**INSTITUTE**

FOR

**COSMIC RAY RESEARCH**

THE UNIVERSITY OF TOKYO

# ANNUAL REPORT
# (APRIL 2013 – MARCH 2014)

5-1-5, Kashiwanoha, Kashiwa, Chiba 277-8582, Japan

Telephone: (81) 4-7136-3102
Facsimile: (81) 4-7136-3115
WWW URL: http://www.icrr.u-tokyo.ac.jp/

# TABLE OF CONTENTS

# PREFACE

This report summarizes the scientific activities of the Institute for Cosmic Ray Research (ICRR) of the University of Tokyo in the Japanese FY 2013.

ICRR is an inter-university research institute for studies of cosmic rays. The headquarters of ICRR is located in Kashiwa, Chiba prefecture, Japan. In order to promote various cosmic-ray-related studies efficiently, ICRR has three research divisions; Neutrino and Astroparticle division, High Energy Cosmic Ray division, and Astrophysics and Gravity division. ICRR has 3 observatories in Japan; Kamioka Observatory (Kamioka underground, Gifu prefecture), Norikura Observatory (2770 meters above sea level, Mt. Norikura, Gifu prefecture), and Akeno Observatory (Yamanashi prefecture), together with 1 research center; Research Center for Cosmic Neutrinos (Kashiwa, Chiba prefecture). In addition, there are 2 major experimental facilities outside of Japan. They are located in Utah in USA, and Yangbajing in Tibet, China.

Many researchers from various Japanese institutions as well as those from overseas are involved in the research programs of ICRR. It should be noted that most of the scientific outputs from this institute are the results of the collaborative efforts by many scientists from various institutions. In order to produce outstanding results, it is very important to carry out an experiment by an international collaboration composed of top-level researchers all over the world. Hence, most of the experimental collaborations that ICRR is involved are international ones. For example, the number of collaborators in the Super-Kamiokande experiment is about 120; about a half of them are from abroad (USA, Korea, China, Poland, Spain and Canada).

Many exciting scientific activities of ICRR are described in this report. One of the highlights in FY 2013 is the results from the Tibet AS gamma experiment, which studied the solar magnetic field using the cosmic ray shadow of the Sun for the first time. It should be noted that the Super-Kamiokande and T2K (which uses Super-Kamiokande as the far detector) experiments have been continuously producing impressive results on neutrino oscillation physics. Another highlight is the construction of the large-scale cryogenic gravitational wave telescope (KAGRA), which intends to detect gravitational waves for the first time and open a new field of gravitational wave astronomy.

As an inter-university research institute, ICRR is reviewed by the top-level researchers in the field. Furthermore, future projects of ICRR are evaluated by a committee composed of top-level researchers from various nearby fields. The report from the ICRR Future Project Evaluation Committee was released in September 2013. The Committee evaluated various possible future projects of ICRR. Several projects have been recommended highly. Among them, joining the CTA project, which is a global TeV gamma ray astronomy project, has been recommended as the top priority ICRR future project. The review report from the External Review Committee, which was released in May 2013 (please see the Annual Review of the last year), also supported joining CTA. ICRR is going to make every endeavor to realize the CTA project as an important international partner of this project.

We hope that this report is useful for the understanding of the current research activities of ICRR. Finally, we appreciate very much the strong support of our colleagues in this research field, the University of Tokyo and the Japanese Ministry of Education, Culture, Sports, Science and Technology. They are indispensable for the continuing, and exciting scientific outcome of ICRR.

Takaaki Kajita,
Director,
Institute for Cosmic Ray Research,
The University of Tokyo

The ICRR building at Kashiwa, Chiba, Japan.

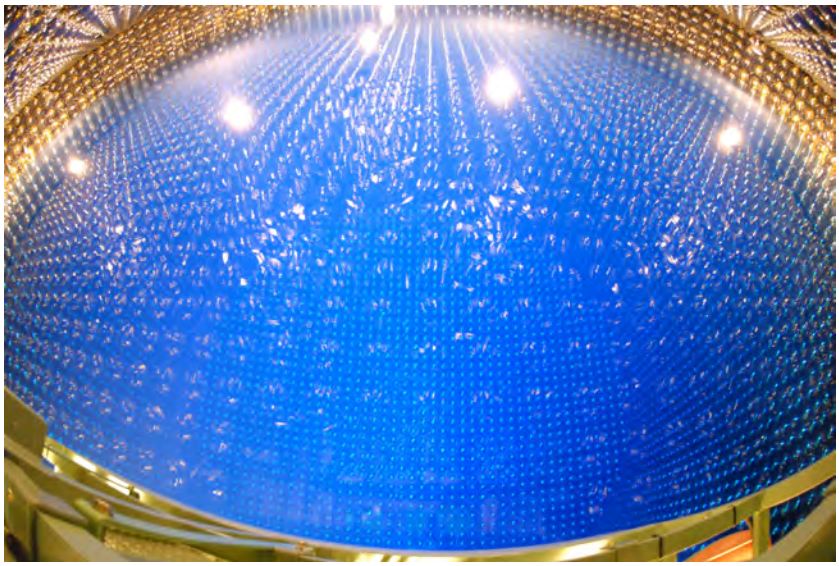

The inner detector of Super-Kamiokande-III during the full reconstruction. The purified water is under filling.

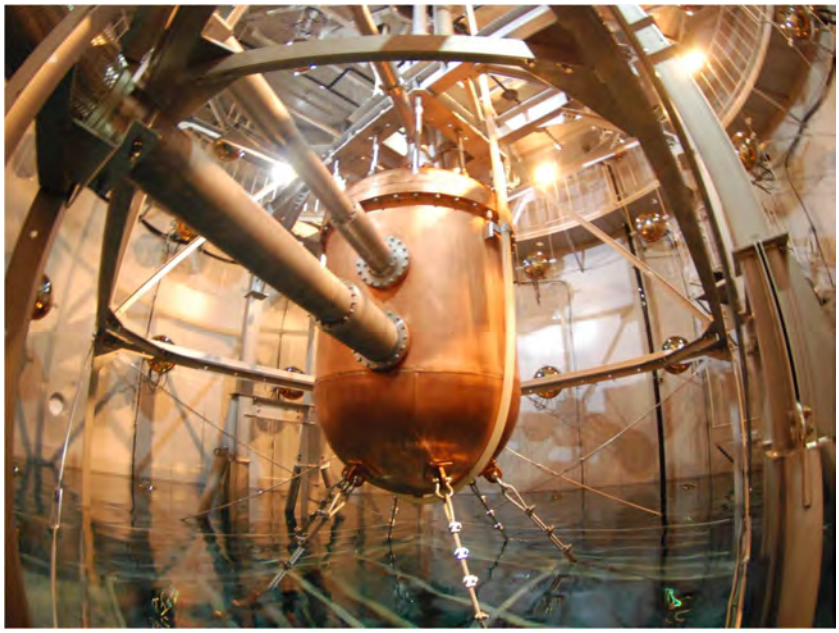

XMASS detector using 835 kg of liquid xenon. Radiations are shielded and cosmic-ray muons can be vetoed by a water-Cherenkov detector outside.

The system of four imaging atmospheric Cherenkov telescopes of 10m diameter of CANGAROO project for detection of very high energygamma-rays The whole system is in operation since March 2004 in Woomera, South Australia.

Tibet-III air shower array (37000 $m^2$) at Yangbajing, Tibet (4300 m in altitude).

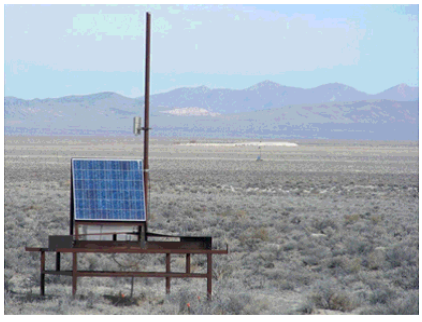

Air fluorescence telescopes (left) and a scintillator surface detector (right) of the Telescope Array experiment in Utah, USA to explore the origin of extremely high energy cosmic rays.

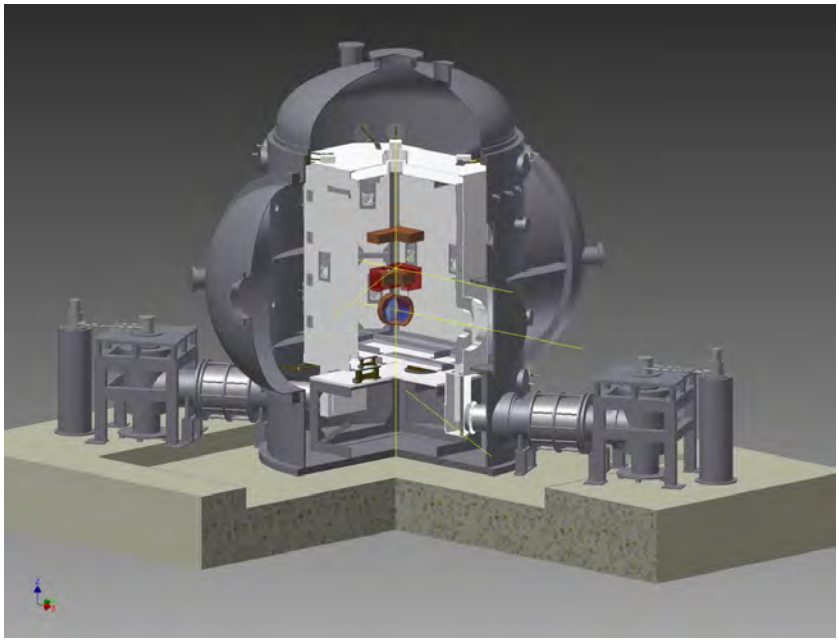

Cryogenic mirror sysytem for KAGRA with a cryostat and a cryocooler.


A public lecture held by Research Center for Cosmic Neutrinos.

## Organization

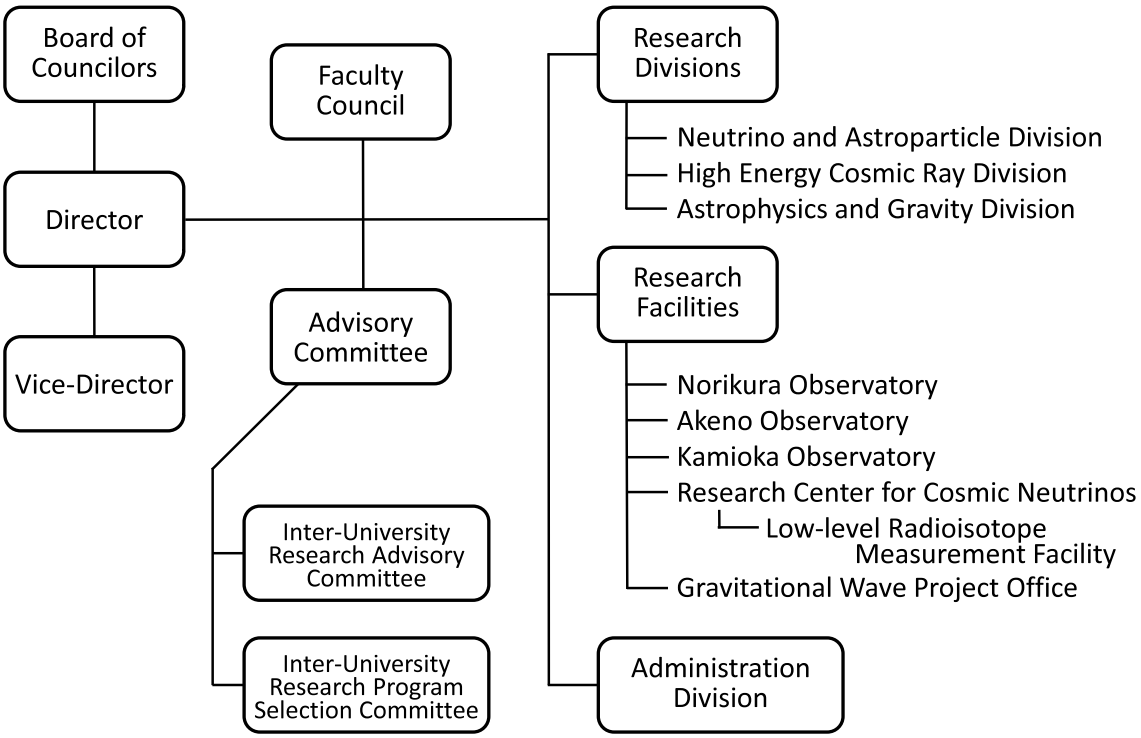


## Number of Staff Members (As of May 1, 2013)

| | Scientific Staff | Technical Staff | Research Fellows | Administrators and Secretaries | Total |
|---|---|---|---|---|---|
| Neutrino and Astroparticle Div. | 24 | 4 | 1 | 17 | 46 |
| High Energy Cosmic Ray Div. | 18 | 11 | 5 | 2 | 36 |
| Astrophysics and Gravity Div. | 14 | 0 | 5 | 8 | 27 |
| Administration | 0 | 0 | 0 | 12 | 12 |
| Total | 56 | 15 | 11 | 39 | 121 |

## FY 2007–2013 Budget

| | 2007 | 2008 | 2009 | 2010 | 2011 | 2012 | 2013 |
|---|---|---|---|---|---|---|---|
| Personnel expenses | 624 000 | 632 000 | 590 000 | 576 000 | 653 000 | 658 000 | 687 000 |
| Non-personnel expenses | 1 253 000 | 1 121 000 | 1 292 000 | 1 048 000 | 1 400 000 | 1 172 000 | 1 034 000 |
| Total | 1 877 000 | 1 753 000 | 1 882 000 | 1 624 000 | 2 053 000 | 1 830 000 | 1 721 000 |

(in 1 000 yen)

# RESEARCH DIVISIONS

## Neutrino and Astroparticle Division

- **Overview**
- **Super-Kamiokande**
- **XMASS Experiment**
- **Hyper-Kamiokande**
- **T2K Experiment**

## High Energy Cosmic Ray Division

- **Overview**
- **Cherenkov Cosmic Gamma-Ray Group**
- **TA: Telescope Array Experiment**
- **Tibet AS$\gamma$ Project**
- **The Ashra Project**
- **High Energy Astrophysics Group**

## Astrophysics and Gravity Division

- **Overview**
- **Gravitational Wave Group**
  - Gravitational Wave Project Office
  - KAGRA Project
  - CLIO Project
- **Observational Cosmology Group**
- **Primary Cosmic Ray Group**
- **Theory Group**
  - Particle Phenomenology
  - Astrophysics and Cosmology

# NEUTRINO AND ASTROPARTICLE DIVISION

## Overview

This division aims to study particle physics with prime interests in physics of neutrinos and proton decay, and astroparticle physics with the use of underground experimental facilities.

Our most important facility is the Super-Kamiokande (SK) detector. It is a 50 kton water Cherenkov detector using 11,129 50 cm-diameter photomultipliers (PMTs) for its inner detector and 1,885 20 cm-diameter PMTs for its outer detector. The data taking of SK started in April 1996. The neutrino oscillations in atmospheric neutrinos were discovered in 1998 and thereby demonstrating that neutrinos have a finite mass. In 2001, the accurate measurements of the $^8$B solar neutrino flux by SK and SNO discovered that neutrino oscillations are the solution of the solar neutrino problem beyond doubt. After those discoveries, precise measurements of atmospheric neutrinos and solar neutrinos have been performed and they unraveled various phenomena of neutrino oscillations. Recently, excess of events induced by $\nu_\tau$ appearance was observed in atmospheric neutrinos, and the day/night difference of the solar neutrino flux, which is expected from the matter effect of neutrino oscillations, was observed in the precise solar neutrino measurement.

The search for nucleon decay at SK gives the current best limit which strongly constrains the grand unification scenario of particle interactions. SK has been searching for neutrinos from supernovae by two methods, one is a search for burst neutrinos originate from nearby supernovae, another is so-called supernova relic neutrinos, which is an accumulated supernova burst neutrinos from the beginning of the universe.

A high intensity neutrino beam experiment using the J-PARC accelerator (T2K) was started in 2009. The T2K experiment uses the SK detector as the far detector. Electron neutrino appearance (the effect of the mixing angle $\theta_{13}$) and the high precision measurement of oscillation parameters are main physics subjects in T2K. An indication of electron neutrino appearance was found in June 2011, and the significance of the appearance has been greatly improved in 2013.

Another activity of the Neutrino and Astroparticle division is a multi-purpose experiment using liquid xenon aiming at the detection of cold dark matter, neutrino absolute mass using neutrinoless double beta decay, and low energy solar neutrinos. The construction of a 800 kg liquid xenon detector was completed at the end of 2010 and subsequent commissioning run continued by June 2012. With the commissioning data, low-mass WIMPs, annual modulation of event rate, and axions were studied. In 2013, detector refurbishment to reduce the surface background had been performed.

In addition to those on-going projects, some R&D projects are also proceeded. GADZOOKS! is a project to add 0.1% of gadolinium into the Super-K tank in order to tag neutrons for $\bar{\nu}_e$ detection. It should enable us to detect supernova relic neutrinos. A feasibility study for GADZOOKS! has been performed using a 200 ton tank which mimics the Super-K detector. The Hyper-Kamiokande (Hyper-K) detector is proposed as a next generation underground water Cherenkov detector. The detector is approximately 20 times larger in volume than Super-K and has discovery potential of leptonic CP violation and proton decays. New photosensor R&D and physics potential studies for Hyper-K has been performed in 2013.

## SUPER-KAMIOKANDE

[Spokesperson : Masayuki Nakahata]
Kamioka Observatory, ICRR, The University of Tokyo

### *Search for nucleon decay*

Proton decays and bound neutron decays (nucleon decays in general) is the most dramatic prediction of Grand Unified Theories (GUTs) in which three fundamental forces of elementary particles are unified into a single force. Super-Kamiokande (SK) is the world's largest detector to search for nucleon decays. Various nucleon decay modes have been looked for, but we have found no significant signal excess so far. In 2013, lifetime limits of major proton decay modes, $p \to e^+\pi^0$ and $p \to \bar{\nu}K^+$, were updated with 260 kton·year exposure. In addition to them, some of nucleon decay modes which violate baryon and lepton number by two have been newly studied. Figure 1 shows summary of nucleon lifetime limits of various decay mode which we have investigated in SK data.

A proton decay into one positron and one neutral pion ($p \to e^+\pi^0$) is one of the most popular decay modes. This decay mode is mediated by super-heavy gauge bosons and discovery of the signal would give us the information of the mass of the gauge mesons. To discriminate the signal from the atmospheric neutrino background, we reconstruct the number of particles (Cherenkov rings) and reconstruct the total visible energy corresponding to parent proton mass and total momentum corresponding to the proton's Fermi momentum. If a proton decays in an oxygen with this mode, generated $\pi^0$ is affected by various interactions (scattering, absorption, charge exchange, multi pion production) with nucleus before go out from the oxygen. In 2012, we have studied pion interaction cross sections which have been measured by other experiments and re-tune final state interaction of pion, which is important also for atmospheric $\nu$ analysis (details in the previous annual report). As a result, the selection efficiency for $p \to e^+\pi^0$ is estimated to be decreased from 45 % to 40 % dominantly due to increasing cross section of pion charge exchange and large angle scattering. Signal and BKG simulations for all period (SK1-SK4) have been regenerated, and data set was also updated until February 2013 corresponding

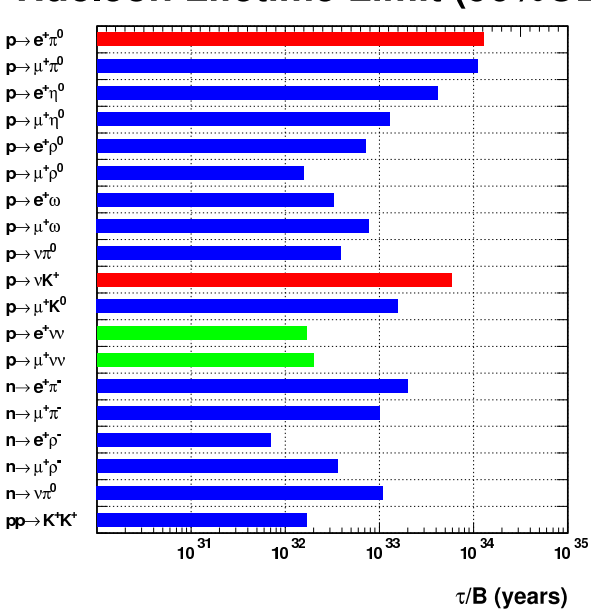


Fig. 1. Nucleon lifetime limits with 90% CL for decay modes which have been investigate by SK. Red histograms shows updated mode and green show new decay mode which have been studied in 2013.

| | kton·yr | Efficiency | BKG |
|---|---|---|---|
| SK1 | 91.7 | 39.2±0.7% | 0.27 |
| SK2 | 49.2 | 38.5±0.7% | 0.15 |
| SK3 | 31.9 | 40.1±0.7% | 0.07 |
| SK4 | 87.3 | 39.5±0.7% | 0.22 |

Table 1. Results of $p \to e^+\pi^0$ mode.

to 260 kton·year exposure, as summarized in Table 1. No candidate has been observed so far and a lower lifetime limit (90% CL) of proton is estimated to be $1.4\times10^{34}$ years.

Total expected background events in 260 kton·year exposure is 0.71 events. In order to keep good sensitivity even in future, it is important to reduce background. A new algorithm to tag neutrons, which are captured in water and emit 2.2 MeV gamma ray, are under developing to distinguish neutrino and anti-neutrino interaction. The neutron tagging is also expected to be useful to reduce atmospheric neutrino background in proton decay searches.

Some GUT models incorporating with Super-symmetry theory, SUSY, favored decay modes which include K mesons in the final state, $p \to \bar{\nu}K^+$. In this mode, we tag the signal by decay products from $K^+$. The momentum of $K^+$ is below the Cherenkov threshold, and is stopped in the water and decay into $\mu^+\nu$ or $\pi^+\pi^0$ with monochromatic momenta. The residual nucleus after proton decay emits $\gamma$ ray ( 40% probability) and it is also useful to tag proton decay signal. There were several improvements in 2012 as described in the previous annual report. Signal and background MC in all period have been reprocessed based on the new analysis, and the exposure of data has been updated to 260 kton·years. There are no candidates for methods tagging proton decay by using $\mu$ with prompt $\gamma$ and $\pi^+\pi^0$ from $K^+$ decay, and no excess can be observed in $\mu$ momentum distribution. The results are summarized in Table 2 and estimated lower limit of lifetime for this decay mode is $5.9\times10^{33}$ years.

In case of above two decay modes, B-L are conserved where B and L are baryon and lepton number, respectively. Trilepton decay modes such as $p \to e^+\nu\nu$ and $p \to \mu^+\nu\nu$, which are based on SO(10) GUT model, can violate B-L by two, $|\Delta(B-L)|$=2. Final states of these two modes should be single ring e- or $\mu$- like event which has momentum in characteristic band due to three body decay. Thus momentum distributions of single ring fully contained (FC1R) events have been examined to check distortions which come from proton decay into three leptons. Figures 2 show momentum distribution of FC1R e-like and $\mu$-like events of data with 273 kton·year exposure, atmospheric $\nu$ MC, and proton decay MC. There were no clear bumps made by proton decays. The data was fitted by atmospheric $\nu$ MC and proton decay MC, and lower limit of proton lifetimes are estimated to be $1.7\times10^{32}$ and $2.0\times10^{32}$ years for $p \to e^+\nu\nu$ and $p \to e^+\nu\nu$, respectively.

If two nucleons decay into meson simultaneously, B-L is not conserved also. In past, $pp \to e^+e^+, \mu^+\mu^+, K^+K^+$ have been studied and it is natural extensions to study two nucleons decay into pions. As a first step, $pp \to \pi^+\pi^+$ has been just started to investigate. The difficult point than other modes studied in the past is that charged pions with high momentum can loose their energy by hadronic interactions which may not be observed by Chrenkov light, which is usually used for estimation of momentum, consequently distributions of total momentum and invariant mass become broader than other modes. "Boosted Decision Tree" analysis has been introduced for this analysis to overcome the difficulty. Once the analysis method is established, it will be extended to $pn \to \pi^+\pi^0$ and $nn \to \pi^0\pi^0$.

### *Atmospheric neutrinos*

Cosmic ray interactions in the atmosphere produce neutrinos via the decay products of secondary hadrons, such as pions and kaons, emerging from these interactions. The atmospheric neutrino flavor ratio, $(\nu_\mu + \bar{\nu}_\mu)/(\nu_e + \bar{\nu}_e)$, is expected to be approximately two based on the structure of the pion decay chain. Though the uncertainty on this ratio is estimated to be only 5 % or less, the absolute scale of the flux for all neutrino species is much less understood and its prediction carries an uncertainty of at least 20 %. It should be noted that despite this uncertainty, above a few GeV where the effects of the geomagnetic field are negligible, the fluxes of upward- and downward-going neutrinos are nearly equal and therefore provide a useful constraint in the study of these neutrinos. Super-Kamiokande has been observing atmospheric neutrinos since 1996 and has accordingly made several important measurements, including the discovery of neutrino oscillations [1, 2].

#### Three flavor oscillations and the neutrino mass hierarchy

The SK atmospheric neutrino data are described at leading order by two-flavor $\nu_\mu \to \nu_\tau$ oscillations with maximal mixing ($\theta_{23}$=$\pi$/4). However, sub-leading contributions via $\nu_\mu$

| | | SK-I | SK-II | SK-III | SK-IV |
|---|---|---|---|---|---|
| Exp.(kton·yrs) | | 91.7 | 49.2 | 31.9 | 87.3 |
| Prompt $\gamma$ | Eff.(%) | 7.9±0.1 | 6.3±0.1 | 7.7±0.1 | 9.1±0.1 |
| | BKG | 0.08 | 0.14 | 0.03 | 0.13 |
| | OBS | 0 | 0 | 0 | 0 |
| $P_\mu$ spec. | Eff.(%) | 33.9±0.3 | 30.6±0.3 | 32.6±0.3 | 37.6±0.3 |
| | BKG | 193 | 94.3 | 69.0 | 223.1 |
| | OBS | 177 | 78 | 85 | 226 |
| $\pi^+\pi^0$ | Eff.(%) | 7.8±0.1 | 6.7±0.1 | 7.9±0.1 | 10.0±0.1 |
| | BKG | 0.18 | 0.17 | 0.09 | 0.18 |
| | OBS | 0 | 0 | 0 | 0 |

Table 2. Summary of the proton decay search $p \to \bar{\nu} K^+$ with selection efficiencies and expected backgrounds for each detector period.

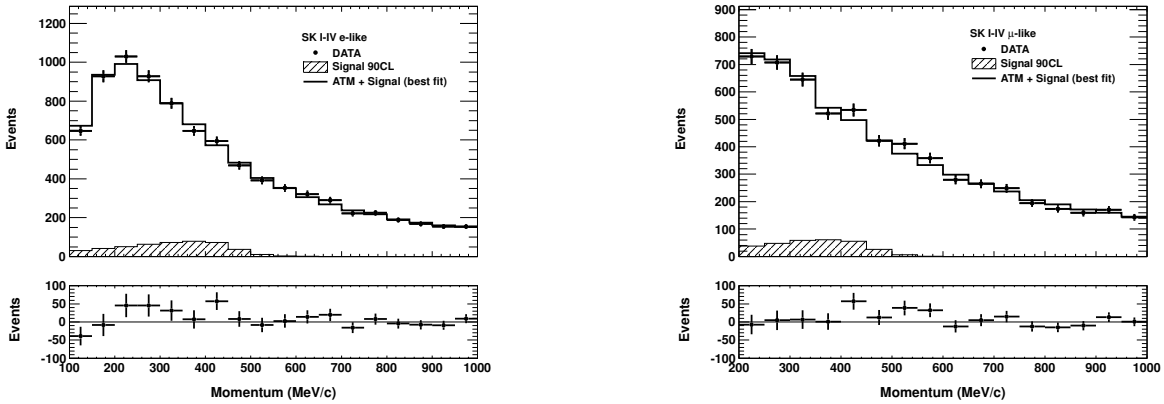


Fig. 2. Reconstructed momentum distribution for 273.4 kton · years of combined SK data (black dots), the best fit result for the atmospheric neutrino background (solid line) and the 90% confidence level allowed amount of nucleon decay signal (hatched histogram) for $p \to e^+\nu\nu$ (left) and $p \to \mu^+\nu\nu$ (right).

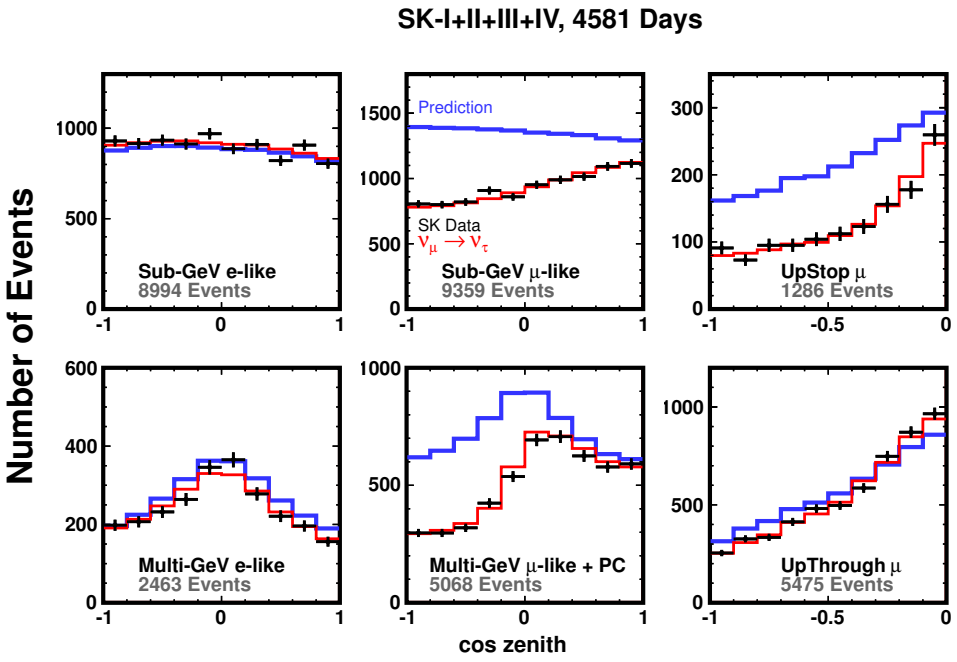


Fig. 3. Zenith angle distributions of SK atmospheric neutrino data. The horizontal axis indicates the cosine of the reconstructed zenith angle ($\cos\theta$ =-1 corresponds to the upward-going direction). The data are shown by the black points with error bars and the MC predictions without oscillations and with two flavor $\nu_\mu \to \nu_\tau$ oscillations are shown by the blue and red lines, respectively.

$\rightarrow \nu_e$ oscillations induced by the mixing angle $\theta_{13}$ as well as the "solar" mixing parameters $(\Delta m^2_{12}, \theta_{12})$ provide the ability to probe currently unknown aspects of the standard neutrino oscillation paradigm, such as the existence of leptonic *CP* violation and the neutrino mass ordering (hierarchy). Understanding these open questions may bring important insight into larger questions, such as the origin and evolution of today's matter-dominated universe.

Several sub-leading oscillation effects are expected to appear in atmospheric neutrinos:

- Resonant enhancement of $\nu_\mu \rightarrow \nu_e$ oscillations due to the effects of matter occur at energies between 2 and 10 GeV and will manifest as an excess of upward-going electron-like events in the atmospheric sample.
- This enhancement exists for either $\nu_e$ or $\bar{\nu}_e$ depending on the mass hierarchy. Therefore the mass hierarchy can be probed by understanding the relative amount of neutrino and antineutrino interactions in the detector.
- The combination of the solar oscillation parameters and the octant of $\sin^2\theta_{23}$, may enhance or suppress the event rate, and to some extent alter the spectral shape, of Sub-GeV electron-like data the due to $\nu_\mu \leftrightarrow \nu_e$ oscillations they induce.
- The *CP* violating term, $\delta_{cp}$, induces several sub-dominant oscillation effects which are predicted to appear across many of the SK atmospheric neutrino samples.

Super-Kamiokande has studied the effects of these oscillations on atmospheric neutrino data separated into fully-contained (FC) events, partially-contained (PC) events, and upward-going muon topologies. Fully-contained events are characterized by a primary interaction vertex that is located inside the 22.5 kton fiducial volume of the detector and whose visible particles stop within the inner detector. On the other hand, though the primary vertex position of PC events is within the fiducial volume, they are characterized by having at least one charged particle escaping the inner detector and depositing light in the outer detector. In most cases the escaping particle is a muon. Upward-going muons originate from high energy muon-neutrino interactions in the rock surrounding the detector. Since all other particles are lost to interactions in the rock, only the muon is penetrating enough to reach the detector and be identified. The FC sample is separated into electron-like and muon-like subsamples by applying a particle identification algorithm to the most energetic Cherenkov ring of each event. Since PC and upward-going events are predominantly produced by muon neutrinos, no particle identification is applied. Though SK cannot distinguish on an event-by-event basis neutrino and antineutrino interactions, since the effect of the mass hierarchy lies in the difference of their oscillations, statistical separation of multi-GeV electron-like subsamples is performed. A likelihood method designed to enhance the kinematic differences between neutrino and antineutrino interactions is applied to separate the events into $\nu_e$-like and $\bar{\nu}_e$-like subsamples.

The atmospheric neutrino data accumulated during SK-I,-II,-III,and -IV and corresponding to 1489+799+518+1775 days of FC/PC and 1646+828+636+1775 days of upward-going muon data have been analyzed. Zenith angle distributions for six data subsamples are shown in Fig. 3. An oscillation analysis considering all mixing parameters from the PMNS framework, including the *CP* violating term, $\delta_{cp}$, and the effects of the earth's matter on neutrino propagation, has been performed assuming that $\theta_{13}$ is constrained to the measured value from reactor neutrino experiments, $\sin^2\theta_{13}$=0.025. It should be noted, however, that the uncertainty on this measurement is included as a systematic uncertainty in this analysis. Fig. 4 shows the allowed region of the atmospheric mass squared difference $(\Delta m^2_{32})$ and $\theta_{23}$ parameters obtained from the analysis. Though accelerator experiments such as T2K and MINOS give more stringent constraints, the atmospheric neutrino measurements are consistent with these results. Comparing the minimum absolute $\chi^2$ values between fits to the normal and inverted hierarchy hypotheses indicate that the Super-K data have a weak preference for the normal mass hierarchy, $\Delta\chi^2 = \chi^2_{NH} - \chi^2_{IH}$ = -0.9. In order to improve sensitivity to the mass hierarchy the analysis has been extended to include external constraints from the T2K experiment. T2K is modeled using atmospheric neutrino MC reweighted to the beam spectrum and incorporates publicly available data and systematic error information for the analysis [4, 4]. The modeled T2K data samples are then fit in conjunction with the atmospheric neutrino data including relevant systematic error correlations. In this fit the normal hierarchy preference is strengthened to $\Delta\chi^2 = -1.2$. The best fit oscillation parameters and minimum $\chi^2$ values from these analyses are shown in Table 3. It should be noted that the data show a slight preference for $\delta_{cp} = 220^\circ$ but include $\sin\delta_{cp}$ = 0 at the 90% C.L. in all fits.

**Neutron tagging**

With SK-IV's upgraded electronics it is now possible to record all PMT hit information in the $500\mu s$ after an event is triggered within the detector. This feature is particularly important for the study of neutrons, which are ordinarily unseen within Super-K. Indeed, neutron capture on hydrogen produces a 2.2 MeV $\gamma$ ray, via $p(n,\gamma)d$, which is just above threshold and therefore difficult to detect in isolation amidst the various radioactive backgrounds occurring in the detector. However, using the $500\mu s$ data following a primary trigger it is possible to correlate and tag signals consistent with neutron capture on water with neutrino interactions. Among water Cherenkov detectors this ability is unique to SK and has the potential to improve separation of charged current neutrino interactions, which dominantly produce a secondary proton, from antineutrino interactions, which dominantly produce a secondary neutron. At increasing energies additional hadronic interactions may produce further neutrons and therefore characterization of this production is an important input for MC generators.

The Super-K neutron tagging algorithm is two stage procedure applied to fully contained neutrino interactions using a few simple precuts followed by a neural network-based selection to define the final neutron candidates. During the preselection, a search is made for time-clustered PMT hits after

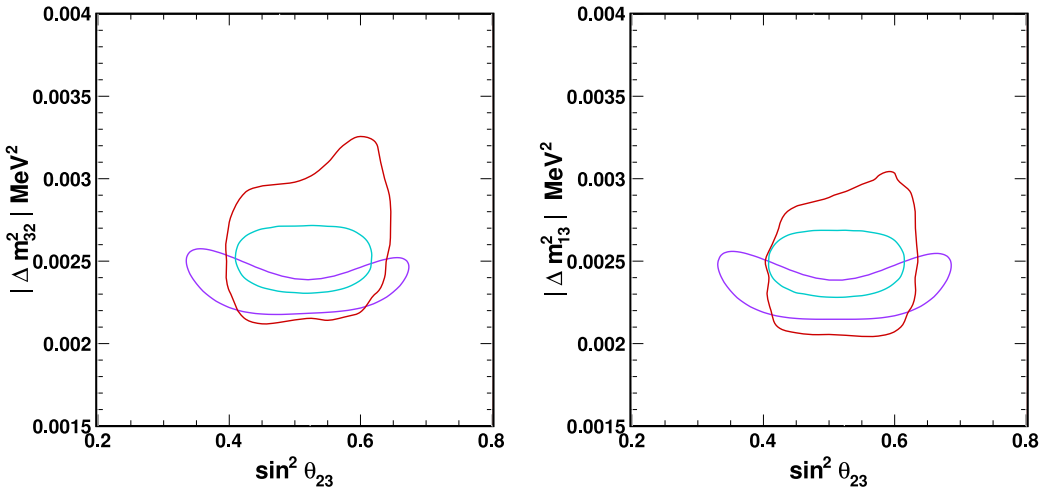


Fig. 4. Allowed regions in the atmospheric mixing plane, $\Delta m^2_{23,31}$ and $\sin^2\theta_{23}$, at the 90% C.L. as measured by Super-Kamiokande atmospheric neutrinos (red), MINOS (purple) [3], and T2K [4] (cyan). Fits to the normal and inverted hierarchy hypotheses are shown in the left and right figures, respectively.

| | $\sin^2\theta_{13}$ | $\delta_{CP}$ | $\sin^2\theta_{23}$ | $\Delta m^2_{32}$ ($\times 10^{-3}$) | $\chi^2$ |
|---|---|---|---|---|---|
| SK only (NH) | 0.025 | 3.84 | 0.57 | 2.6 | 559.8 |
| SK only (IH) | 0.025 | 3.84 | 0.57 | 2.5 | 560.7 |
| SK+T2K (NH) | 0.025 | 4.19 | 0.55 | 2.5 | 578.2 |
| SK+T2K (IH) | 0.025 | 4.19 | 0.55 | 2.5 | 579.4 |

Table 3. Best fit oscillation parameters obtained by the three flavor oscillation analysis. Fits are conducted for both the normal (NH) and inverted (IH) hierarchy assumptions for the atmospheric neutrino data ("SK only") and including constraints from the T2K experiment("SK+T2K"). All fits are performed assuming $\sin^2\theta_{13}$=0.025.

a time-of-flight correction relative to the neutrino interaction vertex has been applied. All clusters with more than seven PMT hits within a 10 *ns* time window and less than 50 (200) hits within a 10(200) *ns* window which occurring during the 18-535$\mu s$ after the initial neutrino interaction are selected as candidates for the neural network. The neural network is composed of 16 variables designed to exploit the following expectations from the signal. Hits from a neutron capture gamma should be produced from a single electromagnetic shower and should therefore have an opening angle near 42°, the critical angle in water, should exhibit low isotropy, and have a tight timing profile. Further, since the majority of neutrons thermalize and capture within 200 cm of the neutrino interaction, hits from a neutron capture have a higher likelihood of occurring on PMTs closer to the initial interaction and their total energy should be consistent with 2.2 MeV. Optimizing the neural network for these criterion, Super-K has achieved 20.5% selection efficiency with an estimated background of 0.018 events per neutrino event. Without applying the neural network these numbers are 33.2% and 4.45% respectively, clearly demonstrating the power of this selection. Applying this algorithm to the atmospheric neutrino data sample a clear neutron capture signal with an exponential time constant of 205.3$\mu s$ is observed and shown in Fig. 5. This measurement compares well with the expectation of 204.8 $\mu s$ [13]. The right panel of the figure shows a comparison between data and MC of the average tagged neutron multiplicity as a function of the initial neutrino's total visible energy. Impressive agreement across most of the energy range has been obtained and establishes the robustness of the method. Future analyses will use this tagging to reduce atmospheric neutrino backgrounds in the SK search for proton decay and to improve the separation between the $\nu_e$- and $\bar{\nu}_e$-like oscillation analysis samples.

**Search for sterile neutrino**

Though the standard three flavor oscillation scheme has been established by a wide range of experiments, there remain "anomalies" which are not consistent in this picture; For example, the LSND experiment observed $\bar{\nu}_e$ appearance over a short baselines, which when interpreted as an oscillation signal suggests a mass difference inconsistent with the results of solar and atmospheric neutrino measurements, $\Delta m^2_s \sim 1\text{eV}^2$ [6]. The MiniBooNE experiment, which was designed to study this anomaly, reported a similar excess of $\bar{\nu}_e$ events [7]. Due to the strong constraint on the number of neutrinos from LEP measurements, the additional neutrino suggested by this new mass difference must not participate in weak interactions. These non-interacting neutrinos are therefore called "sterile." If there is indeed a heavy fourth neutrino state, the effects of the extra oscillation channel atop the dominant $\nu_\mu \to \nu_\tau$ oscillations are expected to be visible in the atmospheric neutrino flux.

The atmospheric neutrino data has been fit searching for

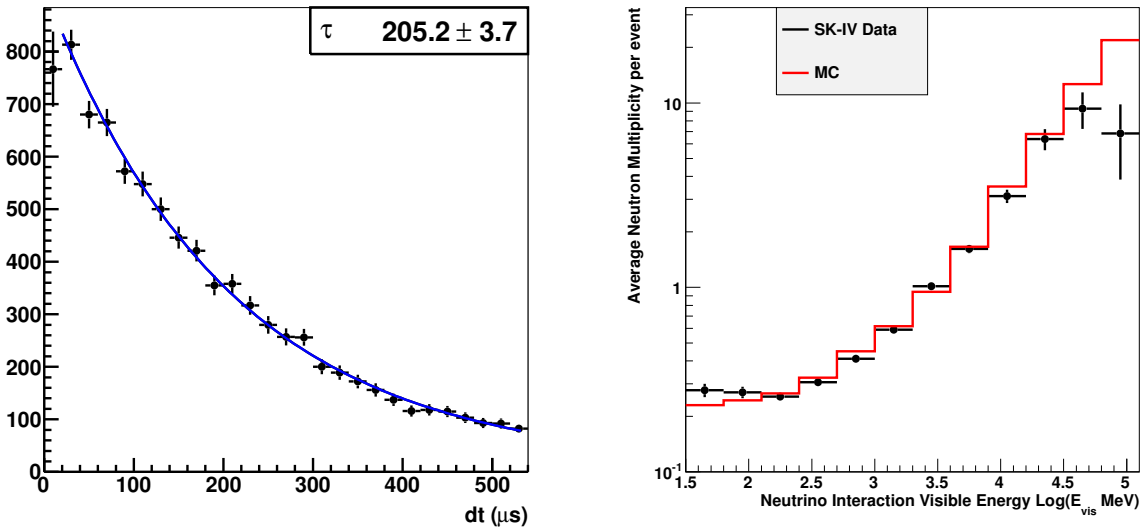


Fig. 5. Time difference between the primary neutrino interaction and tagged neutron capture gamma ray candidates (left) and the average tagged neutron multiplicity as a function of the total visible energy of the neutrino interaction (right). In the latter, the red line indicates the expectation from the Super-K MC.

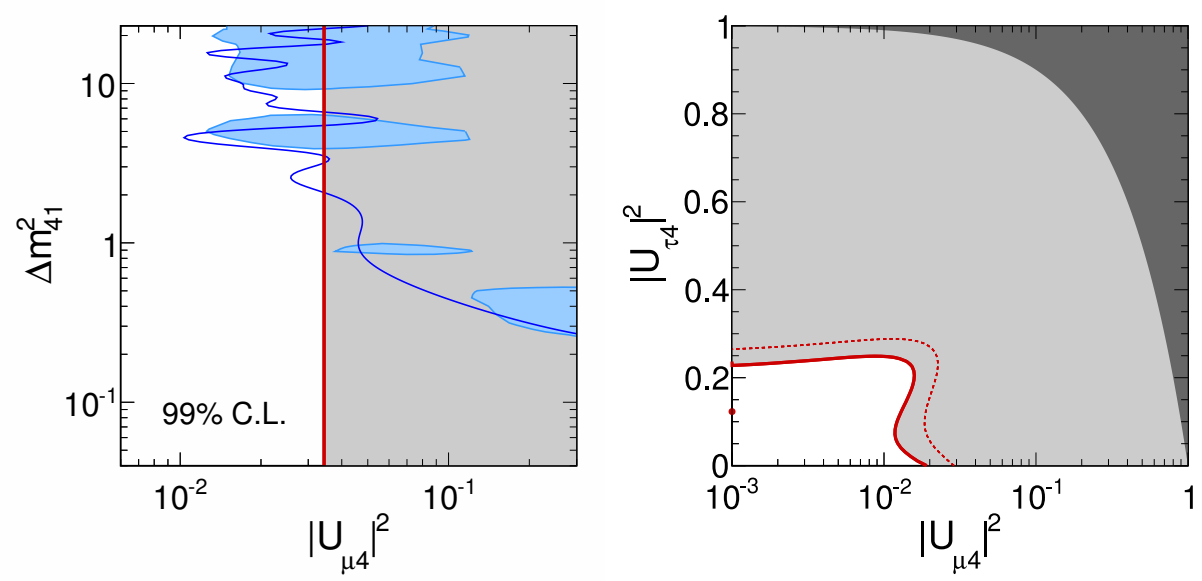


Fig. 6. (Left) Super-Kamiokande's limit on $|U_{\mu 4}|^2$ at the 90% confidence level. (Right) Upper limits on $|U_{\mu 4}|^2$ vs $|U_{\tau 4}|^2$ at 90% and 95% C.L. are shown by the solid and dashed lines, respectively. The light gray region is excluded at 90 % and the dark gray region is disallowed by unitarity.

evidence of these oscillations. However, at large masses atmospheric neutrino oscillations become insensitive to the exact value of the mass splitting and are primarily sensitive to the additional mixing matrix elements between the active and sterile states, $U_{\mu 4}$ and $U_{\tau 4}$. More importantly, the data are insensitive to the precise number of additional sterile neutrinos, a feature unique to atmospheric neutrino studies, so the analysis is performed using a model with only one additional neutrino (the "3+1" model) [9]. The results of two fits, one for $U_{\mu 4}$ with standard matter effects only and one for $U_{\mu 4}$ and $U_{\tau 4}$ including sterile matter effects only, are shown in Fig. 6. Tight constraints on both parameters have been obtained, with $|U_{\mu 4}|^2 < 0.21$ and $|U_{\tau 4}|^2 < 0.22$ at 90% C.L., and a large portion of the allowed region from [9] has been ruled out.

**Limits on Lorentz invariance violation**

Symmetry of physical systems under Lorentz transformations is a fundamental feature of both the Standard Model of particle physics and the General Theory of Relativity. Accordingly, violation of this symmetry, termed Lorentz invariance violation (LIV), would provide striking evidence for new physics and has been the focus of many experiments. Neu-

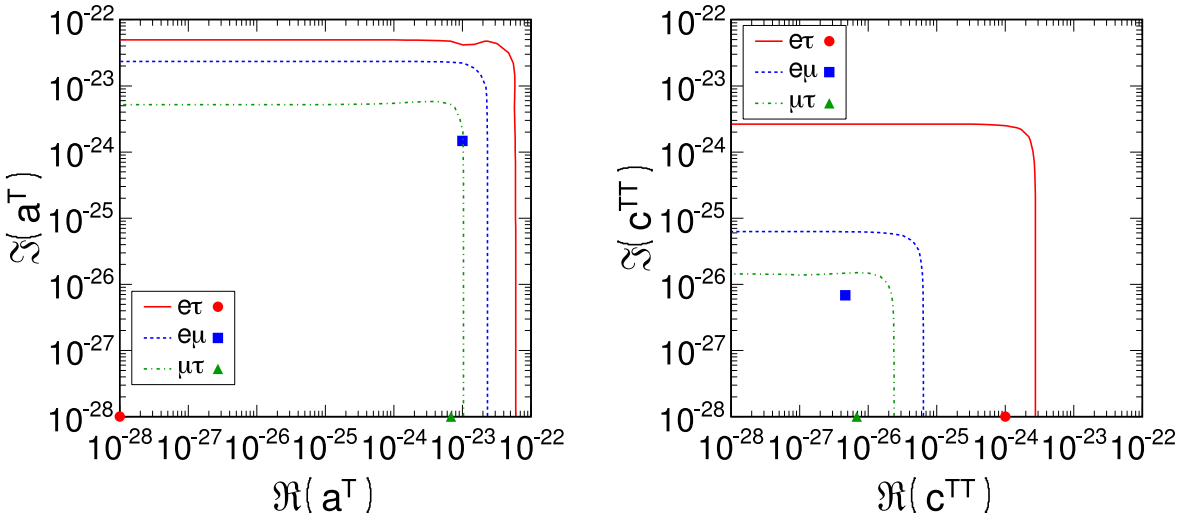


Fig. 7. Contours showing the 95 % confidence level allowed regions for the Lorentz invariance violating parameters $a^T_{e\tau}$ (solid), $a^T_{e\mu}$ (solid), $a^T_{\mu\tau}$ (dot-dashed) appear in the left figure and those for $c^{TT}_{e\tau}$ (solid), $c^{TT}_{e\mu}$ (dashed), $c^{TT}_{\mu\tau}$ (dot-dashed) are shown in the right figure. Best fit points from the six fits are also shown.

trino oscillations are sensitive to two types of LIV phenomena: sidereal effects, in which oscillations are seen to vary as the earth rotates through its sidereal day, and spectral anomalies, which induce oscillation effects whose frequency is proportional to the neutrino pathlength or the product of the neutrino pathlength with its energy. At Super-K LIV is studied within the context of the standard model extension (SME) [12] which introduces a LIV term,$H_{LV}$, into the standard neutrino Hamiltonian,

$$H = UMU^\dagger + V_e + H_{LV},$$

where $U$ is the PMNS mixing matrix, $M$ is the neutrino mass matrix and $V_e$ is the earth matter potential. Though $H_{LV}$ can have many possible complex coefficients corresponding to higher dimensional LIV operators, the present analysis focuses only on the isotropic dimension-three and dimension-four contributions,

$$H_{LV} = \pm \begin{pmatrix} 0 & a^T_{e\mu} & a^T_{e\tau} \\ (a^T_{e\mu})^* & 0 & a^T_{\mu\tau} \\ (a^T_{e\tau})^* & (a^T_{\mu\tau})^* & 0 \end{pmatrix} - E \begin{pmatrix} 0 & c^{TT}_{e\mu} & c^{TT}_{e\tau} \\ (c^{TT}_{e\mu})^* & 0 & c^{TT}_{\mu\tau} \\ (c^{TT}_{e\tau})^* & (c^{TT}_{\mu\tau})^* & 0 \end{pmatrix}.$$

The diagonal elements of $H_{LV}$ have been neglected since they cannot be observed in neutrino oscillations. Though this matrix represents the neutrino Hamiltonian, antineutrino propagation is described by changing the sign of the first matrix and taking the complex conjugate of the $a^T$ and $c^{TT}$ parameters.

It should be noted that this is the first analysis to approach the problem of LIV in the SME without introducing approximations. Indeed, the usual perturbative conditions introduced to simplify analysis in this framework are invalid for the high energy Super-K atmospheric neutrino data, so the complete neutrino evolution equation has been solved when computing oscillation probabilities. After performing oscillation fits including these effects, no evidence for LIV is seen. As a result, Super-K has set limits on the isotropic parameters $a^T$ and $c^{TT}$ in the $e\mu$, $\mu\tau$, and $e\tau$ sectors as shown in Fig. 7. Despite the lack of a positive signal, the SK constraints on the existence of LIV phenomena in neutrino oscillations improve on existing limits [10] for $a^T$ and $c^{TT}$ by four and seven orders of magnitude, respectively.

**Indirect WIMP searches**

Astronomical and cosmological observations point conclusively to the existence of dark matter and though invisible to electromagnetic probes, it is thought to represent 26% of the matter-energy content of the universe. Weakly Interacting Massive Particles (WIMPs), GeV/$c^2$-scale particles which have only gravitational and weak interactions, are a favored candidate to explain the existence of this as yet unknown matter. Though direct dark matter detection experiments search for the elastic scattering interactions of these proposed particles with ordinary baryonic matter, it is also possible that WIMPs decay or annihilate into Standard Model particles which can then be detected to give indirect evidence for WIMPs. If WIMPs become trapped in the gravitational potential of a massive system, such as the center of the Milky Way or the sun, their density may become sufficient for large numbers of these particles to annihilate into particles which then decay into neutrinos. In this case the neutrinos pass undeflected through the universe and would therefore create an additional neutrino signal with a characteristic energy spectrum emerging from a common direction.

At Super-K, though the search for these particles is dominated by the atmospheric neutrino background, the expectation that they are produced at a common location in the sky is a powerful discriminant. Accordingly, the atmospheric neutrino data are binned in both lepton momentum and the reconstructed angle to either the galactic center or to the sun to search for the presence of an extra neutrino signal from those directions. Since there is no knowledge of WIMP interactions,

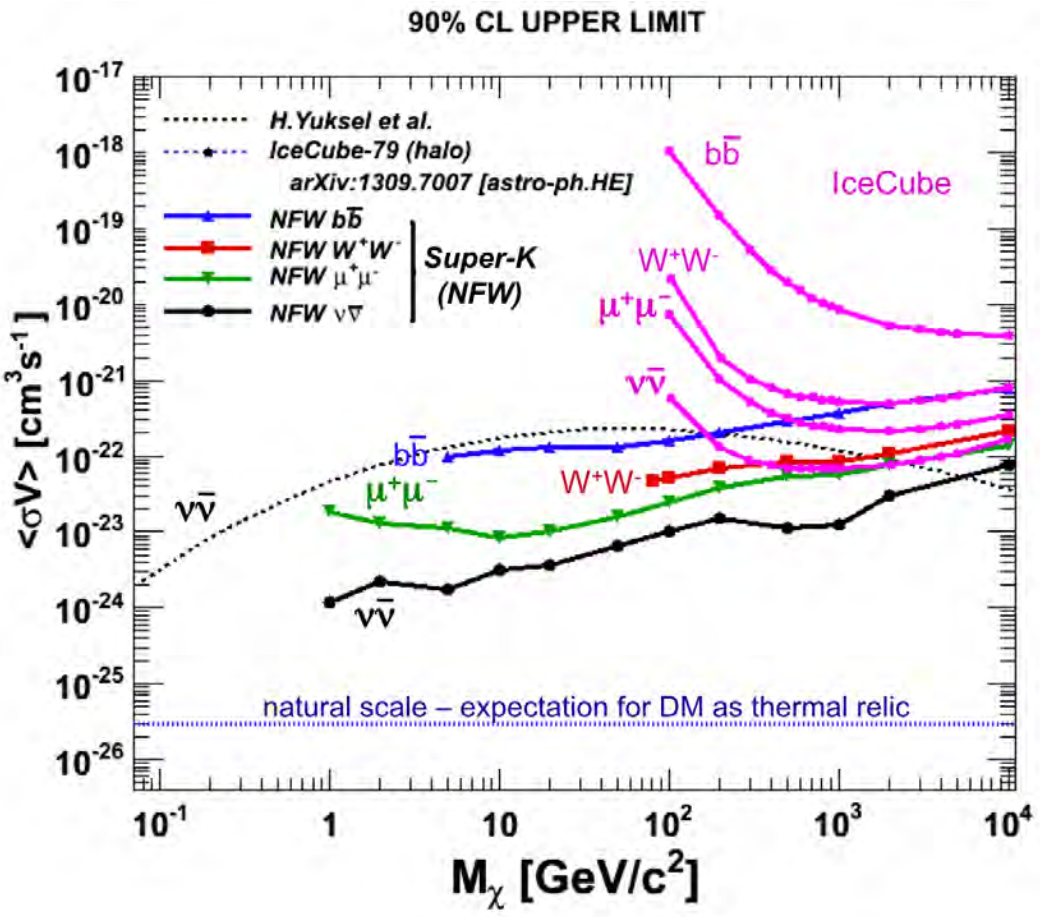


Fig. 8. The 90% C.L. upper limits on the velocity averaged WIMP self-annhilation cross section from a search for WIMP annihilation from the direction of the Galactic Center as a function of WIMP mass. Upper limits assuming branching ratios of 100% for WIMP annihilation into: $\chi\chi \to \nu\bar{\nu}$ (black), $\mu^+\mu^-$ (green), $W^+W^-$ (red), and $b\bar{b}$ (blue) are shown. Limits from the IceCube experiment appear in magenta [11].

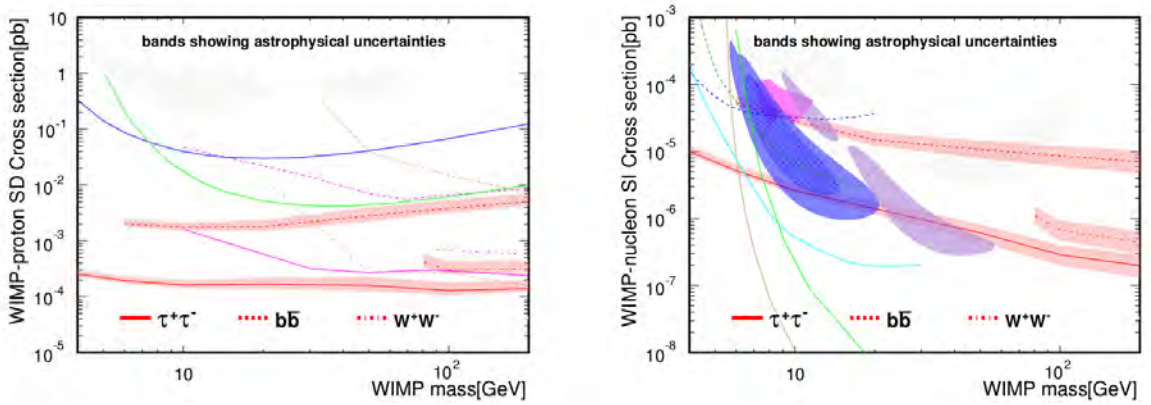


Fig. 9. The 90% C.L. upper limits on the spin-dependent (left) and spin-independent (right) WIMP-nucleon scattering cross section based on a search from WIMP-induced neutrinos coming from the direction of the sun are shown as a function of WIMP mass. These limits are calculated assuming WIMP annihilation into $\tau^+\tau^-$ (red solid), $b\bar{b}$ (red dashed), $W^+W^-$ (red dot-dashed), with 100% branching fraction. Limits and allowed regions from other experiments are also shown.

the analysis proceeds by separately assuming annihilation into each of $\nu\bar{\nu}$, $b\bar{b}$, $t\bar{t}$, and $W^+W^-$ with 100% branching fraction. For each assumed WIMP mass the expected neutrino energy distribution emerging from the decay chains of these particles is computed and used to define the signal spectrum at Super-K. In contrast to previous studies, the entire atmospheric neutrino data set is used and therefore gives access WIMP masses in the range of several GeV/$c^2$ to TeV/$c^2$. No evidence for a neutrino signal on top of the atmospheric neutrino background has been found in the direction of either the

galactic center or the sun. The resulting limits on the velocity averaged WIMP self-annihilation cross section for the galactic center search appear in Fig. 8. Limits on the WIMP-nucleon spin-dependent and spin-independent scattering cross sections from the search for events from the sun are shown in Fig. 9.

## Bibliography


[1] Y. Fukuda *et al.*, "Evidence for Oscillation of Atmospheric Neutrinos", Phys. Rev. Lett. **81** 1562 (1998).

[2] Y. Fukuda *et al.* [Super-Kamiokande Collaboration], Phys. Rev. Lett. **81**, 1562 (1998) [hep-ex/9807003].

[3] P. Adamson *et al.* [MINOS Collaboration], Phys. Rev. Lett. **112**, 191801 (2014) [arXiv:1403.0867 [hep-ex]].

[4] K. Abe *et al.* [T2K Collaboration], Phys. Rev. Lett. **112**, 181801 (2014) [arXiv:1403.1532 [hep-ex]].

[5] K. Abe *et al.* [T2K Collaboration], Phys. Rev. Lett. **112**, 061802 (2014) [arXiv:1311.4750 [hep-ex]].

[6] A. Aguilar-Arevalo et al. (LSND Collaboration), Phys.Rev. **D64**, 112007 (2001), arXiv:hep-ex/0104049 [hep-ex].

[7] A. Aguilar-Arevalo et al. (MiniBooNE Collaboration), Phys.Rev.Lett. **110**, 161801 (2013).

[8] P. Huber, Phys.Rev. **C84**, 024617 (2011), arXiv:1106.0687 [hep-ph].

[9] J. Kopp, P. A. N. Machado, M. Maltoni, and T. Schwetz, JHEP **1305**, 050 (2013).

[10] V. A. Kostelecky, N. Russell and R. Tso, Phys. Lett. B **716**, 470 (2012) [arXiv:1209.0750 [hep-th]].

[11] R. Abbasi *et al.* [IceCube Collaboration], arXiv:1210.3557 [hep-ex].

[12] V. A. Kostelecky, Phys. Rev. D **69**, 105009 (2004) [hep-th/0312310].

[13] D. Cokinos and E. Melkonian, Phys. Rev. C **15**, 1636 (1977).


### *Solar Neutrinos*

Solar neutrino flux measurements from Super-Kamiokande (SK) [1] and the Sudbury Neutrino Observatory(SNO) [2] have provided direct evidence for solar neutrino flavour conversion. However, there is still no clear evidence that this solar neutrino flavour conversion is indeed due to neutrino oscillations and not caused by any other mechanism. Currently there are two testable signatures unique to neutrino oscillations. The first is the observation and precision test of the MSW resonance curve [3]. Based on oscillation parameters extracted from solar neutrino and reactor anti-neutrino measurements, there is an expected characteristic energy dependence of the flavour conversion. The higher energy solar neutrinos (higher energy $^8$B and hep neutrinos) undergo complete resonant conversion within the sun, while the flavour changes of the lower energy solar neutrinos (pp, $^7$Be, pep, CNO and lower energy $^8$B neutrinos) arise only from vacuum oscillations, which limits the average electron flavour survival probability to exceed 50%. The transition from the matter dominated oscillations within the sun, to the vacuum dominated oscillations, should occur near 3 MeV, making $^8$B neutrinos the best choice when looking for a transition point within the energy spectrum. A second signature unique to oscillations arises from the effect of the terrestrial matter density on solar neutrino oscillations. This effect is tested directly by comparing solar neutrinos which pass through the Earth at nighttime to those which do not during the daytime. Those neutrinos which pass through the Earth will in general have an enhanced electron neutrino content compared to those which do not, leading to an increase in the nighttime electron elastic scattering rate (or any charged-current interaction rate), and hence a negative "day/night asymmetry". SK detects $^8$B solar neutrinos over a wide energy range in real time, making it a prime detector to search for both solar neutrino oscillation signatures.

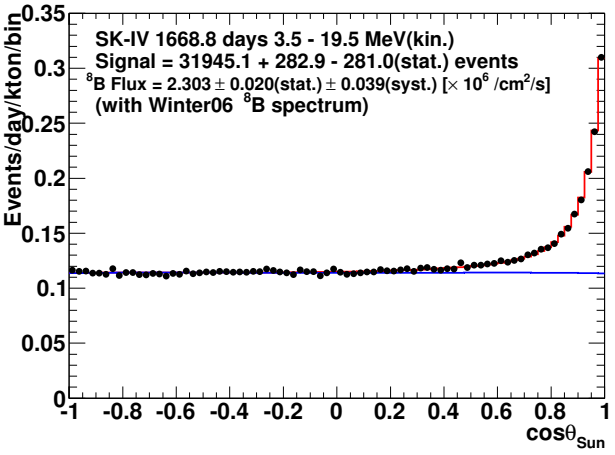


Fig. 10. Solar angle distribution for 3.5-19.5 MeV. $\theta_{\rm sun}$ is the angle between the incoming neutrino direction and the reconstructed recoil electron direction. Black points are data while the blue and red histograms are best fits to the background and signal plus background, respectively.

The start of physics data taking of SK-IV occurred on October 6th, 2008, with this report including data taken until January 31st, 2014. The total livetime is 1668.8 days. The entire data period was taken using the same low energy threshold, with about 85% triggering efficiency at 3.5-4.0 MeV kinetic energy, 99% at 4.0-4.5 MeV kinetic energy and 100% above 4.5 MeV kinetic energy. In the case of $\nu$-e interactions of solar neutrinos in SK, the incident neutrino and recoil electron directions are highly correlated. Fig.10 shows the $\cos\theta_{\rm sun}$ distribution for events between 3.5-19.5 MeV. In order to obtain the number of solar neutrino interactions, an extended maximum likelihood fit is used. This method is also used in the SK-I [1], II [4], and III [5] analyses. The red line of Fig.10 is the best fit to the data. The blue line shows the background component of that best fit.

The combined systematic uncertainty of the total flux in SK-IV is found to be 1.7% as the quadratic sum of all components. This is the best value seen throughout all phases of

SK, much improved over 2.2% in SK-III. The main contributions to the reduction come from improvements in the uncertainties arising from the energy-correlated uncertainties (energy scale and resolution), the vertex shift, trigger efficiency and the angular resolution. SK-III data below 6.0 MeV recoil electron kinetic energy has only about half the livetime as the data above, while SK-IV's livetime is the same for all energy bins. As a consequence, the energy scale and resolution uncertainties lead to a smaller systematic uncertainty of the flux in SK-IV than in SK-III. The higher efficiency of SK-IV between 5.0 and 6.0 MeV (kinetic) of SK-IV and the addition of the 3.5 to 4.5 MeV data lessens the impact of energy scale and resolution uncertainty on the flux determination even further. The number of solar neutrino events (between 3.5 and 19.5 MeV) is $31,945^{+283}_{-281}(\text{stat.}) \pm 543(\text{syst.})$. This number corresponds to a $^8$B solar neutrino flux of $\Phi_{^8B} = (2.303 \pm 0.020(\text{stat.}) \pm 0.039(\text{syst.})) \times 10^6/(\text{cm}^2\text{sec})$, assuming a pure $\nu_e$ flavor content.

Fig.11 shows the resulting SK-IV energy spectrum. SK-IV has $N_{\text{bin}} = 23$ energy bins; 20 bins of 0.5 MeV width between 3.5-13.5 MeV, two energy bins of 1 MeV between 13.5 and 15.5 MeV, and one bin between 15.5 and 19.5 MeV.

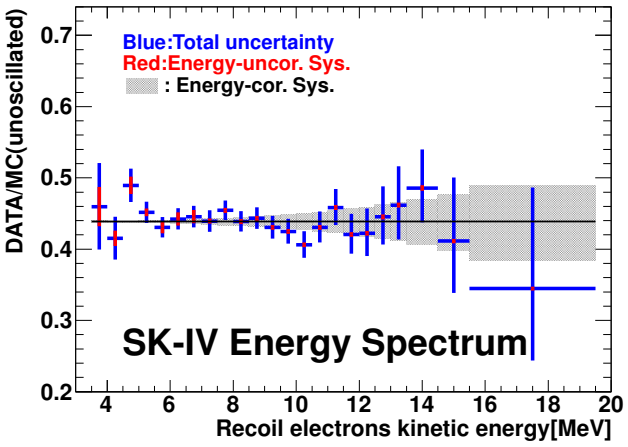


Fig. 11. SK-IV energy spectrum. The horizontal dashed line gives the SK-IV average. Error bars shown are statistical plus energy-uncorrelated systematic uncertainties. Energy-correlated systematic uncertainties are shown separately as shaded region.

To test the expected "upturn" below ~6 MeV from the MSW resonance effects, the best fit oscillation parameters of solar experiments and solar + KamLAND (described later) were fitted to all the SK-I to SK-IV spectra, and it is disfavored by $1\sigma$ and $1.7\sigma$ respectively so far. Fitted results are shown in Fig.12.

The SK-IV livetime during the day (night) is 799.7 days (869.1 days). The solar neutrino flux between 4.5 and 19.5 MeV and assuming no oscillations is measured as $\Phi_D = (2.25 \pm 0.03(\text{stat.}) \pm 0.38(\text{sys.})) \times 10^6/(\text{cm}^2\text{sec})$ during the day and $\Phi_N = (2.36 \pm 0.03(\text{stat.}) \pm 0.40(\text{sys.})) \times 10^6/(\text{cm}^2\text{sec})$ during the night. A more sophisticated method to test the day/night effect is given in [1, 6]. For a given set of oscillation parameters, the interaction rate as a function of the solar zenith angle is predicted. Only the shape of the calculated solar zenith angle variation is used, the amplitude of it is scaled by an arbitrary parameter. The extended maximum likelihood fit to extract the solar neutrino signal is expanded to allow time-varying signals. The likelihood is then evaluated as a function of the average signal rates, the background rates and the scaling parameter which is called the "day/night amplitude". The equivalent day/night asymmetry is calculated by multiplying the fit scaling parameter with the expected day/night asymmetry. In this manner the day/night asymmetry is measured more precisely statistically. Because the amplitude fit depends on the assumed shape of the day/night variation, it necessarily depends on the oscillation parameters, although with very little dependence expected on the mixing angles (in or near the large mixing angle solutions and for $\theta_{13}$ values consistent with reactor neutrino measurements [7]).

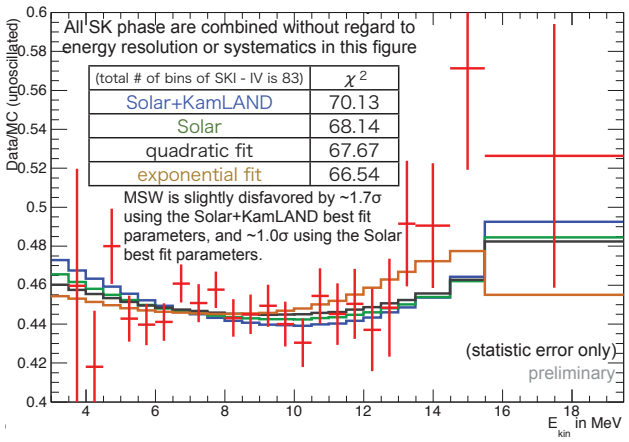


Fig. 12. All SK phase combined energy spectrum and fitted functions.

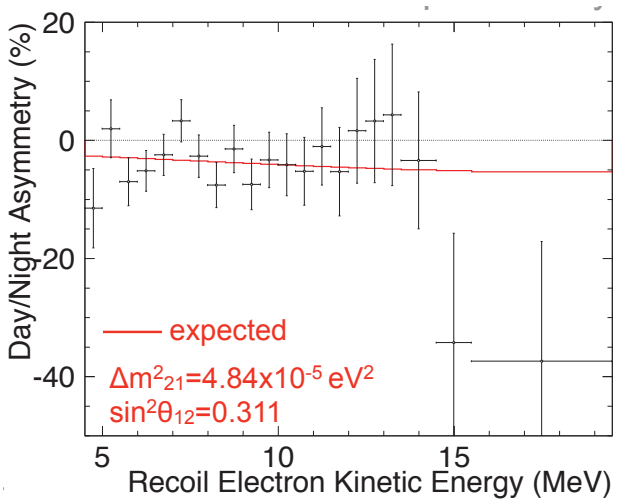


Fig. 13. SK combined energy dependence of the fitted day/night asymmetry (measured day/night amplitude times the expected asymmetry (red)) for $\Delta m^2_{21} = 4.84 \times 10^{-5}\text{eV}^2$, $\sin^2\theta_{12} = 0.311$ and $\sin^2\theta_{13} = 0.025$. The error bars shown are statistical uncertainties only.

The day/night asymmetry coming from the SK-I to IV combined amplitude fit can be seen as a function of recoil electron kinetic energy in Fig.13, for $\Delta m^2_{21} = 4.84 \times 10^5\text{eV}^2$, $\sin^2\theta_{12} = 0.311$ and $\sin^2\theta_{13} = 0.025$. The day/night asymmetry in this figure is found by multiplying the fitted day/night

amplitude from each energy bin, to the expected day/night asymmetry (red distribution) from the corresponding bin.

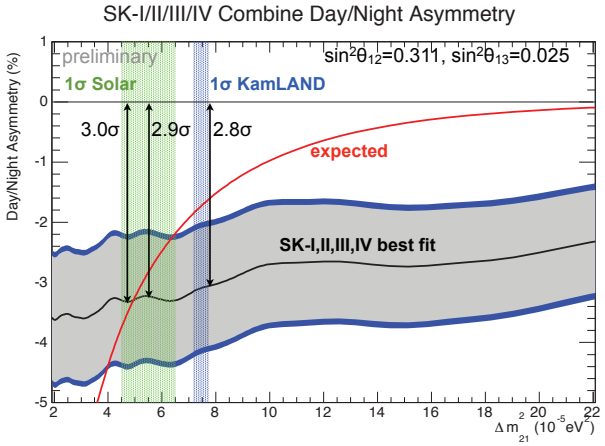


Fig. 14. Dependence of the measured day/night asymmetry (fitted day/night amplitude times the expected day/night asymmetry (red)) on $\Delta m^2_{21}$ (light gray band=stat. error, dark gray band=stat.+syst. error) for $\sin^2\theta_{12} = 0.311$ and $\sin^2\theta_{13} = 0.025$. Overlaid are the allowed ranges from solar neutrino data (green band) and KamLAND (blue band).

Fig.14 shows the $\Delta m^2_{21}$ dependence of the SK all phases combined day/night asymmetry for $\sin^2\theta_{12} = 0.311$ and $\sin^2\theta_{13} = 0.025$. Here the day/night asymmetry is also found by multiplying the fitted day/night amplitude by the expected day/night asymmetry (red curve). The point where the best fit crosses the expected curve represents the value of $\Delta m^2_{21}$ where the measured day/night asymmetry is equal to the expectation. Superimposed are the allowed ranges in $\Delta m^2_{21}$ from the global solar neutrino data fit (green) and from KamLAND (blue). The amplitude fit shows no dependence on the values of $\theta_{12}$ (within the LMA region of the MSW plane) or $\theta_{13}$.

We analyzed the SK-IV elastic scattering rate, the recoil electron spectral shape and the day/night variation to constrain the solar neutrino oscillation parameters. We then combined the SK-IV constraints with those of previous SK phases, as well as other solar neutrino experiments. The allowed contours of all solar neutrino data (as well as KamLAND's constraints) are shown in Fig.15 and 16. In Fig.15 the contours from the fit to all solar neutrino data are almost identical to the ones of the SK+SNO combined fit. In the right panel some tension between the solar neutrino and reactor anti-neutrino measurements of the solar $\Delta m^2_{21}$ is evident. This tension is mostly due to the SK day/night measurement. Even though the expected amplitude agrees well within $1\sigma$ with the fitted amplitude for any $\Delta m^2_{21}$ in either the KamLAND or the SK range, the SK data somewhat favor the shape of the variation predicted by values of $\Delta m^2_{21}$ that are smaller than KamLAND's. The best fit values are $\sin^2\theta_{12} = 0.308 \pm 0.013$, $\Delta m^2_{21} = 7.50^{+0.19}_{-0.18} \times 10^{-5}\mathrm{eV}^2$, and $\sin^2\theta_{13} = 0.027^{+0.016}_{-0.014}$. The significance of non-zero $\theta_{13}$ is about $2\sigma$.

In summary, the analysis threshold was successfully lowered to 3.5 MeV kinetic recoil electron energy in SK-IV and by adding SK-IV data, ~70,000 solar neutrino interactions has been observed in ~4,500 days, by far the largest sample of solar neutrino events in the world. SK spectrum results

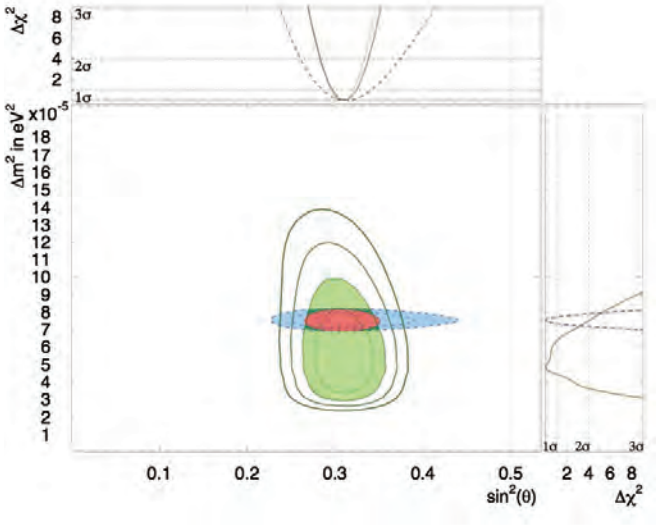


Fig. 15. Allowed contours of $\Delta m^2_{21}$ vs. $\sin^2\theta_{12}$ from solar neutrino data (green) at 1, 2, 3, 4 and 5 $\sigma$ and Kam-LAND data (blue) at the 1, 2 and 3 $\sigma$ confidence levels. Also shown are the combined results in red. For comparison, the almost identical results of the SK+SNO combined fit are shown by the dashed dotted lines. $\theta_{13}$ is constrained by $\sin^2\theta_{13} = 0.0242 \pm 0.0026$.

slightly disfavor the MSW resonance curves, but are consistent with MSW prediction within $1 \sim 1.7\sigma$. SK data provide the first indication (at $2.8 \sim 3.0\sigma$) of terrestrial matter effects on $^8$B solar neutrino oscillation. This is the first observation using a single detector and identical neutrino beams that matter affects neutrino oscillations [8]. These SK measurements strongly constrain neutrino oscillation parameters: SK uniquely selects the Large Mixing Angle MSW region by $> 3\sigma$, gives world's best constraint on $\Delta m^2_{21}$ using neutrinos, and significantly contributes to the measurement of $\theta_{12}$.

## Bibliography


[1] J.Hosaka et al., Phys. Rev. D73, 112001 (2006).

[2] Q.R.Ahmad et al., Phys. Rev. Lett. 87 071301 (2001).

[3] S.P.Mikheyev and A.Y.Smirnov, Sov. Jour. Nucl. Phys. 42, 913 (1985); L.Wolfenstein, Phys. Rev. D17, 2369 (1978).

[4] J.P.Cravens et al., Phys. Rev. D 78, 032002(2008).

[5] K.Abe et al., Phys. Rev. D 83 052010 (2011).

[6] M.B.Smy et al., Phys. Rev. D. 69, 011104(R) (2004).

[7] F.P.An et al., arXiv:1210.6327 (2012); J.K.Ahn et al., Phys.Rev.Lett. 108 191802 (2012); Y.Abe et al.,Phys.Rev. D86 052008 (2012).

[8] A.Renshaw et al., Phys. Rev. Lett. 112, 091805 (2014).

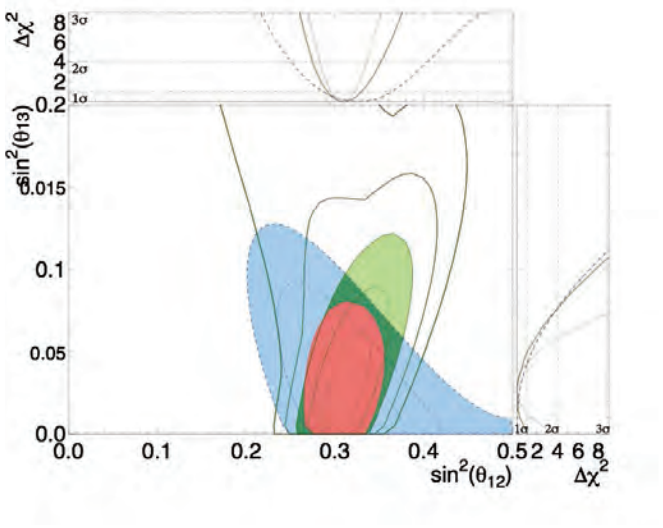


Fig. 16. Allowed contours of $\sin^2\theta_{13}$ vs. $\sin^2\theta_{12}$ from solar neutrino data (green) at 1, 2, 3, 4 and 5 $\sigma$ and KamLAND measurements (blue) at the 1, 2 and 3 $\sigma$ confidence levels. Also shown are the combined results in red.

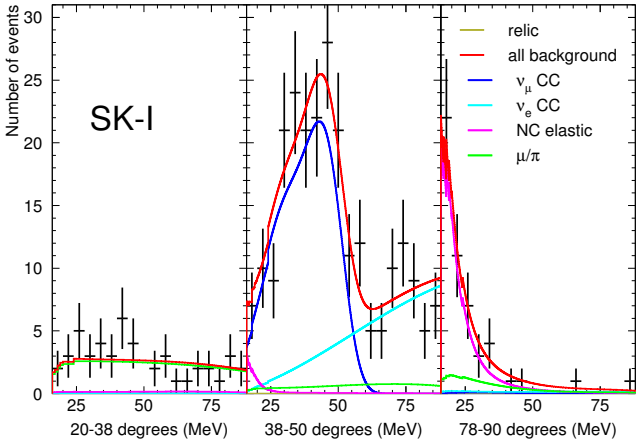


Fig. 17. SK-I best fit result, assuming Ando et al's LMA model. The relic best fit is negative, so a relic fit of 0 is shown. SK-II and SK-III have small but positive relic best fits.

### *Supernova neutrinos*

In 1987, the observation of supernova 1987a by Kamiokande and IMB etc. opend the neutrino astronomy. This observation confirmed that the energy released by neutrinos is about several$\times 10^{53}$ergs. However, the core collaple supernova mechanism is not fully understood yet. Super-Kamiokande would be able to detect several thousand neutrino events if a supernova happened near the centre of our galaxy. Such an observation would enable us to investigate in detail the mechanics of the supernova explosion.

A online program called SNWATCH searches for time clustered events. The current criteria of SNWATCH are (1) more than or equal to 7 events within 0.5 sec, (2) more than or equal to 8 events within 2 sec, and (3) more than or equal to 13 events within 10 sec. When at least one of these criteria are met, SNWATCH reconstructs vertex position and energy of the events together with neighbouring cosmic ray muons. In most cases, these clusters are due to spallation products whose vertex positions are aligned with their parent cosmic ray muon. Since all the SNWATCH processes are now running on online machines, if a supernova happens, we will be able to detect it within about one minute.

If SNWATCH finds an event cluster whose vertex spread is larger than a given criterion, an alarm signal is sent to experts by e-mail and an automatic call to their cellphones. Then, the experts check whether it is a real supernova signal or not by looking at various plots which are uploaded to a secured site accessible from the Internet. These alarms are usually due to the accidental coincidence of two cosmic ray induced clusters. We have a supernova drill at least once per year. So far, no real supernova neutrino burst signal has been observed at Super-Kamiokande.

In the drill, the SNWATCH conveners and the executive committee members meet via TV conference system, and discuss to make a decision for a prompt announcement to outside researchers and the press. We practice this drill as if a real supernova happened. We also have SK shift training by illuminating an LED in the SK detector a few times every month. SK shift members are notified by a dummy alarm that SNWATCH makes when the LED is illuminated. The shift members then call to the SNWATCH experts and give a report. The SK collaborators will be ready for the real supernovae through the drill and the training.

Not only the supernova burst, signals from Supernova Relic Neutrinos (SRNs) are also searched at SK. The SRN signal is the diffuse supernova neutrino background from all the supernovae in the past. This signal has never been detected, but it is expected to be detectable in the 16-30 MeV energy region, which is the gap between the energy ranges of solar neutrinos and atmospheric neutrinos. Our published result utilizes SK-I, II and SK-III data with analysis energy threshold 16MeV. A maximum likelihood search was performed in multiple regions of the Cherenkov angle distribution to extract the most accurate flux limit(Fig.17). The obtained flux limit is between 2.7 and 3.0 $\bar{\nu}cm^{-2}s^{-1}$ (positron energy $>$ 16 MeV), which actually depends on the shape of the neutrino spectrum assumed. This result currently provides the world's best limit on SRN flux. Furthermore, a new method of presenting the SRN flux limit is also ready which is of great use to theorists and does no depend on any particular model (Fig.18).

### *R&D for the gadolinium project*

As mentioned above, although at SK a few SRN events a year are expected, SRNs have not been detected yet because the large backgrounds constrain our search. The main goal of our research is to reduce these backgrounds and be able to detect SRNs. The observation of SRNs in general or neutrinos from distant supernovae in particular, would give us some information about the universe, for example the core collapse

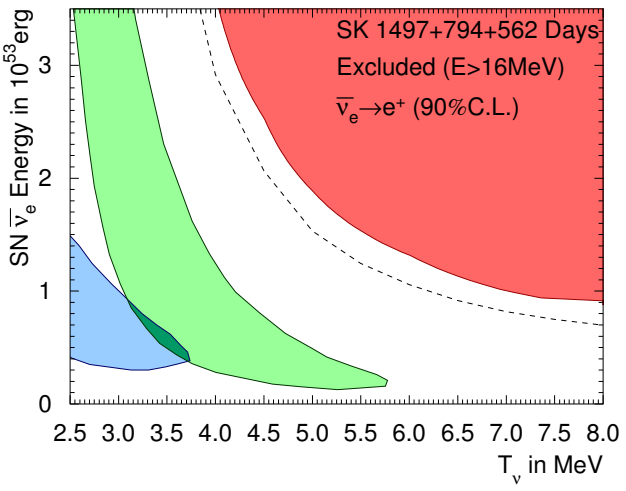


Fig. 18. Results plotted as an exclusion contour in SN neutrino luminosity vs. neutrino temperature parameter space. The green and blue contours show IMB and Kamiokande allowed areas for 1987a data, respectively. The red shows our new 90% c.l. result. The dashed line shows the individual 90% c.l. results of each temperature considered separately, which is not a true 2-D exclusion contour.


Fig. 19. In the new cavern the Gd pre-mixing and pre-treatment 15 ton tank (front left), the selective filtration system (front right) and the 200 ton tank (rear of the hall) have been installed.

rate from SRNs, and about the neutrino itself too, for example its lifetime. Since most of the neutrinos that can be detected at SK undergo inverse beta decay, electron anti-neutrinos are the most copiously detected neutrinos:

$$\bar{\nu}_e + p \rightarrow e^+ + n \quad (1)$$

Presently, the SK detector can only detect the positrons efficiently but if we could detect the neutrons, we could greatly reduce the backgrounds that constrain our SRN search. This could be attained by the coincidence detection of positron and neutron (in space, vertices within tens of cm and in time, with the neutron capture delayed about 20 $\mu$sec). By adding 0.2% of gadolinium (Gd) sulfate into the water tank we could achieve this goal. Gadolinium has a neutron capture cross section of 49.000 barns (about 5 orders of magnitude larger than of protons) and emits a gamma cascade of 8 MeV that can be easily detected at SK.

We want to show that adding Gd into the SK water, SK will become an electron anti-neutrino detector, able to tag inverse beta decays, while keeping all its previous capabilities in the other analyses like solar and atmospheric neutrinos.

The EGADS (Evaluation Gadolinium's Action on Detector Systems) project was funded in 2009. Since then, a new hall near the SK detector has been excavated and a 200 ton tank with its ancillary equipment has been installed, see Fig.19, to mimic the conditions at SK. Of special importance is the selective water filtration system, that filters out water impurities while it keeps the Gd in the water.

From January 2010 to July 2011 we circulated pure water through the 200 ton tank and proved that our water system is stable and achieves a high water quality. In 2013, from February 6th to April 20th, the 200 ton tank has been stepwise loaded with Gd until the final 0.2% concentration was reached. By measuring Gd concentration at some detector positions, we confirmed that the Gd sulfate dissolves homogeneously in the 200 ton tank, and we can achieve and maintain a good water quality.

In summer 2013, we installed 240 photomultipliers and the data taking has started from September without Gd. After the water quality became good and stable, detector caibrations were performed. At the end of March, few batches of Gd were dissolved into water corresponding 115 ppm Gd concentration. Soon after that, the first signal from Gd neutron capture was detected with a Am/Be (gamma and neutron source) installed at the detector center. Figure 20 (left) shows the time difference between the prompt gamma event and the delayed neutron capture event. The time constant is obtained as 123 $\mu$sec which is in good agreement with our expectation (120.8 $\mu$sec). Am/Be data were also taken with 230 ppm Gd concentration, and it was confirmed that the time difference became shorter due to a higher neutron capture rate by Gd (Figure 20). Next year, we will make a final configuration with 0.2% Gd concentration and provide detailed information, such as the water transparency and its uniformity, PMT signal stability, Rayleigh scattering measurement using EGADS detector, and the neutron capture rate. Aftre all these evaluations finished, EGADS will become a detector with instant supernova detection capabilities.

## XMASS EXPERIMENT

[Spokesperson : Yoichiro Suzuki]
Kavli IPMU, University of Tokyo

### *XMASS experiment*

XMASS is a multi-purpose experiment (detection of dark matter, neutrino-less double beta decay, and $^7$Be/pp solar neutrinos) using ultra-pure liquid xenon [1]. The first stage of XMASS experiment (XMASS-I) is to look for dark matter using 800 kg liquid xenon (100 kg fiducial mass).

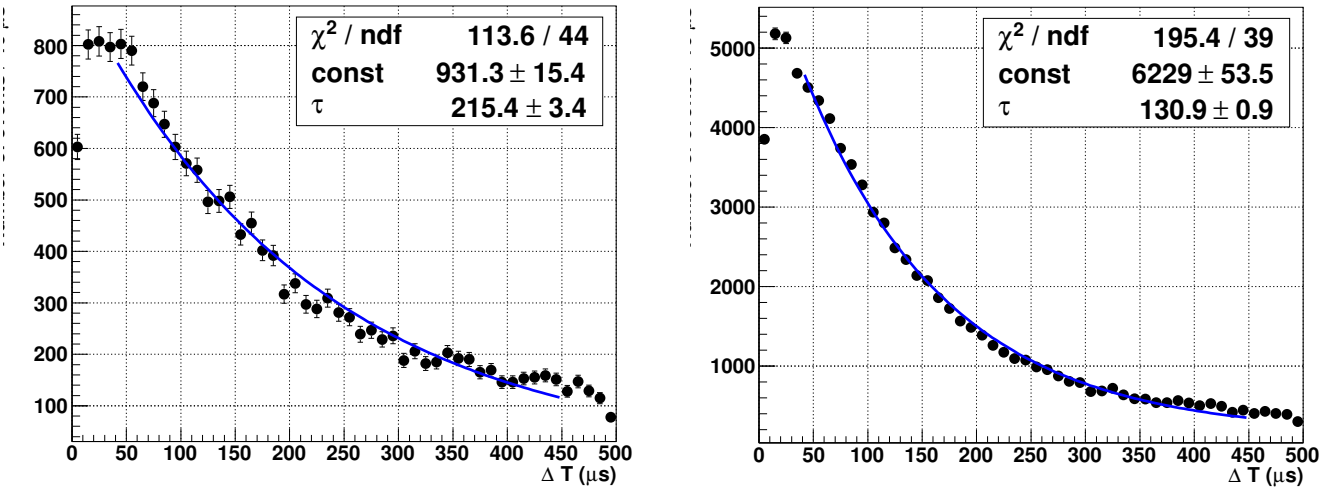


Fig. 20. Time difference between a prompt event and a delayed event obtained in Am/Be calibration in 115 ppm (left) and 230 ppm (right) Gd concentration. Back shows data and blue line shows fitted line.

The existence of dark matter is recognized through gravitational effects in astronomical observations. It is indicated that the universe contains a large amount of nonbaryonic dark matter. One of the most plausible candidates for the nonbaryonic dark matter is a weakly interacting massive particle (WIMP) conceived by the supersymmetry in the form of a lightest supersymmetric particle. WIMPs can be directly detected through their elastic scattering off target nuclei in a detector. The XMASS-I searches for the WIMP-xenon nucleus interaction in liquid xenon.

Two phase liquid xenon detectors achieve low background by removing electron and gamma ray events, but XMASS aims at realizing low background even with electron and gamma ray events. This introduces a unique advantage in a search for dark matter particles through electromagnetic interactions as well. This is particularly important since no indications of supersymmetric particles have obtained so far even from the large hadron collider. Dark matter particles other than WIMPs are also quite interesting. In parallel to the search for WIMP-xenon nucleus interactions, ability to detect e/gamma events enables us to search for broad range of dark matter particles. For example, axion-like particles, bosonic super-WIMPs, inelastic scattering by WIMPs can be searched for with our unique detector.

As the first stage of the XMASS experiment, the XMASS-I detector was constructed. In the following sections, we describe:

- Construction and commissioning data taking. After the construction of the detector, we took data to understand the performance of the XMASS-I detector. By introducing radioactive sources, number of photoelectrons per keV was measured. Vertex reconstruction algorithm was confirmed to work properly. Origins of background were also investigated and found one of the parts used in photomultipliers contained natural radioactivity more than expected.
- Physics analysis using commissioning data. We have achieved the lowest energy threshold, and the largest target mass. The level of background without rejection of e/gamma events are modest. Therefore the data from the world largest detector, XMASS-I, is valuable to search for low-mass WIMPs, solar axions, inelastic scattering by WIMPs, and bosonic super-WIMPs. We have conducted these searches.
- Refurbishment. Based on the investigation with commissioning data, we devised a plan to reduce background. Covering the contaminated parts by copper covers and plates, we could reduce background more than one order of magnitude. This strengthen our understanding of background and reinforces the future design of XMASS detectors.

We succeeded the background reduction of the XMASS-I detector. However, in order to get into the new regime, we need more sensitive detectors. We are designing XMASS-1.5 detector as described in following section.

### *XMASS-I detector*

The construction of the XMASS-I detector was started in April 2007 and was completed in September 2010. The XMASS-I detector uses a cylindrical water tank with 72 50 cm PMTs and spherical liquid xenon detector with 642 2 inch PMTs is placed at the center of the water tank as shown in Fig. 21. This is the first case to adopt a pure-water tank as an active and passive shield for dark matter experiments. The spherical array of PMTs is arranged in a double wall vessel. The vessel consisting of inner and outer vacuum chamber (IVC and OVC) is made from oxygen free high conductivity copper. The layer between IVC and OVC is kept vacuum for thermal isolation.

After the construction, commissioning data was taken from October 2010 to May 2012. Based on calibration data, we found that the detector has the largest photoelectron yield (≈14

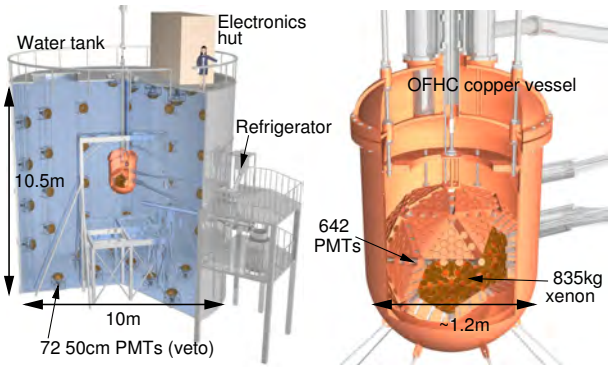


Fig. 21. Schematic view of the water tank and the liquid xenon vessel.

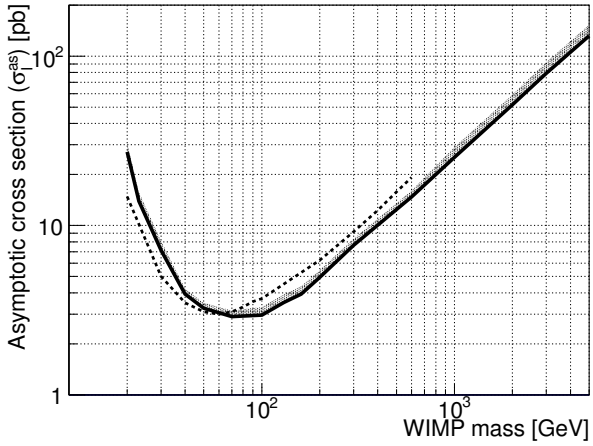


Fig. 22. The black solid line is our 90% C.L. upper limit on the asymptotic cross section $\sigma_l^{as}$ for inelastic scattering on $^{129}$Xe (black solid line) using the same form factors as DAMA. The gray band covers its variation with our systematic uncertainty. The dotted line is the limit obtained by the DAMA group that was derived after statistically subtracting background. Our low background allows us to derive this limit without such background subtraction. Observed energy spectrum and predictions for various mass of dark matter.

photoelectrons/keV). This enables us to realize low-energy threshold which is important for dark matter search. We also conducted various performance tests on XMASS-I, such as reconstruction by scintillation patterns. The details of these are described in Ref. [2].

### *Results using commissioning data*

We analyzed the commissioning data to search for low-mass dark matter and solar axions [3, 4]. In our recent analysis, we have achieved an unprecedented low-background level of $3\times10^{-4}\,\mathrm{kg^{-1}keV^{-1}kg^{-1}}$ in the energy range around a few 10's of keV close to our ultimate goal at 5 keV. This background level was one order of magnitude lower than XENON100 and LUX before their $e/\gamma$ rejection. This results demonstrated the unique feature mentioned above.

- *A search for inelastic scattering of WIMPs on the isotope $^{129}$Xe [5].* WIMPs are expected to cause inelastic scattering on nucleus $^{129}$Xe has an excited state at 39.58 keV that can be excited through spin-dependent

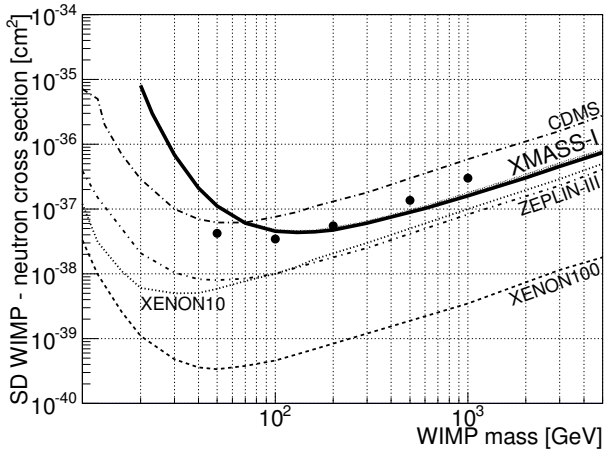


Fig. 23. The thick line and dots represent our limit on the spin-dependent cross section of WIMPs on neutron using two different recent calculations of form factors. The gray shaded part of the thick line shows systematic uncertainty. The dashed, dotted, dash-dotted, and long dash-dotted lines represent experimental constraints on spin dependent WIMP nucleon cross sections extracted from elastic scattering data. Our own limit is the first derived exclusively from data on inelastic scattering.

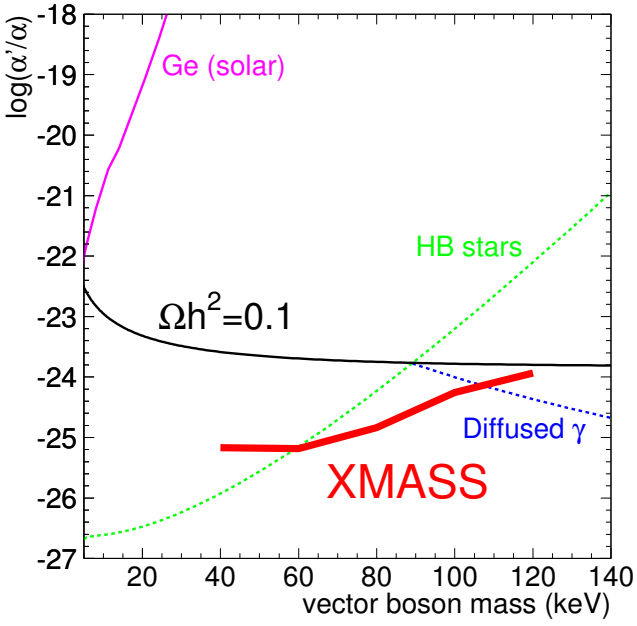


Fig. 24. Our first experimental limit on coupling constants between electrons and vector bosons in 90% C.L. (thick solid line) assuming dark matter consists of the vector bosons. The thin black line corresponds to the coupling constant required to reproduce the observed dark matter abundance through thermal production mechanism. The green and blue dotted lines correspond to the upper limit from He-burning lifetime in horizontal branch (HB) stars and from the $\gamma$ ray background from $3\gamma$ decays in the Galaxy, respectively. The purple line shows an experimental constraint derived in a search for particles produced in the Sun. See text for details.

coupling. A peak at 39.58 keV with a high-energy tail is expected since the scintillation lights from gamma rays emitted after the excitation [1] and from the additional nuclear recoil cannot be separated. Using a restricted target mass (∼41 kg of LXe at the center of our detector) we observed no significant excess of events in 165.9 live days of data. Our background reduction allowed us to derive our limits as shown in Fig. 22 for the WIMP-nucleus cross section and Fig. 23 for the spin-dependent cross section on neutron [2]. These limits have been the first derived exclusively from data on inelastic scattering.

- *A search for vector boson super-WIMPs [6].* We have searched for superweakly interacting particles (super-WIMPs), with 40-120 keV mass. These particles are motivated since they soften some problems in the cold dark matter models [3]. In particular, the vector super-WIMPs in this mass range are not experimentally constrained and are a good candidate for thermally generated dark matter in the Universe. Interestingly, the bosonic nature of the particles means that they cause a monochromatic peak at the rest mass when they are absorbed in the target. In the 165.9 days data no signal was observed and stringent limits on the electron coupling with a mass in the 40-120 keV range were obtained. For vector bosons in some of this mass range our direct detection limit (Fig. 24) surpasses existing astrophysical constraints, covering new territory.

### *Refurbishment of XMASS-I*

In the commissioning data we found that majority of the background was from the radioactive contamination in the aluminum seal of PMT windows. Some radioactive contamination on the inner wall of the detector was also identified. Since the understanding of the origins of background is essentially important for future design of the detector, we decided to refurbish the detector. By covering the aluminum using copper rings and copper plates, we can demonstrate the correctness of the understandings and reduce background of the XMASS-I detector. The actual modification of the detector are shown in Fig. 25. The copper rings and plates are expected to stop scintillation lights and radiations practically caused by the radioactive contamination.

The refurbishment was completed in November, 2013, and data taking was resumed. The comparison before and after the refurbishment is presented in Fig. 26. It is clearly seen that numbers of event in lower energy region (5-10 k$e$V) are reduced around one order of magnitude. Further analysis based on event reconstruction is expected to give better background reduction.

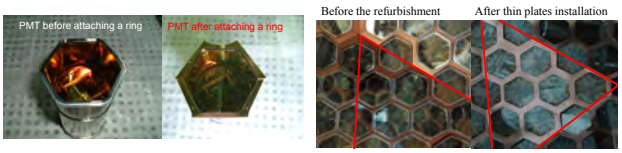


Fig. 25. Left two photographs show PMTs before and after installing a copper ring. Right two photographs show the inner wall of the detector before and after the refurbishment.

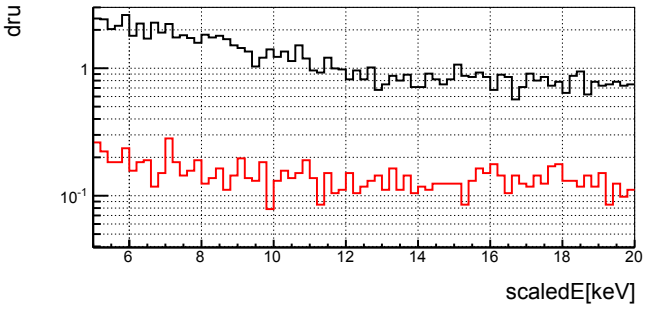


Fig. 26. Energy spectrum before the refurbishment(black) and after(red) is respectively plotted after a set of simple noise reduction is applied.

### *XMASS-1.5*

We are planning to build the next stage detector, XMASS-1.5, with 1 ton fiducial mass. Increasing the fiducial mass is indispensable to examine cross sections smaller than current constraints for standard WIMPs. The basic design of the detector is same as the one for the 100 kg fiducial mass detector but with an essential improvement of the discrimination between the surface background and the inner events. For that purpose, we are developing a new type of PMTs. They have convex-shape photocathodes which has advantage to detect direct light from the inner surface of the detector. As shown in Fig. 27 (left), the dome-shaped PMTs are more efficient for detecting scintillation photons originated at the inner surface of the detector than the flat-shaped PMTs used for the XMASS-I detector. In fact, our simulation shows that three PMTs surrounding the event vertices on the surface should detect 40%–50% of photoelectrons. This strongly indicates that reducing surface events is much easier and more reliable. With this improvement, we can search for heavy WIMPs with cross sections less than $10^{-46}$cm$^2$ even for the same background level of the XMASS-I. Figure 27 (right) shows the expected sensitivity of this detector.

It is noteworthy that the XMASS-1.5 has an unique feature that it has a very low energy threshold as well as high sensitivity for other types of dark matter. The low energy threshold is essentially important for a low mass WIMP search and achieved by the high light yield as confirmed in the XMASS-1 detector. The detector is sensitive to axion-like particles as well as bosonic super-WIMPs as discussed above because the detector is designed to realize low background even without $e/\gamma$ rejection. These unique features are particularly important to have a detector sensitive to broad range of dark matter candidates.

*1 P. Belli *et al.*. Phys. Lett. B **387**, 222 (1996); R. Bernabei *et al.*, New J. Phys. **2**, 15 (2000).

*2 L. Baudis *et al.*, Phys. Rev. D **88**, 115014 (2013); J. D. Vergados, H. Ejiri, and K. G. Savvidy, Nucl. Phys. B **877**, 36 (2013).

*3 M. Pospelov, A. Ritz, and M. Voloshin, Phys. Rev. D 78 (2008) 115012; J. Redondo, M. Postma, J. Cosm. Astropart. Phys., 02 (2009) 005; R. Horvat, D. Kekez, M. Krčmar, Z. Krečak, A. Ljubičić, Phys. Lett. B 721 (2013) 220.

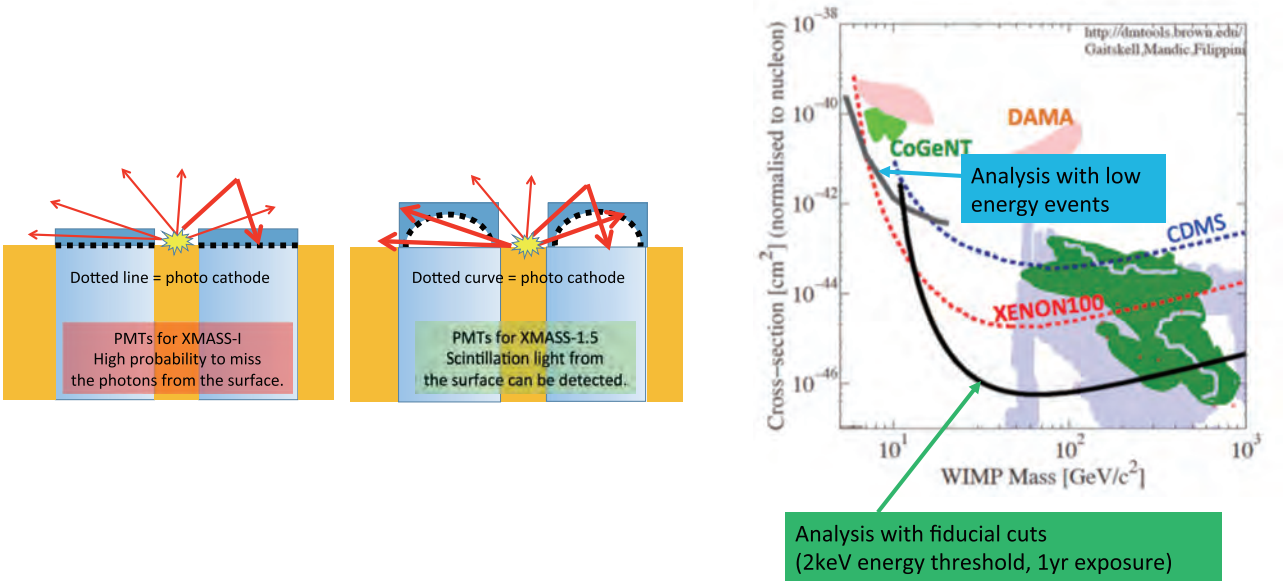


Fig. 27. (Left) Response to surface events of PMT with flat photocathode and a dome-shaped photocathode. Because the dome-shaped photocathode has a large acceptance for scintillation light from the inner surface of the detector, identification of surface events is much more efficient with the dome-shaped PMTs. (Right) Expected sensitivity with the XMASS-1.5 detector.

## Bibliography


[1] Y. Suzuki *et al.*, "Low energy solar neutrino detection by using liquid xenon", Aug. 2000, hep-ph/0008296.

[2] K. Abe *et al.*, Nucl. Instr. Meth. 716 (2013) 78

[3] K. Abe *et al.*, the XMASS collaboration, Phys. Lett. B 719 (2013) 78.

[4] K. Abe *et al.*, the XMASS collaboration, Phys. Lett. B 724 (2013) 46.

[5] H. Uchida *et al.*, the XMASS collaboration, Prog. Theor. Exp. Phys. 2014, 063C01.

[6] K. Abe *et al.*, the XMASS collaboration, arXiv: 1406.0502.


## HYPER-KAMIOKANDE PROJECT


[Project Leader: Masato Shiozawa]

Kamioka Observatory, ICRR, The University of Tokyo


The Hyper-Kamiokande is the third generation nucleon decay and neutrino detector at Kamioka, that aims to explore unification of elementary particles and full picture of neutrino masses and mixings [1, 2]. The schematic view of the Hyper-K detector is illustrated in Fig. 28 and 29.

A letter of intent [3] of the Hyper-Kamiokande project has been released, in which the baseline design of the detector and physics potential of Hyper-K are described. The water Cherenkov detector with the mass of 1 million tones has capability to search for the nucleon decays with sensitivity of

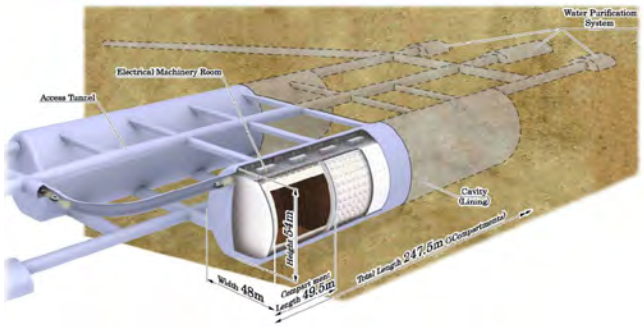


Fig. 28. Schematic view of the Hyper-Kamiokande. The detector consists of two cylindrical tanks holding $\sim$ 500 kton ultrapure water ($\sim$ 1 Mton in total). The each tank is divided by segmentation walls every 50 m.

10 times longer than the lifetime limits given by the Super-Kamiokande. For example, the sensitivity for the decay mode $p \to e^+\pi^0$ is expected to be beyond $1 \times 10^{35}$ years [3]. The detector also aims to study neutrino properties, such as Dirac $CP$ phase $\delta_{CP}$, mass hierarchy, octant of $\theta_{23}$, by using a high power accelerator based neutrino beam and atmospheric neutrinos. In particular, the neutrino oscillation physics sensitivities of Hyper-K with J-PARC neutrino beam and atmospheric neutrinos have been updated and compiled in a proposal, and that has been submitted to J-PARC Physics Advisory Committee in 2014. Fig. 30 shows the expected size of allowed regions for the parameter space of $\theta_{13}$ and $\delta_{CP}$ by using upgraded J-PARC neutrino beam with the power of 0.75 MW $\times$10 years and the Hyper-Kamiokande detector with the fiducial volume of 0.56 Megaton. Hyper-K has a good sensitivity in the whole relevant $\theta_{13}$ and $\delta_{CP}$ parameter space. The high statistics data sample of atmospheric neutrinos obtained by Hyper-K will also allow us to extract information on the mass hierarchy and the octant of $\theta_{23}$ (Fig. 31). With a full 10 year period of data taking, the significance for the mass hierarchy

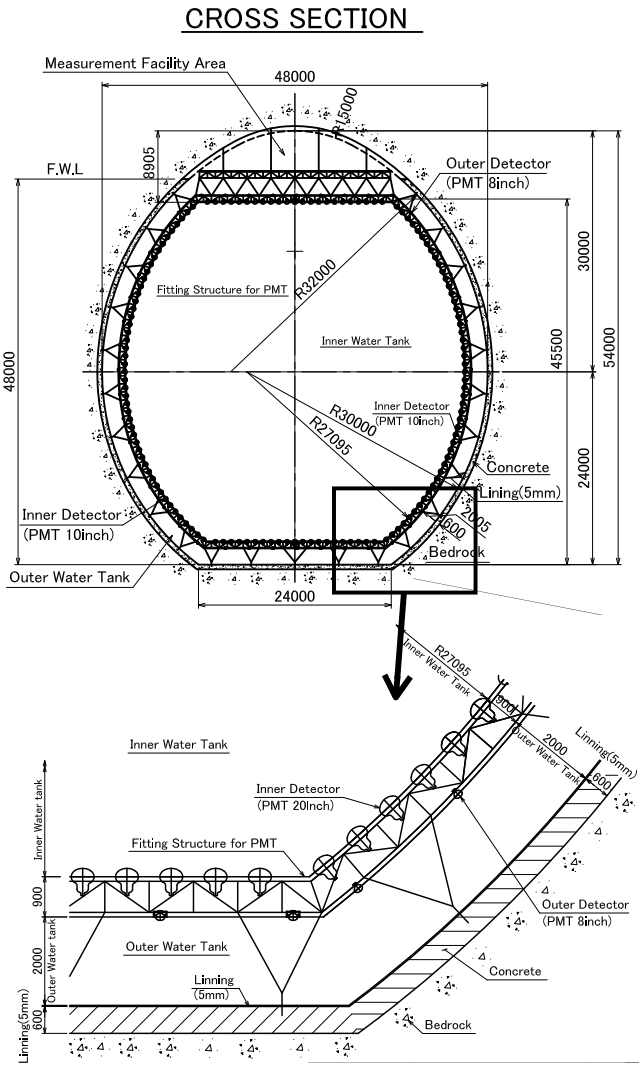


Fig. 29. The cross section of the Hyper-Kamiokande water tank.

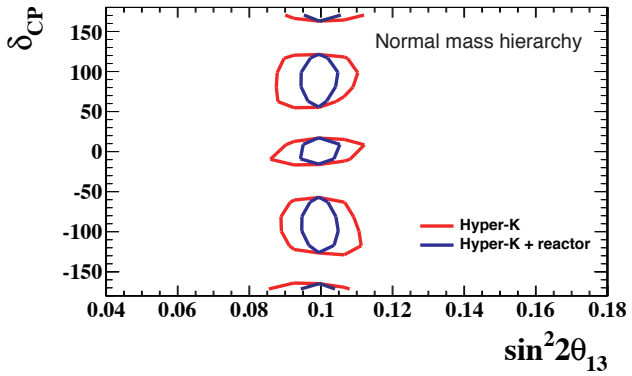


Fig. 30. Expected sensitivity for $\sin^2 2\theta_{13}$ and $CP$ phase $\delta_{CP}$ (normal mass hierarchy case). Red (blue) lines show the result with Hyper-K only (with $\sin^2 2\theta_{13}$ constraint from reactor experiments).

determination is expected to reach $3\sigma$ or greater as is shown in left panel of Fig. 31.

T2K has observed $\nu_\mu \to \nu_e$ oscillations (electron neutrino appearance) with more than $7\sigma$ significance [4]. The T2K result with the world average value of $\theta_{13}$ disfavored some values of $\delta_{CP}$ and showed a slight preference for $\delta_{CP} \sim -\pi/2$.

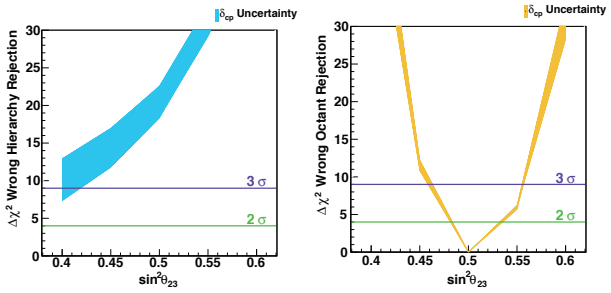


Fig. 31. Atmospheric neutrino sensitivities for a ten year exposure of Hyper-K assuming the mass hierarchy is normal. Left: the $\Delta\chi^2$ discrimination of the wrong hierarchy hypothesis as a function of the assumed true value of $\sin^2\theta_{23}$. Right: the discrimination between the wrong octant for each value of $\sin^2\theta_{23}$. The uncertainty from $\delta_{CP}$ is represented by the thickness of the band.

The results highly encourage and boost the activities toward realization of the future detector.

For Hyper-K R&D, design studies and constructing a detector prototype, five years Grant-in-Aid has been approved and started in 2013. Hyper-Kamiokande project has been selected as one of top 27 important large-scale projects in the "Master plan 2014" [5] of Science Council of Japan.

International Hyper-Kamiokande Working Group consists of about 240 people in 67 institutes from 12 countries. The working group intensively develop various aspects of Hyper-K project such as geological surveys at the detector candidate sites, design of cavern and tank, water purification and circulation system design, new photon-sensor and DAQ system, detector calibration system, analysis software, and physics sensitivities. A technical design report of Hyper-K cavern and tank constructions has been written up, and that will be released in near future. Although the detector baseline design and the physics sensitivities studies of Hyper-K assume to use Super-K style 20-inch PMTs, new photo-sensors that are potentially lower-cost and higher-sensitivity are pursued since the photo-sensor is a major cost driver in Hyper-Kamiokande project. Hyper-Kamiokande Working Group has been developing new photo-sensor candidates, hybrid photo-detector (HPD) and high quantum efficiency (HQE) PMT. Prototypes of these photo-sensors have been produced, and eight 8-inch HPDs and five HQE 20-inch PMTs were installed in a 200-ton water Cherenkov detector (EGADS detector, Fig. 32) to evaluate the basic performance and a long term stability of the photo-sensors. The testing with the 200-ton detector is well

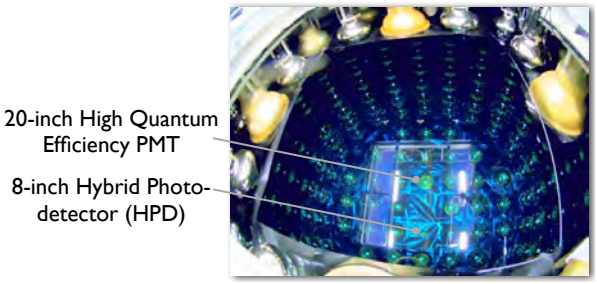


Fig. 32. Photo of 200-ton water Cherenkov detector in which new photo-sensor prototypes have been installed and filled with ultrapure water.

progressing, and it is confirmed that new photo-sensors have better performances than Super-K style PMTs. Other types of photo-sensors, such as box and line dynode PMT, are also being developed. 20-inch prototypes for these photo-sensors will be available and their performances will be evaluated in 2014. Hyper-Kamiokande Working Group plans to publish a technical paper summarizing the results of new photo-sensor R&D. Several other R&D and studies are also making good progresses. Hyper-Kamiokande Working Group holds 'Open Meeting for Hyper-Kamiokande Project' once in about every six months to discuss the progresses of studies and various aspects of the project face to face.

## Bibliography


[1] M. Shiozawa, "The Hyper-Kamiokande project," Nucl. Phys. B (Proc. Suppl.) **237-238**, 289-294 (2013).

[2] M. Diwan, R. Edgecock, T. Hasegawa, T. Patzak, M. Shiozawa and J. Strait, "Future long-baseline neutrino facilities and detectors," Adv. High Energy Phys. **2013**, 460123 (2013).

[3] K. Abe, T. Abe, H. Aihara, Y. Fukuda, Y. Hayato, K. Huang, A. K. Ichikawa and M. Ikeda *et al.*, "Letter of Intent: The Hyper-Kamiokande Experiment — Detector Design and Physics Potential —," arXiv:1109.3262 [hep-ex].

[4] K. Abe *et al.* [T2K Collaboration], "Observation of Electron Neutrino Appearance in a Muon Neutrino Beam," Phys. Rev. Lett. **112**, 061802 (2014) [arXiv:1311.4750 [hep-ex]].

[5] "Master plan 2014" of Science Council of Japan http://www.scj.go.jp/ja/info/kohyo/pdf/kohyo-22-t188-1.pdf (in Japanese)


# T2K EXPERIMENT


[Spokesperson : Takashi Kobayashi]

High Energy Accelerator Research Organization (KEK)


The T2K (Tokai-to-Kamioka) experiment [1] is a 295 km long-baseline neutrino oscillation experiment, employing a high intensity muon neutrino beam sent from the Japan Proton Accelerator Research Complex (J-PARC) in Tokai to the Super-Kamiokande (SK) water Cherenkov detector in Kamioka. The primary goals of the experiment are to observe electron neutrino appearance in this muon neutrino beam and thereby measure the last unknown mixing angle, $\theta_{13}$, as well as to precisely determine the oscillation parameters, $\Delta m^2_{32}$ and $\theta_{23}$, by simultaneously observing muon neutrino disappearance.

The T2K beam is composed primarily of muon neutrinos, which are produced in the decays of charged pions and kaons created in the interactions of 30 GeV protons from the J-PARC accelerator striking a graphite target. An electron neutrino background, produced in the decays muons as well as these hadrons, represents less than 1% of the neutrino flux around the beam's peak energy. T2K is the first long-baseline experiment to adopt an off-axis beam [2]. The beam is directed 2.5° away from the direction to Super-K, which creates a narrow muon neutrino energy spectrum peaking around 0.6 GeV, the location of the first oscillation maximum for the T2K baseline.

Table 4. T2K data taking periods and integrated numbers of protons on target (POT) for SK (off-axis ND280) used in the neutrino oscillation analyses. References for T2K results from each data update are also listed.

| Period | Dates | $\times 10^{20}$ POT (ND) |
|---|---|---|
| Run 1 | Jan.2010 - Jun.2010 | 0.32 (0.17) |
| Run 2 | Nov.2010 - Mar.2011 | 1.11 (0.79) [5],[6] |
| Run 3 | Mar.2012 - Jun.2012 | 1.58 (1.56) [7],[8] |
| Run 4 | Oct.2012 - May.2013 | 3.56 (3.38) [9],[10] |

The near detector (ND) site located 280 m from the T2K target consists of two detector complexes one each on and off the beam axis. The on-axis interactive neutrino grid (INGRID [3]), composed of an array of iron scintillator sandwiches, monitors the neutrino beam intensity, direction and profile. The off-axis detector (ND280) is situated along the same direction to SK and measures the neutrino beam flux, composition and energy spectrum prior to neutrino oscillations. ND280 provides important information on the neutrino flux and interaction models, both of which are essential to T2K's oscillation measurements.

The far detector, SK [4], is a 50 kton water Cherenkov detector which uses timing information synchronized to the Global Positioning System (GPS) to records events coincident with the operation of the T2K beam. All data within $\pm 500\,\mu$s of the beam arrival time at SK are recorded for use in later analysis.

This report uses T2K neutrino data collected during the four run periods listed in Table 4 and corresponds to $6.57 \times 10^{20}$ protons on target (POT) in total. The proton beam reached an intensity of 220 kW during this period and produced $1.2 \times 10^{14}$ protons per pulse. The expected number of events at ND280 and SK is calculated using a flux, cross section and detector simulation assuming a certain oscillation parameter set. The systematic uncertainties in this prediction are largely reduced by measurements using the T2K near detectors, whose data constrain the neutrino flux and interaction model parameters used throughout the experiment.

The neutrino flux is calculated with a Monte Carlo (MC) simulation considering the T2K beamline and measurements of the primary proton beam profile, the magnetic fields produced by the focusing horns, and hadron production data from the NA61/SHINE measurements [11, 12]. Neutrino interactions are then simulated based on the flux predictions at both the ND280 and SK sites using the NEUT framework [13].

Parameters in the neutrino interaction model are constrained with three control samples from ND measurements [14]. Charged current (CC) samples were selected at the ND280 using tracking information from its FGD and TPC subdetectors and

further divided based on pion multiplicity into a (i) CC-0$\pi$ sample with no identified pions and therefore enriched in CCQE interactions, a (ii) CC-1$\pi^+$ sample with only one identified $\pi^+$ to constrain CC resonant pion production and a (iii) CC-other sample with all other CC events. Using $5.90\times10^{20}$ POT (c.f. Table 4) the observed event rates for these samples were 17369, 4047, and 4173 events, respectively.

Charged current quasi-elastic (CCQE) scattering at SK, $\nu_l + N \to l + N'$, is a dominant interaction in the T2K energy region, which produces a single charged lepton ($l$ = muon, or electron) from an initial nucleon, $N$, with a final state nucleon, $N'$. This processes appears as a single Cherenkov ring at SK and the parent neutrino energy can be inferred using this ring's reconstructed information. For this reason events with only one Cherenkov ring are selected at SK and the T2K analysis studies oscillations using in two independent data samples separated by particle identification: $\nu_\mu \to \nu_e$ with single-ring $e$-like events, and $\nu_\mu \to \nu_{(X\neq\mu)}$ with single-ring $\mu$-like events. Neutral current (NC) production of a single pion is a main background source in these single-ring events.

The value of $\theta_{13}$ has been evaluated using the observation of electron neutrino appearance at SK. The analysis sample is enriched in $\nu_e$ CCQE by selecting fully contained single-ring $e$-like events consistent with the T2K beam timing and located within the SK fiducial volume. Residual $\nu_\mu$ events generating decay-electrons which can mimic the CCQE signal and pion backgrounds from NC interactions are reduced by requiring that there are no delayed decayed electrons observed and that the reconstructed momentum of electron exceeds 100 MeV/$c$. Furthermore, requiring the reconstructed neutrino energy be less than 1250 MeV is used to elected to avoid a small amount of high-energy electron neutrinos intrinsic to the beam. A new SK event reconstruction algorithm, fiTQun, was introduced in the 2013 analysis in order to improve the rejection of $\pi^0$s that are misidentified as a single electron ring. FiTQun uses all photomultiplier hit information in its fit and achieves improved background rejection while maintaining good signal efficiency.

In the Run 1-4 data, out of 377 fully contained fiducial volume neutrino candidates at Super-K 28 events passed all of the selection cuts [9]. Compared to the prediction of $4.92\pm0.55$ events assuming $\theta_{13}=0$, this is a significant excess.

Two independent analyses were performed, one using the reconstructed energy of the neutrino and one using both the momentum and the angle of the observed electron direction relative to the beam direction, and both gave consistent results. Figure 33 shows the reconstructed neutrino energy distribution assuming all events underwent CCQE interactions, where the solid line represents the expected distribution at the best fit for $\theta_{13}$ assuming fixed values of the oscillation parameters: $\sin^2\theta_{12}=0.306$, $\Delta m^2_{21}=7.6\times10^{-5}\mathrm{eV}^2$, $\sin^2\theta_{23}=0.5$, $\Delta m^2_{32}=2.4\times10^{-3}\mathrm{eV}^2$ and $\delta_{CP}=0$. The parameter $\delta_{CP}$ describes a CP (charge parity) phase, where the CP conservation in leptonic sector is unknown. The prediction agrees well with the observed distribution.

The best fit as well as 68% and 90% confidence intervals for $\sin^2 2\theta_{13}$ from the momentum and angle binned analysis are shown at each fixed value of $\delta_{CP}$ in Fig. 34 and with the following parameter assumptions: $\sin^2\theta_{12}=0.306$, $|\Delta m^2_{21}|=7.6\times10^{-5}\mathrm{eV}^2$, $\sin^2\theta_{23}=0.5$ and $\Delta m^2_{32}=2.4\times10^{-3}\mathrm{eV}^2$. The best fit values of $\sin^2 2\theta_{13}$ with the 68% confidence intervals are evaluated to be $\sin^2 2\theta_{13}=0.140^{+0.038}_{-0.032}$ ($0.170^{+0.045}_{-0.037}$) at $\delta_{CP}=0$ for the normal (inverted) hierarchy assumption. The 28 observed $\nu_e$ events are a clear indication of electron neutrino appearance and non-zero $\theta_{13}$ with $7.3\sigma$ significance. Therefore, the $\nu_\mu \to \nu_e$ oscillation mode has been definitely discovered by T2K using its data up until 2013.

As the precision of the T2K measurement improves, uncertainties in the other oscillation parameters become increasingly important and have been included in the subsequent analysis. The measured values of $\theta_{23}$ and $\Delta m^2_{32}$ from the T2K $\nu_\mu$ disappearance analysis [8], corresponding to $3.01\times10^{20}$

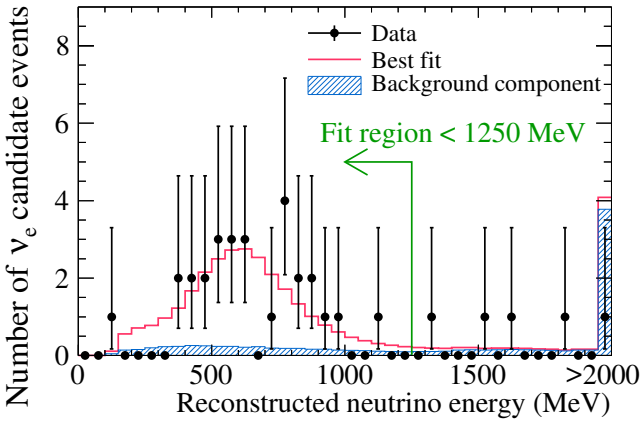


Fig. 33. Observation and best fit reconstructed neutrino energy distribution ($\sin^2 2\theta_{13}=0.144$, $\delta_{CP}=0$, normal hierarchy). The contribution from $\nu_e$ appearance is shown by the white histogram.

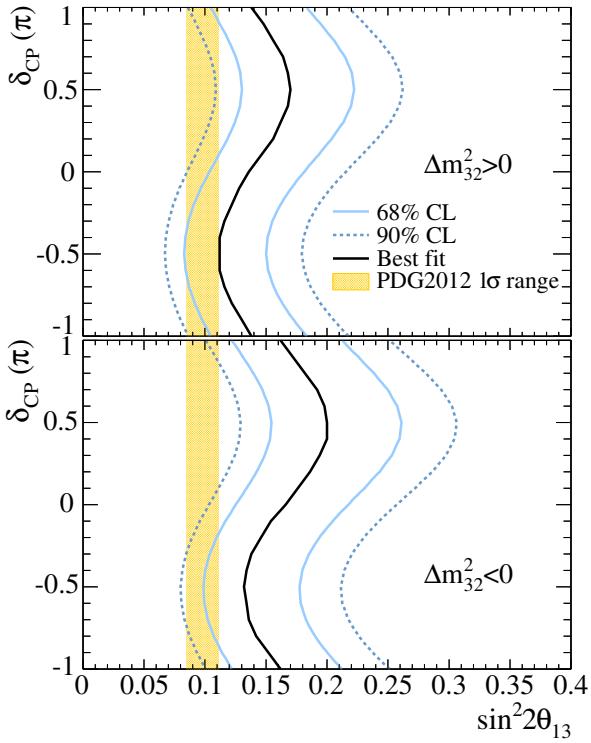


Fig. 34. The 68% and 90% confidence intervals for $\sin^2 2\theta_{13}$ scanned over values of $\delta_{CP}$ assuming $\sin^2\theta_{23}=0.5$ Results from a fit to the normal hierarchy (top) and inverted hierarchy (bottom) are shown.

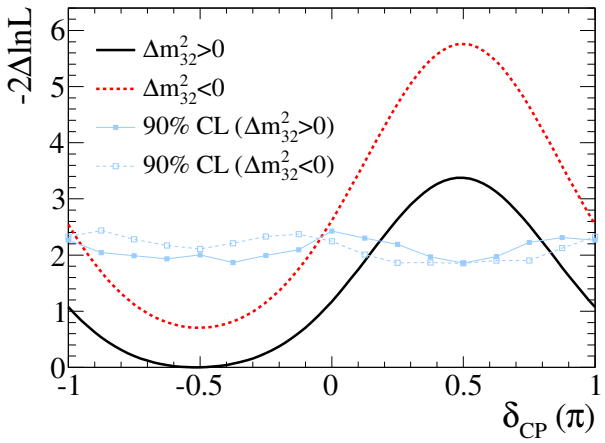


Fig. 35. The $-2\Delta lnL$ and 90% CL of $\delta_{CP}$ obtained by incorporating results of the T2K $\nu_\mu$ disappearance result ($3.01\times20^{20}$, 2012) and average value of $\theta_{13}$ from reactor experiments in the appearance analysis.

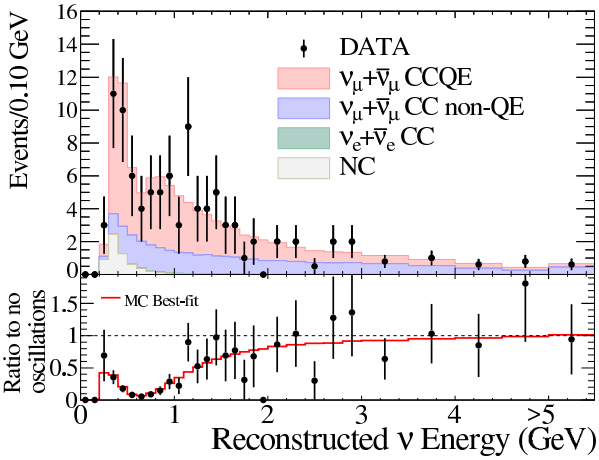


Fig. 36. The reconstructed energy spectrum of single-ring $\mu$-like events at SK for the Run 1-4 data with the best fit MC expectation broken down by neutrino flavor and interaction type appears in the top panel. The ratio of the observed and best-fit MC expectations from the top figure relative to the no oscillation hypothesis is shown in the bottom panel.

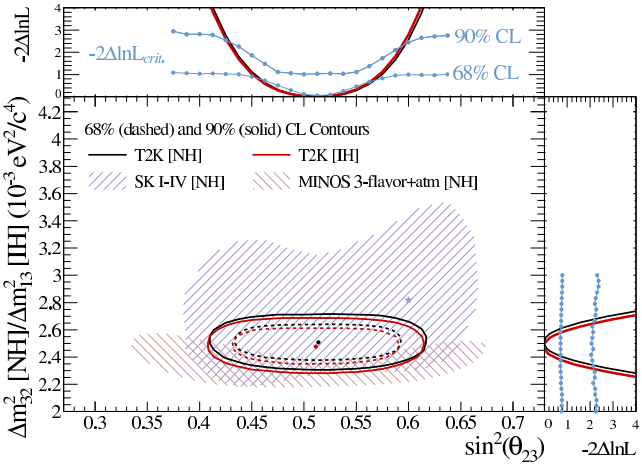


Fig. 37. The 68% and 90% confidence region from the T2K $\nu_\mu$ disappearance measurement for both hierarchy assumptions. The 1-d profile likelihoods for each parameter are separately shown at the top and right of the figure with the 68% and 90% confidence levels determined using the Feldman-Cousins method.

POT, are $\sin^2 2\theta_{13} = 0.136^{+0.044}_{-0.033}$ ($0.166^{+0.051}_{-0.042}$) in the case of the normal (inverted) hierarchy at $\delta_{CP} = 0$.

The first evaluation of the allowed region of $\delta_{CP}$ in T2K was performed with the help of precision measurements of $\theta_{13}$ by reactor $\bar{\nu}_e$ disappearance experiments. The value of $\sin^2 2\theta_{13}$ value was to $0.098 \pm 0.013$ based on the PDG2012 average [15]. The $-2\Delta lnL$ curve as a function of $\delta_{CP}$ is shown in Fig. 35 with a 90% confidence level (CL) determined with the Feldman-Cousins method [16]. T2K data indicate at the 90% CL that $\delta_{CP}$ is excluded between $0.19\pi$ and $0.80\pi$ ($-\pi$ and $-0.97\pi$, and $-0.04\pi$ and $\pi$) assuming a normal (inverted) hierarchy.

The T2K $\nu_\mu$ disappearance analysis is performed separately on a $\nu_\mu$ CCQE enriched sample by selecting single-ring $\mu$-like events with cuts on the reconstructed muon momentum ($p_\mu > 200\,\mathrm{MeV}/c$) and the number of delayed signals from Michel electrons (less than or equal to one). In the Run 1-4 data 446.0±22.5 events are expected without neutrino oscillations, while just 120 events have been observed [10]. The best fit MC expectation and data as a function of reconstructed neutrino energy are shown in the top portion of Fig. 36. The bottom panel shows the ratio of the observation and best fit expectation relative to the expectation from the null oscillation hypothesis, clearly demonstrating the presence of $\nu_\mu \to \nu_{(X\neq\mu)}$ oscillations in the data. In Fig. 37, the T2K allowed regions for the parameters $\sin^2\theta_{23}$ and $\Delta m^2_{32}$ (or $\Delta m^2_{13}$) for both hierarchy assumptions are shown. T2K has achieved the most stringent constraint on $\theta_{23}$, surpassing the SK atmospheric neutrino measurement.

T2K data sets are also used to determine neutrino cross sections. The result of the measurement for $\nu_\mu$ inclusive charged current interactions was published [17]. The first measurement of the neutrino-oxygen neutral current quasi-elastic (NCQE) cross section was also reported [18]. With $3.01 \times 10^{20}$ POT, a search for $\gamma$-ray events from nuclear de-excitation following NC interactions in Super-K has yielded 43 events with energy between 4-30 MeV and corresponds to a flux-averaged NCQE cross section measurement of $1.35^{+0.59}_{-0.29} \times 10^{-38}$ cm$^2$.

Although the discovery of electron neutrino appearance and the most constraining measurement of $\theta_{23}$ have been achieved the current T2K exposure is still only 8% of the design goal. The T2K experiment has also analyzed both the appearance and disappearance samples simultaneously incorporating parameter correlations and the first preliminary result was obtained using the Run 1-4 data. In 2014, an anti-neutrino run with a $\bar{\nu}_\mu$ beam will start. This will allow T2K to independently study $\nu_e$ and $\bar{\nu}_e$ oscillations and improve sensitivity to the CP violating parameter, $\delta_{CP}$.

## Bibliography

[1] K. Abe *et al.* [T2K Collaboration], Nucl. Instrum. Meth. A **659**, 106 (2011) [arXiv:1106.1238 [physics.ins-det]].

[2] D. Beavis, A. Carroll, I. Chiang, *et al.*, Long Baseline Neutrino Oscillation Experiment at the AGS (Proposal E889), 1995. Physics Design Report, BNL 52459.

[3] M. Otani, N. Nagai, D. Orme, A. Minamino, K. Nitta, O. Drapier, F. Moreau and M. Besnier *et al.*, Nucl. Instrum. Meth. A **623**, 368 (2010).

[4] Y. Fukuda *et al.* (Super-Kamiokande Collaboration), Nucl. Instrum. Meth. A501, 418 (2003).

[5] K. Abe *et al.* [T2K Collaboration], Phys. Rev. Lett. **107**, 041801 (2011) [arXiv:1106.2822 [hep-ex]].

[6] K. Abe *et al.* [T2K Collaboration], Phys. Rev. D **85**, 031103 (2012) [arXiv:1201.1386 [hep-ex]].

[7] K. Abe *et al.* [T2K Collaboration], Phys. Rev. D **88**, 032002 (2013) [arXiv:1304.0841 [hep-ex]].

[8] K. Abe *et al.* [T2K Collaboration], Phys. Rev. Lett. **111**, 211803 (2013) [arXiv:1308.0465 [hep-ex]].

[9] K. Abe *et al.* [T2K Collaboration], Phys. Rev. Lett. **112**, 061802 (2014) [arXiv:1311.4750 [hep-ex]].

[10] K. Abe *et al.* [T2K Collaboration], Phys. Rev. Lett. **112**, 181801 (2014) [arXiv:1403.1532 [hep-ex]].

[11] N. Abgrall *et al.* [NA61/SHINE Collaboration], Phys. Rev. C **84**, 034604 (2011) [arXiv:1102.0983 [hep-ex]].

[12] N. Abgrall *et al.* [NA61/SHINE Collaboration], Phys. Rev. C **85**, 035210 (2012) [arXiv:1112.0150 [hep-ex]].

[13] Y. Hayato, Nucl. Phys. (Proc. Suppl.) B112, 171 (2002).

[14] K. Abe *et al.* [T2K Collaboration], Phys. Rev. D **89**, 092003 (2014) [arXiv:1403.2552 [hep-ex]].

[15] J. Beringer *et al.* [Particle Data Group], Phys. Rev. D **86**, 010001 (2012).

[16] G.J. Feldman and R.D. Cousins, Phys. Rev. D **57**, 3873 (1998).

[17] K. Abe *et al.* [T2K Collaboration], Phys. Rev. D **87**, 092003 (2013) [arXiv:1302.4908 [hep-ex]].

[18] K. Abe *et al.* [T2K Collaboration], arXiv:1403.3140 [hep-ex].

# HIGH ENERGY COSMIC RAY DIVISION

## Overview

There are three major experimental research activities in the High Energy Cosmic Ray Division, the study of high energy gamma rays and the development of the next generation gamma-ray telescopes by the Cherenkov Cosmic Gamma Ray group, the study of extremely high energy cosmic rays by the Telescope Array (TA) group, and the study of very high energy cosmic rays and gamma rays by the Tibet AS$\gamma$ group.

Other activities, such as experiments utilizing the Akeno observatory, the Norikura observatory, the Mt. Chacaltaya observatory (jointly operated with Bolivia) are closely related to inter-university joint research programs. Also an all-sky high resolution air-shower detector (Ashra) is in partial operation on the Hawaii island. The High Energy Astrophysics group created in the fiscal year 2009 aims to explore various high energy astrophysical phenomena, through theoretical and observational approaches.

The CANGAROO telescopes had been in operation in South Australia since 1992, with a 3.8 m small telescope and then with four 10 m telescopes. The major scientific objective was the study of Very High Energy (VHE) gamma-ray sources in our galaxy in the southern hemisphere. The mission of these telescopes was completed and the CANGAROO observation site was closed in 2011.

For further development of VHE gamma-ray astronomy, the Cherenkov Cosmic Gamma Ray group is working on the design study and development of the next generation international ground-based gamma-ray observatory CTA which will offer an order of magnitude better sensitivity than currently running Cherenkov telescopes, three times better angular resolution, and wider energy coverage from 20 GeV to 100 TeV or higher.

At the Akeno observatory, a series of air shower arrays of increasing geometrical sizes were constructed and operated to observe extremely high energy cosmic rays (EHECRs). The Akeno Giant Air Shower Array (AGASA) was operated from 1991 to January 2004 and covered the ground area of 100 km$^2$ as the world largest air shower array. In 13 years of operation, AGASA observed a handful of cosmic rays exceeding the theoretical energy end of the extra-galactic cosmic rays (GZK cutoff) at $10^{20}$ eV.

The Telescope Array (TA), a large plastic scintillator array with air fluorescence telescopes, has been constructed in Utah, USA, which succeeds AGASA and measures the EHECRs with an order of magnitude larger aperture than that of AGASA for the further study of EHECRs. The full-scale TA is accumulating data as the largest array viewing the northern sky and observed the energy spectrum with high statistics, which is in good agreement with the GZK suppression.

An air shower experiment aiming to search for celestial gamma-ray point sources started in 1990 with Chinese physicists at Yangbajing (Tibet, 4,300 m a.s.l.). This international collaboration is called the Tibet AS$\gamma$ Collaboration. An extension of the air shower array was completed in 1995 and an emulsion chamber has been combined with this air shower array since 1996 to study the primary cosmic rays around the knee energy region. After successive extensions carried out in 1999, 2002 and 2003, the total area of the air shower array amounts to 37,000 m$^2$. The sun's shadow in cosmic rays affected by the solar magnetic field was observed for the first time in 1992, utilizing its good angular resolution at multi-TeV energy region.

A new type of detector, called Ashra (all-sky survey high resolution air-shower detector), was developed. The first-phase stations were installed near the Mauna Loa summit in the Hawaii Island and high-efficiency observation is continuing. It monitors optical and particle radiation from high-energy transient objects with a wide field-of-view.

The High Energy Astrophysics group is conducting theoretical researches on fundamental processes responsible for non-thermal particle acceleration in various astrophysical environments, including first-order diffusive shock acceleration, second-order stochastic acceleration in shock downstream regions, modification of shock structure by pick-up interstellar neutrals, as well as injection processes of suprathermal particles. In addition to these theoretical works, R/D studies for radio observations of pulsars and cosmic ray air showers are also being made.

## Cherenkov Cosmic Gamma-Ray Group

### *CTA Project (Cherenkov Telescope Array)*

**CTA-Japan Consortium**
[Spokespersons : M.Teshima and H.Kubo]

Collaboration list:
Institute for Cosmic Ray Research, The University of Tokyo, Chiba, Japan; Department of Physics, Aoyama Gakuin University, Tokyo, Japan; Department of Physics, Hiroshima University, Hiroshima, Japan; Hiroshima Astrophysical Science Center, Hiroshima University, Hiroshima, Japan; Faculty of Science, Ibaraki University, Ibaraki, Japan; Institute of Particle and Nuclear Studies, High Energy Accelerator Research Organization (KEK), Ibaraki, Japan; Department of Physics, Konan University, Hyogo, Japan; Faculty of Medical Engineering and Technology, Kitasato University, Kanagawa, Japan; Graduate School of Science and Technology, Kumamoto University, Kumamoto, Japan; Department of Physics, Kyoto University, Kyoto, Japan; Department of Applied Physics, University of Miyazaki, Miyazaki, Japan; Department of Physics, Nagoya University, Aichi, Japan; Solar-Terrestrial Environment Laboratory, Nagoya University, Aichi, Japan; Kobayashi-Maskawa Institute, Nagoya University, Aichi, Japan; Depart-

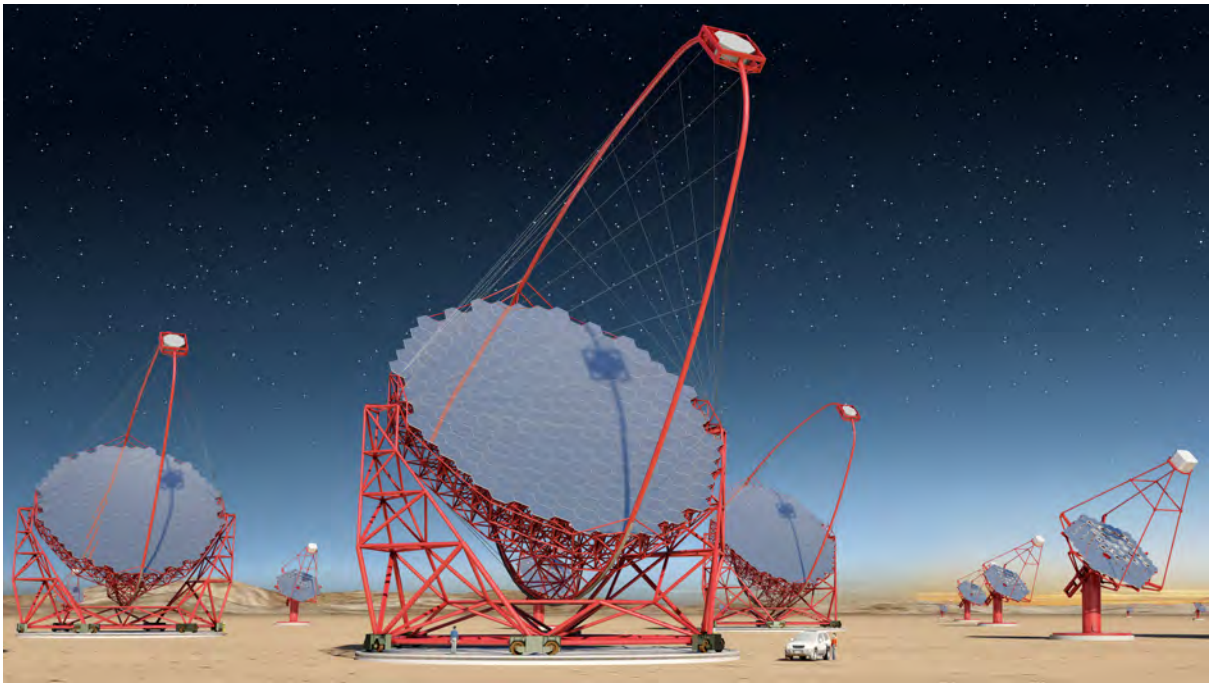

Fig. 1. Artist view of the CTA observatory. CTA consists of three types of telescopes, Large Size Telescopes (23m diameter), Mid Size Telescopes (12m) and Small Size Telescopes (4m), and covers the broad energy band from 20GeV to 100TeV.

ment of Earth and Space Science, Osaka University, Japan; Department of Physics, Kinki University, Osaka, Japan; Astrophysical Big Bang laboratory, RIKEN, Wako, Japan; Department of Physics, Saitama University, Saitama, Japan; Institute of Space and Astronautical Science, JAXA, Kanagawa, Japan; Department of Physics, Tokai University, Kanagawa, Japan; Department of Radiation Oncology, Tokai University, Kanagawa, Japan; Faculty of Integrated Arts and Sciences, The University of Tokushima; Department of Astronomy, The University of Tokyo, Tokyo, Japan; Department of Physics, The University of Tokyo, Tokyo, Japan; Faculty of Science and Engineering, Waseda University, Tokyo, Japan; Department of Physics, Yamagata University, Yamagata, Japan; Faculty of Management Information, Yamanashi Gakuin University, Yamanashi, Japan; Center for Cosmology and AstroParticle Physics, Ohio State University, Ohio, USA; Max-Planck-Institute for Physics, Munich, Germany [1].

### *CTA Project*

During the past several years, Very High Energy (VHE) gamma-ray astronomy has made spectacular progress and has established itself as a vital branch of astrophysics. To advance this field even further, we propose the Cherenkov Telescope Array (CTA) [2], the next generation VHE gamma ray observatory, in the framework of a worldwide, international collaboration. CTA is the ultimate VHE gamma ray observatory, whose sensitivity and broad energy coverage will attain an order of magnitude improvement above those of current Imaging Atmospheric Cherenkov Telescopes (IACTs). By observing the highest energy photons known, CTA will clarify many aspects of the extreme Universe, including the origin of the highest energy cosmic rays in our Galaxy and beyond, the physics of energetic particle generation in neutron stars and black holes, as well as the star formation history of the Universe. CTA will also address critical issues in fundamental physics, such as the identity of dark matter particles and the nature of quantum gravity.

VHE gamma rays from 100GeV to 10TeV can be observed with ground-based IACTs. The history of VHE gamma ray astronomy began with the discovery of VHE gamma rays from the Crab Nebula by the Whipple Observatory in 1989. To date, the current generation IACTs featuring new technologies, such as H.E.S.S., MAGIC, VERITAS, and CANGAROO, have discovered more than 100 Galactic and extragalactic sources of various types.

CTA is designed to achieve superior sensitivity and performance, utilizing established technologies and experience gained from the current IACTs. The project is presently in its preparatory phase, with international efforts from Japan, the US and EU. It will consist of several 10s of IACTs of three different sizes (Large Size Telescopes, Mid Size Telescopes, and Small Size Telescopes). With a factor of 10 increase in sensitivity (1m Crab $\sim 10^{-14} erg\ s^{-1}\ cm^{-2}$), together with a much broader energy coverage from 20GeV up to 100TeV, CTA will bring forth further dramatic advances for VHE gamma ray astronomy. The discovery of more than 1000 Galactic and extragalactic sources is anticipated with CTA.

CTA will allow us to explore numerous diverse topics in physics and astrophysics. The century-old question of the origin of cosmic rays is expected to be finally settled through detailed observations of supernova remnants and other Galactic objects along with the diffuse Galactic gamma ray emission, which will also shed light on the physics of the interstellar medium. Observing pulsars and associated pulsar wind nebulae will clarify physical processes in the vicinity of neutron stars and extreme magnetic fields. The physics of accretion

onto supermassive black holes, the long-standing puzzle of the origin of ultrarelativistic jets emanating from them, as well as their cosmological evolution, will be addressed by extensive studies of active galactic nuclei (AGN). Through dedicated observing strategies, CTA will also elucidate many aspects of the mysterious nature of gamma ray bursts (GRBs), the most energetic explosions in the Universe. Detailed studies of both AGNs and GRBs can also reveal the origin of the highest energy cosmic rays in the Universe, probe the cosmic history of star formation including the very first stars, as well as provide high precision tests of theories of quantum gravity. Finally, CTA will search for signatures from elementary particles constituting dark matter with the highest sensitivity yet. Realization of the rich scientific potential of CTA is very much feasible, thanks to the positive experience gained from the current IACTs.

The CTA-Japan consortium [1] is aiming at contributing in particularly to the construction of the Large Size Telescopes (LSTs) and is involved in their development. The LST covers the low energy domain from 20GeV to 1000GeV and is especially important for studies of high redshift AGNs and GRBs. The diameter and area of the mirror are 23m and 400m$^2$, respectively, in order to achieve the lowest possible energy threshold of 20GeV. All optical elements/detectors require high specifications, for example, high reflectivity, high collection efficiency, high quantum efficiency and ultra fast digitization of signal, etc. For this purpose, CTA-Japan is developing high quantum efficiency photomultipliers, ultrafast readout electronics and high precision segmented mirrors. On the strength of their experience gained from construction of the MAGIC telescope, the Max-Planck-Institute for Physics in Munich is responsible for the design of the 23m diameter telescope structure, based on a carbon fiber tube space frame. The LSTs require very fast rotation (180 degrees/20seconds) for promptly observing GRBs.

The Cherenkov Cosmic Gamma Ray group is also operating the MAGIC Telescopes [6] on La Palma, Canary Islands. This facility is used not only for scientific observations but also for technological development toward the future observatory CTA.

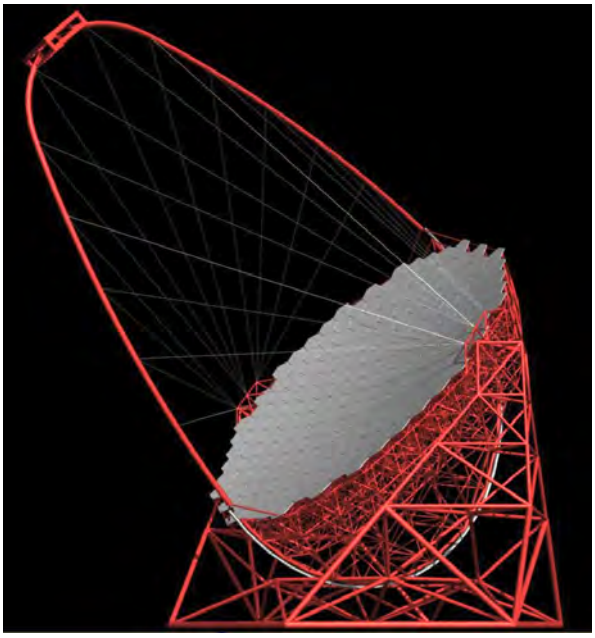

Fig. 2. Large Size Telescope (23m diameter) designed by Max–Planck-Institute for Physics. CTA Japan is contributing to the design and prototyping of the imaging camera at the focal plane, ultrafast readout electronics, and high precision segmented mirrors.

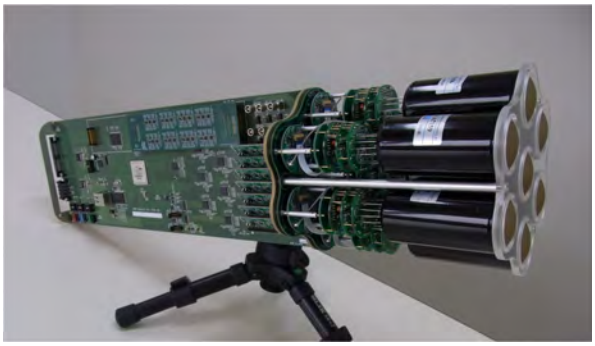

Fig. 3. Camera cluster for the Large Size Telescope (LST) developed by CTA-Japan. This cluster consists of seven high quantum efficiency photomultipliers (R11920-100), CW High Voltages, pre-amplifier, Slow Control Board, DRS4 Ultra fast waveform recording system and Trigger. The LST camera can be assembled with 265 of these clusters, cooling plates and camera housing.

Fig. 4. The high precision segmented mirrors for the Large Size Telescope (LST) developed by CTA-Japan in cooperation with Sanko Co.LTD. The mirror is made of a 60mm thick aluminum honeycomb sandwiched by 3mm thin glass on both sides. A surface protection coat consisting of the materials SiO2 and HfO2 is applied to enhance the reflectivity and to elongate the lifetime.

## Bibliography


[1] CTA Consortium website: `http://www.cta-observatory.jp/` and `http://www.cta-observatory.org/`.

[2] Design Concepts for The Cherenkov Telescope Array, The CTA Consortium, Exper. Astron. 32 (2011) 193-316.

[3] Status of Very High Energy Gamma Ray Astronomy and Future Prospects, M. Teshima, The Astronomical Herald, 104 (2011) 333-342.

[4] Design Study of a CTA Large Size Telescope, Proc. of ICRC2012 at Beijing China, M. Teshima, arXiv:1111.2183.

[5] Introducing the CTA Concept, B. Acharya et al., Astroparticle Physics, 34 (2013) 3.

Fig. 5. MAGIC Stereo System with two Cherenkov telescopes of 17m diameters, so far achieved the threshold energy of 25GeV. It locates near the mountain top of the Roque de los Muchachos on the Canary Island of La Palma. Two telescopes are located with the distance of 85 meters.

[6] MAGIC Collaboration website: `http://magic.mppmu.mpg.de/`.

### *MAGIC*

The MAGIC Collaboration has built in 2002 / 2003 a first large atmospheric imaging Cherenkov telescope, MAGIC-I, with a mirror surface of 236 sq.m. and equipped with photomultiplier tubes of optimal efficiency. In 2009, a second telescope of essentially the same characteristics was added; MAGIC-II was installed at a distance of 85m from MAGIC-I. With the accent of these instruments on large mirror surface and best light collection, cosmic gamma-rays at an energy threshold lower than any existing or planned terrestrial gamma-ray telescope have become accessible. So far achieved has been a threshold of 25 GeV. The Japanese group has joined the MAGIC collaboration since 2010, and contributed to the operation, observations and data analysis. The MAGIC telescopes are operated by an international collaboration of 17 institutes from 8 countries.

The recent highlights from MAGIC are, 1) the successful observation of pulsed gamma ray signal from the Crab pulsar up to TeV regime [1], 2) the discovery of the most distant blazer 3S 0218 + 35 with the redshift of 0.944 above 100GeV [2], 3) the observation of the very fast flare of 1min time scale from the blazar inside Perseus cluster, IC310 [3]. These results brought new questions on the pulsar emission mechanism, the EBL energy density, and gamma ray emission mechanism from the supermassive blackholes or vicinity of them.

## Bibliography

[1] Phase-resolved energy spectra of the Crab pulsar in the range of 50-400 GeV measured with the MAGIC telescopes, the MAGIC Collaboration, Aleksić et al. A&A 540 (2012) A69.

[2] ATEL 6349.

[3] ATEL 4583.

### *Other Activities*

As a test bench for domestic R & D activities of future ground-based gamma-ray observatory projects, a used atmospheric Cherenkov telescope of a 3 m diameter was obtained and placed at the Akeno Observatory in November 2010. This is currently the only atmospheric Cherenkov telescope located in Japan. In the fiscal year 2013, we readjusted the telescope optics consisting of 18 segment mirrors, which had been recoated by 2012 at the Okayama Astrophysical Observatory (OAO), the National Astronomical Observatory of Japan (NAOJ) (Fig. 6). An R & D system of 32 pixel (PMT) imaging camera and electronics were installed to the telescope, and test observations of air-shower events are going to be carried out with this system in the next fiscal year [1, 2]. Test observations with some prototype imaging cameras for CTA are also planned with the telescope in the near future.

Fig. 6. Akeno atmospheric Cherenkov telescope with 18 segment mirrors readjusted as the Davies-Cotton optics.

## Bibliography

[1] M. Ohishi et al., Proc. of 33rd Internat. Cosmic Ray Conf. (Rio de Janeiro), in press (2013).

[2] T. Yoshikoshi et al., Proc. of 32nd Internat. Cosmic Ray Conf. (Beijing), **9**, 226–229 (2011).

---

# TA: Telescope Array Experiment

---

[Spokespersons: H. Sagawa[1], G. B.Thomson[2] ]

1 : ICRR, The Univ. of Tokyo, Kashiawa, Chiba 277-8582
2 : Dept. of Physics, University of Utah

Collaborating Institutions:

Chiba Univ., Chiba, Japan; Earthquake Research Institute, Univ. of Tokyo, Tokyo, Japan; Ehime Univ., Matsuyama, Japan; Ewha W. Univ., Seoul, Korea; Hiroshima City Univ., Hiroshima, Japan; Hanyang Univ., Seoul, Korea; ICRR, Univ. of Tokyo, Kashiwa, Japan; INR, Moscow, Russia; IPMU, Univ. of Tokyo, Kashiwa, Japan; Kanagawa Univ., Yokohama, Japan; KEK/IPNS, Tsukuba, Japan; Kinki Univ., Higashi-Osaka, Japan; Kochi Univ., Kochi, Japan; Kyoto Univ., Kyoto, Japan; Nat. Inst. of Rad. Sci., Chiba, Japan; Osaka City Univ., Osaka, Japan; RIKEN, Wako, Japan; Ritsumeikan Univ., Kusatsu,

Japan; Rutgers Univ., Piscataway, NJ, USA; Saitama Univ., Saitama, Japan; Tokyo City Univ., Tokyo, Japan; Tokyo Inst. of Tech., Tokyo, Japan; Tokyo Univ. of Science, Noda, Japan; ULB, Brussels, Belgium; UNIST, Ulsan, Korea; Univ. of Utah, Salt Lake City, UT, USA; Univ. of Yamanashi, Kofu, Japan; Waseda Univ., Tokyo, Japan; Yonsei Univ., Seoul, Korea

### *Overview and Status of TA*

The Telescope Array (TA) is the largest Ultra-High-Energy Cosmic-Ray (UHECR) observatory in the Northern Hemisphere, located in the West Desert in Utah, USA (latitude 39.3° N, longitude 112.9° W, altitude ∼1400 m). TA is designed to observe extensive air showers (EAS) induced by UHECRs with energies from $\sim 10^{18}$ to $\sim 10^{20.5}$ eV, and measures the energy spectrum, mass composition, and arrival direction distribution of UHECRs, and searches for ultra-high-energy photon and neutrino primaries. The aim of these measurements is to explore the origin, propagation and interaction of UHECRs. The TA detector consists of an air shower surface detector (SD) array of plastic scintillation counters to measure the lateral distribution of secondary particles on the ground, and fluorescence detectors (FDs) to measure the longitudinal development of the EAS in the atmosphere. The SD array consists of 507 counters with an area of 3 $m^2$, which were deployed on a square grid of 1.2-km spacing, covering ∼700 $km^2$. Three FD stations are located at the periphery, looking inward over the SD array. The Middle Drum (MD) FD site is located to the north of the SD array, and is instrumented with 14 refurbished telescopes from the High-Resolution Fly's Eye (HiRes) station. The Black Rock Mesa (BRM) and Long Ridge (LR) FD sites are located to the southeast and southwest of the SD array, respectively. They are each instrumented with 12 new telescopes. TA is operated by an international collaboration of researchers from Japan, USA, Korea, Russia, and Belgium. Hybrid observations using both SDs and FDs commenced in March 2008.

### *Results*

#### Energy Spectrum

The energy spectrum for four years of TA SD data has been published [1]. Here, we update this energy spectrum using the SD data for the five years of observations from May 2008 to May 2013 with an exposure of ∼4500 $km^2$ sr yr. The Monte Carlo (MC) data were generated by a CORSIKA air shower simulation with the QGSJET-II-03 model. A GEANT4 simulation was used for the detector simulation. We use the correlation of $S_{800}$, which is the charge density at a distance of 800 m from the shower core, and zenith angle with primary energy from the MC study for the first estimation of the cosmic-ray energy.

The energy scale uncertainty in the SD MC simulation can be large, mainly due to the modeling of hadronic interactions. The energy scale uncertainty is experimentally controlled for the FD, because the energy measurement is calorimetric. We correct our energy scale to the TA FD using events detected by both the FD and SD. The observed differences between the FD and SD events are well described by a simple proportionality relationship, where the SD energy must be reduced by 27% to agree with the FD energy.

The resulting energy spectrum is shown together with the measurements of other experiments in Figure 7. Using a broken power-law fit, we found the two breaks at $(5.04 \pm 0.27) \times 10^{18}$ eV and $(5.68 \pm 1.05) \times 10^{19}$ eV. These are consistent with the ankle and the GZK suppression [2, 3], respectively. We observed 26 events above the suppression, whereas a linear extrapolation of the power law below the break predicts 68.1 events above the break. This result provides evidence for the flux suppression with a statistical significance of $5.74\sigma$. The Auger spectrum after energy-scale shift by +10% agrees with the TA spectrum below the suppression, whereas the suppression points differ between the two spectra.

We check the compatibility of the measured TA spectrum above $10^{18.2}$ eV using the MC code for cosmic-ray propagation (CRPropa) with modifications [4] by setting the injection spectral index ($p$ for $E^p$), the source evolution ($m$ for $(1+z)^m$) and energy scale as free parameters, where $z$ is the red shift. We obtain the preliminary best fit $\chi^2/d.o.f. = 12.5/17$ with $p = 2.21^{+0.15}_{-0.10}$, $m = 6.6^{+1.7}_{-1.2}$, and $\Delta \log E = -0.03^{+0.03}_{-0.02}$. Similar results are obtained for the isotropic model and the large-scale structure (LSS) model, and the difference is included as a systematic error. The LSS model used in this analysis is explained in Section .

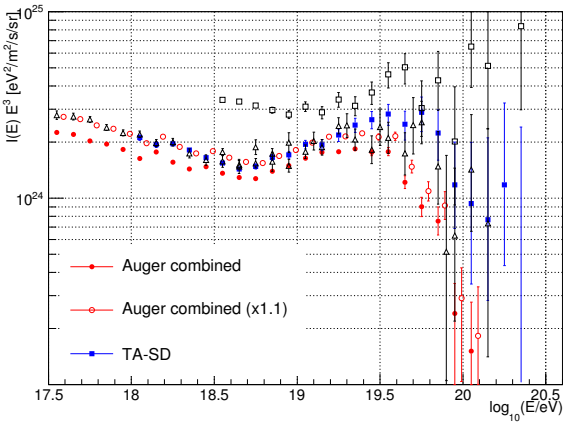


Fig. 7. The preliminary TA SD spectrum together with the spectra from other experiments: the TA SD (blue closed squares), AGASA (black open squares), Auger [5] (red closed circles), HiRes (black open triangles). Red open circles are Auger spectrum after energy-scale shift by +10%. .

With each of the three sites acting independently, the FD measurement of the spectrum in "monocular" mode [6] provides a larger dynamic range of energy measurements and a bolometric measurement of the EAS energy, but the duty cycle is only ∼10% due to its operation being restricted to moonless nights. The geometrical reconstruction of the EAS is also poorer than with the SD alone. The "hybrid" measurement [7, 8] combines the bolometric FD measurements with the geometrical precision of the SD at the cost of the duty cycle and reduced dynamic range of each method. For the monocular and hybrid measurements of the spectra, two separate analyses were performed, and these separate analyses are combined appropriately to allow us to present a TA monocular

spectrum and a TA hybrid spectrum. Figure 8 shows the preliminary results for the combined monocular spectrum, combined hybrid spectrum, and SD spectrum [9]. These spectra are consistent with each other.

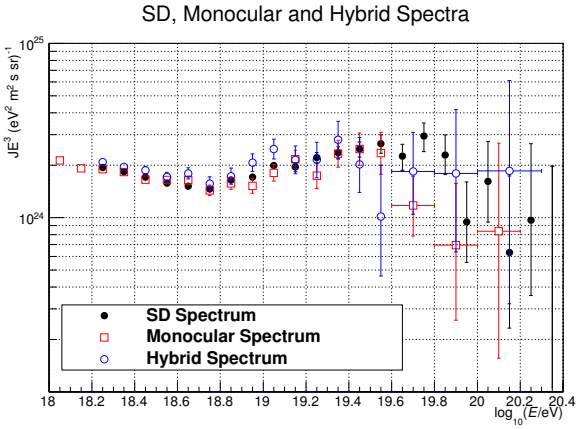


Fig. 8. The TA combined monocular FD spectrum, TA combined hybrid spectrum, and TA SD spectrum (preliminary).

## Mass Composition

The dependence of shower maximum depth, $X_{\rm max}$, on the primary energy is used to determine the mass composition. The HiRes result is consistent with proton-dominated composition for E $> 10^{18}$ eV [10], whereas the Auger result is compatible with mixed composition [5].

The events observed simultaneously at two new FD stations (stereo events) from November 2007 through November 2012 are presented [11]. The distribution of reconstructed $X_{\rm max}$ for the TA data is in agreement with the QGSJET-II-03 proton distribution in each energy range as shown in Figure 9. Here the $X_{\rm max}$ values include reconstruction and acceptance bias both for the TA data and MC simulation. The evolution of the average $X_{\rm max}$ with energy for TA stereo data is shown with the MC simulation in the energy range of $10^{18.2}$ to $10^{19.8}$ eV in Figure 10. The TA stereo data are in agreement with the proton prediction.

A similar result was obtained using the MD hybrid data for four years (2008–2012) [8]. The evolution of the average $X_{\rm max}$ with energy is shown with the MC simulation in the energy range of $10^{18.2}$ to $10^{19.6}$ eV in Figure 11. The MD hybrid data are in agreement with the proton prediction.

## Search for Ultra-high-energy Photons

It is expected that a photon-induced shower would have a deeper shower maximum than a hadronic shower and exhibit a larger shower-front curvature on the ground. We present results from the TA 5-year SD data set [12]. Figure 12 shows the distribution of Linsley curvature parameter for events with zenith angles between 45° and 60°. For each event, we determined the percentile rank below the observed Linsley parameter value for photon primaries. The distribution of this percentile rank for photon primaries is flat between 0 and 1, whereas the actual distribution in the data is strongly non-uniform (mostly below 0.5). Based on this, the obtained 95%

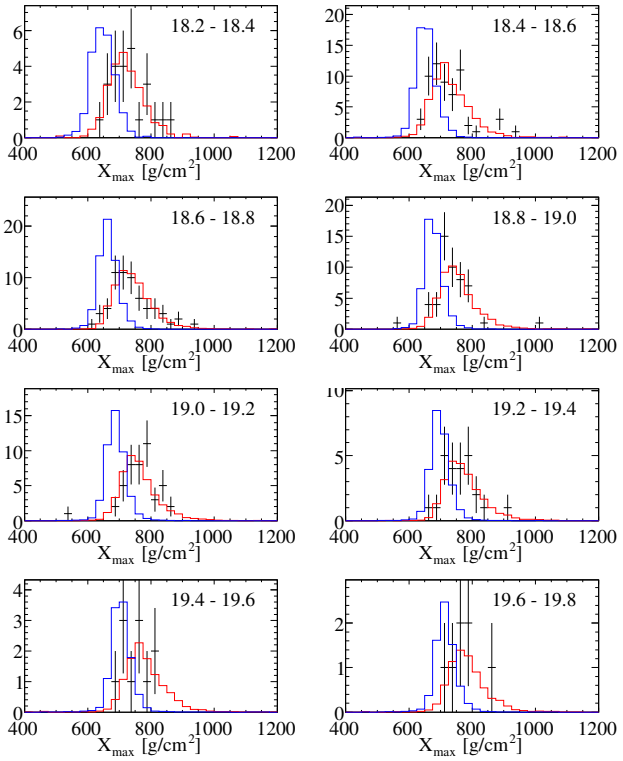


Fig. 9. The preliminary reconstructed $X_{\rm max}$ distributions for the stereo data (points) with QGSJET-II-03 MC simulation for eight energy regions between $10^{18.2}$ and $10^{19.8}$ eV. The red and blue histograms are the proton and iron predictions, respectively.

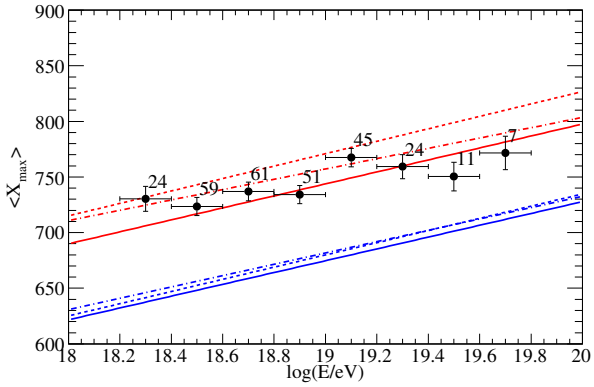


Fig. 10. The preliminary average reconstructed $X_{\rm max}$ (black points) as a function of energy for the TA stereo data. The red lines are the pure proton predictions with three interaction models: QGSJET-01 (solid line), QGSJET-II-03 (dot-dash line), and SYBILL (dotted line). The blue lines show the iron predictions.

CL upper limits on the photon fluxes are 0.019, 0.0097, and 0.0071 km$^{-2}$sr$^{-1}$yr$^{-1}$@ for $E_\gamma > 10^{19}$, $10^{19.5}$ and $10^{20}$ eV, respectively.

## Search for Ultra-high-energy Neutrinos

Neutrino-induced showers are expected to produce young showers for all zenith angles. For each event, we count the total number of peaks in SD waveforms over the upper and lower layers of all detectors. Very inclined hadronic showers are old, and contain mostly muons. These propagate recti-

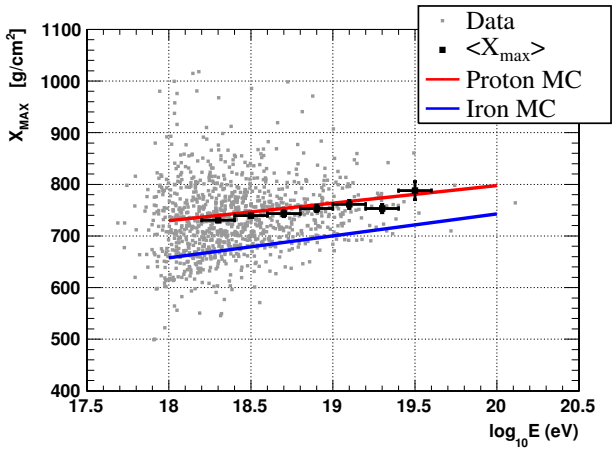


Fig. 11. The preliminary result of $X_{\rm max}$ vs. energy for the TA MD-hybrid data. The gray points show the distribution of $X_{\rm max}$ measurements of the data as a function of energy. The black points with error bars are the average $X_{\rm max}$ measurements of the data for the various energy slices. The red line is the pure proton prediction with QGSJET-II-03 model. The blue line is the iron prediction.

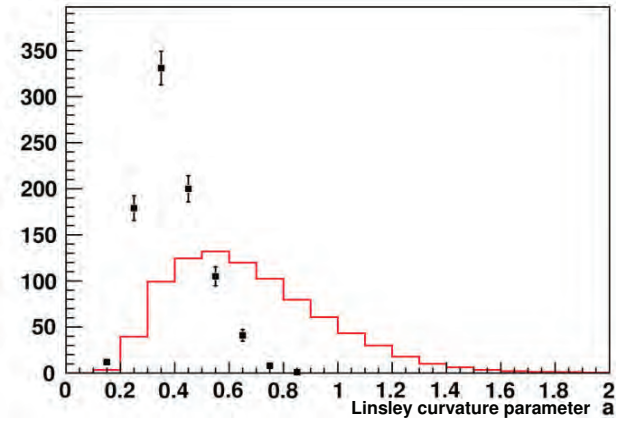


Fig. 12. Linsley curvature parameter distribution for zenith angle region between 45° and 60° for reconstructed $E_\gamma > 10^{19}$ eV. Black points refer to the data and the red histogram represents a photon MC simulation with $E^{-2}$ spectrum.

linearly, producing mostly single-peaked waveforms. On the contrary, young showers produce long, indented waveforms. Figure 13 shows the number of peaks per layer versus zenith angle for the TA 5-year data [13]. There are no apparent neutrino candidates in the data set. We define the percentile rank of the number of peaks per layer for neutrino primaries, and obtain the following preliminary differential flux limit at $10^{20}$ eV: $E^2\Phi_{\nu_e} < 5\times10^{-5}$ GeV cm$^{-2}$s$^{-1}$sr$^{-1}$ (90% CL).

### Anisotropy in Arrival Directions of UHECRs

We have published an analysis of UHECRs for correlations with Active Galactic Nuclei (AGNs), as well as for autocorrelations and correlations with the LSS for a 40-month TA data set [14]. Here, we update the anisotropy results using the full 5-year TA data, which contains 2130 events with $E > 10^{19}$ eV, 132 events with $E > 4\times10^{19}$ eV, and 52 events with $E > 5.7\times10^{19}$ eV for zenith angles below 55° for autocorrelations and LSS correlations. There are 42 events with $E > 5.7\times10^{19}$ eV for zenith angles below 45° for AGN correlations [15, 16]. For the 40-month TA data set, we published the result of the search for the correlations of the arrival directions of UHECRs with extragalactic objects for several catalogs [17].

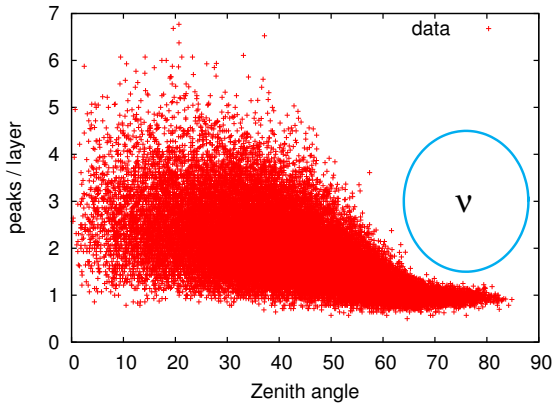


Fig. 13. The number of peaks per layer in the TA data set. Young inclined neutrino-induced showers are expected to lie within the circle.

### Correlations with AGNs

Auger reported correlations between the arrival directions of UHECRs with $E > 5.7\times10^{19}$ eV and the positions of nearby AGNs from the Véron 2006 catalog with $0< z \leq 0.018$ in 2007 [18]. They reported the probability that correlations for angular separations of less than 3.1° occurred by chance is $1.7\times10^{-3}$. The number of correlating events was 9 out of 13, which is about 69%. The Auger analysis has been updated, and it was found that the number of correlating events was 21 out of 55, which corresponds to about 38% of events [19].

We searched for AGN correlations using the same requirements as Auger, and found 17 correlating events (40%) out of 42 total events with $E > 5.7\times10^{19}$ eV . The number of random coincidences expected for this total number of events is 10. Using a binomial distribution with a single-event correlation probability of $p_{iso} = 0.24$, the probability of this excess occurring by chance is 1.4%, assuming an isotropic distribution.

### Autocorrelations

Figure 14 shows the dependence of the $p$-value, $P(\delta)$, on the pair separation angle, $\delta$, for events with zenith angles below 55° for two energy thresholds: $4\times10^{19}$ eV and $5.7\times10^{19}$ eV. There is no excess of small-scale clusters. For energies above $5.7\times10^{19}$ eV, there is a hint of some grouping of events at angular scales with a minimum $p$-value of about 0.2% in the angular range between 20° and 30°.

### Correlations with LSS

We use galaxies at distances of 5 to 250 Mpc and with Ks magnitudes of less than 12.5 in the 2MASS Galaxy Redshift Catalog (XSCz) [20]. This catalog provides the most accurate information about the three-dimensional distribution of galaxies. We assume that UHECRs are protons, and that the

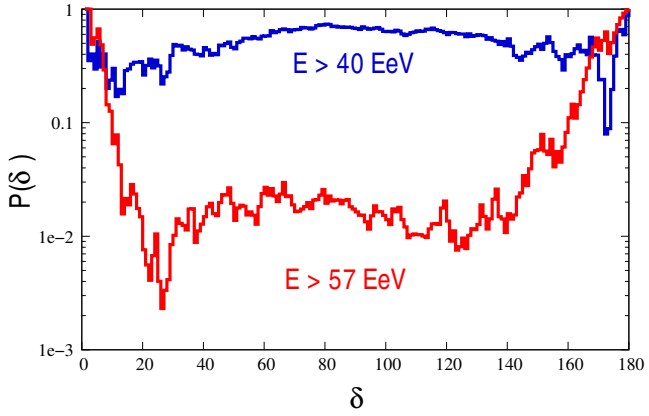


Fig. 14. The dependence of the $p$-value, $P(\delta)$, on the pair separation angle, $\delta$, for two energy thresholds: $4\times10^{19}$ eV and $5.7\times10^{19}$ eV (upper blue and lower red lines, respectively).

effects of galactic and extragalactic magnetic fields on each arrival direction can be approximated by a Gaussian probability density function with an angular resolution (called a smearing angle) of $\theta$, which is treated as a free parameter. The data above $5.7\times10^{19}$ eV is compatible with the LSS model, of which $p$-value is about 10%, and is incompatible with the isotropy model, of which $p$-value is about 0.1% at a smearing angle of 6°.

### Hotspot for highest-energy cosmic rays

We search for intermediate-scale anisotropy of cosmic-ray events with energy greater than $5.7\times10^{19}$ eV [21]. Here we use the event selection somewhat looser than the above analyses in order to increase the number of events with maintaining reasonable energy and angular resolution. By the looser cuts, of which major change is abolishing the cut of the SD array edge, we obtain 72 cosmic-ray events. Figure 15 (a) shows a sky map in equatorial coordinates of these events. A cluster of events that we call a "hotspot" appears in this map centered near right ascension ∼150° and declination ∼40°, with a diameter of ∼30° to 40°. In order to estimate the significance of this hotspot, we use oversampling with a 20° radius. Figure 15 (b) shows a significance map of the events above $5.7\times10^{19}$ eV. The maximum excess in our Field-of-View (FoV) appears as a hotspot centered at right ascension of 146.7° and declination of 43.2° with a statistical significance of $5.1\sigma$ (the number of observed events = 19, and the number of events expected in an isotropic cosmic-ray sky = 4.49). The probability of such a hotspot appearing by chance in an isotropic cosmic-ray sky is estimated to be $3.7\times10^{-4}$ ($3.4\sigma$).

### Search for point-like sources and large-scale anisotropy at around EeV

We search for steady point-like sources of neutral particles around EeV energy observed by the TA SD [22]. The air-shower reconstruction and data selection are optimized for the EeV air showers. The number of air showers above 0.5 EeV is increased by ∼10 times, which corresponds to 172,125 events, after the optimization. In order to search for the point-like sources, the Equi-Zenith Angle method is adopted to these cosmic-ray air showers taken by the TA SD during the period

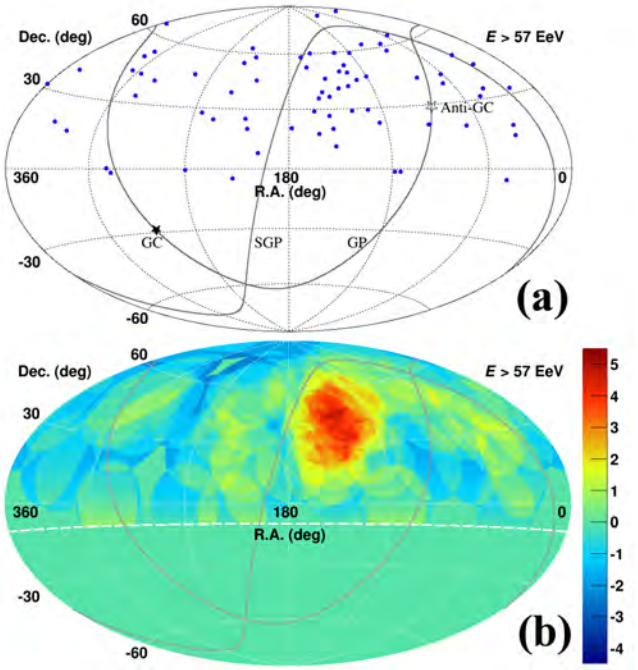


Fig. 15. Aitoff projection of the UHECR maps in equatorial coordinates. The solid curves indicate the galactic plane (GP) and supergalactic plane (SGP). Our FoV is defined as the region above the dashed curve at declination of −10°. (a) The points show the directions of the UHECRs with $E > 5.7\times10^{19}$ eV observed by the TA SD array, and the closed and open stars indicate the Galactic center (GC) and the anti-Galactic center (Anti-GC), respectively. (b) Significance map using oversampling with a 20° radius. Color scale denotes significance value.

between 2008 May and 2011 October. As a result, we find overall no significant excess above 0.5 EeV in the northern sky. Hence, we set upper limits at 95% C.L. on the neutron flux, which is an averaged flux 0.067 $\mathrm{km^{-2}yr^{-1}}$ above 1 EeV in the northern sky. This is the most stringent flux upper limit in the northern sky survey assuming the point-like sources.

We search also for the large-scale cosmic-ray anisotropy in the energy region between $10^{18.0}$ eV and $10^{18.4}$ eV based on the dataset taken during the period between 2008 May and 2012 October [23]. The number of analyzed air shower events is approximately 1.6 times larger than that of the AGASA observation which claimed the presence of the large-scale anisotropies before. In order to estimate the significance, we use oversampling with a 20° radius. We find no such excesses or deficit in the TA SD data.

### TA SD burst events in association with lightning

By SD shower trigger, we record events that are detected by not less than three neighboring SDs, of which trigger rate is $\sim5\times10^{-3}$ per second. Contrarily to this average trigger rate, we detected 10 bursts that consisted of not less than three events recorded by SD shower triggers generated within 1 millisecond in the 5-year SD data. The chance probability of obtaining such burst event rate was $10^{-4}$. The SDs of each event spread over up to about 10 $\mathrm{km^2}$. Some events were reconstructed using cosmic-ray air-shower reconstruction program, and we found some differences of the event characteristics from the usual air-shower events induced by cosmic rays.

And we observed temporal and spatial correlations between the burst events and lightning. Figure 16 shows a burst example with reconstructed SD events in association with lightning.

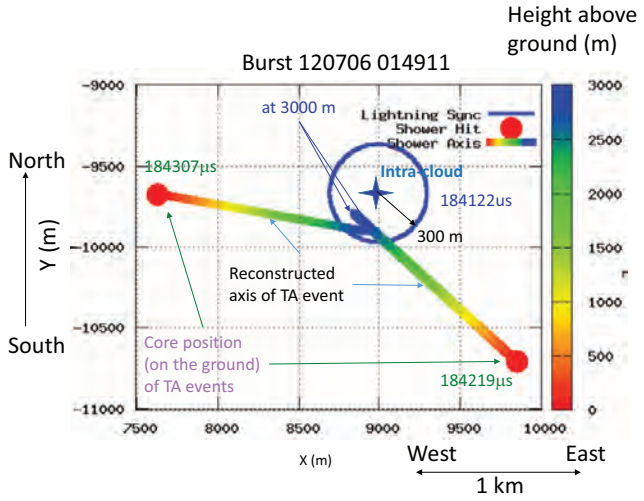


Fig. 16. Geometrical information of reconstructed SD events in the burst at 01 hr. 49 min. 11 sec. on July 6 in 2012 UTC in association with lightning. The vertical and horizontal axes show the north-south and east-west directions, respectively. The unit of the coordinates is meter, and the values are measured from the Central Laser Facility (CLF) in the TA site. The blue circle with 300-m radius denotes median location error of the lightning flash and the blue cross mark is its measured position provided by the National Lightning Detection Network (NLDN) in US. The red points denote the core positions on the ground of the two reconstructed SD events. The axes show the directions of the two reconstructed showers. The blue ends show the x-y positions at 3,000 m above ground level. The six digits of three values in $\mu$sec correspond to the timing of the lightning flash and two SD events.

## *Prospects*

We present preliminary results from the ELS, and outline the status of joint studies by the TA and Auger collaborations. We also describe extensions, proposals, and R&D of future detectors.

### The Electron Light Source: Measurement of Fluorescence Yield

The basic idea of the end-to-end calibration of the FD with the ELS is to compare measured ADC values with those from a MC simulation, and then correct the MC simulation for the difference from the data, which affects the energy scale. The beam energy is measured with an accuracy of less than 1% using a bending magnet. We worked for the precise measurement of the beam charge using a Faraday cup, and checked the relevant geometry with GEANT4 simulation. The first step of calibrating the TA FD using the ELS involves measuring the air fluorescence yield. This requires all of the FD calibration parameters. For this purpose, we select the following two air fluorescence models described.

The first model uses a fluorescence spectrum measured by the FLASH experiment [24] for 300–420 nm. The fluorescence yield integrated over 300–400 nm in the above-mentioned fluorescence spectrum is normalized to the yield measured by Kakimoto *et al.* [25]. This model is used in the analysis of air showers by the TA. The second is a combined model for air fluorescence yield [26] proposed by the dedicated working group of the UHECR2012 symposium [27]. This model adopts the fluorescence spectrum measured by AIRFLY. This spectrum is normalized for the air fluorescence yield at 337 nm measured by AIRFLY [28].

The air fluorescence yield is measured by comparing the ELS data with the MC simulation. The average fluorescence yield ratios of the data to the MC simulation for the first and second models were presented at ICRC2013 [29] and the updated preliminary results are $1.18 \pm 0.01\ (\mathrm{stat}) \pm 0.18\ (\mathrm{sys})$ and $0.96 \pm 0.01\ (\mathrm{stat}) \pm 0.15\ (\mathrm{sys})$.

In addition, the ELS is being used by groups from around the world to calibrate a new telescope that is under development [36], and to search for radio signals from cosmic ray showers. Several groups are searching for molecular bremsstrahlung signals [30, 31] and radar echoes.

### TA and Auger Joint Studies

The TA and Auger collaborations began a program of joint studies in order to understand the differences of the TA and Auger results for the energy spectrum, $X_{\mathrm{max}}$, and arrival directions. The following progress reports were presented at ICRC2013 [32]:

- The light source developed by the Auger collaboration was brought to the TA site and measured by the TA FD in 2012 and 2013.
- A large-scale anisotropy result with full sky coverage using the TA and Auger data above $1\times10^{19}$ eV was reported by developing a method to combine the two data sets.
- The $X_{\mathrm{max}}$ analysis of ad hoc data that is compatible with the Auger composition model via TA reconstruction is being studied in order to know how well the TA detector distinguishes between the Auger mixed composition and the pure proton composition.

### Low Energy Extension

The TA Low Energy Extension (TALE) will enable detailed studies of the energy spectrum and composition from $10^{16.5}$ eV upwards. Previous experiments reported the second knee in the cosmic-ray spectrum around the $10^{17}$-eV decade. The energy scales of these detectors differed by about a factor of two, so the energy at which this spectral break occurs is quite uncertain. There is a possibility that the transition from galactic cosmic rays to extragalactic cosmic rays occurs in this energy region. Thus we expect to observe the transition from heavier to lighter composition. A 14-TeV center-of-mass collision at the LHC corresponds to a proton of about $10^{17}$ eV colliding with another proton at rest. The cosmic-ray data observed by TALE could be compared with the air shower MC simulation tuned by the results of the LHC experiments.

Ten additional TALE FDs view 31°–59° in elevation angle, and are constructed from refurbished HiRes-II telescopes.

The TALE infill SD array consists of approximately 100 scintillation counters, which are identical to those of the TA SD array. These counters have graded spacings, ranging from 400 m near the FD to 600 m further away, which merge with the TA SD array at its northwestern corner. The TALE FD operation was commenced in the spring of 2013. About one third of the surface detectors were deployed at this time. Figure 17 shows an air shower event recorded with the combined TA MD and TALE FDs, and TALE SDs.

The Non-Imaging CHErenkov (NICHE) array is proposed to cover an energy range of $10^{15.8}$ to $10^{18}$ eV [33]. With an array of simple Cherenkov counters (PMTs looking upwards) deployed within the TALE infill array, we can use counter timing to reconstruct the shower geometry, counter pulse heights to reconstruct the shower energy, and counter signal widths to reconstruct $X_{\rm max}$.

**TA×4 proposal**

The TA result is consistent with the proton LSS model with GZK suppression, and there are some indications of anisotropy of arrival directions of highest-energy cosmic rays at a level of $3\sigma$. Based on this picture, we propose TA×4, which quadruples the SD array by building additional 500 counters of the current TA SD design, and deploying them in a square grid with 2.08-km spacing [34]. Including the existing TA SD, this array would reach an overall design size of $\sim$3000 km$^2$. The new array would need an FD overlooking it to confirm the energy scale and increase the number of hybrid events. This FD will be formed from additional reconditioned HiRes telescopes. The layout of TA×4 is shown in Figure 18. Assuming two-year construction and three-year observation for additional SD array and FD and five-year observation by the current TA, we expect the equivalent of 20 and 14 years of TA SD and hybrid exposures, respectively, by adding the 6-year data recorded so far, After five years, the recorded data will clarify anisotropy of arrival directions of highest-energy cosmic rays, which can be originated from the matter structure or extreme phenomena in the nearby universe, with a significance greater than $5\sigma$ if the correlation continues at the current level.

**R&D for future detectors with larger aperture**

To collect much better statistics at the highest energies, significantly larger detectors are needed to identify sources via anisotropy studies. Because of the prohibitive cost, it may be difficult to build a sufficiently large detector using existing technologies. Hence, it is important to explore new detection techniques.

It is advantageous that the FD on the ground detects air showers at a distance, but the FD has only a 10% duty cycle. Radio echoes from EASs have not been proven to be a successful technology. The TA RAdar Experiment (TARA) provides a controlled test of the bistatic radar technique, and is now operating a 40-kW transmitter at 54.1 MHz in the TA site, with receivers located 40 km away, west of the SD [35]. This project aims to look for coincidences between radar signals and either the SD or FD of TA.

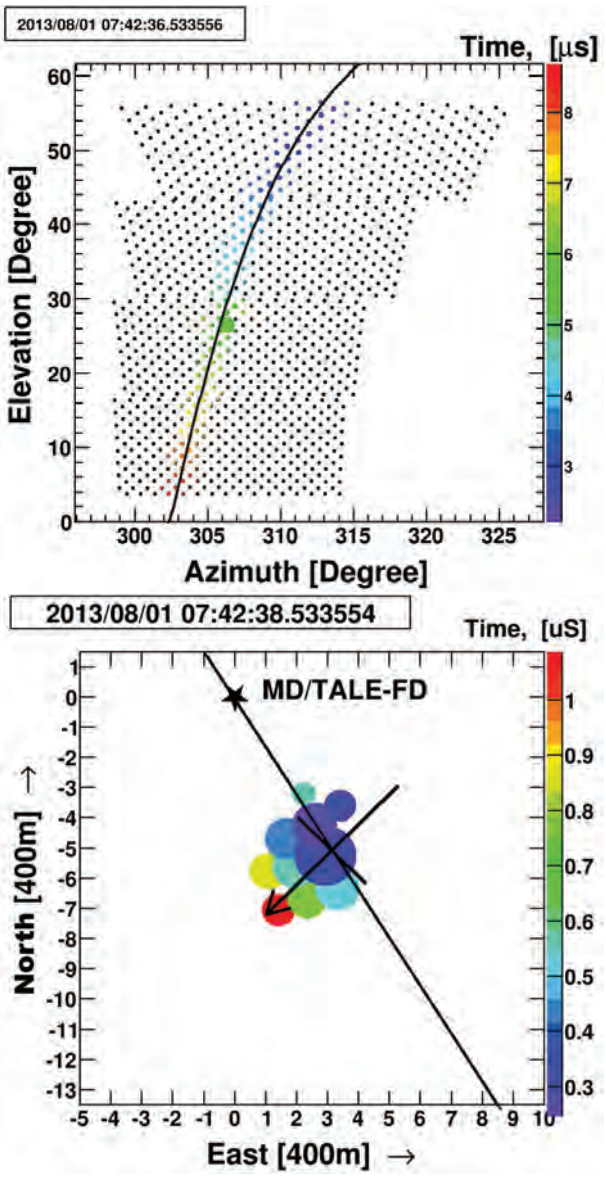


Fig. 17. An air shower event recorded with the combined TA MD and TALE FDs, and TALE SDs. In the first panel, the top two cameras correspond to the TALE and the bottom two cameras correspond to the TA MD. The circles represent the PMTs that were hit, whereas the points represent PMTs that were not hit. The solid line shows the reconstructed shower-detector plane. The second panel shows the corresponding SD hit map. The arrow and the cross point denote the arrival direction and the core position of the reconstructed shower, respectively.

JEM-EUSO is a new type of observatory that will utilize very large volumes of the earth's atmosphere as a detector of the highest-energy cosmic rays in the Universe. It will be mounted to the International Space Station (ISS) at an altitude of approximately 400 km. The sensor is a very wide-field, very fast, and large telescope, and observes brief UV flashes in the earth's atmosphere caused by highest-energy cosmic rays. In ICRR, we preliminarily set up the calibration system of Multi-Anode PMTs (MAPMT) which will be used at the focal surface detector of JEM-EUSO [36]. The test of JEM-EUSO prototype is been performed at a TA FD site.

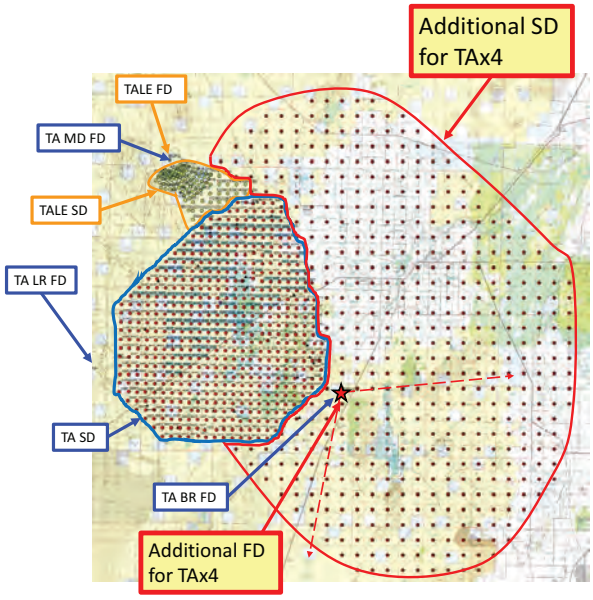


Fig. 18. The layout of the proposed TA×4. The array of 507 SDs (red filled circles inside a blue closed curve) is the current TA SD array. There are three TA FD stations (MD to the north, LR to the west, and BRM to the east of the TA array). The array of surface detectors (yellow filled circles inside an orange closed curve) to the north of the TA SD array is the TALE SD array. An additional array of 500 surface detectors (rouge filled circles inside a red curve) for TA×4 is located to the east of the TA SD array. An additional FD station with refurbished HiRes telescopes for TA×4 is located at the BRM FD site and views to the southeast as denoted by red dashed lines.

### *Summary*

The TA confirmed flux suppression above $5.68 \times 10^{19}$ eV, which is consistent with the GZK suppression expected for protons, with a statistical significance of $5.74\sigma$ and the ankle at $5.04 \times 10^{18}$ eV. The preliminary $X_{\rm max}$ measurement above $10^{18.2}$ eV is consistent with QGSJET-II-03 proton model. We found an indication of a cluster of cosmic rays with energy greater than $5.7\times10^{19}$ eV by oversampling using 20°-radius circles. Its significance appearing in an isotropic cosmic-ray sky is $3.7\times10^{-4}$ ($3.4\sigma$). Analyses of these highest-energy cosmic-ray arrival directions for correlations with AGNs, correlations with the LSS proton model, and autocorrelation show a hint of anisotropy at a level of $2\sigma$ to $3\sigma$.

The TA results suggest that anisotropy of arrival directions of highest-energy cosmic rays could be related to the matter distribution or extreme phenomena in the nearby universe. We propose to build TA×4, an extension of the SD area by a factor of four and one FD station. After five years, the expanded array will provide 20 years of TA SD data and 14 years of TA hybrid data by adding 6 years of TA data taken before TA×4. The signal at a level of $3\sigma$ in the current anisotropy studies is expected to result in an observation at more than $5\sigma$. And we will have more events for the measurement of energy spectrum and $X_{\rm max}$.

TA, TALE, and the proposed TA×4 and NICHE will provide important measurements of the spectrum, composition, and anisotropy from the knee region up over five decades in energy, with a single energy scale calibrated with the ELS.

For the future detectors with larger aperture,the R&D of a new technology investigating the detection of radio echoes from EASs (TARA) and JEM-EUSO prototype test are been performed in the TA site. The preliminary calibration test of JEM-EUSO MAPMTs has just started in ICRR.

## Bibliography

[1] T. Abu-Zayyad *et al.*, Astrophys. J. Lett. 768 (2013) L1 (5pp).

[2] K. Greisen, Phys. Rev. Lett. 16 (1966) 748-750.

[3] G.T. Zatsepin and V.A. Kuz'min, JETP Lett. 4 (1966) 78-80.

[4] O.E. Kalashev and E. Kido, arXiv:1406.0735 [astro-ph.HE].

[5] A. Aab *et al.*, arXiv:1307.5059.

[6] T. Abu-Zayyad *et al.*, Astropart. Phys. 48 (2013) 16-24.

[7] D. Ikeda *et al.*, ICRC 2013 #0358.

[8] M. Allen *et al.*, ICRC 2013 #0794.

[9] D. Bergman *et al.*, ICRC 2013 #0221.

[10] R.U. Abbasi *et al.*, Phys. Rev. Lett. 104 (2010) 161101.

[11] Y. Tameda *et al.*, ICRC 2013, #0512.

[12] T. Abu-Zayyad et al., Phys. Rev. D 88 (2013) 112005.

[13] G. Rubtsov *et al.*, ICRC 2013, #0149.

[14] T. Abu-Zayyad *et al.*, Astrophys. J. 757 (2012) 26 (11pp).

[15] P. Tinyakov *et al.*, ICRC 2013, #0935.

[16] P. Tinyakov *et al.*, ICRC 2013, #1033.

[17] T. Abu-Zayyad *et akl.*, Astrophys. J. 777 (2013) 88 (8pp).

[18] J. Abraham *et al.*, Science 318 (2007) 939; J. Abraham *et al.*, Astropart. Phys. 29 (2008) 188-204.

[19] P. Abreu *et al.*, Astropart. Phys. 34 (2010) 315-326.

[20] T. Jarrett, arXiv:astro-ph/0405069.

[21] R.U. Abbasi *et al.*, Astrophys. J. Lett. 790 (2014) 21.

[22] K. Kawata *et al.*, ICRC 2013, #0310.

[23] K. Kawata *et al.*, ICRC 2013, #0311.

[24] R. Abbasi *et al.*, Astrophys. J. 29 (2008) 77.

[25] F. Kakimoto *et al.*, Nucl. Instrum. and Meth. Phys. Res. A 372 (1996) 527.

[26] B. Keihauer *et al.*, arXiv:1210.1319.

[27] http://www.epj-conferences.org/index.php?option=com_toc&url/articles/epjconf/abs/2013/14/contents/contents.html

[28] M. Ave *et al.*, Astropart. Phys. 42 (2013) 90.

[29] T. Shibata *et al.*, ICRC 2013, #0507.

[30] R. Engel *et al.*, ICRC 2013, #1200.

[31] T. Yamamoto *et al.*, ICRC 2013, #1003.

[32] T. Abu-Zayyad *et al.*, arXiv:1310.0647 [astro-ph.HE].

[33] J. Krizmanic *et al.*, ICRC 2013, #0365.

[34] H. Sagawa *et al.*, ICRC 2013, #0121.

[35] J. Belz *et al.*, ICRC 2013 #1192.

[36] M. Casolino *et al.* ICRC 2013, #1213.

## Tibet AS$\gamma$ Project

[Spokespersons : M. Takita]
ICRR, The Univ. of Tokyo, Kashiawa, Chiba 277-8582

### *Experiment*

The Tibet air shower experiment has been successfully operated at Yangbajing (90°31' E, 30°06' N; 4300 m above sea level) in Tibet, China since 1990. It has continuously made a wide field-of-view (approximately 2 steradian) observation of cosmic rays and gamma rays in the northen sky.

The Tibet I array was constructed in 1990 and it was gradually upgraded to the Tibet II by 1994 which consisted of 185 fast-timing (FT) scintillation counters placed on a 15 m square grid covering 36,900 m$^2$, and 36 density (D) counters around the FT-counter array. Each counter has a plastic scintillator plate of 0.5 m$^2$ in area and 3 cm in thickness. All the FT counters are equipped with a fast-timing 2-inch-indiameter photomultiplier tube (FT-PMT), and 52 out of 185 FT counters are also equipped with a wide dynamic range 1.5-inch-indiameter PMT (D-PMT) by which we measure up to 500 particles which saturates FT-PMT output, and all the D-counters have a D-PMT. A 0.5 cm thick lead plate is put on the top of each counter in order to increase the counter sensitivity by converting gamma rays into electron-positron pairs in an electromagnetic shower. The mode energy of the triggered events in Tibet II is 10 TeV.

In 1996, we added 77 FT counters with a 7.5 m lattice interval to a 5,200 m$^2$ area inside the northern part of the Tibet II array. We called this high-density array Tibet HD. The mode energy of the triggered events in Tibet HD is a few TeV.

In the late fall of 1999, the array was further upgraded by adding 235 FT-counters so as to enlarge the high-density area from 5,200 m$^2$ to 22,050 m$^2$, and we call this array and further upgraded one Tibet III. In 2002, all of the 36,900 m$^2$ area was covered by the high-density array by adding 200 FT-counters more. Finally we set up 56 FT-counters around the 36,900 m$^2$ high density array and equipped 8 D-counters with FT-PMT in 2003. At present, the Tibet air shower array consists of 761 FT-counters (249 of which have a D-PMT) and 28 D-counters as in Fig. 19.

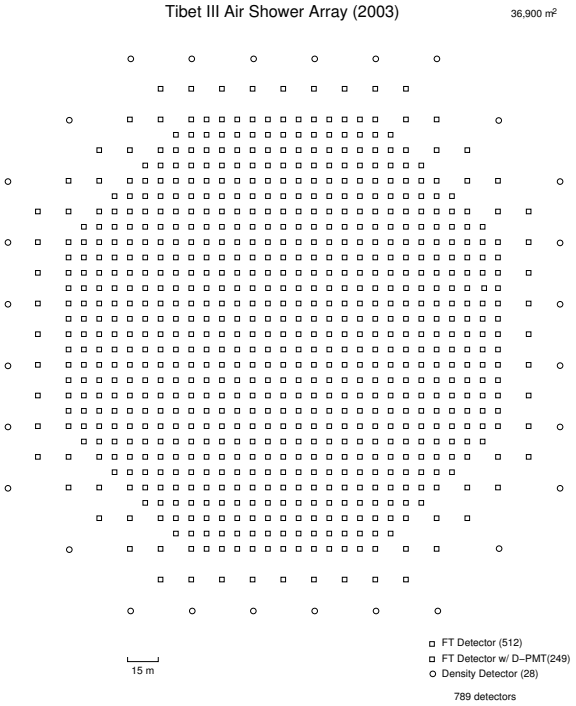


Fig. 19. Schematic view of Tibet III.

The performance of the Tibet air shower array has been well examined by observing the Moon's shadow (approximately 0.5 degrees in diameter) in cosmic rays. The deficit map of cosmic rays around the Moon demonstrates the angular resolution to be around 0.9° at a few TeV for the Tibet III array. The pointing error is estimated to be better than $\sim$0.01°, as shown in Fig. 20, by displacement of the shadow's center from the apparent center in the north-south direction, as the east-west component of the geomagnetic field is very small at the experimental site. On the other hand, the shadow center displacement in the east-west direction due to the geomagnetic field enables us to spectroscopically estimate the energy scale uncertainty at $\pm$12 % level, as shown in Fig. 21. Thus, the Tibet air shower experiment introduces a new method for energy scale calibration other than the conventional estimation by the difference between the measured cosmic-ray flux by an air shower experiment and the higher-energy extrapolation of cosmic-ray flux measured by direct measurements by baloon-borne or satellite experiments.

### *Physics Results*

Our current research theme is classified into 4 categories:
(1) TeV celestial gamma-ray point/diffuse sources,

(2) Chemical composition and energy spectrum of primary cosmic rays in the knee energy region,

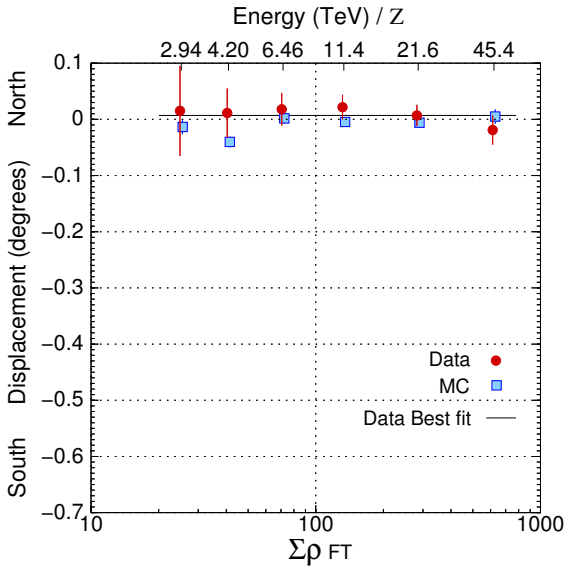


Fig. 20. From [1]. The Moon's shadow center displacement from the apparent position in the north-south direction as a function of energy, observed by Tibet III.

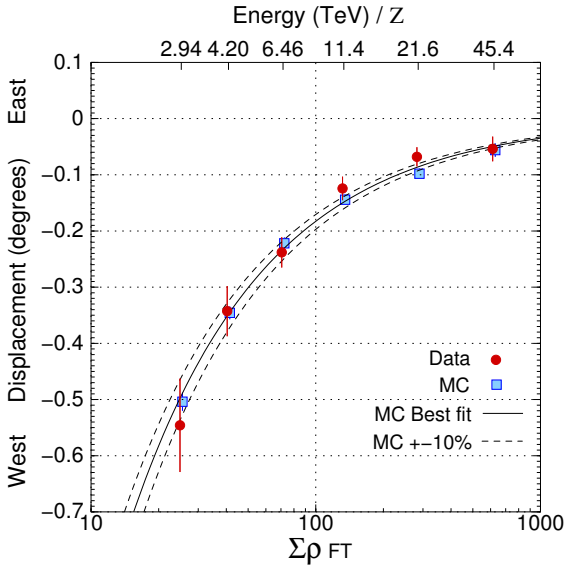


Fig. 21. From [1]. The Moon's shadow center displacement from the apparent positionin the east-west direction as a function of energy, observed by Tibet III.

(3) Cosmic-ray anisotropy in the multi-TeV region with high precision,

(4) Global 3-dimensional structure of the solar and interplanetary magnetic fields by observing the Sun's shadow in cosmic rays.

We will introduce a part of the results obtained in this fiscal year.

An understanding of the structure of the Sun's magnetic field between it and the Earth is essential if humanity is to venture into space. However, it is extremely difficult to directly observe the coronal magnetic structure within the Earth's or-

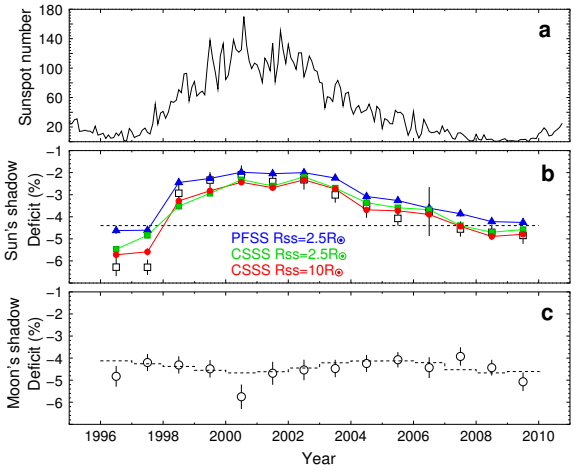


Fig. 23. From Ref. [2]. Temporal variations of (a) the monthly mean sunspot number, (b) the deficit intensity due to the Sun's shadow and (c) the deficit intensity due to the Moon's shadow. The open squares in the panel (b) are the observed central deficit ($D_{\rm obs}$). The blue triangles, green squares and red circles indicate the central deficits ($D_{\rm MC}$) by the MC simulations assuming the PFSS ($R_{\rm ss}$ = $2.5R_{\odot}$), the CSSS ($R_{\rm ss}$ = $2.5R_{\odot}$) and the CSSS ($R_{\rm ss}$ = $10.0R_{\odot}$) models, respectively. The dashed lines in the panels (b) and (c) are the deficits expected from the apparent angular size of the Sun and the Moon.

bit, and while spacecraft such as Voyager and Ulysses have carried out some observations, the solar neighborhood is an extremely harsh environment characterized by high temperatures and high levels of radiation. Even the latest spacecraft cannot get close to the Sun, and as a result our understanding of this region is limited.

The Tibet AS $\gamma$ experiment observed the Sun's shadow of cosmic rays at 10 TeV energies from 1996 to 2009, created when it shields galactic cosmic rays reaching the Earth, as is shown in Fig. 22.

The coronal magnetic field deflects these charged particles as they pass near the Sun, causing variation in the form of the Sun's shadow. The analyzed data were recorded over the 14-year period from 1996 to 2009, and a correlation was discovered between the 11-year solar cycle and this variation, as shown in Fig. 23. The stable size of the Moon's shadow in cosmic rays over the same period demonstrates that the systematic uncertainty is negligible.

We have also developed and performed numerical simulations of the Sun's shadow in galactive cosmic rays, based on two major coronal magnetic field models - the Potential Field Source Surface (PFSS), and the Current Sheet Source Surface (CSSS). The PFSS model leaves out the effect of the electric current in the vicinity of the Sun on the structure of the coronal magnetic field, while the CSSS model assumes the effect of the electric current. The magnetic field lines near the Sun are drawn in Fig. 24 in both cases.

The simulation of the trajectories of galactic cosmic rays based on the two models found that the CSSS model better describes the size variation of the Sun's shadow, as shown in Fig. 23.

This is the world's first and most successful analysis of the coronal magnetic structure using the data obtained by the observation of the cosmic ray shadow of the Sun. This re-

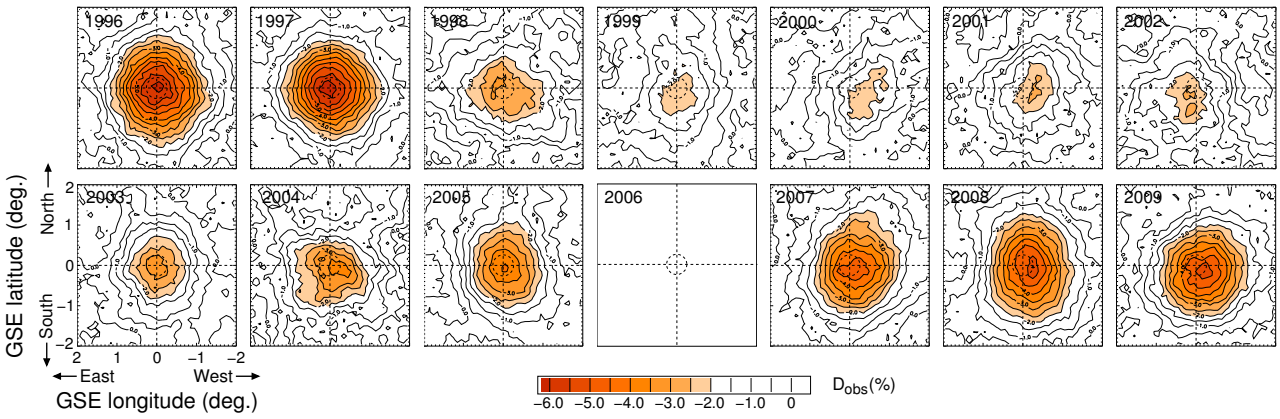


Fig. 22. From Ref. [2]. Year-to-year variation of the observed Sun's shadow between 1996 and 2009. Each panel displays a 2 dimensional contour map of the observed flux deficit ($D_{\rm obs}$).The map in 2006 is omitted because of insufficient statistics for drawing a map.

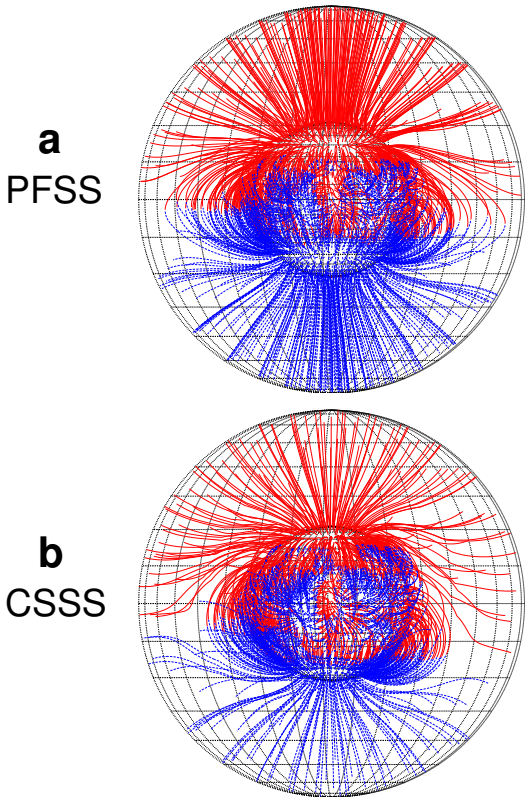


Fig. 24. From Ref. [2]. Magnetic field line structures calculated using (a) the PFSS model and (b) the CSSS model in CR1910 (Year 1996), in a region between the photosphere and the source surface at 2.5$R_{\odot}$, represented by the inner and outer spheres, respectively. The red (blue) lines represent the field lines directing away from (toward) the photosphere.

search provides a new approach to exploring the Sun's magnetic structure and, with future increased in accuracy, should provide even more detailed knowledge of the magnetic filed between the Sun and the Earth. This research employed the phenomenon that the path of charged cosmic rays is bent when it passes through a magnetic field, and was made possible by the long-term accumulation of cosmic radiation data over a period of 14 years, and is a major step forward in the long-term observation of cosmic radiation. The paper from this result was highlighted as one of the "Editor's Suggestions" in Physical Review Letters (PRL) in 2013. The American Physical Society (APS) also featured this paper on its website with short summary: Synopsis: Catching Rays in the Sun' Shadow.

### *Other Activities*

The emulsion-pouring facilities can meet the demands for making any kind of nuclear emulsion plates which are used for cosmic ray or accelerator experiments. The thermostatic emulsion-processing facilities are operated in order to develop nuclear emulsion plates or X-ray films. Using these facilities, it is also possible to make and develop emulsion pellicles in 600-micron thickness each. In this way, these facilities have been open to all the qualified scientists who want to carry out joint research programs successfully. Of recent, however, the shrinking demand for the facilities let us decide that we should suspend calls for joint research programs to utilize the emulsion-pouring facilities, starting from 2012.

### *Future Plans*

(1) Chemical composition of primary cosmic rays making the knee in the all-particel energy spectrum

We have measured the energy spectra of primary cosmic-ray protons, heliums, all particles around the knee energy region. The main component responsible for making the knee structure in the all particle energy spectrum is heavier nulei than helium. The next step is to identify the chemical component making the knee in the all particle energy spectrum. We have a plan to install an Yangbajing Air shower Core detector array (YAC) around the center of Tibet III to distinguish the chemical component making the knee. We completed construction of YAC2 ($\sim$100 detectors over $\sim$160m$^2$ in area), as is shown in Fig. 25, and started data-taking in March 2013. YAC2 aims at mainly studying the energy specta of proton and helium components in the knee energy region.

Currently, we are planning to set up YAC3 ($\sim$400 detectors over $\sim$5000m$^2$ in area) to measure the iron flux in the knee energy region.

Fig. 25. YAC2 set up at Yangbajing.

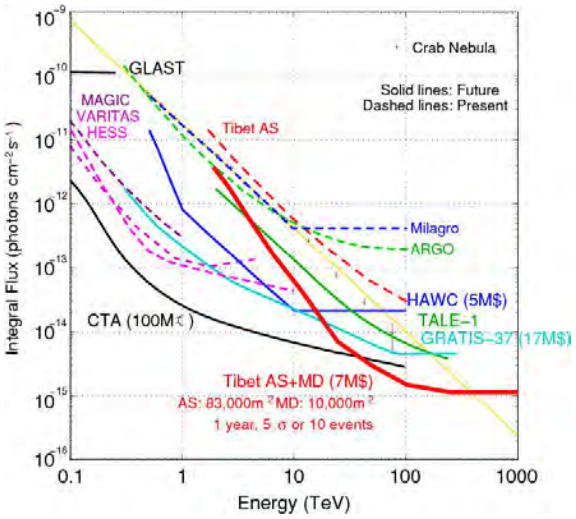


Fig. 26. Tibet AS + MD (red curve) integral flux sensitivity ($5\sigma$ or 10 events/1yr) for a point source.

(2) Gamma-ray astronomy in the 100 TeV region

We have a plan[3] to construct a large ($\sim 10,000\,\mathrm{m}^2 \times 1.5$m deep) underground ($\sim 2.5$ m soil+concrete overburden) water Cherenkov muon detector array (Tibet MD) around an extended version (Tibet AS, $\sim$83,000 m$^2$) of Tibet III. By Tibet AS + MD, we aim at background-free detection of celestial point-source gamma rays in the 100 TeV region (10 TeV – 1000 TeV) with world-best sensitivity and at locating the origins of cosmic rays accelerated up to the knee energy region in the northern sky. The measurement of cut off energies in the energy spectra of such gamma rays in the 100 TeV region may contribute significantly to understanding of the cosmic-ray acceleration limit at SNRs. Search for extremely diffuse gamma-ray sources by Tibet AS + MD, for example, from the galactic plane or from the Cygnus region may be very intriguing as well. Above 100 TeV, the angular resolution of Tibet AS with 2-steradian wide field of view is $0.2^\circ$ and the hadron rejection power of Tibet MD is 1/10000. The proposed Tibet AS + MD, demonstrated in Fig. 26, has the world-best sensitivity in the 100 TeV region, superior to HESS above 10-20 TeV and to CTA above 30-40 TeV.

In addition to unknown point-like sources, we expect to detect established sources in the 100 TeV region: TeV J2032 + 4130, HESS J1837-069, Crab, MGRO J2019+37, MGRO J1908+06, Milagro candidate sources, Mrk421, Mrk501 are sufficiently detectable and Cas A, HESS J1834-087, LS I+63 303, IC443 and M87 are marginal.

Furthermore, our integral flux sensitivity to diffuse gamma rays will be the world-best as well. The diffuse gamma rays from the Cygnus region reported by the Milagro group and also diffuse gamma-rays from the galactic plane will be clearly detected. Diffuse gamma-rays of extragalacitic origin may be an interesting target as well.

In fall, 2007, a prototype underground muon detector, composed of two 52m$^2$ water pools, was successfully constructed in Tibet to demonstrate the technical feasibility, cost estimate, validity of our Monte Carlo simulation. Data analyses demonstrate that our MC simulation reproduces real data quite reasonably.

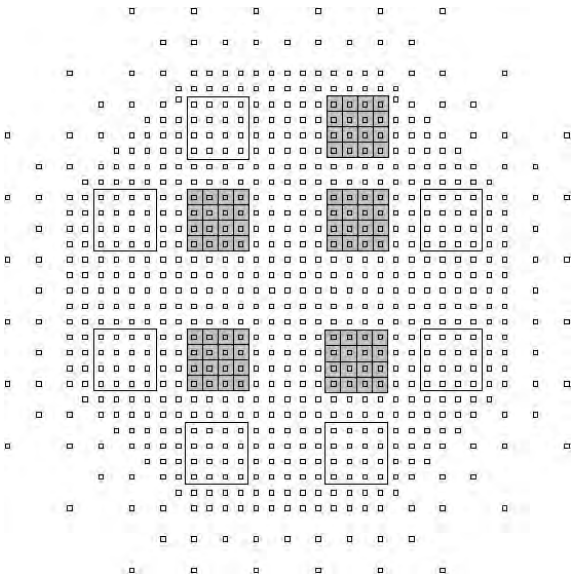

Fig. 27. The 5 shaded squares represent the constructed 5 MD pools.

In March 2013, construction of 5/12 of the full-scale MD, as is shown in Fig. 27, was successfully completed and data-taking started. One of the detector cell filled with water is demonstrated in Fig. 28

## Bibliography

### Papers in refereed journals

[1] "Multi-TeV Gamma-Ray Observation from the Crab Nebula Using the Tibet-III Air Shower Array Finely Tuned by the Cosmic-Ray Moon's Shadow", M. Amenomori *et al.*, Astrophysical Journal, **692** , 61-72 (2009).

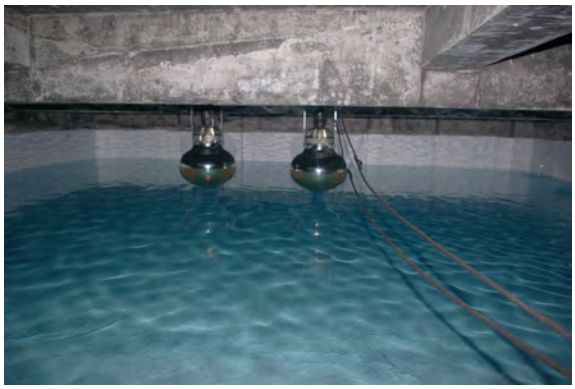

Fig. 28. PMTs mounted in a MD cell filled with water.

[2] "Probe of the Solar Magnetic Field Using the "Cosmic-Ray Shadow of the Sun", M. Amenomori *et al.*, Physical Review Letters, **111** , 011101-1-011101-5 (2013).

[3] "Exploration of a 100 TeV gamma-ray northern sky using the Tibet air-shower array combined with an underground water-Cherenkov muon-detector array", T.K. Sako *et al.*, Astroparticle Physics, **32** , 177-184 (2009).

### Papers in conference proceedings

The Tibet AS$\gamma$ Collaboration

M. Amenomori,[1] X. J. Bi,[2] D. Chen,[3] T. L. Chen,[4] W. Y. Chen,[2] S. W. Cui,[5] Danzengluobu,[4] L. K. Ding,[2] C. F. Feng,[6] Zhaoyang Feng,[2] Z. Y. Feng,[7] Q. B. Gou,[2] Y. Q. Guo,[2] H. H. He,[2] Z. T. He,[5] K. Hibino,[8] N. Hotta,[9] Haibing Hu,[4] H. B. Hu,[2] J. Huang,[2] H. Y. Jia,[7] L. Jiang,[2] F. Kajino,[10] K. Kasahara,[11] Y. Katayose,[12] C. Kato,[13] K. Kawata,[14] Labaciren,[4] G. M. Le,[2] A. F. Li,[15,6,2] H. J. Li,[4] W. J. Li,[2,7] C. Liu,[2] J. S. Liu,[2] M. Y. Liu,[4] H. Lu,[2] X. R. Meng,[4] K. Mizutani,[11,16] K. Munakata,[13] H. Nanjo,[1] M. Nishizawa,[17] M. Ohnishi,[14] I. Ohta,[18] S. Ozawa,[11] X. L. Qian,[6,2] X. B. Qu,[2] T. Saito,[19] T. Y. Saito,[20] M. Sakata,[10] T. K. Sako,[12] J. Shao,[2,6] M. Shibata,[12] A. Shiomi,[21] T. Shirai,[8] H. Sugimoto,[22] M. Takita,[14] Y. H. Tan,[2] N. Tateyama,[8] S. Torii,[11] H. Tsuchiya,[23] S. Udo,[8] H. Wang,[2] H. R. Wu,[2] L. Xue,[6] Y. Yamamoto,[10] Z. Yang,[2] S. Yasue,[24] A. F. Yuan,[4] T. Yuda,[14] L. M. Zhai,[2] H. M. Zhang,[2] J. L. Zhang,[2] X. Y. Zhang,[6] Y. Zhang,[2] Yi Zhang,[2] Ying Zhang,[2] Zhaxisangzhu,[4] X. X. Zhou[7]

[1]*Department of Physics, Hirosaki University, Hirosaki 036-8561, Japan*
[2]*Key Laboratory of Particle Astrophysics, Institute of High Energy Physics, Chinese Academy of Sciences, Beijing 100049, China*
[3]*National Astronomical Observatories, Chinese Academy of Sciences, Beijing 100012, China*
[4]*Department of Mathematics and Physics, Tibet University, Lhasa 850000, China*
[5]*Department of Physics, Hebei Normal University, Shijiazhuang 050016, China*
[6]*Department of Physics, Shandong University, Jinan 250100, China*
[7]*Institute of Modern Physics, SouthWest Jiaotong University, Chengdu 610031, China*
[8]*Faculty of Engineering, Kanagawa University, Yokohama 221-8686, Japan*
[9]*Faculty of Education, Utsunomiya University, Utsunomiya 321-8505, Japan*
[10]*Department of Physics, Konan University, Kobe 658-8501, Japan*
[11]*Research Institute for Science and Engineering, Waseda University, Tokyo 169-8555, Japan*
[12]*Faculty of Engineering, Yokohama National University, Yokohama 240-8501, Japan*
[13]*Department of Physics, Shinshu University, Matsumoto 390-8621, Japan*
[14]*Institute for Cosmic Ray Research, University of Tokyo, Kashiwa 277-8582, Japan*
[15]*School of Information Science and Engineering, Shandong Agriculture University, Taian 271018, China*
[16]*Saitama University, Saitama 338-8570, Japan*
[17]*National Institute of Informatics, Tokyo 101-8430, Japan*
[18]*Sakushin Gakuin University, Utsunomiya 321-3295, Japan*
[19]*Tokyo Metropolitan College of Industrial Technology, Tokyo 116-8523, Japan*
[20]*Max-Planck-Institut für Physik, München D-80805, Deutschland*
[21]*College of Industrial Technology, Nihon University, Narashino 275-8576, Japan*
[22]*Shonan Institute of Technology, Fujisawa 251-8511, Japan*
[23]*Japan Atomic Energy Agency, Tokai-mura 319-1195, Japan*
[24]*School of General Education, Shinshu University, Matsumoto 390-8621, Japan*

## The Ashra Project

[Spokesperson: Makoto Sasaki]
ICRR, Univ. of Tokyo, Kashiwa, Chiba 277-8582
In collaboration with the members of:
ICRR, University of Tokyo, Kashiwa, Japan; Toho University, Funabashi, Japan; University of Hawaii at Manoa, Honolulu, USA; University of Hawaii at Hilo, Hilo, USA; Nagoya University, Nagoya, Japan; Kanagawa University, Yokohama, Japan

### *Overview*

Ashra (*All-sky Survey High Resolution Air-shower detector*) [1, 2, 3, 4] is a project to build an unconventional optical telescope complex that images very wide field of view, covering 77% of the sky, yet with the angle resolution of a few arcmin, sensitive to the blue to UV light with the use of image intensifier and CMOS technology.

Detection of PeV-EeV neutrinos ($\nu$'s) is direct evidence for the acceleration of hadrons into the EeV range and of photo-pion interactions in a violent object such as GRBs[5]. The earth-skimming tau neutrino technique, which detects extensive air showers [6], has the advantage of providing a large

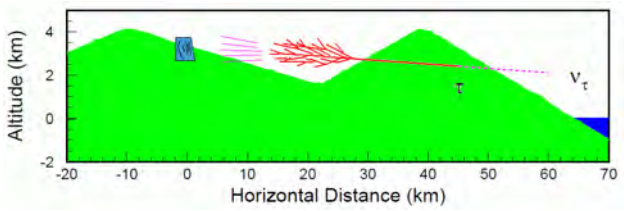


Fig. 29. Conceptual drawing of Cherenkov $\tau$ shower method. The right mountain is Mauna Kea and the left is Mauna Loa.

Fig. 30. The Ashra main and sub stations at the Mauna Loa site (top), and a light collector towards Mauna Kea (bottom).

target mass. The technique uses air shower produced by decay particles of tau leptons in the atmosphere as the observed signal. The air shower emits intense Cherenkov lights in front, which could be detected by the mountain or the ground faced detector (Figure 29). The method is realized by Ashra-1 experiment [7]. The air shower also emits isotropic fluorescence lights. In order to enhance the tau neutrino detectability, the detector should be capable of detecting fluorescence signal.

The observatory firstly consists of one main station having 12 detector units and two sub-stations having 8 and 4 detector units. One detector unit has a few light collecting systems with segmented mirrors. The main station and one of the sub stations were constructed on Mauna Loa (3,300 m) on Hawaii Island in 2007 as shown in Figure 30.

Since January 2012, we highly efficiently made physics observation runs (Observation03) with triple types of triggers for Cherenkov tau showers induced by earth-skimming tau neutrinos, Cherenkov cosmic ray showers, and optical flashes from transient objects like GRBs.

### *Ashra detector*

All-sky survey high-resolution air-shower detector (Ashra) is designed to hold 77% of the entire night sky in the field of view with a resolution of a few arcminutes. Ashra detector is a complex of unconventional optical light collectors (LCs) , each of those has 42° diameter field of view. An image of the optical collector is focused on the large electrostatic lens [8] followed by the image pipeline, which is shown in Figure 31. The image pipeline split and transport the image to both a trigger device and a high-gain, high-resolution complementary metal-oxide semiconductor image sensor.

Ashra will acquire optical images every 1 second with 1-second exposure without dead time. This enables us to explore optical transients, possibly associated with gamma ray bursts (GRBs), flares of soft gamma-ray repeaters (SGRs), supernovae explosion, and so on, in so far as they are brighter than $B \simeq 13$ mag, for which we expect 3-$\sigma$ signals.

The split image is transported a trigger device via the 4m long optical fiber bundle. The bundle is made of 500 $\mu$m $\phi$ optical fiber. $64 \times 64$ optical fibers are arranged to have $32mm \times 32mm$ square cross section. Central position of each fiber is arranged according to 500 $\mu$m lattice within the accuracy of less than $100\mu m$. The transmittance is measured to be greater than 85% including coupling loss at each end of the fiber.

One end of the bundle is connected to multi-anode PMTs. PMT signal is injected to the custom made trigger LSI . Each LSI chip has $16 \times 16$ pixels, each size of those is 500 $\mu$m $\times$ 500 $\mu$m. Total 4096 channels of 16 LSI chips are implemented on the ceramic board. In order to process different time scale lights, Cherenkov light and fluorescence light, band-pass frequency of the filter is designed to be adjustable by external voltage. The threshold level on each pixel can be chosen from 8 levels to compensate pixel-to-pixel sensitivity discrepancy.

"Wired OR" signal, summed signal of 64 pixels along axes, are sent to the FPGA based trigger circuit. Decision of the first level Cherenkov trigger is based on geometrical criteria. The aperture of one trigger pixel is $\sim 0.65° \times 0.65°$, adjacent two of which well contain Cherenkov lights from an air shower.

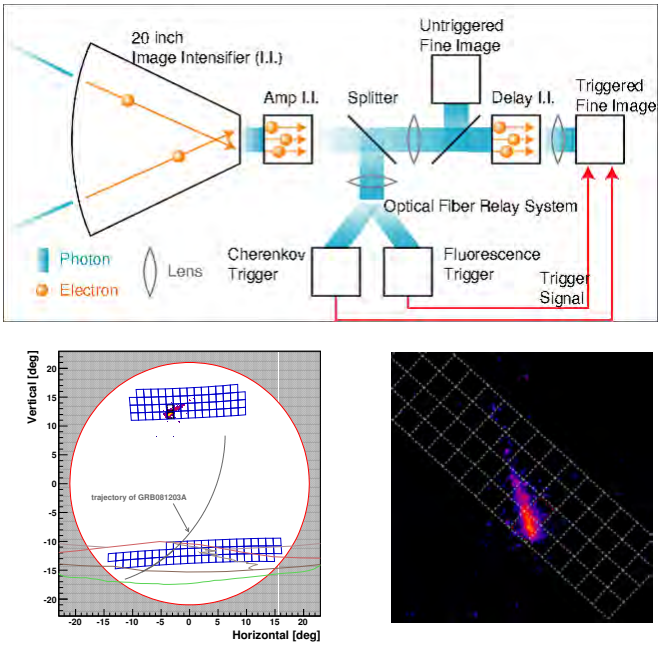


Fig. 31. Schematic view of Ashra image pipeline (top), trigger pixel configuration in FOV (bottom left) and real image of triggered 200ns-expusure for an air-shower (bottom right).

The calibration chain is designed to obtain not only an absolute energy scale to air shower measurement, but also uniformed sensitivity over the large field of view (positional) and in time (temporal). Environmental monitors systems, a cloud monitor, weather monitors, a far Lider and a near Lidar have already been installed or are ready for installation. Especially Ashra detector observes stars in the view every 1 second, which would give us an absolute calibration of the transparency of atmosphere. LED flasher system was developed in order to obtain positional and temporal flat calibration

of the detector sensitivity.

LED flasher is composed of a LED, a photo diode and optical lenses in a black box. Collimated light of $\lambda = 405nm$ is divided by a half mirror in two directions. One illuminates a photo diode monitoring LED luminous intensity and the other illuminates the input window of the photoelectric tube via off -focusing optical lenses. Thermal variations of LED luminosity and photo diode sensitivity were carefully studied using a thermostatic chamber. LED luminosity variable coefficient (Photo diode output variable coefficient) was measured to be -0.21ppc/$^\circ C$( -0.07ppc/$^\circ C$ ) in the temperature range from 35$^\circ C$ to 47$^\circ C$. Radiance uniformity was also measured to be sufficiently flat in the view; namely the variation was less than 1%.

### *Experiment and Observation*

Experiment of the Cherenkov light trigger was carried out at Ashra observational site on Mauna Loa in Hawaii. The trigger LSI module and the trigger board were installed on one LC and a half of the PMT channels are read out in place of old handmade discriminator module. The LC which dedicates Mauna Kea and the above sky to the view allows to observe the earth skimming tau neutrino and also extensive air showers. Pilot observation was carried out for a total of 44.4 hours in 2008 December [5, 7] Data was also taken in the 3rd observation period from January 2012 to end of February 2013, more than 1720 hours.

Arrays of trigger pixels and their aperture are shown in the field of view of the detector (Figure 31). Cherenkov light observation was carried out using this trigger pixel configuration. In Figure 31, shown are the boundary (large red circle) between the inside (open circle) and outside (hatched area) of the FOV of the Ashra-1 light collector, which faces Mauna Kea, and the layout of trigger pixel FOVs and blue boxes for Cherenkov $\tau$ shower observation [7]. We repositioned array of the trigger pixel FOVs (upper blue boxes) to check the detection sensitivity with ordinary cosmic-ray air showers at a higher elevation. Firing trigger pixels (thick blue boxes) of an observed image of a cosmic-ray air shower readout along the trigger (points) is overlaid. An extended portion of the trajectory of GRB081203A counterpart (circular arc), the segment of this trajectory used in the $\nu_\tau$ search (thick circular arc), the ridge lines of Mauna Kea (red) and Mauna Loa (green) mountains, the horizon, and Mauna Kea access road are shown. Observed cosmic-ray flux was consistent with Monte Carlo simulation in PeV to EeV region [7].

Gamma-ray bursts (GRBs) eject the most energetic outflows in the observed universe, with jets of material expanding relativistically into the surrounding interstellar matter with a Lorentz factor $\Gamma$ of 100 or more. Energy dissipation processes involving nonthermal interactions between particles are thought to play an important role in GRBs. The GRB standard model [9], which is based on internal/external shock acceleration, has been used to describe the general features of a GRB, but the jet structure and particle acceleration details remain observationally unresolved. In the context of the GRB standard model, the interaction of an expanding relativistic shell with the intersteller medium (ISM) involves two shocks: the forward shock, which explains observed multi-wavelength afterglow, and the reverse shock, which is predicted to produce a strong optical flash [10, 11]. The explanation of optical flashes by the reverse shock has led to some estimates of the initial Lorentz factor $\eta$ [11, 12]. The presence of accelerated protons at the GRB site must be a reality. The detection of PeV–EeV neutrinos ($\nu$s) from a GRB provides direct evidence for the acceleration of hadrons into the EeV range, and of photopion interactions in the GRB. Even the non-detection of neutrino can provide valuable information about GRB's key physical parameters such as the emission radius $R_d$, and the bulk Lorentz factor $\Gamma$ [13].

| Satellite | GRB Name | $t_{inFOV} - t_0$ [sec] |
|---|---|---|
| Swift | GRB081203A | $-1.2\times10^4 - 5.6\times10^3$ |
| Fermi | GRB090428 | $-8.1\times10^3 - 5.9\times10^3$ |
| Fermi | GRB090429C | $-4.1\times10^3 - 1.7\times10^3$ |
| Swift | GRB091024 | $-1.6\times10^3 - 3.3\times10^2$ |
| Fermi | GRB100216A | $-4.0\times10^3 - 1.1\times10^4$ |
| Swift | GRB100906A | $-1.0\times10^4 - 4.0\times10^3$ |
| Fermi | GRB120120 | $-1.4\times10^3 - 8.9\times10^3$ |
| Fermi | GRB120129 | $-1.6\times10^3 - 6.7\times10^3$ |
| Fermi | GRB120327 | $-9.9\times10^3 - 8.2\times10^1$ |
| Swift | GRB120911 | $-2.4\times10^4 - 6.8\times10^1$ |
| Fermi | GRB121019 | $-1.7\times10^3 - 7.3\times10^3$ |
| Swift | GRB121212A | $-5.8\times10^3 - 2.6\times10^4$ |
| Fermi | GRB130206 | $-3.3\times10^3 - 7.5\times10^4$ |
| Fermi | GRB130215 | $-2.7\times10^3 - 4.3\times10^2$ |

Table 1. Summary of coincidence events with satellite GRB triggers [16, 17]. List of gold-plated events which must be observable geometrically within the FOV of our light collector at satellite triggers during our observation time.

Ashra-1 acquires optical images every 1$\sim$6 s with short readout deadtime. This enables us to explore optical transients, possibly associated with violent objects such as GRBs in so far as they are brighter than $B = 12 \sim 13$ mag, for which we expect $3\sigma$ signals assuming 4 s exposure. The unique advantage is the on-time detection of the events without resorting to usual satellite alerts. In each detector unit FOV, 1$\sim$2 events per year are expected in coincodence with the Swift gamma-ray events. The total Ashra field of view that is wider than satellite instruments allows to detect more optical transients, including an interesting possibility for an optical flash, not visble with gamma-rays.

The earth-skimming tau neutrino ($\nu_\tau$) technique, which detects extensive air showers [6], has the advantage of a large target mass, since it uses air showers produced by decay particles of tau leptons ($\tau$s) in the atmosphere as the observed signals. $\tau$s emerge out of the side of the mountain or the ground facing the detector; they are the product of interactions between VHE $\nu_\tau$ and the earth matter they traverse. Above 1 EeV, air fluorescence observations based on the earth-skimming $\nu_\tau$ technique have been reported [14]. Ashra-1 has reported the first observational search for $\nu_\tau$ from a GRB based on the earth-skimming $\nu_\tau$ technique with air showers induced by $\tau$ decays (hereafter referred to as the Cherenkov $\tau$ shower method) [15]. It can achieve sufficient detection sensitivity in the PeV–EeV region to be useful in the search for $\nu$s originating from hadrons accelerated to EeV at astronomical objects.

Additional advantages of the Cherenkov $\tau$ shower method are its perfect shielding of cosmic-ray secondary particles, highly precise arrival direction determination for primary $\nu_\tau$ and negligible background contamination by atmospheric $\nu$s in the PeV–EeV energy range.

Two of the Ashra-1 light collectors has been used for optical flash observation, of which FOV centers are in the direction of 60° (0°N) and 12° (22.5°N) in the elevation (azimuthal) angles respectively. We recorded more than 3 million non-trigger reccuring images of the FOV of 0.83 sr for 5637 hr of 1121 night runs between June 28 in 2008 and March 23 in 2013. The observation time corresponds to 20 % of all time without the shutdown period for the maintenance and 95 % of the maximum observable time defined by the solar and the lunar conditions where the altitudes of the sun and the moon must be lower than -18° and 0° respectively with the moon fraction less than 0.2.

To investigate GRB optical emission, we define three specific observational time domains with respect to satellite triggers; precursor ($0<t_0$-$t_e<24$ hr), prompt ($t_s<t_0<t_e$), and afterglow ($0<t_s$-$t_0<3$ hr ) where $t_0$ is a satellite trigger time, $t_s$ is the time when the trajectry of the center position of GRB counter part object triggered by the satellite enters into a FOV of an Ashra-1 light collector and $t_e$ is the time when it exits the FOV. Throughout the above observation time for optical flashes and afterglows, we preselected and categolized 32 (86), 6 (21), and 1 (4) GRBs triggers by Swift (Fermi) satellite, which were circulated through The Gamma-ray Coordinates Network (GCN) [16, 17], into the three time domains respectively as optical transient cadidates. Futhermore, we selected gold-plated samples of 14 prompt GRB candidate events for our cross observation with Swift or Fermi satellites requiring the events triggered are reported as trigger type of GRB as summarized in Table1.

One of the Ashra light collectors built on Mauna Loa has the geometrical advantages of not only facing Mauna Kea, allowing it to encompass the large target mass of Mauna Kea in the observational FOV, but has also an appropriate distance of ∼30 km from Mauna Kea, yielding good observational efficiency when imaging air-shower Cherenkov lights which are directional with respect to the air-shower axis. Using the advanced features, we performed commissioning search for Cherenkov $\tau$ showers for 197.1 hr between October and December of 2008 and have already published [15]. We served limited 62 channels of photomultiplier tubes (PMTs) as trigger sensors prepared for the commissioning runs to cover the view of the surface area of Mauna Kea, maximizing the trigger efficiency for Cherenkov $\tau$ showers from Monte Carlo (MC) study. Adjacent-two logic was adopted to trigger the fine imaging, by judging discriminated waveform signals from each pixel of the multi-PMT trigger sensor. During the commissioning search period, ∼2 hr before the trigger of GRB081203A [21]. We accumulated nealy 44 million images with the air-shower Cherenkov light triggers for 1863 hr of 323 night runs of the $\nu_\tau$ search between January 12 in 2012 and March 23 in 2013.

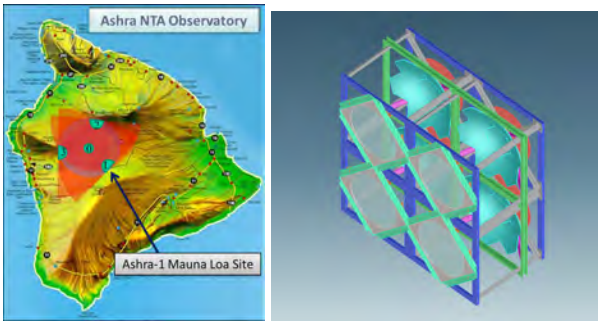


Fig. 32. NTA Observatory layout (left) and NTA detector unit of four same LCs (right).

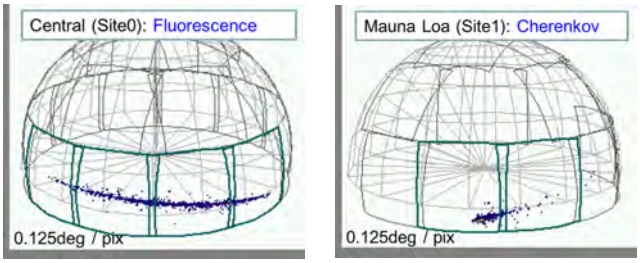


Fig. 33. Simulated event with $E_{\nu_\tau} = 10^{17}$eV: (left) fluorescence track image by Site0; (right) Cherenkov track image by Site1. Trigger pixel and fine image FOV angles are $0.5^\circ$ and $0.125^\circ$, respectively.

### *Prospects*

In this Ashra-1 experiment, we were performing device installation and specific observation in a step-by-step way to enhance the scientific impacts as shown in the previous sections. We have already made a referee journal publication of PeV-EeV tau neutrino search [20] as important physics results with the Ashra-1 detector unit adding to publications on the detector or methodorogical developments and circulations [8, 21, 22]. We are now preparing for a few physics publications from the optical observation data of the 2.5 years from the Obs01 to Obs02 as well as keeping highly efficient observation runs in Obs03 for optical transients, VHE CRs and tau neutrinos. Adding that, the R&D for the direct Cherenkov method applied to Ashra-1 has been granted and under development.

The planned full Ashra (Neutrino Telescope Array (NTA)) observatory consists of four sites: Site0-3, as shown in Fig. 32 (left), with the x-y-z coordinates and corresponding FOV coverage. Site1-3 form a 25 km triangle, observing the total air mass surrounded by Mauna Loa, Mauna Kea, and Hualalai. The central Site0 has full-sky coverage. Each site has a group of detector units each of which has several LC systems (Fig. 32 (right)) instrumented with segmented mirrors. Performance was studied based on Ashra-1 experience. Detailed design studies for the NTA detector are currently underway.

The z-axis points to zenith and y-axis points north, with z-coordinates determined from topography data. Site1-3 are the vertices of an equilateral triangle of side length 25 km, with Site0 at their geometric center. Site1 is located at ML-OS (on Mauna Loa) and Site2 at 25 km distant from ML-OS in the direction of the Kilohana Girl Scout Camp. To simulate the

performance of the Ashra NTA detector, we assume each LC has $32^\circ \times 32^\circ$ total FOV, $0.5^\circ \times 0.5^\circ$ for trigger pixel FOV, and $0.125^\circ \times 0.125^\circ$ image sensor pixel FOV. The Site0 system consist of 12 LCs in the lower, 8 LCs in the middle, and 4 LCs in the higher elevation angle regions which together cover the full-sky solid angle of $2\pi$ sr. The remaining sites have only 12 LCs in the lower elevation angle region covering $\pi$ sr. The bottom edge of the lower elevation angle region is defined to be $-9^\circ$ (below the horizon).

In our simulation program, we take density profile of the Earth, use the $\nu_\tau$ distribution from CTEQ4 citeGandhi96, inelasticity parameter from [29], and parameterize energy loss in Earth by citeTseng03,Dutta2001. We use $\tau$ decay from TAUOLA and air-shower generation of Gaisser-Hillas + NKG [30]. We use a constant average $\nu_\tau$ energy fraction of 40% (lab frame) from $\tau$ decays. The error from this approximation is found negligible. For detector simulation, we incorporate light collection and throughput with simplified triggering logic. Event reconstruction is not yet implemented. All candidate events must satisfy the trigger conditions (1) number of detected photoelectrons per LC $> 61$; (2) S/N estimated in track-associated 4 pixels $\times$ 64 pixels box (air-shower track included) $>4$ [31].

A simulated event with primary $\nu_\tau$ energy $E_{\nu_\tau} = 10^{17}$ eV consistent with the above conditions is shown in the r.h.s. of Fig. 33. The error for $\nu_\tau$ arrival direction reconstruction is $0.08^\circ$. Fig. 34 shows estimated effective detection areas simulated for $\nu_\tau$ from point source with azimuthal arrival direction. NTA can survey $\nu_\tau$ point source objects with the best-yet sensitivity in the detection solid angle for $\nu_\tau$ defined as $-30^\circ < \theta_{elev} < 0^\circ$ and $0^\circ < \phi_{azi} < 360^\circ$ , and for 10 PeV $< E_{\nu_\tau} < 1$ EeV. The location of NTA on Hawaii Island allows us to survey the galactic center for more than several hundred hours each year.

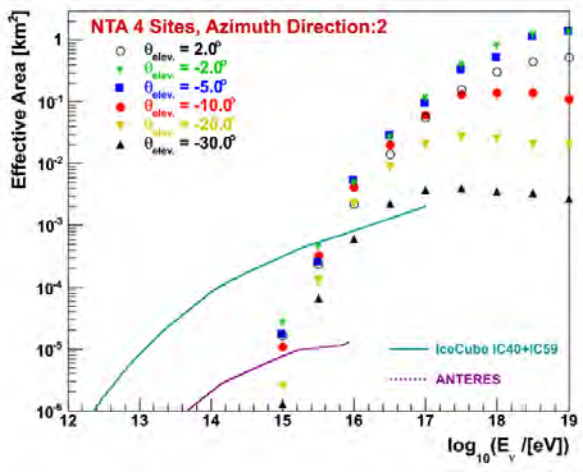


Fig. 34. Estimated effective detection areas simulated for $\nu_\tau$ from point source with azimuthal arrival direction $\phi_2$ of the Mauna Loa summit with respect to the central Site0, and dip angles $2.0^\circ$ (black open circle), $-2.0^\circ$ (green star), $-5.0^\circ$ (blue filled box), $-10.0^\circ$ (red filled circle), $-20.0^\circ$ (yellow filled triangle), and $-30.0^\circ$ (black filled triangle).

Further discussion on angular resolution and background simulation can be found in the LOI, which is to be published.

### *Preparation for Observation 4*

We are now preparing for the fourth observation period (Obs04) as a next step during the long shutdown after the Obs03 as well as proceeding several physics analysis streams using observed data. The aim of the Obs04 is primarily a commissioning of Ashra-1 as a fluorescence detector for holizontal air-showers with good sensitivity and well established detector calibration of statistically dominating further events.

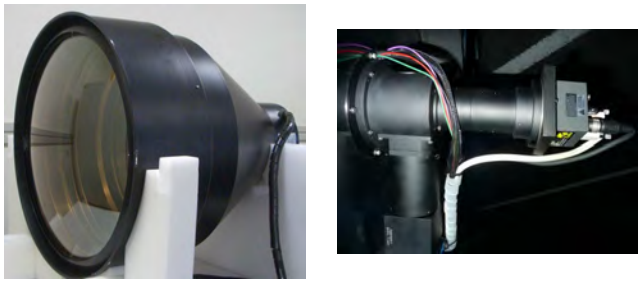

Fig. 35. PLI (left) and PIP (right) mounted on LC.

The photoelectric lens imaging tube (PLI) installed on the facul sphere of the Ashra-1 optical system and the image pipeline (PIP) following PLI have worked stably so far at the Mauna Loa observational site (Figure 35).

Fig. 36. Trigger decision board

For the readout of images from PLI and PIP, we uses a trigger decision processing board with programmable two field-programmable gate arrays (FPGAs) and one Digital Signal Processor (DSP). During Obs03, we used a trigger condition for Cherenkov light of air-shower image requring adjacent two triggered pixels as the first level and a global readout of the image just after the trigger decision. For the aim of fluorescence trigger and readout, we need to implement more complicated trigger logic to adapt to long sustained fluorescence signal with the typical duration of several micro seconds. We have been developing such control programs to be implemented onto the combination of the FPGAs and DSP installed on the board (Figure 36). The trigger decision processing board includes a function of automatic adjustment of the

threshold of the 1st level (exposure control) trigger to keep the total trigger frequence stable even if the night sky background change time to time due to natural weather or/and artificial conditions. The trigger decision processing board sends, to the fine image sensor with trigger (FST) as described later, the decided triggers of the 1st and 2nd levels with the addresses corresponding to 64×64 cell regions of FOV.

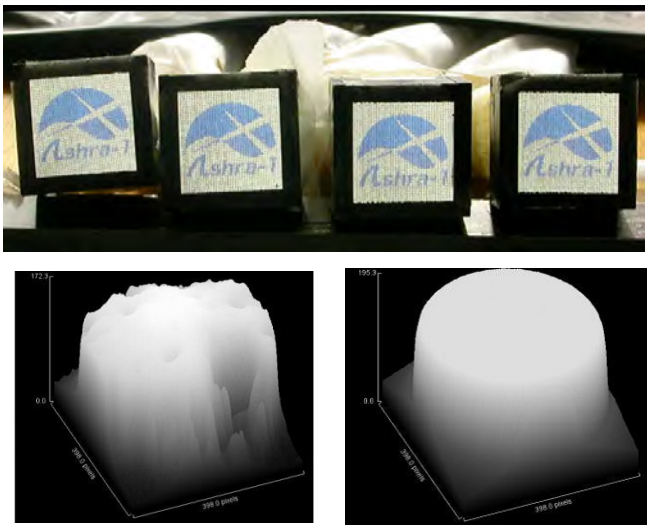

Fig. 37. Fiber bundles attached to PIP trigger ports (top), images of fiber ends before (bottom left) and after (bottom right) fine polish with the achieved transmittance more than 95%.

The PIP can split and relay the same image from the output of PLI into the trigger pixel sensor and fine image sensor with trigger (FST). To transmit the trigger image into trigger pixel sensor, we use the 64×64 optical fiber bundle with 4m length. The fiber bundles have been developed and assembled by Ogawa group of Toho University (Figure 37 top). The fabrication and assembling process has been established well. Particularly the technique of alignment and polish of the end of each optical fiber is essential. Now we have confirmed that the alignment accuracy is achieved to be within 0.1 mm and transmission of the 4m-length fiber to be more than 95% after the original technique of polishing the end of fibers (Figure 37 bottom).

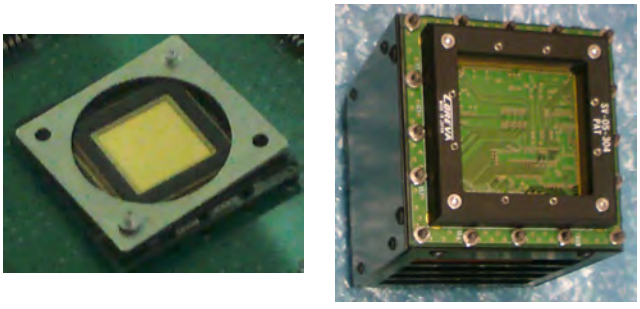

Fig. 38. FST CMOS sensor chip (left) and camera control box (right).

Comparing with Cherenkov image trigger, the fluorescence image trigger requres the trigger process to reduce the contamination of night sky background more severely. For the reason, we have developed custom fine image sensor with trigger (FST), which can start exposure of any of 64×64 subdivided cell regions on the sensor after the 1st level (exposure control) trigger signal and start readout to data acquisition computer through a Camera Link cable after the 2nd level (readout control) trigger signal sent from the trigger processor as described before. The FST chip with 2048×2048 pixels on 19 mm×19 mm area mounted on the camera box as shown in Figure 38 has been tested in a laboratory. The achieved parameters are the saturation capacity of more than 4500 electrons, the dark current of about 600 electrons/s, the temporal dark noise of 16 electrons, the total quantum efficiency of 58.3% at wave length of 525 nm, the dark signal non-uniformity of 4%, and the photoresponse non-uniformity of 7%, where the last two types of non-uniformity can be eliminated after careful off-chip fixed pattern noise correction as usual CMOS sensor technology. The FST sensor mounted on the control camera box is now ready for integration tests in a laboratory and use of the field test observation after the total integration on the LC.

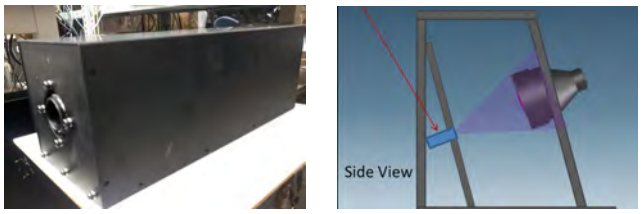


Fig. 39. LED flusher (left) and the schematic view of the installation on LC (right).

As a basic step of the Ashra-1 gain calibration chain, the importance and the function of the LED flusher (Figure 39) has been already described before. The achieved status is as follows. To ensure the uniform lights on the focal sphere of the PLI input window, the spot size of the virtual point source is required to be small and the numerical aperture of the output light to be large after the output of the LED flusher optical system. The measured HWHM spot size at the output window of the LED flusher is 300 $\mu$m without any spiky structure. We have also measured the non-uniformity on the PLI input window surface to be less than 1%. The optical system inside of the LED flusher box may cause some systematic error of the alightment. We measured the misalignment error to be less than 23 $\mu$m which corresponds to 1.7 mrad (0.1°). We can expect the LED flusher can be used even every second during the observation to confirm the stability of the total gain of the readout system and calibrate it time to time if necessary.

Fig. 40. Shelters for a laser and LC (left) and LC (right) in the shelter.

We have already set up the test facility to integrate the readout system on the LC for test in a shelter at Akeno Ob-

servatory (Figure 40). The LC for test is ready for mounting and integrating the trigger and readout system. A 355 nm and 532 nm YAG laser system with 130 mJ/puse has been installed in the next shelter, which will be used for virtual fluorescence signals for test. The YAG laser pulse at the appropriate distance yields Rayleigh scattering light, some of which reaches the puple of the optical system of Ashra-1 LC, corresponds to the emission of fluorescence light from an air-shower with the primary energy up to several $10^{19}$ eV. The integratin test of the trigger and readout procedure with the facilities at Akeno observatory will be useful just before the installation and the commissioning at the Ashra-1 Mauna Loa observatory.

## Bibliography


[1] http://www.icrr.u-tokyo.ac.jp/∼ashra

[2] Sasaki, M., Progress of Theoretical Physics Supplement, **151**, 192 (2003).

[3] Sasaki, M., et al., Proc. 29th Int. Cosmic Ray Conf. (Pune, India), Vol. 8, 197-200, 2005.

[4] M. Sasaki, 30th Intl. Cosmic Ray Conf. (Merida), ID1232, 2007.

[5] M. Sasaki *et al.*, in 32th International Cosmic Ray Conference, Rio de Janeiro 2013.

[6] D. Fargion, ApJ, 570:909, 2002.

[7] Y. Aita *et al.* ApJ, 736:L12, 2011.

[8] Y. Asaoka and M. Sasaki, Nucl. Instr. and Meth. A647, 34, 2011.

[9] Mészaros, P. 2006, Rep. Prog. Phys., 69, 2259

[10] Mészaros, P., & Rees, M.J. 1997, ApJ, 476, 232

[11] Sari, R., & Piran, T., 1999. ApJ, 517, L109

[12] Mészaros, P., & Rees, M.J. 1999, MNRAS, 306, L39

[13] Gao, S., *et al.* 2013, arXiv:1305.6055

[14] Abraham, J., et al. 2008, Phys. Rev. Lett., 100, 211101

[15] Aita, Y., et al. 2011, ApJL, 736, L12

[16] http://gcn.gsfc.nasa.gov/swift_grbs.html

[17] http://gcn.gsfc.nasa.gov/fermi_grbs.html

[18] Antoni, T., et al. 2005, Astropart. Phys., 24, 1

[19] Amenomori, M., et al. 2008, ApJ, 678, 1165

[20] Y. Aita *et al.*, ApJL**736**, L12 (2011).

[21] Y. Aita *et al.*, GCN Circ., 8632 (2008).

[22] Y. Asaoka *et al.*, GCN Circ., 11291 (2010).

[23] Bertin, E. and Arnouts, S. 1996, A&AS, 117, 393

[24] H$\phi$g, E., *et al.*, 2000, A&A, 355, L27

[25] Kobayashi, S. and Zhang, B., 2003, ApJ, 582, 641

[26] http://gcn.gsfc.nasa.gov/other/081203A.gcn3

[27] Asaoka, Y. and Sasaki, M., 2013, Astropart. Phys., 41, 7

[28] Sasaki, M., Manago, N., Noda, K., Asaoka, Y., GCN Circ. 3421, 2005.

[29] R. Gandhi, C. Quigg, M.H. Reno and I. Sarcevic, Phys. Rev. D **58** (1998) 093009.

[30] M. Sasaki, Y. Asaoka, M. Jobashi, Astropart. Phys. 19 (2003) 37.

[31] M. Sasaki, J. Phys. Soc. Jpn. **70** (Suppl. B) (2001) 129.


# High Energy Astrophysics Group


**[Spokesperson: T. Terasawa]**
ICRR, Univ. of Tokyo, Kashiawa, Chiba 277-8582


### *Overview*

Since its creation in December 2009, the high energy astrophysics group has been making theoretical and observational studies of violent astrophysical phenomena in which nonthermal cosmic ray particles are being accelerated. In April 2013, new members, a research associate and a postdoc, joined the group, who have been contributing to extend the group activity significantly. Targets of the group's study include high energy astrophysical objects such as supernova remnants/pulsar magnetospheres, giant flares and repeating bursts of magnetars, a giant galactic explosion called 'Fermi bubble', neutron star merger events, fast radio bursts (FRBs), jets from active galactic nuclei (AGN), as well as mysterious gamma ray bursts (GRBs). Research works on the origin of ultra high energy cosmic rays (UHECRs) are also within the coverage of the group.

### *Research topics: 1. Particle acceleration and emissions in GRBs and AGNs*

The origin of ultra high-energy cosmic-rays (UHECRs) is one of the most important research targets in ICRR. The sources may be ultra-relativistic jets such as gamma-ray bursts (GRBs) or acitive galactic nuclei (AGNs). The physical condition to produce UHECRs can be verified via studies of electromagnetic emission, in which the information on the acceleration mechanism and efficiency is concealed. The first step to unveil the UHECR sources is the identification of the photon emission processes in relativistic jets.

In the standard model of GRB, electrons are accelerated via shocks, and emit synchrotron photons. In such a situation, protons should be accelreated to ultra high-energies. However, several alternative models have been proposed by many authors. In the photosphere model, one of such alternative

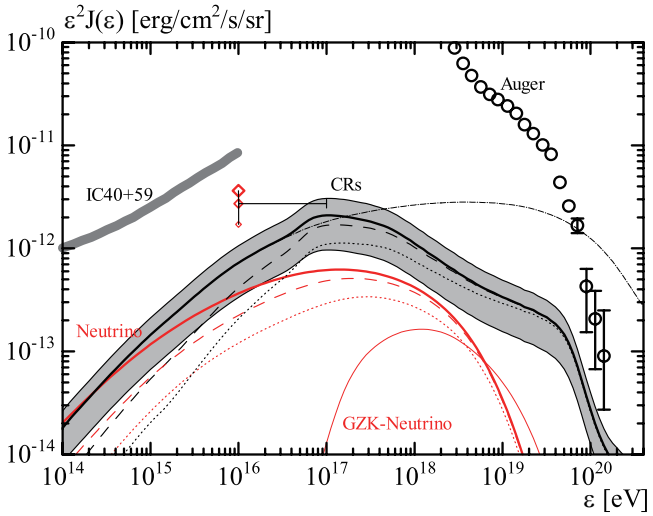


Fig. 41. Fluxes of UHECRs and neutrinos from GRBs calculated with time-dependent simulations of the hadronic cascade processes [5]. The results are consistent with the upper-limit of the neutrino flux (IC40+59) and observed UHECR flux (AUGER).

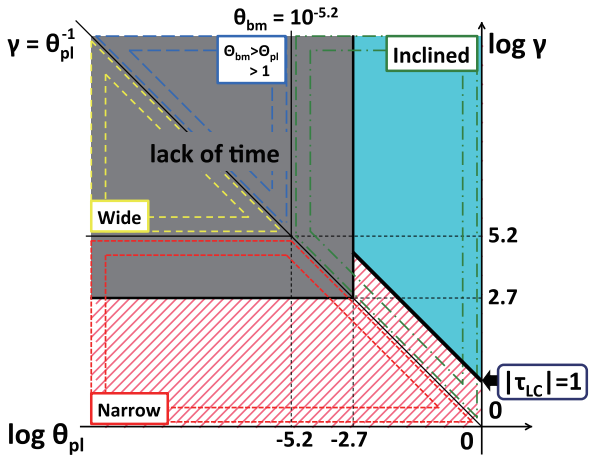


Fig. 42. The $\gamma - \theta_{\rm pl}$ diagram of the pulsar wind where $\gamma$ is the Lorentz factor of the pulsar wind and $\theta_{\rm pl}$ is the inclination angle with respect to the propagation direction of the radio pulses [8]. Here, we do not consider the gray region. The black solid line of $\tau_{\rm LC} = 1$ means the optical depth for induced Compton scattering of unity. The blue region corresponds $\tau_{\rm LC} < 1$, i.e., the radio pulses are allowed to escape from the scattering by the pulsar wind. The fuctional form of $\tau_{\rm c} = 1$ is not shown in the diagram because it depends on the magnetization of the pulsar wind and the size of the emission region of the radio pulses.

models, thermal emission is a main spectral component. In the high photon density of this model, the UHECR production is difficult owing to the cooling due to the photopion production. However, our time-dependent simulations show that the photosphere model is hard to reconcile with the observed GRB spectra [3]. In another study [5], based on the standard picture, we quantitatively estimate the UHECR and neutrino production rates from GRBs with our numerical simulations. As shown in Figure 41, our results indicate that GRBs are still possible UHECR sources avoiding the neutrino limit by IceCube.

On the other hand, there are several open questions in the wide-band photon spectra of AGN jets. Generally electrons are supposed to be accelerated via shocks in jets. However, the maximum energy of electrons is comparable to that in young supernova remnants in spite of stronger magnetic fields in AGN jets. The spectra show curved feature, while the simple shock acceleration theory predicts power-law spectra. We try to fit wide-band spectra assuming the stochastic acceleration by turbulences instead of shocks. The spectra for 1ES 1101-232 and Mrk 421 are well fitted by our models [4]. If the stochastic acceleration is common mechanism in AGN jets, the UHECR production seems to be difficult.

### *Research topics: 2. Theoretical studies of pulsars*

*2a: Pulsar wind properties*

High energy emissions from pulsars and their nebulae are unambiguous evidences that the pulsars generate high energy particles, i.e., cosmic rays. However, because of their extreme physical condtions, we have not fully understood the particle acceleration and creation processes at the pulsar magnetosphere. We do not even achieve consensus on the physical conditions, such as the number density, the kinetic energy and the magnetization of the high energy particles which is called

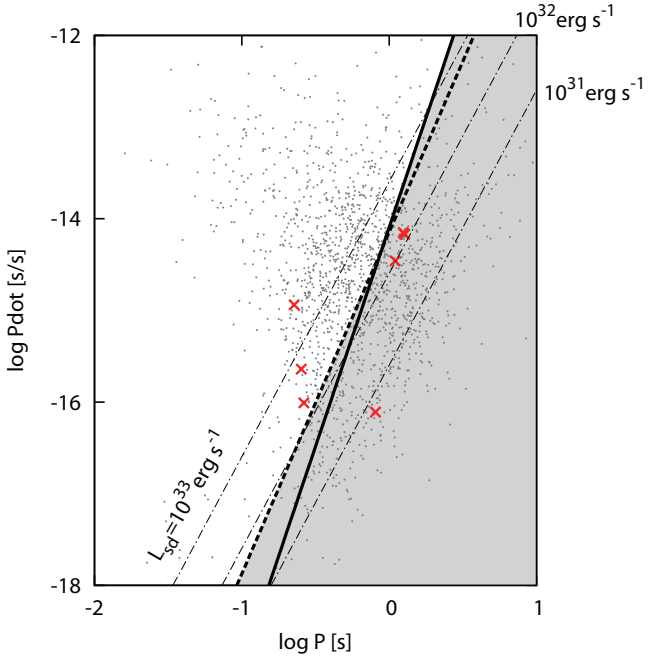


Fig. 43. Synchrotron radiation death lines (thick solid and dashed lines) on the $P$-$\dot{P}$ diagram, where $P$ is the period and $\dot{P}$ is its derivative (Kisaka and Tanaka, in press). The thin dot-dashed lines denote the spin-down power of $L_{\rm sd} = 10^{33}, 10^{32}$ and $10^{31}$ erg s$^{-1}$. Each large cross denotes X-ray detected old pulsars. Four of our samples locate in the filled region (below the death lines) so that the synchrotron radiation model does not explain their non-thermal X-ray emissions.

pulsar wind. We study the induced Compton scattering off radio pulses of the pulsar by the pulsar wind generated by the pulsar itself to constrain the physical conditions of the pulsar wind. One of our results are shown in Figure 42, the $\gamma - \theta_{\rm pl}$ diagram of a pulsar wind, where the Lorentz factor $\gamma$ and the inclination angle with respect to the radio pulse $\theta_{\rm pl}$. In Figure 42, blue region is allowed for escaping the radio pulses from scattering and tells us the allowed pulsar wind velocity characterized by $\gamma$ and $\theta_{\rm pl}$. For example, when $\gamma$ and $\theta_{\rm pl}$ are sufficiently high, radio pulses escape from induced Compton scattering. In terms of the number density, sufficiently low density is required for escaping of the radio pulses from scattering. We find the small value of the Lorentz factor and also the large value of the number density of the pulsar wind compared with the study by Wilson & Rees (1978) are allowed when we consider the inclined pulsar wind with respect to the radio pulses.

*2b: High energy emission from old pulsars*

Observationally, pulsars are characterized by their spin period and its derivative. We obtain the characteristic age and the spin-down power from them. We know the young energetic pulsars are efficient particle accelerator and emit bright non-thermal radiation mostly in X-rays and $\gamma$-rays. However, a dozen of old (typically $> 1$ Myr) and less energetic pulsars have been also detected in X-rays. Their non-thermal X-ray signatures give a great opportunity to study the evolution of how and where to accelerate particles. We study the non-thermal X-ray emission from old pulsars based on synchrotron radiation models which are usually considered as the non-thermal X-ray emission mechanism for young pulsars. Figure 43 shows X-ray emission death lines for the one of four types of synchrotron radiation model which we considered. The death line means that the significant non-thermal X-ray emission is not expected for the pulsars below this line. Although we consider fairly optimistic model of synchrotron X-ray emission, the detected X-ray flux for some old pulsars is not explained by the synchrotron radiation. In addition, we require the different particle acceleration process from that of young pulsars even for the pulsars above the death line. Our results indicate that the particle acceleration and creation processes at pulsar magnetospheres significantly change around 1 Myr.

*2c: Electric field screening and particle ejection in a pulsar magnetosphere*

We study the screening of the rotationally induced electric field above pulsar polar caps including backflow-particles from the outer gap region. We apply a simple numerical model for the dynamics of the charged particles using Particle-in-Cell methods. Although the field-line footpoints of the outer gap are considered to the return current region where the sign of the average current density flowing along the magentic field line $j$ and the Goldreich-Julian current density $j_{\rm GJ} = c\rho_{\rm GJ}$ is opposite ($j/j_{\rm GJ} < 0$), we find that the electric field can be screened without pair creation under the certain conditions. For the arbitrary value of current density, we find that if another backflow components with small average Lorentz factor $\bar{\gamma} \sim 1$ are come into the polar cap, the development of the electric field is prevented. If ions are extracted from the surface,

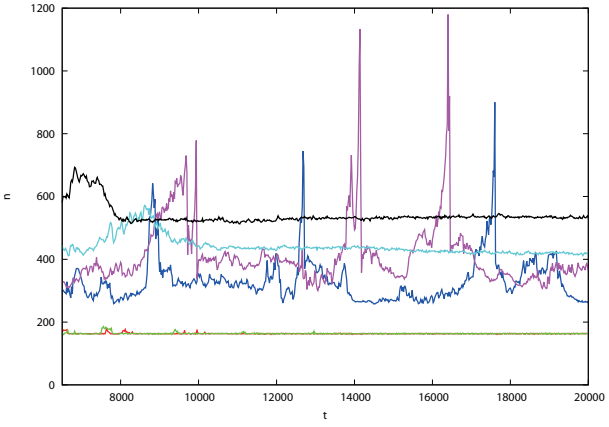


Fig. 44. Periodic ejection of particles into a pulsar magnetosphere. The number of particles through the outer domain boundaries as a function fo the compultational time. The value of the vertical axis is normalized by $0.01 n_{\rm GJ}$, where $n_{\rm GJ}$ is the Goldreich-Jullian density. The colors show the number of injected particles $n_{\rm inj}/n_{\rm GJ} =$ 0.1 (red), 0.2 (light green), 0.4 (blue), 0.6 (purple), 0.8 (light blue) and 1.0 (black) from the outer boundary (Kisaka, Asano, and Terasawa, in preparation).

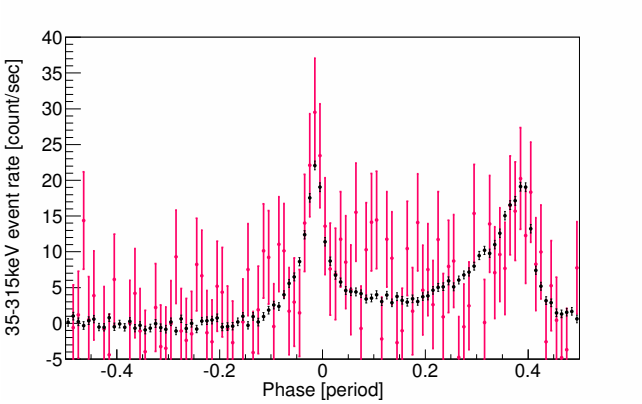


Fig. 45. The pulse profile of the Crab pulsar for soft $\gamma$-ray photons (35-315 keV, the average photon energy $\sim$113 keV), observed with the HXD/GSO sensor on board of the Suzaku satellite. Red dots shows the count rates folded over only the periods simultaneous with GRPs, while black dots shows those accumlated only for non–GRP periods. We estimate the upper limit on soft-gamma-ray flux enhancement ($1\sigma$) concurrent with the GRPs to be $\sim 10\%$, which is more stringent than the previous value ($\sim 19\%$, Lundgren et al., 1995). Phase 0 correspond to the main peak of radio pulses.

the bunches of particles are ejected to the outer region quasi-periodically (Figure 44). We suggest that this behavior may be one of the origin of pulsar radio emission.

### *Research topics: 3. Observational study of the Crab pulsar*

Crab pulsar, the remnant of the supernova explosion in 1054 A.D., is one of the most studied neutron stars. While its physical properties have been investigated for more than 40 years since its discovery, there remains an enigma about the origin of giant radio pulses (GRPs). While for a long time the Crab's GRPs had been regarded as a pulsar phenomenon lim-

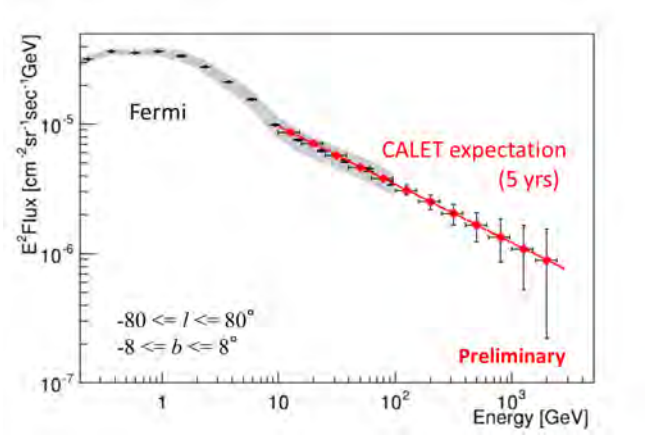


Fig. 46. Energy spectrum of diffuse gamma-rays by Fermi (M. Ackermann et al. 2012) and an expectation of CALET 5-year observation.

ited to the radio frequency, a 3% enhancement of the optical emission at the GRP timing was discovered recently (Shearer et al., 2003; Strader et al. 2013). However, in other frequency bands, no significant flux enhancement was found and only the upper limits were set. We have been making simulatenous observations of the Crab pulsar at the GHz frequency range and X-ray/soft-gamma-ray energy ranges. Figure 45 shows an example, where we made the correlation study between GRPs and the soft-gamma-ray pulses.

### *Research topics: 4. CALET project — a R/D study*

CALET, CALorimetric Electron Telescope, is a new mission for the Japanese Experiment Module-Exposed Facility (JEM-EF) on the International Space Station. The CALET mission aims at revealing unsolved problems in high energy phenomena of the Universe by carrying out accurate measurements of high energy spectra of electrons, gamma-rays and nuclei. The instrument will be flown in JFY 2014, and is scheduled to be operated for five years. CALET is focused on investigating the high energy total electron spectrum into the trans-TeV energy range. CALET can also perform a gamma-ray all-sky survey, complementing Fermi and atmospheric Cerenkov telescope, to detect intense high energy sources, study the diffuse component. CALET has an imaging and deep calorimeter with 30 radiation lengths for electromagnetic particles, which provides superior energy resolution and excellent separation between hadrons and electrons/gamma-rays and between charged particles and gamma-rays. We developed analysis methods such as particle identification and arrival direction, and evaluated detection performance such as angular resolution, energy resolution and point spread function, using Monte Carlo simulations and CERN-SPS beam test data. Figure 46 shows energy spectrum of diffuse gamma-rays expected by CALET 5-year observation. We note that CALET can make an important contribution by extending the Fermi gamma-ray observations to energies above $\sim$ 100 GeV.

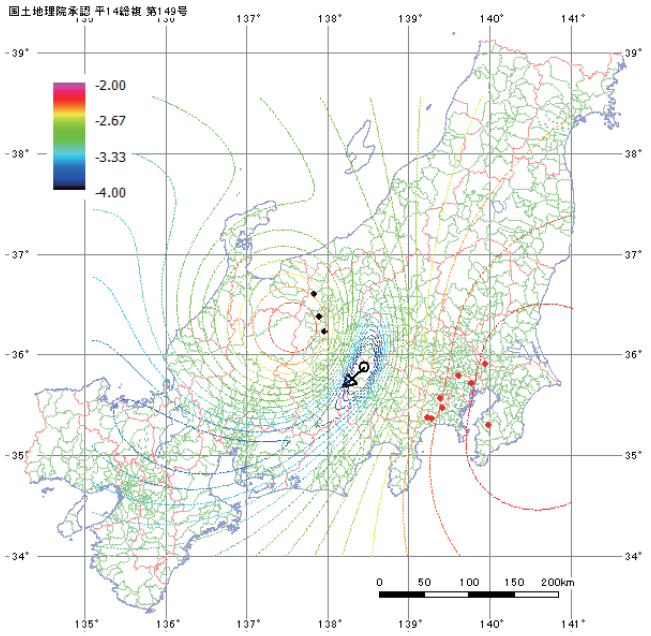


Fig. 47. A multi-point observation of forward scattering meteor echo made on 30 July 2013 at 02:45:07 JST (29 July 2013 at 17:45:07 UT). In this example, we utilized three transmitters (solid black dots) and eight receivers (solid red dots) making possible to derive meteor parameters, such as the radiant position (RA=5.96$\pm$0.18 hour, DEC=47.90$\pm$6.04 deg) and the meteor velocity (32.31$\pm$0.95 km/s), from which we concluded that this meteor was a sporadic meteor not belonging to any known meteor shower group. The contour curves represent the error residuals in the parameter–fitting procedure, where a open black dot shows the geographical position giving the error minimum (longitude=138.4$\pm$0.2 deg, latitude=35.9$\pm$0.3 deg). An arrow starting from there shows the meteor velocity direction projected to the horizontal plane.

### *Research topics: 5. R/D study for radar detection of UHECRs and extraterrestrial grains*

Wide attention has been attracted to the detection of ultra high energy cosmic rays (UHECRs) with radio techniques, either passive and active, towards future large-scale UHECR observatory on the ground. Collaborating with the TA group of ICRR, we have made a R/D study of the active method, namely, the detection of radar echoes from extensive air showers of UHECRs (UHECR echoes, hereafter) [13]. Parallel to the above R/D study, we have also made a radar research research project for extraterrestrial grains (meteors). Despite more than three orders of magnitude difference in the echo duration between UHECR echoes ($<\sim \mu$s, expected but not yet identified) and meteor echoes (several - several tens of ms, observed), the know-how developed in the latter project (Figure 47) can provide a technical basis for the former.

## Bibliography

### Papers in refereed journals

1. Ackermann, M., M. Ajello, K. Asano et al. The First Fermi LAT Gamma-Ray Burst Catalog, ApJS 209, 11 (90pp) (2013)

2. Ackermann, M., M. Ajello, K. Asano et al., Fermi-LAT Observations of the Gamma-Ray Burst GRB 130427A,

Science Vol. 343, 42-47 (2014)

3. Asano, K., and P. Meszaros. Photon and Neutrino Spectra of Time-Dependent Photospheric Models of Gamma-Ray Bursts, JCAP 09, 008 (2013)

4. Asano, K., F. Takahara, M. Kusunose, K. Toma, and J. Kakuwa, Time-Dependent Models for Blazar Emissions with the Second-Order Fermi Acceleration ApJ 780, 64(12pp) (2014)

5. Asano, K., and P. Meszaros, Neutrino and Cosmic-Ray Release from Gamma-Ray Bursts: Time-Dependent Simulations, ApJ 785, 54 (2014)

6. Mikami, R., T. Terasawa, S. Kisaka, H. Miyamoto, K. Asano, N. Kawai, Y. Yamakoshi, K. Nagata, R. Kataoka, K. Takefuji, M. Sekido, H. Takeuchi, H. Odaka, S. Sato, Y. T. Tanaka, Search for a correlation between giant radio pulses and hard X-ray emissions in the Crab pulsar, JPS Conf. Proc., 1, 015106 (2014)

7. Takamoto, M., Kisaka, S., Suzuki, T., and T. Terasawa, The Evolution of High Temperature Plasma in Magnetar Magnetospheres and its Implications for Giant Flares, ApJ, in press (2014)

8. Tanaka, S. J., and Takahara, F., Constraint on Pulsar Wind Properties from Induced Compton Scattering off Radio Pulses, PTEP 12, 123E01 (2013)

9. Yatsu, Y., K. Asano, N. Kawai, Y. Yano, and T. Nakamori, Spatially Resolved Spectroscopy of a Pulsar Wind Nebula in MSH 15-56 ApJ 773, 25(14pp) (2013)

10. Yokota, S., Y. Saito, K. Asamura, M. N. Nishino, T. I. Yamamoto, H. Tsunakawa, H. Shibuya, M. Matsushima, H. Shimizu, F. Takahashi, M. Fujimoto, and T. Terasawa, Kaguya observation of the ion acceleration around a lunar crustal magnetic anomaly, Planetary and Space Science, 93-94, 87-95 (2014)

**Thesis**

11. Higuchi, C., "Statistical study of lightning activity: Periodicity and possible link with solar activity", (in Japanese), Master thesis, Department of Physics, Tokyo Institute of Technology (2014)

**Conference papers**

12. Akaike, Y., for the CALET collaboration, "CALET observational performance expected by CERN beam test", Proceedings of the 33rd International Cosmic Ray Conference (2013)

13. Asano, K., "Wide-Band Spectra of Prompt Emission", EAS Publications Series, 61, 115 (2013)

14. Belz, J., M. Abu Bakr Othman, C. Allen, E. Barcikowski, D. Besson, B. Farhang-Boroujeny, D. Ikeda, W. Hanlon, S. Kunwar, J. P. Lundquist, I. Kravchenko, S. Larson, I. Myers, T. Nakamura, J. S. Rankin, H. Sagawa, P. Sokolsky, H. Takai, T. Terasawa, and G. B. Thomson, "TARA: Forward-scattered radar detection of UHECR at the telescope array", EPJ Web of Conferences 53, 08012 (2013)

15 Fujisawa, K., and S. Kisaka, "Axisymmetric and stationary magnetic field structures in neutron star crusts under various boundary conditions", Proceedings of IAU Symposium 302, Magnetic fields throughout stellar evolution (2013)

16. Guzik, T., for the CALET collaboration, "The CALorimetric Electron Telescope (CALET) ground data handling and processing system", Proceedings of the 33rd International Cosmic Ray Conference (2013)

17. Kisaka, S., and T. Terasawa, "Electric field screening at the pulsar polar cap", Proceedings of SKA Science Workshop in East Asia (2013)

18. Marrocchesi, P. S., for the CALET collaboration, "CALET measurements with cosmic nuclei and performance of the charge detectors", Proceedings of the 33rd International Cosmic Ray Conference (2013)

19. Marrocchesi, P. S., for the CALET collaboration, "CALET Measurement of Ultra-Heavy Cosmic Rays", Proceedings of the 33rd International Cosmic Ray Conference (2013)

19. Mikami, R., T. Terasawa, S. Kisaka, K. Asano, S. J. Tanaka, M. Sekido, K. Takefuji, H. Takeuchi, H. Odaka, T. Sato, Y. T. Tanaka and N. Kawai, "Hard X-ray observations with Suzaku HXD at the time of giant radio pulses from the Crab pulsar", Proceedings of SUZAKU - MAXI conference (2014)

20. Moiseev, A., for the CALET collaboration, "CALET perspectives in high-energy gamma-ray observations", Proceedings of the 33rd International Cosmic Ray Conference (2013)

21. Mori, M., for the CALET collaboration, "Expected Performance of CALET as a High Energy Gamma Ray Observatory", Proceedings of the 33rd International Cosmic Ray Conference (2013)

22. Niita, T., and the CALET collaboration, "CALET Calibration on ISS Orbit Using Cosmic Rays", Proceedings of the 33rd International Cosmic Ray Conference (2013)

23. Rauch, B., for the CALET collaboration, "CALET Positron / Electron Measurements Using the Geomagnetic Field", Proceedings of the 33rd International Cosmic Ray Conference (2013)

25. Tamura, T., for the CALET collaboration, "Particle Beam Tests of the Calorimetric Electron Telescope", Proceedings of the 33rd International Cosmic Ray Conference (2013)

26. Tanaka, S. J., “Broadband Emission Structure of Pulsar Wind Nebulae”, Proceedings of the 33rd International Cosmic Ray Conference (2013)

27. Tanaka, S. J., “High Energy Emission from Spherically Symmetric Pulsar Wind Nebulae”, Proceedings of SUZAKU-MAXI Conference (2014)

28. Tanaka, S. J., and S. Kisaka, “Synchrotron Emission from Old Pulsars”, Proceedings of SUZAKU-MAXI Conference (2014)

29. Tanaka, Y. T., M. Hayakawa, Y. Hobara, J. Raulin, Y. Takahashi, M. Sato, and T. Terasawa, T. ELF and VLF observations of ionospheric disturbances caused by extra-terrestrial origin, American Geophysical Union, Spring Meeting, SM24A-03 (2013)

30. Torii, S., for the CALET collaboration, “The Calorimetric Electron Telescope (CALET) for High Energy Astroparticle Phsycis on the International Space Station”, Proceedings of the 33rd International Cosmic Ray Conference (2013)

31. Ueyama, Y., for the CALET collaboration, “The CALET Structure and Thermal Model used for beam test at CERN”, Proceedings of the 33rd International Cosmic Ray Conference (2013)

32. Yamaoka, K., for the CALET collaboration, “CALET Gamma-ray Burst Monitor (CGBM)”, Proceedings of the 33rd International Cosmic Ray Conference (2013)

# ASTROPHYSICS AND GRAVITY DIVISION

## Overview

Astrophysics and Gravity Division consists of Gravitational Wave Group, The Observational Cosmology Group, Primary Cosmic Ray Group and Theory Group. The Gravitational Wave Group conducts experimental research of gravitational wave with researchers of gravitational wave experiment and theory in Japan. The main items are the construction of the large scale cryogenic interferometer(KAGRA) at Kamioka underground and the operation of CLIO.

The Observational Cosmology Group studies the cosmic history based on deep multi-wavelength observations in collaboration with worldwide researchers. This group has started a new optical deep survey project with the wide-field imager of Hyper Suprime-Cam mounted on the Subaru telescope.

Theory Group conducts both theoretical study of the Universe and astroparticle physics.

## Gravitational Wave Group

### *Gravitational Wave Project Office (GWPO)*

[Spokesperson : Kazuaki KURODA]

ICRR, The Univ. of Tokyo, Kashiwa, Chiba 277-8582

**Overview**

Gravitational wave project office was established at the beginning of the financial year of 2011 to assist the construction of KAGRA[4] gravitational wave telescope. The organization of this office is illustrated in Fig. 1. Main office is set in Kashiwa campus and its Kamioka branch is in Kamioka. It is an internal office belonging to Astrophysics and Gravity Division of ICRR.

KAGRA project is hosted by ICRR, which means the funding comes through the University of Tokyo and all procurements are made through ICRR. However, the number of researchers working for KAGRA construction belonging to other organizations is larger than the staffs belonging to ICRR. Therefore, three collaboration members of KEK are recruited as guest researchers of ICRR and one research staff is temporarily moved to ICRR from NAOJ.

The role of this office is to support execution of KAGRA project by ICRR staffs together with these collaboration members. Main works are

- finance planning
- management of collaboration
- support for the execution of KAGRA budget
- coordination of collaboration meetings
- technical supports for the KAGRA construction
- support for education of graduate students
- bridging collaboration members and ICRR administration office
- others

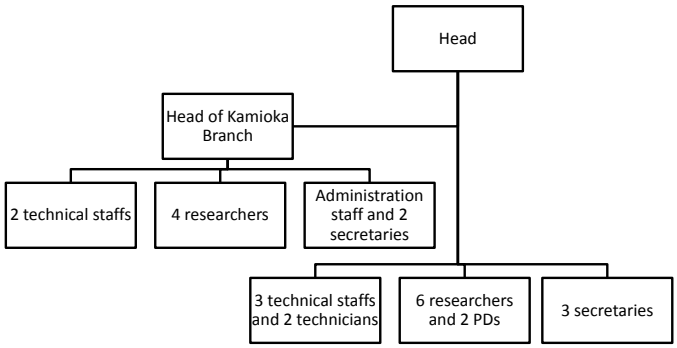


Fig. 1. Organization of the Gravitational Wave Project Office in 2013

**Activity in FY 2013**

We supported the collaboration meetings held in Kashiwa campus. They were two face-to-face international collaboration meetings[5] and four KAGRA collaobration remote meetings (two international and two domestic) [6]. We supported the KAGRA council meeting on 17th, September, Program Advisory Board meeting on 2nd-3rd, November and 2nd ELiTES general meeting held at Euro Tokyo delegation house on 4th, December and at Sanjo Conferene Hall on 5th, December.

We took care of travel supports for the following events:
- External Peer Review of KAGRA in April, 2014 (which was for FY2014 but had to be processed in FY 2013)
- 4th Korea-Japan Workshop on 10th-11th, June in Osaka University
- 5th Korea-Japan Workshop in Seoul on 29th-30th, November

We supported the execution of research programs adopted as ICRR collaborative researches listed in Table 1 in processing invoices for experimental goods and domestic travels.

*4 nicknamed in January, 2012 by public contribution for LCGT

*5 http://gwwiki.icrr.u-tokyo.ac.jp/JGWwiki/KAGRA/Meeting/F2F

*6 http://gwwiki.icrr.u-tokyo.ac.jp/JGWwiki/KAGRA/Meeting/Collaboration

| Title | Representative | Affiliation |
|---|---|---|
| Research and Development for the ultra high sensitivity quantum interferometer in KAGRA | Yutaka Shikano | IMS |
| Development of optical cavities for ultranarrow stable laser | Tetsuya Ido | NICT |
| Gravitational Wave Detector in Kamioka (XII) | Masatake Ohashi | ICRR, UTokyo |
| Data analysis using CLIO data (IV) | Hirotaka Takahashi | Nagaoka U TEC |
| Application of geophysical observations in the Kamioka mine to the dynamics of snow and water | Yuichi Imanishi | ERI, UTokyo |
| Study for LCGT data analysis and Research for its System (III) | Nobuyuki Kanda | Osaka CU |
| Development of beam position minitoring and controling systems for KAGRA | Takashi Sato | Niigata U |
| The development of a super sensitive shadow sensor for a gravitational antenna | Ruggero Micheletto | Yokohama CU |
| Research on ultra-low frequency anti-vibration system for KAGRA | Ryutaro Takahashi | ICRR/NAOJ |
| Research of Large-scale Gravitational wave Telescope (III) | Kazuaki Kuroda | ICRR, UTokyo |
| Development of Sapphire Mirror Suspension for KAGRA(LCGT) (X) | Toshikazu Suzuki | KEK/ICRR |
| Development of Very Low Vibration Cryo-Cooler System | Nonuhiro Kimura | KEK/ICRR |
| Gravitational Wave Detection using Non-Harmonic Analysis | Shigeki Hirobayashi | Univ. of Toyama |
| Characterization of Sapphire mirror for KAGRA using electron spin resonance | Yukinori Ono | Univ. of Toyama |
| R&D for the intensity stabilization of the laser system in KAGRA | Fusakazu Matsushima | Univ. of Toyama |
| Development of the output mode-cleaner for KAGRA | Kentaro Somiya | TITEC |
| Development of precision profiler for mirrors of LCGT interferometer 3 | Toshiyuki Takatsuji | AIST |
| Development of a stabilization system for the KAGRA laser source | Norikatsu Mio | PSC, UTokyp |
| Real time control for interferometer using computers (II) | Osamu Miyakawa | ICRR, UTokyo |
| Numerical simulation of Electric-Magnetic Wave Propagation in Gravitational wave Detector | Shinji Miyoki | ICRR, UTokyo |
| Research on cryogenic payload for KAGRA | Kazuhiro Yamamoto | ICRR, UTokyo |

Table 1. List of research titles adopted as ICRR Cooperative researches in FY 2013

**Kamioka branch of GWPO**

The manpower of the Kamioka branch consists of 5 research staffs, one adminstration staff, 2 secretaries and 2 technicians as shown in Fig. 1, which is increased from the previous year.

The data acquisition & Analysis building was designed and constructed by the end of this financial year as shown in Fig. 2. The building is jointed to the adjacent Hokubu Kaikan building where the office & laboratory rooms for Kamioka branch of GWPO are located (refurbished part from previous Kinder garten).

The Kamioka branch mainly executes the following works:

- Supporting research activity for KAGRA project
- Planning coordination and schedule of the KAGRA construction
- Making liason with the construction company, Kamioka Observatory and local government for condcuting KAGRA construction
- Outreach activity with local communities
- Accepting visitors from various fields

The Kamioka branch held an exchange meeting with local residents in collaboration with the Kamioka Observatory on 12th, July and had an information session about the construction and schedule of KAGRA for local residents on 20th, August. Research staffs gave lectures at several weekends from April to July at Public Exposition Hall of Inotani as listed in Appendices.

Fig. 2. Data acquisition & analysis building for KAGRA

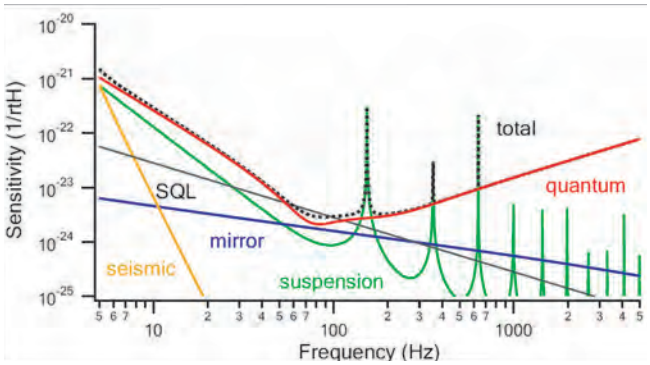


Fig. 3. Ultimate sensitivity limit of KAGRA.

### *KAGRA Project Status*

[Spokesperson : Seiji KAWAMURA]
ICRR, The Univ. of Tokyo, Hida, Gifu 506-1205

**Overview**

KAGRA, Large-scale Cryogenic Gravitational wave Telescope, aims at detection of gravitational waves for the first time and establishing a new astronomy, gravitational wave astronomy, by a 3 km baseline laser interferometer with a cryogenic mirror system placed underground at Kamioka. The KAGRA development is divided into two stages: the initial KAGRA (iKAGRA) and baseline KAGRA (bKAGRA). The iKAGRA detector will be a simple Fabry-Perot Michelson interferometer with mirrors at room temperature and a simple seismic isolation system. We plan to operate the iKAGRA detector by the end of 2015 with a one-month observation run at the end of the stage. Then we will proceed to bKAGRA. The bKAGRA detector will employ a Resonant Sideband Extraction (RSE) interferometer with cryogenic mirrors and an advanced Seismic Attenuation System (SAS). The bKAGRA detector should attain the sensitivity high enough for the detection of gravitational waves with the help of the RSE interferometer to reduce the quantum noise, the cryogenic mirrors to reduce the thermal noise, and the SAS to reduce the seismic noise. We plan to start operating the bKAGRA detector by the end of 2017, then repeat short-time observation runs and noise hunting to improve the sensitivity until it reaches the aimed sensitivity of KAGRA.

Fig. 3 shows the estimated ultimate sensitivity limits of KAGRA where incoherent sum of the fundamental noise sources is assumed. The observation range for an inspiral and merger of neutron-star binary with the ultimate sensitivity limit of KAGRA is about 173Mpc. It should be noted that the definition of the observation range, which used to be different from the one used by LIGO and Virgo, was changed to be the same as LIGO and Virgo to avoid possible confusion.

Major milestones we had accomplished and important progress we had made between April 2013 and March 2014 are the following:

- The excavation of the tunnel was completed.
- A building for data analysis was built in the Mozumi area.
- Various kinds of cooling tests with the cryostats, including measuring the cooling time of the mirror and measuring the vibration level caused by the cryo-coolers were performed successfully.
- Some of the mirrors/beam splitter were polished and coated successfully.
- The prototype test of the inverted pendulum, which is an important element of the advanced seismic isolation system, was successfully finished, and the payload prototype was assembled.
- The digital control system and the data acquisition system were completed.

We also enhanced the international and domestic collaborations with the Einstein Telescope (ET) project, LIGO and Virgo, the Korean and other Asian groups, and Toyama University by exchanging researchers and having international workshops.

The rapidly progressing status of KAGAR were presented in several international conferences.[1] Some papers about the progress of KAGRA were also published.[2] We also presented activities in our web-page.[3]

## Bibliography

[1] Seiji Kawamura for the KAGRA collaboration, "Progress and Challenges of KAGRA", 10th Amaldi Conference on Gravitational Waves, July 7-13, 2013, Uniwersytet Warszawski, Warsaw, Poland.

[2] Yoichi Aso, et al. (The KAGRA Collaboration), "Interferometer design of the KAGRA gravitational wave detector", Phys. Rev. D **88** (2013) 043007.

[3] http://gwcenter.icrr.u-tokyo.ac.jp/en/

**Tunnel for KAGRA**

[Spokesperson : Takashi UCHIYAMA]
ICRR, The Univ. of Tokyo, Hida, Gifu 506-1205

KAGRA is a laser interferometric gravitational-wave detector with a 3 km arm length. It is to be constructed in tunnels of Kamioka mine (Hida, Gifu, Japan). The use of an underground site for small seismic motion is a key feature of KAGRA. Kajima corporation (Kajima) in Japan carried out KAGRA tunnel excavation work from 22th May, 2012 to the end of March, 2014. The total length and the total volume of the tunnels are 7,697 m and 156.301 $m^3$, respectively. Kajima used the New Austrian Tunneling Method.

Figure 4 shows a location map of the KAGRA tunnels. The tunnels have been excavated in Mt. Ikenoyama of Kamioka mine, whose top is at about 1,300 m. There are two 3,000 m arm tunnels connected perpendicularly. One arm tunnel in north-east direction is called Xarm; the other arm tunnel is called Yarm. The Center area, Xend area and Yend area, where some experiment rooms exist are located at the connecting corner of the arm tunnels and at the end of both arm tunnels, respectively. All of the areas are inside at more than 200 m from the surface of the mountain, in order to obtain a quiet seismic motion environment as we expected at the underground site. Both arm tunnels are tilted by 1/300 for natural water drainage. The Xend area is at the highest altitude of about 382 m, and the Yend area is at the lowest altitude of about 362 m.The altitude of the Center area is 372 m. The KAGRA tunnels have two entrances: New Atotsu entrance and Mozumi entrance. The New Atotsu entrance was newly constructed for the KAGRA tunnels, whose dimensions are a width of 4 m and a height of 4 m. The cross section of the New Atotsu entrance is the same of standard cross section of the arm tunnels.

Figure 5 shows how to conduct the excavation work. Excavation work must be done at multi working positions by multi worker groups. The first blast was conducted at the Mozumi access tunnel by a worker group that entered from the Mozumi entrance on 22th May, 2012. This worker group proceeded with the excavation work of the Mozumi access tunnel, the Yend area, and the Yarm tunnel, and stopped at the Ikenoyama fault because of spring water. All work from the Mozumi entrance was completed on 27th April, 2013. Another worker group started excavation of the New Atotsu access tunnel on 18th June, 2012, and reached the Center area on 1st October, 2012. This worker group completed the 1st floor of the Center area in 2012, and then started excavation of the Xarm tunnel and the Yarm tunnel on 24th December, 2012 and on 9th January, 2013, respectively. The Yarm tunnel was completed on 5th December, 2013. The Xarm tunnel was completed on 1st March, 2014. After completing the Xarm tunnel, excavation of the Xend area and the bypass tunnel started. All the excavation work for the KAGRA tunnels was completed by the end of March, 2014.

**Vibration Isolation Subsystem**

[Spokesperson : Ryutaro TAKAHASHI]
NAOJ, Mitaka, Musashisakai 181-8588

The vibration isolation is a very important system for the success of KAGRA. It should provide the seismic noise attenuation in the detection band and should reduce the mirror speed at low frequencies. It consist of several components including the pre-isolator, the mechanical filters based on the geometric anti-spring (GAS) filter, and the socalled "payload", which includes the mirror and all the components required for its suspension and control. Schematic view of the system is shown in figure 6.

The control of the inverted pendulum (IP) in the pre-isolator prototype was tested. The resonancies were inertially damped by the active control system successfully. The payload prototype was assembled and tested. The dummy test mass was suspended by two-loop wires with 10-mm gap so as to make the pitch mode frequency be lower ($\sim 1$ Hz). The optical sensor and electro-magnetic actuator module (OSEM) is used to control the test mass. Four OSEMs are attached onto the recoil mass, and the sensors and actuators were diagonalized to three degrees of freedom (transverse pitch, and yaw) successfully.

## Bibliography

[1] R. Takahashi, "Vibration Isolation System for Mirrors", J. Vac. Jpn **54** (2011) 24-27.

**Fabrication of cryostat and R&D for cryogenic items**

[Spokesperson : Kazuhiro YAMAMOTO]
ICRR, The Univ. of Tokyo, Kashiwa, Chiba 277-8582

***Outlines*** A key feature of KAGRA is the operation of the interferometer mirrors made from sapphire at cryogenic temperatures. This mirror is a part of the cryogenic payload and this payload is cooled. In 2013, a cooling test of KAGRA cryostats was performed and we studied radiation shield vibration and initial cooling time of a cryogenic payload in this cooling test. Other R&D research (cryogenic duct and sapphire suspension and so on) is also in progress. In the following, the details of these items and an international collaboration (ELiTES) are explained.

***Cooling test of KAGRA cryostat in 2013*** In fiscal year 2012, all four KAGRA cryostats were fabricated by Toshiba Keihin Product Operations and the cooling test of the all KAGRA cryostats themselves was conducted. We tried the cooling test for one cryostat again in 2013 at Toshiba Keihin Product Operations. The main purposes of this test were to measure the radiation shield vibration around 10 K and evaluate the initial cooling time of a cryogenic payload with heat links.

Any vibration of the radiation shield could contaminate the gravitational wave signal, being introduced through the heat links that is necessary to cool the mirrors as well as through scattered light. In order to evaluate this noise, the horizontal and vertical cryogenic accelerometers were developed at ICRR and University of Rome La Sapienza, respectively. We measured the vibration of the radiation shield around 10K. After this measurement, we derived the noise by the vibration

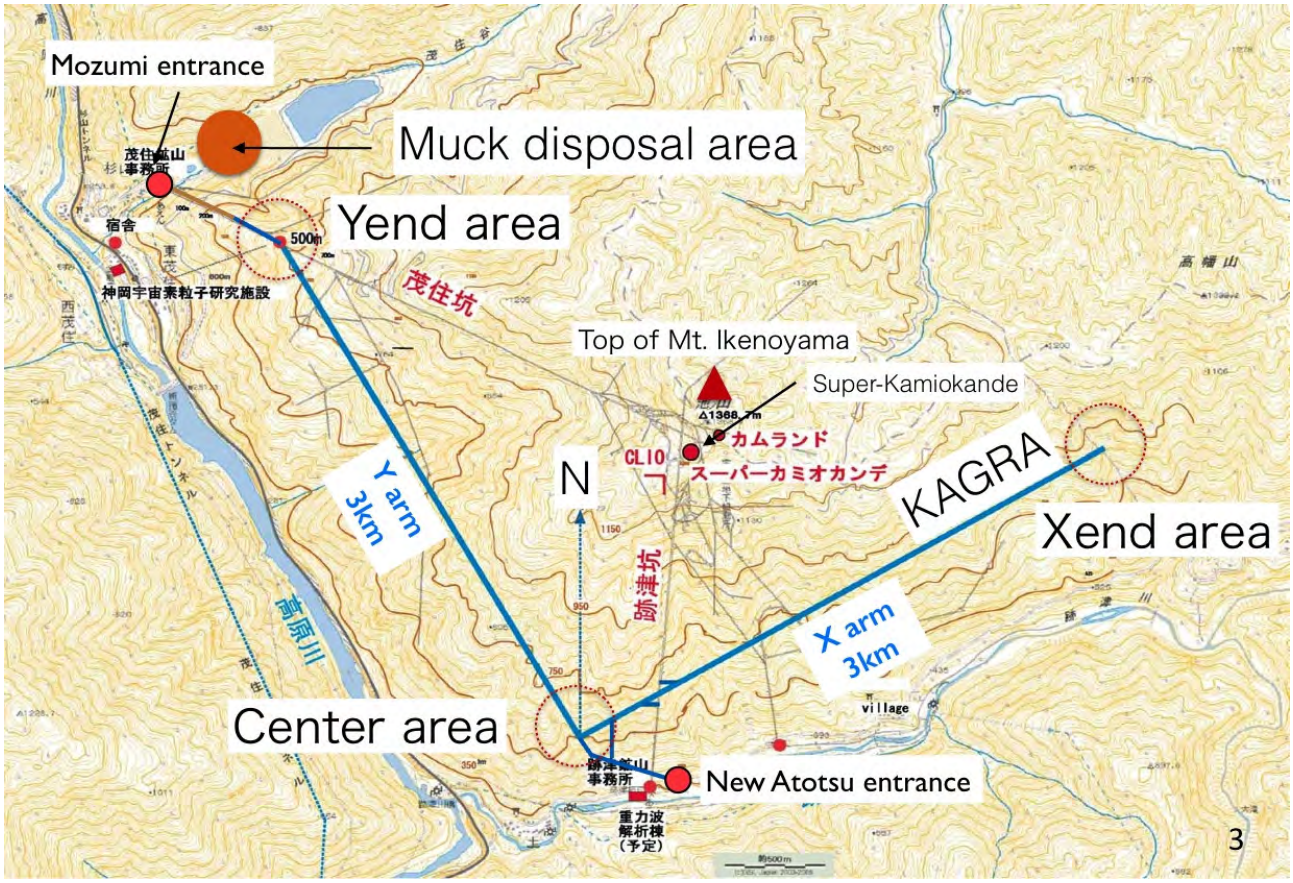


Fig. 4. Location map of the KAGRA tunnels. The tunnels are in Mt. Ikenoyama of Kamioka mine, whose top is at about 1,300 m. There are two 3,000 m arm tunnels connected perpendicularly. One arm tunnel in the north east direction is called Xarm; the other arm tunnel is called Yarm. The Center area, Xend area and Yend area, contain some experiment rooms, which are located at the connecting corner of the arm tunnels and at the end of both arm tunnels, respectively. All of the areas are inside at more than 200 m from the surface of the mountain in order to obtain the quiet seismic motion environment that we expected to be achieved at the underground site. Both arm tunnels are tilted by 1/300 for natural water drainage. The Xend area is at the highest altitude of about 382 m, and the Yend area is at the lowest altitude of about 362 m.The altitude of the Center area is 372 m.

via heat links from our measurement. We found that extra pendulums are necessary to reduce the vibration via the heat links. The details of these pendulums will be considered. We submitted the paper about this investigation to Classical and Quantum Gravity.

In the cooling test of 2012, we installed a half size cryogenic payload prototype without heat links in order to investigate the cooling time by radiation. In the cooling test of 2013, we installed the prototype cryogenic payload with pure copper heat links in order to evaluate the cooling time by the thermal conduction in the heat links. We found that the thermal conductivity of pure copper was not as high as that we expected. However, our other experiment showed annealing increases the thermal conductivity. We calculated the initial cooling time of a KAGRA cryogenic payload based on these experiment results. It is about 1 month. We submit the paper about this study to Classical and Quantum Gravity. We must take the thermal resistance at both ends of the heat links into account. The investigation is in progress.

***Cryogenic duct*** The radiation shields should have two large holes for the laser beam which are comparable in size with the diameter of the cooled mirror (220 mm). Through these holes, 300 K radiation will invade the radiation shield. Cryogenic ducts with baffles are necessary to prevent the propagation of 300 K radiation. We measured the heat transfer by this cryogenic duct and found that it is enough small for KAGRA as our calculation result (using ZEMAX). The scattered light by these cryogenic ducts could contaminate the output of KAGRA interferometer. We calculated the scattered light noise (again, using ZEMAX) with some assumptions. Fortunately, it is smaller than the KAGRA goal. However, for more precise evaluation, we have plans to measure cryogenic duct vibration and amplitude of the scattered light.

***1/4 cryostat*** Since the cryogenic payload is a complicated system, a test is necessary before the installation in the Kamioka mine. The 1/4 cryostat for this test was delivered on the September.

***Sapphire suspension*** The cooled mirror will be suspended by four sapphire fibers. These fibers must have nail heads on the fiber ends. MolTech GmbH and IMPEX HighTech GmbH (both of them are German companies) delivered the sapphire fibers with the nail heads. These sapphire fibers must have a high thermal conductivity to extract heat from the mir-

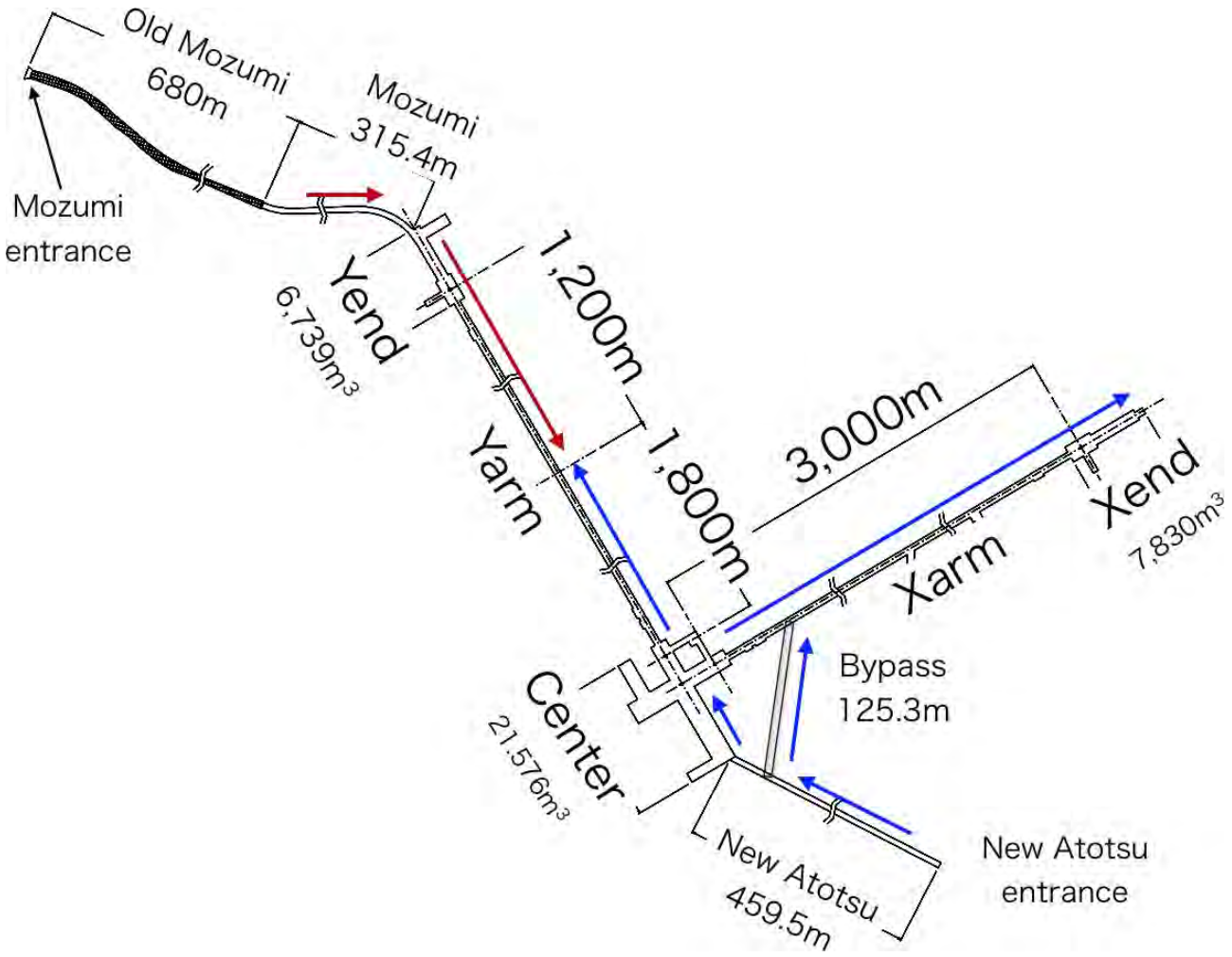


Fig. 5. Schematic view of the KAGRA tunnels. Arrows indicate the progress direction of excavation. Excavation work has been done at multi working positions by multi worker groups. A worker group entered from the Mozumi entrance and excavated the Mozumi access tunnel, the Yend area, and the Yarm tunnel of 1,200 m. Another worker group entered from the New Atotsu entrance and excavated the New Atotsu access tunnel and the Center area. After completing the 1st floor of the Center area, excavation of the Xarm and the Yarm has started. Excavation of the Xend area and the bypass tunnel was completed in the final period.

ror and high Q-values for small thermal noise. We measured these values and found that IMPEX fibers satisfy the requirements. The result of the thermal conductivity experiment was published (Classical and Quantum Gravity 31(2014)105004). Institute for Gravitational Research, University of Glasgow investigated the strength of the fibers and they are enough strong. The nail head in above experiments is a cylinder. However, for connection with the mirror, a square nail head is better. The fibers with the square nail heads were delivered and the investigation is in progress.

Sapphire blade springs are necessary to compensate the difference of the sapphire fibers. This spring was designed based on the strength test of sapphire plates at Glasgow. These springs are delivered soon and will be checked performance.

For connection between each part, bonding techniques are necessary. We are studying the Hydroxide Catalysis Bonding and Indium Bonding. The Hydroxide Catalysis Bonding is adopted in the room temperature gravitational wave detectors, Advanced LIGO and Advanced Virgo. The Indium Bonding is also necessary because the fibers and mirror can be taken apart when the fibers are broken. We tried the strength test of the Hydroxide Catalysis Bonding and the analysis is in progress. We are measuring thermal resistance of the bonding and have plans to investigate mechanical loss of bonding at cryogenic temperature.

***ELiTES*** ELiTES (ET-LCGT interferometric Telescope Exchange of Scientists) is a European grant (European 7th Framework Programme Marie Curie action between Mar. 2012 and Feb. 2016) for the collaboration between KAGRA and Einstein Telescope (European future project). People in Europe visit Japan for KAGRA. In 2013, a total of 25 visitors (from Germany, Netherland, U.K., Italy) were supported by ELiTES. Many of them helped the development of the sapphire suspension; the development of an automatic measurement system (and measurement with this system) of the thermal conductivity and Q-values of sapphire fibers and so on, sapphire fiber and plate strength tests, the lecture about how to make the Hydroxide Catalysis Bonding, the investigation of how to make the Indium Bonding, strength tests of Hydroxide Catalysis Bonding, the measurement of thermal resistance and mechanical loss of the Hydroxide Catalysis Bonding and Indium

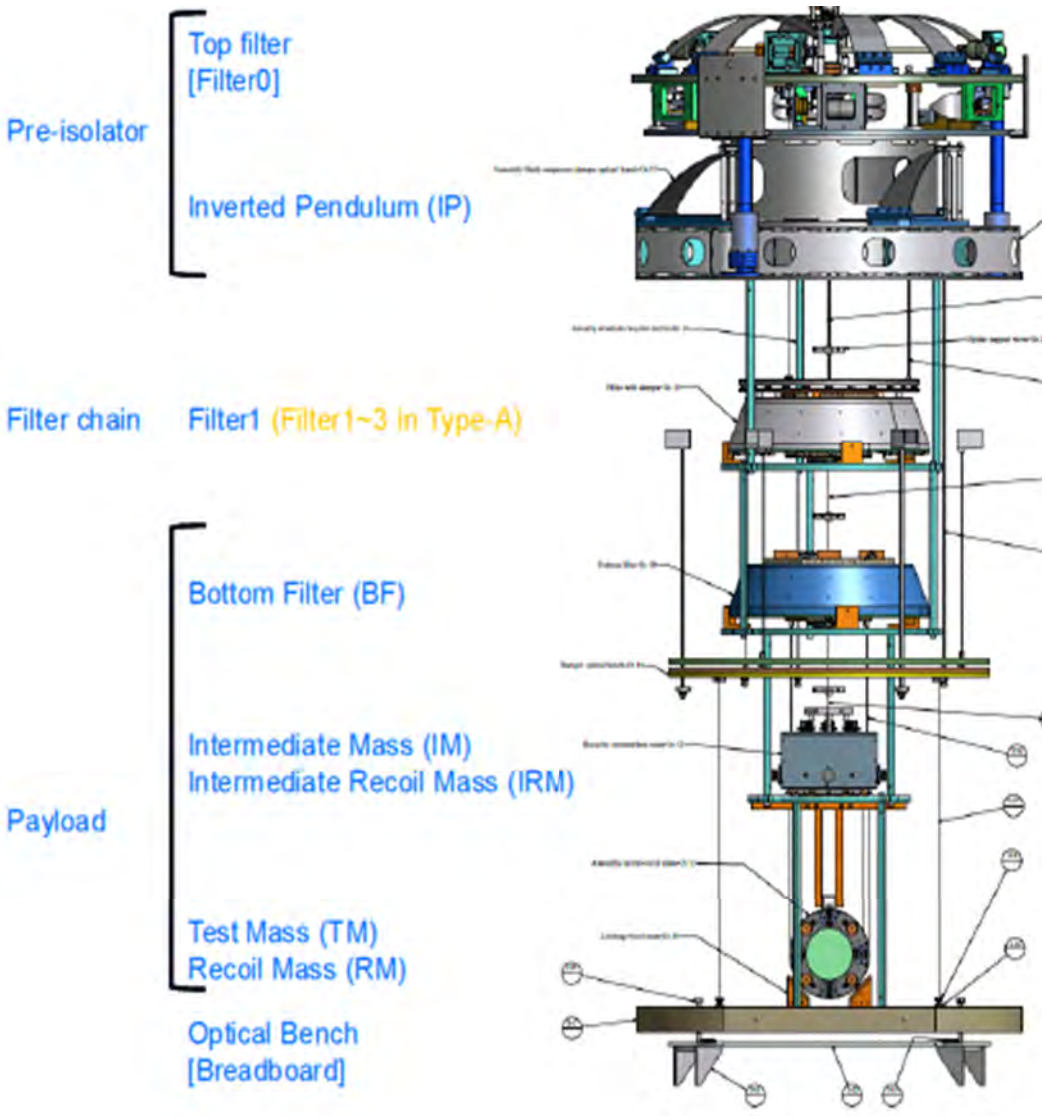


Fig. 6. Schematic view of the seismic attenuation system. The system for the cryogenic mirror has additional two filters (Filter2 and 3).

Bonding. Some other people supported the measurement of the radiation shield vibration, the development of the vibration isolation system at room temperature, the investigation of annealed tungsten, the control system for cryogenic payload, the measurement of the reflective coating mechanical loss at low temperature, the study of the reflective coating on the mirror with smaller thermal noise, the ponderomotive squeezing experiment, environmental sensors and so on.

Moreover, ELiTES stimulated Japanese graduate students to visit Europe. Three graduate students in Ph.D. course of our project office stayed at University of Glasgow and Friedrich-Schiller-Universitaet Jena, NIKHEF (Amsterdam), University of Rome La Sapienza, respectively, within a few months.

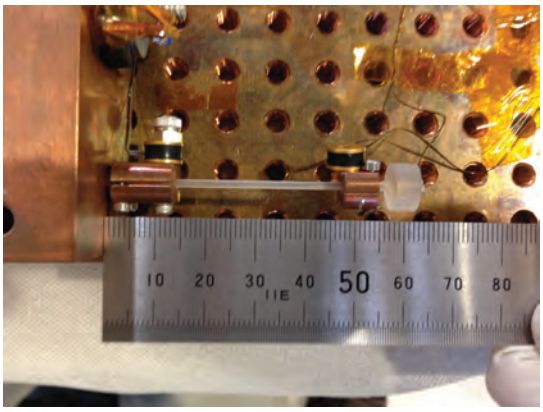


Fig. 7. A test piece of the sapphire fiber with nail heads (a white bar with a white nail head on the right hand side). This piece is installed in an apparatus to measure the thermal conductivity. The actual KAGRA fibers to suspend the mirror are about 300 mm in length.

**Data aqcuisition and control**

[Spokesperson : Osamu MIYAKAWA]
ICRR, The Univ. of Tokyo, Hida, Gifu 506-1205

KAGRA collects many signals from all of subsystems in the interferometer, not only for a main gravitational wave sig-

nal but also additional control signals for length and alignment of optics, physical environmental monitor signals from sensors and so on. The total number of signals will be more than 2000 channels. These signals are collected into a data acquisition (DAQ) system. In this fiscal year, we have constructed and tested a full scale DAQ system for KAGRA as a preparation of installation into the mine (see Fig.8). DAQ system consists of 3 parts, Data Concentrator (DC), Network Data Service (NDS) and Frame Writer (FW). All the data from KAGRA is collected into the DC server once, and it is distributed into the NDS and FW servers through 10GB network with a low latency protocol. The NDS server works as a data manager which is responsible for requests from users or data analysis software. The FW server stores some selected data as DAQ channels into disks. We have prepared 200 TB disk storage for the initial operation of KAGRA for one month full data and one-two years commissioning data for full KAGRA. Whole KAGRA may require several Peta-byte class data storage for observation in several years.

Fig. 8. Part of DAQ system for KAGRA. All data from KAGRA is collected into these computers. The DAQ system and real time front-end computers are synchronized by timing system shown in blue chassis in this picture.

Another important part of KAGRA's control system is the real time front-end (RTFE) which consists of a server class computer, PCIe extension chassis, ADC (analog to digital converter) and DAC (digital to analog converter) modules. ADC is a front-end of DAQ, on the other hand DAC is a front-end of control. Signals from sensors in an interferometer are collected by ADC, then they are filtered in computers, and finally they are fedback to mirrors to actuate the interferometer. A transmission of control signals among computers is very critical. Even a small delay which may happen in the general network protocol can break control loops easily. To establish a very low latency connection, the reflective memory (RFM) networks are used in this system. Memories of remote computers are immediately reflected on memories of the local computer through the RFM.

We have tested connections between multiple RTFM computers and above the DAQ system, and we verified that all the data from computers is collected in the DC server and transmitted into downstream with 10GB speed. This system is called a Large scale Network System (LNS) in altogether. This LNS is a preparation of KAGRA's control system which has been constructed outside of the mine, and the whole system of this LNS will be directly moved into the mine. It will be used as an actual full scale KAGRA's control system with some additional RTFE computers connected into subsystems of KAGRA, e.g. vibration isolation system or photo detectors.

Between the digital system and subsystem, or to make subsystem itself work, many analog circuits will be used in KAGRA. The total number of circuit will be more than 800 boxes. We are designing and manufacturing the circuits. Recently we have just started providing the circuits to people who need circuits for their subsystem.

Combined system with analog and digital will provide us not only to control the interferometer but also to establish a total monitoring/diagnostic system for an observation of the gravitational waves in the future.

**Collaboration research with the Korean gravitational wave group**

[Spokesperson : Seiji KAWAMURA]
ICRR, The Univ. of Tokyo, Hida, Gifu 506-1205

We have a close collaboration on KAGRA with the Korean gravitational wave group since 2012. We exchanged some researchers to perform some collaboration research with the help of the JSPS core-to-core program we obtained starting from April, 2013. For the instrument development, Tai Hyun Yoon (Korea University) spent two months in the summer of 2013 at ICRR as a visiting professor to develop the fiber ring cavity with his student and another student of Norikatsu Mio (University of Tokyo). He successfully stabilized the laser frequency using the fiber ring cavity. Later in the KAGRA input/output optics group led by Seiji Kawamura (ICRR) we discussed and decided to use the technology for iKAGRA if the frequency stability attained is satisfactory. Then it was decided and approved that Tai Hyun Yoon will visit ICRR again for two months in the summer of 2014 as a visiting professor to refine the system and measure the stability. For the data analysis led by Hideyuki Tagoshi (Osaka University), as one of the collaboration research between Japan and Korea, we worked on the Bayesian parameter estimation method of the gravitational waves from colasescing compact binaries in the KAGRA data analysis. From the Korean side, Hyung Won Lee (Inje University), Jeongcho Kim (Inje University), and

Chunglee Kim (Seoul National University) participated this research. We had been working on the research of basic papers on the Bayesian parameter estimation methods and the profiling the pipeline used in the LIGO data analysis. For the detector characterization led by Kazuhiro Hayama (Osaka City University), in order for KAGRA to reach its design sensitivity quickly, one of important activities was to develop a system to localize noise sources to be suppressed using information from the auxiliary instrumental channels. We collaborated with the Korean detector characterization group, involving John J. Oh (NIMS), Sang-Hoon Oh (NIMS), Edwin J. Son (NIMS), and Young-Ming Kim (PNU), to develop the system based on the multi-channel analysis method based on the artificial neural network (ANN) algorithm, which the Korean group had developed. The Japanese members were granted accounts to access the KISTI cluster in Korea and start collaborating development using the LIGO S5 auxiliary channel data on the cluster. We have been integrating the ANN based multi-channel analysis software package into our detector-characterization software package called HasKAL. For the data management, we considered the data tier plans, including usage of GRID computing. We also contacted Japanese and Korean astronomers who were working on optical observations, or X- and Gamma-Ray detectors. Between April, 2013 and March, 2014, we had two Korea-Japan workshops on KAGRA and we discussed the past activities and future plan in details.

### *CLIO Project*

[Spokesperson : Masatake Ohashi]

ICRR, The Univ. of Tokyo, Kashiwa, Chiba 277-8582
In collaboration with members of: KEK, Tsukuba; Kyoto-U, Kyoto; ERI of UT, Tokyo

#### Overview of CLIO

CLIO (Cryogenic Laser Interferometer Observatory) is a 100 m-baseline underground cryogenic interferometer at the Kamioka Mine. CLIO forms a bridge connecting the CLIK (7 m prototype cryogenic interferometer at Kashiwa campus) and the KAGRA (3 km cryogenic interferometer at Kamioka). The site of CLIO, near the Super-Kamiokande neutrino detector, is shown in Fig. 9. The tunnel was dug in 2002, and a strain meter for geophysics was installed in 2003 [1]. The construction of CLIO began in late 2003, and installation of the mode cleaner vacuum system was reported in the annual report (2003–2004). Four sets of cryostats and whole vacuum system were installed (annual report 2004–2005). We started the operation of CLIO in 2006 (annual report 2006).

The prime purpose of CLIO is to demonstrate mirror thermal noise reduction with cryogenic mirrors. We achieved the design sensitivity at the room temperature after noise hunting taken in 2008 (Annual report 2008) [2, 3]. After then, we started out cooling the mirrors and noise hunting with the mirrors under 20K had been done. We firstly observed the sensitivity improvement due to the mirror thermal noise reduction.

CLIO sensitivity curve with cooled mirrors (cryogenic sensitivity) and without cooling (300K sensitivity) are shown in Fig. 12 with estimation curves of the mirror thermal noise. The 300K sensitivity and the cryogenic sensitivity were measured at 2008/11/5 and at 2010/03/20, respectively. When the cryogenic sensitivity was measured, two front mirrors were cooled and the rest of two end mirrors were at the room temperature. Temperature of the front mirrors were 17K and 18K. Modifications possibly affecting the sensitivity at the cryogenic sensitivity measurement are exchange of final suspension wires and addition of heat link wires to the suspension systems. Cooling the mirror took about 250 hours and vacuum pressure was better than $10^{-4}$Pa for both sensitivity measurements.

Fig. 10. Overview of the CLIO interferometer.

The noise floor level of the cryogenic sensitivity from 90Hz to 240Hz is below the 300K sensitivity. Observation range for GWs from neutron star binary coalescence was also improved to 159kpc from 148kpc for the optimum direction. This is the first observation of sensitivity improvement by the cryogenic mirrors. The noise floor at 165Hz was reduced to $2.2 \times 10^{-19}\,\mathrm{m}/\sqrt{\mathrm{Hz}}$ from $3.1 \times 10^{-19}\,\mathrm{m}/\sqrt{\mathrm{Hz}}$ after cooling the front mirrors. Amount of this noise floor reduction is consistent with the estimation of mirror thermal noise reduction due to cooling. This achievement has been published in 2012 [4].

#### Digital control in CLIO

Since KAGRA will have a very complicated control topology in its optical configuration called as RSE (resonant sideband extraction). A digital control system using multiple computers will be used since the computer based human interface provides us a very good flexibility to control such a complicated interferometer, and it is expected to reduce noise hunting time for KAGRA.

We are continuously developing a standalone based digital controls system in CLIO. CLIO is a very good test bench for the control system since we can use a whole function of the begin operated interferometer, and the gravitational wave data and the control signal data produced by CLIO are quite similar as KAGRA's data. Advanced lock acquisition techniques were tested with this system and it was shown that the noise performance using whitening/dewhitening filters was almost the same as the analog control servo. Recently some data monitoring system and timing synchronization have been de-

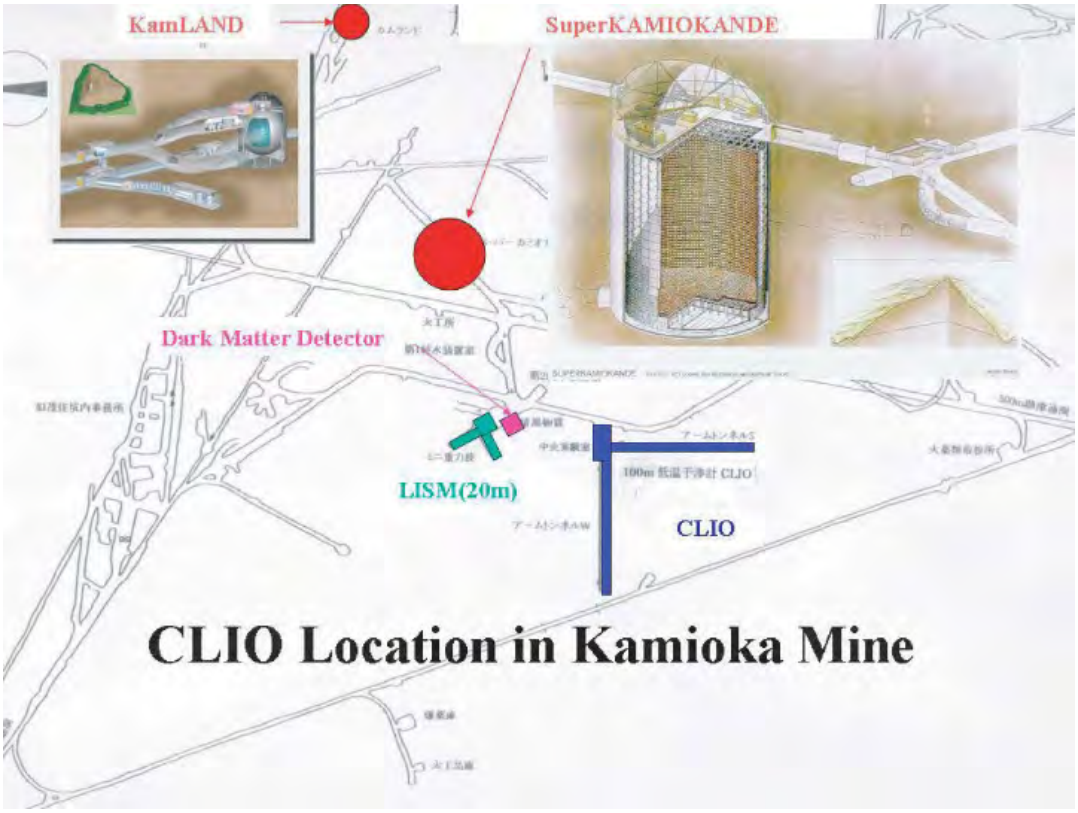


Fig. 9. Location of the CLIO interferometer.

Fig. 11. A sapphire mirror and cryogenic suspension system

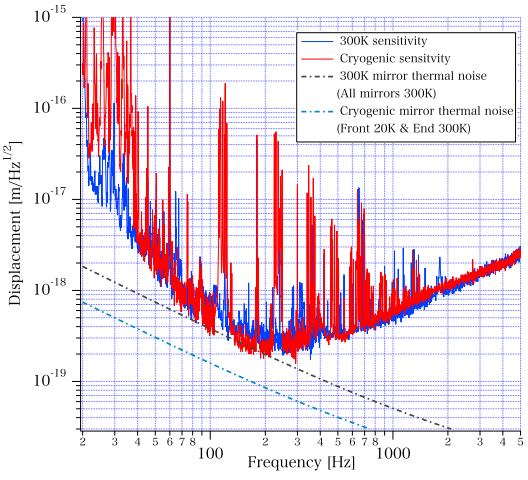


Fig. 12. Comparison of CLIO sensitivity curves. 300K sensitivity (solid blue line) and Cryogenic sensitivity (solid red line) show CLIO sensitivity curves without cooling mirrors measured at 2008/11/05 and with front mirrors under 20K measured at 2010/03/20, respectively. 300K mirror thermal noise (dot dash gray line) and Cryogenic mirror thermal noise (dot dash blue line) show estimation curve of mirror thermal noise corresponding to the each sensitivity measurements.

veloped and tested, and the results are ready to be used in a larger scale control systems for KAGRA.

**Study for the next generation techniques**

Although construction of KAGRA is on going, researches and developments of techniques to realize much more sensitive detectors are still important. Since CLIO still maintains the sensitivity, CLIO is a suitable apparatus to test techniques which need a cryogenic laser interferometer. Two study topics using CLIO for the next generation techniques are on going. One is development of low-loss optical coating. Another is development of a high finesse Fabry-Perot cavity using NQD method[5].

The mirror thermal noise is still a serious fundamental noise even using the cryogenic mirror. Dissipation in optical coatings on a mirror surface will be dominate the amplitude of the thermal noise in cryogenic temperature. Purpose of the development of low-loss mirror coatings is to reduce the mirror thermal noise further more. The current status of the study is looking for a recipe of a low-loss optical coatings using dissipation measurements of samples of coatings made by an Ion Beam Spattering machine at NAOJ Mitaka. After finding the recipe, we will make mirrors whose substrates are monolithic sapphire, dimensions are the same as the mirrors of CLIO. The mirrors will be installed in CLIO and we will investigate the mirror thermal noise reduction in cryogenic temperature.

A Fabry-Perot cavity having a high finesse and a long cavity length is important to realize Resonant Sideband Extraction (RSE) method with a higher gain. The high gain RSE provides not only a sensitivity improvement in high frequency region, but also decreasing heat generation in test masses caused by laser absorption in substrates. The decreasing heat generation is important for cooling test masses at cryogenic temperature. The most difficult issue to realize a Fabry-Perot cavity having a high finesse and a long cavity length is a lock acquisition for an optical cavity to resonance. Since we have already developed NQD method[5] to solve this issue using the Mode Cleaner optical cavity of CLIO, we will apply this method to the 100 m arm cavity of CLIO to demonstrate a Fabry-Perot cavity having a high finesse and a long cavity length. We are making new test masses made of sapphire as well as the current test masses of CLIO, and new test masses will have laser reflection coating whose reflection ratio of 0.99999 instead of the current value of 0.999. We will exchange new test masses with high reflection with the current test masses, and construct Fabry-Peort cavities whose length is 100 m and Finesse is 300,000 instead of the current Finesse of 3,000.

## Bibliography


[1] S. Takemoto, *et al.*, Journal of Geodynamics **41** (2006) 23.

[2] S. Miyoki, *et al.*, Journal of Physics: Conference Series **203** (2010) 012075.

[3] T. Uchiyama and S. Miyoki, "Experimental Demonstration of Cryogenic Mirror Technique - Achievements of CLIO-", J. Cryo. Super. Soc. Jpn., **46** (2011) 392-399.

[4] Takashi Uchiyama, Shinji Miyoki, Souichi Telada, Kazuhiro Yamamoto, Masatake Ohashi, Kazuhiro Agatsuma, Koji Arai, Masa-Katsu Fujimoto, Tomiyoshi Haruyama, Seiji Kawamura, Osamu Miyakawa, Naoko Ohishi, Takanori Saito, Takakazu Shintomi, Toshikazu Suzuki, Ryutaro Takahashi, Daisuke Tatsumi, "Reduction of thermal fluctuations in a cryogenic laser interferometric gravitational wave detector", Phys. Rev. Lett. **108**, 141101 (2012) [5 pages].

[5] S. Miyoki, S.Telada and T.Uchiyama, "Expansion of linear range of Pound-Drever-Hall signal", Applied Optics, Vol. 49, Issue 28, pp.5217-5225 (2010) .


# Observational Cosmology Group


[Spokesperson : Yoshiaki Ono]

ICRR, The Univ. of Tokyo, Kashiwa, Chiba 277-8582


### *An Intensely Star-Forming Galaxy at* $z \sim 7$ *with Low Dust and Metal Content Revealed by Deep ALMA and HST Observations* [1]

In collaboration with the members of The University of Tokyo, Kavli Institute for the Physics and Mathematics of the Universe, California Institute of Technology, The Graduate University for Advanced Studies, Joint ALMA Observatory, Harvard-Smithsonian Center for Astrophysics, and National Astronomical Observatory of Japan.

We report deep ALMA observations complemented by associated *HST* imaging for a luminous ($m_{\rm UV} = 25$) galaxy, "Himiko", at a redshift $z = 6.595$. The galaxy is remarkable for its high star formation rate, $100 M_\odot {\rm yr}^{-1}$, which has been securely estimated from our deep *HST* and *Spitzer* photometry, and the absence of any evidence for strong AGN activity or gravitational lensing magnification. Our ALMA observations probe an order of magnitude deeper than previous IRAM observations, yet fail to detect a 1.2 mm dust continuum, indicating a flux of $< 52 \mu$Jy, which is comparable to or weaker than that of local dwarf irregulars with much lower star formation rates (Figure 13). We likewise provide a strong upper limit for the flux of [CII] 158$\mu$m, $L_{\rm [CII]} < 5.4 \times 10^7 L_\odot$, which is a diagnostic of the hot interstellar gas that is often described as a valuable probe for early galaxies. In fact, our observations indicate that Himiko lies off the local $L_{\rm [CII]}$–star formation rate scaling relation by a factor of more than 30. Both aspects of our ALMA observations suggest Himiko is a unique object with a very low dust content and perhaps nearly primordial interstellar gas. Our *HST* images provide unique insight into the morphology of this remarkable source, highlighting an extremely blue core of activity and two less extreme associated clumps. Himiko is undergoing a triple major merger event whose extensive ionized nebula of Ly$\alpha$ emitting gas, discovered in our earlier work with Subaru, is powered by star formation and the dense circumgalactic gas. We are likely witnessing an early massive galaxy during a key period of its mass assembly close to the end of the reionization era.

## Bibliography


[1] Ouchi, M., et al. 2013, Astrophys. J., 778, 102


### *Evolution of the Sizes of Galaxies over* $7 < z < 12$ *Revealed by the 2012 Hubble Ultra Deep Field Campaign* [2]

In collaboration with the members of The University of Tokyo, Kavli Institute for the Physics and Mathematics of the Universe, University of Edinburgh, California Institute of Tech-

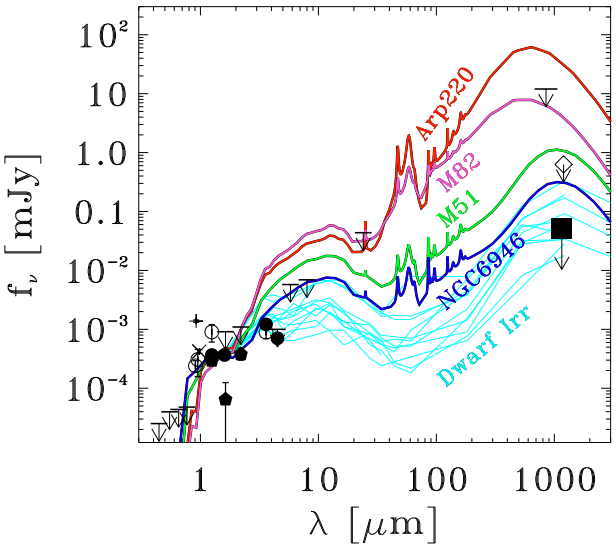


Fig. 13. Optical to far-infrared SED of Himiko in the observed frame. The filled square shows the upper limit from our deep ALMA Band 6 observations and the filled circles represent photometry from *HST*/WFC3 $J_{125}$ and $H_{160}$ photometry and *Spitzer* SEDS 3.6 and 4.5$\mu$m. The filled pentagons indicate the UKIDSS-UDS DR8 $J$, $H$, and $K$ photometry. The cross and plus symbols denote *HST*/WFC3 $F098M$ and Suprime-Cam $NB921$ photometry that includes Ly$\alpha$ emission and the Gunn-Peterson trough in their bandpasses. The open circles and arrows are data points and the upper limits taken from the literature. The open diamond with an arrow shows the upper limit from the IRAM observations. The red, magenta, green, and blue lines represent the SEDs of local galaxies, Arp220, M82, M51, and NGC6946, respectively, redshifted to $z = 6.595$. SEDs of local dwarf irregular galaxies similarly redshifted are presented with cyan lines. All local galaxy SEDs are normalized in the rest-frame UV, where Himiko's SED is reliably determined. This figure is reproduced by permission of the AAS.

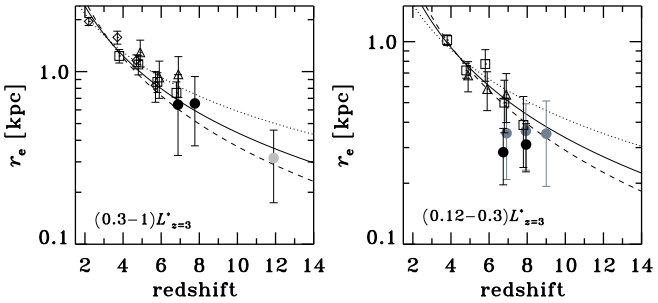


Fig. 14. *Left*: evolution of the half-light radius across the redshift range from $z \sim 2$ to 12 in $(0.3-1)L^*_{z=3}$. The filled circles show the average sizes of our $z_{850}$-dropouts and $Y_{105}$-dropouts, and the size of the $z \sim 12$ object. The open symbols are taken from the literature After excluding the sample overlaps, we fit simple functions of $(1+z)^s$ with the data in both luminosity bins, and obtain $s = -1.30^{+0.12}_{-0.14}$. which is shown as the solid line. The dotted and dashed lines correspond to the case of $s = -1.0$ and $-1.5$, respectively. *Right*: evolution of the half-light radius across the redshift range from $z \sim 4$ to 8 in $(0.12-0.3)L^*_{z=3}$. The open and filled black symbols denote the same as those in the top panel. The gray filled circles are dropout galaxies in the fainter luminosity bin, $(0.048-0.12)L^*_{z=3}$. The solid, dotted, and dashed lines are the same as those in the left panel. This figure is reproduced by permission of the AAS.

nology, University of Arizona, Space Telescope Science Institute, Institut d'Astrophysique de Paris, and University of California.

We analyze the redshift- and luminosity-dependent sizes of dropout galaxy candidates in the redshift range $z \sim 7-12$ using deep images from the 2012 Hubble Ultra Deep Field (UDF12) campaign, which offers two advantages over that used in earlier work. First, we utilize the increased signal-to-noise ratio offered by the UDF12 imaging to provide improved measurements for known galaxies at $z \simeq 6.5-8$ in the HUDF. Second, because the UDF12 data have allowed the construction of the first robust galaxy sample in the HUDF at $z > 8$, we have been able to extend the measurement of average galaxy size out to higher redshifts. Restricting our measurements to sources detected at $> 15\sigma$, we confirm earlier indications that the average half-light radii of $z \sim 7-12$ galaxies are extremely small, $0.3-0.4$ kpc, comparable to the sizes of giant molecular associations in local star-forming galaxies. We also confirm that there is a clear trend of decreasing half-light radius with increasing redshift, and provide the first evidence that this trend continues beyond $z \simeq 8$ (Figure 14). Modeling the evolution of the average half-light radius as a power-law, $\propto (1+z)^s$, we obtain a best-fit index of $s = -1.30^{+0.12}_{-0.14}$ over $z \sim 4-12$. A clear size-luminosity relation is evident in our dropout samples. This relation can be interpreted in terms of a constant surface density of star formation over a range in luminosity of $0.05-1.0L^*_{z=3}$. The average star formation surface density in dropout galaxies is $2-3$ orders of magnitude lower than that found in extreme starburst galaxies, but is comparable to that seen today in the centers of normal disk galaxies.

## Bibliography

[2] Ono, Y., Ouchi, M., et al. 2013, Astrophys. J., 777, 155

### *What is the Physical Origin of Strong Ly$\alpha$ Emission? I. Demographics of Ly$\alpha$ Emitter Structures* [3]

In collaboration with the members of The University of Tokyo, The University of Tsukuba, and Kavli Institute for the Physics and Mathematics of the Universe.

We present the results of structure analyses for a large sample of 426 Ly$\alpha$ emitters (LAEs) at $z \sim 2.2$ that are observed with *HST*/ACS and WFC3-IR during deep extra-galactic legacy surveys. We confirm that the merger fraction and the average ellipticity of LAE's stellar component are $10-30\%$ and $0.4-0.6$, respectively, that are comparable with previous study results. We successfully identify that some LAEs have a spatial offset between Ly$\alpha$ and stellar-continuum emission peaks, $\delta_{\mathrm{Ly}\alpha}$, by $\sim 2.5-4$ kpc beyond our statistical errors. To uncover the physical origin of strong Ly$\alpha$ emission found in LAEs, we investigate the Ly$\alpha$ equivalent width (EW) dependences of three structural parameters: merger fraction, $\delta_{\mathrm{Ly}\alpha}$, and ellipticity of stellar distribution in the range of $EW(\mathrm{Ly}\alpha) = 20-250$ Å. Contrary to expectations, we find that the merger fraction does not significantly increase with Ly$\alpha$ EW (Figure 15). We reveal an anti-correlation between $\delta_{\mathrm{Ly}\alpha}$ and $EW(\mathrm{Ly}\alpha)$ using a Kolmogorov–Smirnov (K-S) test. There is a trend that the LAEs with a large Ly$\alpha$ EW have a small ellipticity. This

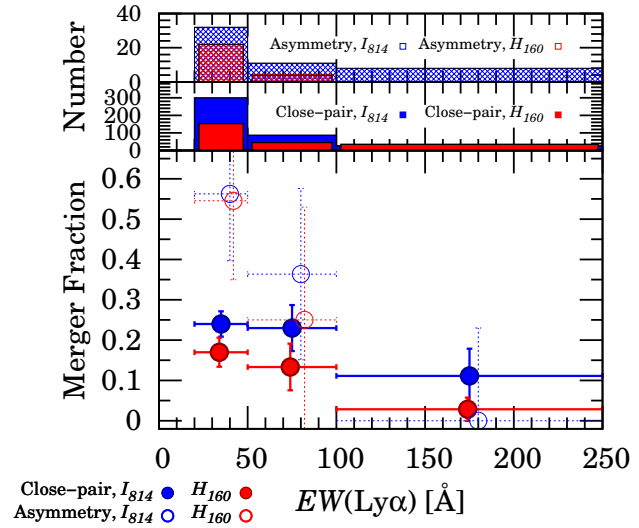


Fig. 15. Merger fraction of $z = 2.2$ LAEs as a function of Ly$\alpha$ EW. The blue and red symbols indicate the merger fractions in $I_{814}$ and $H_{160}$, respectively. The filled and open circles denote the merger fraction in the close-pair method and the $A$ classification, respectively. Error bars in each plot include the Poisson statistical error. Error bars in Ly$\alpha$ EW indicate the bin widths. The symbols are slightly shifted along the $x$-axis for the sake of clarity. There are no LAEs in $H_{160}$ in the highest EW bin for the $A$ classification, because no mergers are found in this EW bin. The histograms in the upper and middle panels show the number of LAEs in each Ly$\alpha$ EW bin in the $A$ classification and the close-pair method, respectively. This figure is reproduced by permission of the AAS.

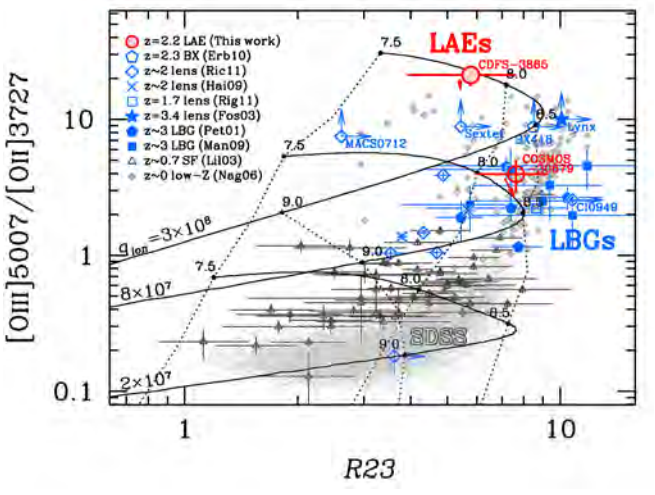


Fig. 16. Emission line flux ratio [O III]/[O II] vs. $R23$-index for our $z = 2.2$ LAEs (CDFS-3865: the solid red circle; COSMOS-30679: the open red circle) and non-LAEs (the blue symbols); the metal-poor BX galaxy at $z = 2.3$ (the open pentagon), lensed galaxies at $z \sim 2$ (the crosses, the open diamonds, and the open square), the lensed galaxy at $z = 3.4$ (the solid star), and $z \sim 3$ LBGs (the solid pentagons, the solid squares), as well as the star-forming galaxies at $0.47 < z < 0.92$ (the black open triangles), and local star-forming galaxies in the low-metallicity range ($7 \lesssim 12+\log(\mathrm{O/H}) \lesssim 8.5$: the gray diamonds) and high-metallicity range ($12+\log(\mathrm{O/H}) \gtrsim 8.2$: the gray dots). The values on this plot are not corrected for dust extinction, except for the local data points. For CDFS-3865 and COSMOS-30679, effects of their extinction corrections are indicated by the red small arrows. The black grid shows photoionization model calculations. For reference, the relations of $q_{ion} = 3\times10^8$, $8\times10^7$, and $2\times10^7$ cm s$^{-1}$ are shown, linked to each other at same metallicities, which are denoted by $12+\log(\mathrm{O/H})$ values with dots. This figure is reproduced by permission of the AAS.

is consistent with the recent theoretical claims that Ly$\alpha$ photons can more easily escape from face-on disks having a small ellipticity, due to less inter-stellar gas along the line of sight, although our KS test indicates that this trend is not statistically significant. Our results of Ly$\alpha$-EW dependence generally support the idea that an H I column density is a key quantity determining Ly$\alpha$ emissivity.

## Bibliography

[3] Shibuya, T., Ouchi, M., et al. 2014 Astrophys. J., 785, 64

### *First Spectroscopic Evidence for High Ionization State and Low Oxygen Abundance in Ly$\alpha$ Emitters* [4]

In collaboration with the members of The University of Tokyo, Kavli Institute for the Physics and Mathematics of the Universe, Space Telescope Science Institute, and Observatories of the Carnegie Institution of Washington.

We present results from Keck NIRSPEC and Magellan MMIRS follow-up spectroscopy of Ly$\alpha$ emitters (LAEs) at $z = 2.2$ identified in our Subaru narrowband survey. We successfully detect H$\alpha$ emission from seven LAEs, and perform a detailed analysis of six LAEs free from AGN activity, two out of which, CDFS-3865 and COSMOS-30679, have [O II] and [O III] line detections. They are the first [O II]-detected LAEs at high-$z$, and their [O III]/[O II] ratios and $R23$-indices provide the first simultaneous determinations of ionization parameter and oxygen abundance for LAEs (Figure 16). CDFS-3865 has a very high ionization parameter ($q_{ion} = 2.5^{+1.7}_{-0.8} \times 10^8$ cm s$^{-1}$) and a low oxygen abundance ($12+\log(\mathrm{O/H}) = 7.84^{+0.24}_{-0.25}$) in contrast with moderate values of other high-$z$ galaxies such as Lyman break galaxies (LBGs). COSMOS-30679 also possesses a relatively high ionization parameter ($q_{ion} = 8^{+10}_{-4} \times 10^7$ cm s$^{-1}$) and a low oxygen abundance ($12+\log(\mathrm{O/H}) = 8.18^{+0.28}_{-0.28}$). Both LAEs appear to fall below the mass-metallicity relation of $z \sim 2$ LBGs. Similarly, a low metallicity of $12+\log(\mathrm{O/H}) < 8.4$ is independently indicated for typical LAEs from a composite spectrum and the [N II]/H$\alpha$ index. Such high ionization parameters and low oxygen abundances can be found in local star-forming galaxies, but this extreme local population occupies only $\sim 0.06\%$ of the SDSS spectroscopic galaxy sample with a number density $\sim 100$ times smaller than that of LAEs. With their high ionization parameters and low oxygen abundances, LAEs would represent an early stage of galaxy formation dominated by massive stars in compact star-forming regions. High-$q_{ion}$ galaxies like LAEs would produce ionizing photons efficiently with a high escape fraction achieved by density-bounded HII regions, which would significantly contribute to cosmic reionization at $z > 6$.

## Bibliography

[4] Nakajima, K., Ouchi, M., et al. 2013 Astrophys. J., 769, 3

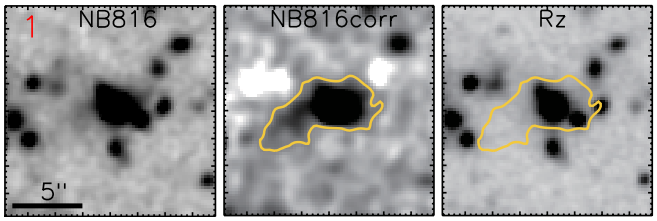


Fig. 17. *NB816*, *NB816*$_{\rm corr}$, and *Rz* images of O IIB 1. North is up and east is left. Each panel is $15'' \times 15''$ (corresponding to 124 kpc $\times$124 kpc at $z = 1.19$) with the O IIB at the center. The spatial scale is indicated in the *NB816* images. The yellow contours in the *Rz* images show the isophotal area above $2\sigma$ arcsec$^{-2}$ in the *NB816*$_{\rm corr}$ image. This figure is reproduced by permission of the AAS.

### *First Systematic Search for Oxygen-Line Blobs at High Redshift: Uncovering AGN Feedback and Star-Formation Quenching* [5]

In collaboration with the members of The University of Tokyo, Liverpool John Moores University, Tohoku University, and University of Tsukuba.

We present the first *systematic* search for extended metal-line [O II]$\lambda\lambda$3726,3729 nebulae, or [O II] blobs (O IIBs), at $z = 1.2$ using deep narrowband imaging with a survey volume of $1.9 \times 10^5$ Mpc$^3$ on the 0.62 deg$^2$ sky of Subaru–*XMM* Deep Survey (SXDS) field. We discover a giant O IIB, dubbed "O IIB 1" (Figure 17), with a spatial extent over $\sim$ 75 kpc at a spectroscopic redshift of $z = 1.18$, and also identify a total of 12 O IIBs with a size of $>$ 30 kpc. Our optical spectrum of O IIB 1 presents [Ne V]$\lambda$3426 line at the $6\sigma$ level, indicating that this object harbors an obscured type-2 AGN. The presence of gas outflows in this object is suggested by two marginal detections of Fe II$\lambda$2587 absorption and Fe II$^*\lambda$2613 emission lines both of which are blueshifted at as large as $500-600$ km s$^{-1}$, indicating that the heating source of O IIB 1 is AGN or associated shock excitation rather than supernovae produced by starbursts. The number density of O IIB 1-type giant blobs is estimated to be $\sim 5 \times 10^{-6}$ Mpc$^{-3}$ at $z \sim 1.2$, which is comparable with that of AGNs driving outflow at a similar redshift, suggesting that giant O IIBs are produced only by AGN activity. On the other hand, the number density of small O IIBs, $6 \times 10^{-5}$ Mpc$^{-3}$, compared to that of $z \sim 1$ galaxies in the blue cloud in the same $M_B$ range, may imply that 3% of star-forming galaxies at $z \sim 1$ are quenching star formation through outflows involving extended [O II] emission.

## Bibliography

[5] Yuma, S., Ouchi, M., et al. 2013, Astrophys. J., 779, 53

### *Star Formation On Subkiloparsec Scale Triggered by Non-linear Processes in Nearby Spiral Galaxies* [6]

In collaboration with the members of The University of Tokyo, National Astronomical Observatory of Japan, Stony Brook

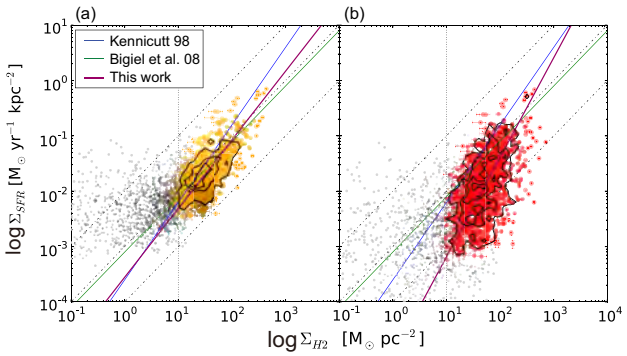


Fig. 18. K-S plot on 500 pc scale, (a) without and (b) with BG subtraction, for our 10 sample galaxies. The dot-dashed lines are SFEs of $10^{-8}$, $10^{-9}$ and $10^{-10}$ yr$^{-1}$, from top to bottom. The green and blue lines are the best-fit results taken from the literature. The light purple lines are the best-fit linear regressions through our data, yielding slopes of 1.3 (a) and 1.8 (b), respectively. The overlaid black contours are density distributions of the data points. We also plot all data points below $3\sigma$ as black dots. This figure is reproduced by permission of the AAS.

University, University of Cambridge, Japan Aerospace Exploration Agency, University of Massachusetts, California Institute of Technology, and Joint ALMA Observatory.

We report a super-linear correlation for the star formation law based on new CO($J$ = 1–0) data from the CARMA and NOBEYAMA Nearby-galaxies (CANON) CO survey. The sample includes 10 nearby spiral galaxies, in which structures at sub-kpc scales are spatially resolved. Combined with the star formation rate surface density traced by H$\alpha$ and 24 $\mu$m images, CO($J$ = 1–0) data provide a super-linear slope of $N = 1.3$ (Figure 18a). The slope becomes even steeper ($N = 1.8$) when the diffuse stellar and dust background emission is subtracted from the H$\alpha$ and 24 $\mu$m images (Figure 18b). In contrast to the recent results with CO($J$ = 2–1) that found a constant star formation efficiency (SFE) in many spiral galaxies, these results suggest that the SFE is not independent of environment, but increases with molecular gas surface density. We suggest that the excitation of CO($J$ = 2–1) is likely enhanced in the regions with higher star formation and does not linearly trace the molecular gas mass. In addition, the diffuse emission contaminates the SFE measurement most in regions where the star formation rate is low. These two effects can flatten the power-law correlation and produce the apparent linear slope. The super-linear slope from the CO($J$ = 1–0) analysis indicates that star formation is enhanced by non-linear processes in regions of high gas density, e.g., gravitational collapse and cloud-cloud collisions.

## Bibliography

[6] Momose, R., et al. 2013, Astrophys. J. (Letters), 772, L13

# Theory Group

### *Overview*

We have theoretically studied particle physics (mainly particle physics phenomenology) and astroparticle physics (mainly particle cosmology).

2013 was one of the important milestone for the particle physics and the cosmology. The observed "Higgs-like scalar particle" in the mass region around 126 GeV has been confirmed to be "the Higgs boson" consistent with the standard model of particle physics, and also the AMS-02 experiment has reported an excess of the cosmic-ray positron fraction, which is consistent with the previous observations. The latter result would give a considerable clue to find dark matter candidate. BICEP2 experiment has given us a significant impact by reporting the observation of B-mode polarization of the cosmic microwave background (CMB), which might be a fingerprint of the inflationary universe. While these experiments make us confirm the standard model of particle physics and Big bang Universe, they also give us many implications for extensions of the standard scenarios.

The supersymmetric (SUSY) extension of the standard model (SM) in the particle physics is considered to be one of the most promising models beyond the standard model. It solves the naturalness problem for the Higgs boson mass term in the standard model, and it is also compatible with the grand unified theories (GUTs). Our group has been studying phenomenological and cosmological aspects of the SUSY models.

Recent cosmological observations including the Planck data determine precisely the mean densities of matter and baryon in the Universe, and existence of non-baryonic dark matter is established. Weakly interacting massive particles (WIMPs) are considered to be good candidates of the dark matter. They act as the cold dark matter in the structure formation of the universe. Our group has been studying model building for dark matter and detectability in direct and indirect search experiments.

For understanding of the early universe, a role of the elementary particle physics is crucial. Recent progress in the particle physics such as grand unification theories and supersymmetry leads us to a more deeper insight into the fundamental aspects of the early universe. In the inflationary universe, the quantum fluctuations of the scalar field which drives the inflation become the density fluctuations and lead to formation of the structure observed in the present universe. On the other hand cosmology and astrophysics are used to test new theories in particle physics. Such particle cosmology is one of main subjects of our group.

Big Bang Nucleosynthesis (BBN) is one of the most important subjects in modern cosmology. Predicted abundances of the light elements are very sensitive to the cosmological scenario. On the other hand, physics beyond the standard model predicts the new particles which would have existed at the BBN epoch. Such particles may spoil the success of BBN, which leads to constraints on the new particles and the particle physics models.

The grand unified theories (GUT) predict that our universe undergoes several vacuum phase transitions. In the course of phase transitions topological defects (monopoles, cosmic strings and domain walls) are generally produced depending on symmetries of the vacua. Our group has studied evolution of various topological defects.

### *Particle Phenomenology*

[Spokesperson : M. Ibe]
ICRR, The Univ. of Tokyo, Kashiwa, Chiba 277-8582

**Dark Matter, Inflation**

• *Recent Result of the AMS-02 Experiment and Decaying Gravitino Dark Matter in Gauge Mediation*

In collaboration with the members of ICRR, IPMU and University of Tokyo

The AMS-02 collaboration has recently reported an excess of cosmic-ray positron fractions, which is consistent with previous results at PAMELA and Fermi-LAT experiments. The result indicates the existence of new physics phenomena to provide the origin of the energetic cosmic-ray positron. We pursue the possibility that the enhancement of the positron fraction is due to the decay of gravitino dark matter. We discuss that such a scenario viably fits into the models in which the soft SUSY breaking parameters are dominantly from gauge-mediation mechanism with superparticle masses of around 10 TeV. Our scenario is compatible with 126 GeV Higgs boson, negative searches for SUSY particles, and non-observation of anomalous FCNC processes. We also point out that the scenario will be tested in near future by measuring the electric dipole moment of the electron and the lepton flavor violating decay of the muon.

• *AMS-02 Positrons from Decaying Wino in the Pure Gravity Mediation Model*

In collaboration with the members of ICRR, IPMU and UC Berkeley

The AMS-02 collaboration has recently reported an excess of the cosmic-ray positron fraction, which turned out to be consistent with previous results reported by the PAMELA and Fermi-LAT collaborations. A decaying dark matter with the mass around 1 TeV can be responsible for the excess of the positron fraction when it is interpreted as a dark matter signal. Interestingly, the pure gravity mediation model provides such a dark matter, namely an almost pure neutral wino dark matter, when a tiny $R$-parity violation through $LLE^c$ interactions is introduced. We show that the decaying wino dark matter well reproduces the energy spectrum of the fraction with being consistent with constraints from cosmic-ray anti-proton and gamma-ray observations.

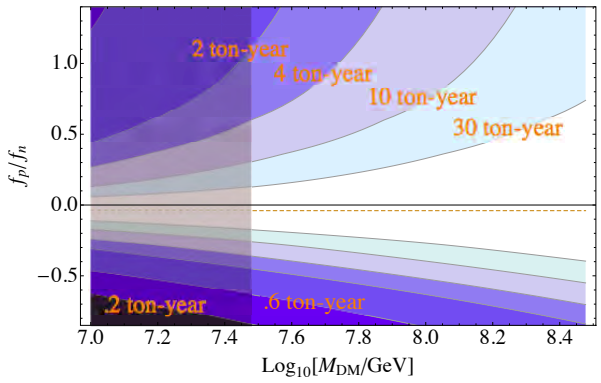


Fig. 19. The required effective exposures for a 90%C.L. exclusion of the isospin violation dark matter for a given hypercharged dark matter mass. Isospin preserving dark matter corresponds to $f_p/f_n = 1$, and $Z$-mediated scattering (this model) is shown as the dashed line. The shaded region has been excluded by the XENON100 experiments.

• *Hypercharged Dark Matter and Direct Detection as a Probe of Reheating*

In collaboration with the members of ICRR, and IPMU

The lack of new physics at the LHC so far weakens the argument for TeV scale thermal dark matter. On the other hand, heavier, non-thermal dark matter is generally difficult to test experimentally. Here we consider the interesting and generic case of hypercharged dark matter, which can allow for heavy dark matter masses without spoiling testability. Planned direct detection experiments will be able to see a signal for masses up to an incredible $10^{10}$ GeV, and this can further serve to probe the reheating temperature up to about $10^9$ GeV, as determined by the non-thermal dark matter relic abundance. The $Z$-mediated nature of the dark matter scattering may be determined in principle by comparing scattering rates on different detector nuclei, which in turn can reveal the dark matter mass. We will discuss the extent to which future experiments may be able to make such a determination (see Fig. 19).

• *Lower Bound on the Garvitino Mass $m_{3/2} > O(100)$ TeV in R-Symmetry Breaking New Inflation*

In collaboration with the members of ICRR, and IPMU

In supersymmetric theories, the $R$-symmetry plays a unique role in suppressing a constant term in the superpotential. In single chiral field models of spontaneous breaking of a discrete $R$-symmetry, an $R$-breaking field can be a good candidate for an inflaton in new inflation models. In this paper, we revisit the compatibility of the single-field R-breaking new inflation model with the results of the Planck experiment. As a result, we find that the model predicts a lower limit on the gravitino mass, $m_{3/2} > O(100)$ TeV. This lower limit is consistent with the observed Higgs mass of 126 GeV when the masses of the stops are of order the gravitino mass scale.

• *Mixed (Cold+Warm) Dark Matter in the Bino-Wino co-annihilation scenario*

In collaboration with the members of ICRR, and IPMU

We study phenomenological aspects of the bino-wino co-annihilation scenario in high-scale supersymmetry breaking models. High-scale SUSY breaking scenarios are considered to be promising possibility after the discovery of the Higgs boson with a mass around 126 GeV. In this paper, we discuss the bino lightest supersymmetric particle (LSP) accompanied by the at most around 30 GeV heavier wino. With the suitable mass splitting between the bino and the wino, the bino LSP has the correct relic abundance of dark matter. For the smaller mass splitting, the late-time decay of the gravitino can provide the correct abundance of the bino dark matter. It is extremely challenging to find signals from the bino dark matter in direct and indirect detections. By utilizing multi-jets plus missing transverse momentum events at the LHC, we can constraint the gluino mass and thus probe the bino-wino co-annihilation scenario indirectly. The collider experiment, however, can not search the bino dark matter directly. In this paper, we suggest the direct probe of the bino dark matter. We show that the bino dark matter leaves imprints on the small-scale matter power spectrum when the bino dark matter is produced by the decay of the gravitino. The non-thermal bino dark matter behaves as mixed (cold+warm) dark matter.

• *Dynamical Chaotic Inflation in the Light of BICEP2*

In collaboration with the members of ICRR and IPMU

The measurement of a large tensor-to-scalar ratio by the BICEP2 experiment, r = 0.20 (-0.05)(+0.07), severely restricts the landscape of viable inflationary models and shifts attention once more towards models featuring large inflaton field values. In this context, chaotic inflation based on a fractional power-law potential that is dynamically generated by the dynamics of a strongly coupled supersymmetric gauge theory appears to be particularly attractive. We revisit this class of inflation models and find that, in the light of the BICEP2 measurement, models with a non-minimal gauge group behind the dynamical model seem to be disfavored, while the model with the simplest group, i.e. SU(2), is consistent with all results. We also discuss how the dynamical model can be distinguished from the standard chaotic inflation model based on a quadratic inflaton potential.

• *High-Scale SUSY Breaking Models in light of the BICEP2 Result*

In collaboration with the members of ICRR and IPMU

The large value of the tensor-to-scalar ratio in the cosmic microwave background radiation reported by the BICEP2 collaboration gives strong impact on models of supersymmetry (SUSY). The large ratio indicates inflation with a high-energy scale and thus a high reheating temperature in general, and various SUSY models suffer from the serious gravitino and Polonyi problems. In this article, we discuss a class of the high-scale SUSY breaking models which are completely free

from those problems. With especially focusing on the dark matter relic abundance, we examine how the BICEP2 result narrows down the parameter space of the models, assuming the simplest chaotic inflation model. We find that the mass of the dark matter is predicted to be less than about 1 TeV thanks to the non-thermal production in the early universe through the decay of abundant gravitinos produced after the reheating process. We also discuss implications in some details to dark matter searches at collider and indirect dark matter detection experiments.

## Bibliography


[1] M. Ibe, S. Iwamoto, S. Matsumoto, T. Moroi and N. Yokozaki, JHEP **1308**, 029 (2013) [arXiv:1304.1483 [hep-ph]].

[2] M. Ibe, S. Matsumoto, S. Shirai and T. T. Yanagida, JHEP **1307**, 063 (2013) [arXiv:1305.0084 [hep-ph]].

[3] B. Feldstein, M. Ibe and T. T. Yanagida, Phys. Rev. Lett. 112, 101301 [arXiv:1310.7495 [hep-ph]].

[4] K. Harigaya, M. Ibe and T. T. Yanagida, Phys. Rev. D **89**, 055014 (2014) [arXiv:1311.1898 [hep-ph]].

[5] M. Ibe, A. Kamada and S. Matsumoto, Phys. Rev. D **89**, 123506 (2014) [arXiv:1311.2162 [hep-ph]].

[6] K. Harigaya, M. Ibe, K. Schmitz and T. T. Yanagida, Phys. Lett. B **733**, 283 (2014) [arXiv:1403.4536 [hep-ph]].

[7] K. Harigaya, M. Ibe, K. Ichikawa, K. Kaneta and S. Matsumoto, arXiv:1403.5880 [hep-ph].


### Supersymmetric extensions of the Standard Model

• *Non-Universalities in Pure Gravity Mediation*

In collaboration with the members of ICRR, IPMU and Minnesota U.

The simplest model of pure gravity mediation contains only two free parameters: the gravitino mass and $\tan\beta$. Scalar masses are universal at some high energy renormalization scale and gaugino masses are determined through anomalies and depend on the gravitino mass and the gauge couplings. This theory requires a relatively large gravitino mass ($m_{3/2} \gtrsim 300$ TeV) and a limited range in $\tan\beta \simeq 1.7 - 2.5$. Here we generalize the theory to allow for non-universality in the Higgs soft masses. This introduces zero, one or two new free parameters associated with Higgs soft masses. This generalization allows us to greatly increase the allowed range in $\tan\beta$ and it allows one to find viable solutions with lower $m_{3/2}$. The latter is important if we hope to find a low energy signal from gluinos. Some special cases of these non-universalities are suggestive of Higgs bosons as Nambu-Goldstone bosons or a partial no-scale structure for the Higgs doublets. Thus, we probe signatures at the weak scale and structures at the GUT and/or Planck scale.

• *Peccei-Quinn symmetry from a gauged discrete R symmetry*

In collaboration with the members of ICRR, and IPMU

The axion solution to the strong CP problem calls for an explanation as to why the Lagrangian should be invariant under the global Peccei-Quinn (PQ) symmetry, U(1)PQ, to such a high degree of accuracy. In this paper, we point out that the U(1)PQ can indeed survive as an accidental symmetry in the low-energy effective theory, if the standard model gauge group is supplemented by a gauged and discrete R symmetry, ZNR, forbidding all dangerous operators that explicitly break the Peccei-Quinn symmetry. In contrast to similar approaches, the requirement that the ZNR symmetry be anomaly-free forces us, in general, to extend the supersymmetric standard model by new matter multiplets. Surprisingly, we find a large landscape of viable scenarios that all individually fulfill the current experimental constraints on the QCD vacuum angle as well as on the axion decay constant. In particular, choosing the number of additional multiplets appropriately, the order N of the ZNR symmetry can take any integer value larger than 2. This has interesting consequences with respect to possible solutions of the problem, collider searches for vectorlike quarks and axion dark matter.

• *A Closer Look at Gaugino Masses in Pure Gravity Mediation Model/Minimal Split SUSY Model*

In collaboration with the members of ICRR, and IPMU

We take a closer look at the gaugino masses in the context of pure gravity mediation models/minimal split SUSY models. We see that the gaugino mass spectrum has a richer structure in the presence of vector-like matter fields even when they couple to the supersymmetry breaking sector only through Planck suppressed operators. For example, the gluino mass can be much lighter than in anomaly mediation, enhancing the detectability of the gluino at the LHC experiments. The rich gaugino spectrum also allows new possibilities for dark matter scenarios such as the bino-wino co-annihilation, bino-gluino co-annihilation, or even wino-gluino co-annihilation scenarios, which affects future collider experiments as well as dark matter search experiments.

• *One-loop anomaly mediated scalar masses and $(g-2)_\mu$ in pure gravity mediation*

In collaboration with the members of ICRR, IPMU and Minnesota U.

We consider the effects of non-universalities among sfermion generations in models of Pure Gravity Mediation (PGM). In PGM models and in many models with strongly stabilized moduli, the gravitino mass may be $O(100)$ TeV, whereas gaugino masses, generated through anomalies at 1-loop, remain relatively light $O(1)$ TeV. In models with scalar mass universality, input scalar masses are generally very heavy ($m_0 \simeq m_{3/2}$) resulting in a mass spectrum resembling that in split supersymmetry. However, if one adopts a no-scale or partial no-scale structure for the Kähler manifold, sfermion masses may vanish at the tree level. It is usually assumed that the

leading order anomaly mediated contribution to scalar masses appears at 2-loops. However, there are at least two possible sources for 1-loop scalar masses. These may arise if Pauli-Villars fields are introduced as messengers of supersymmetry breaking. We consider the consequences of a spectrum in which the scalar masses associated with the third generation are heavy (order $m_{3/2}$) with 1-loop scalar masses for the first two generations. A similar spectrum is expected to arise in GUT models based on $E_7/SO(10)$ where the first two generations of scalars act as pseudo-Nambu-Goldstone bosons. Explicit breaking of this symmetry by the gauge couplings then generates one-loop masses for the first two generations. In particular, we show that it may be possible to reconcile the $(g-2)_\mu$ discrepancy with potentially observable scalars and gauginos at the LHC.

• *Flat Higgs Potential from Planck Scale Supersymmetry Breaking*

In collaboration with the members of ICRR, and IPMU

The observed Higgs boson mass poses a new puzzle in addition to the longstanding problem of the origin of the electroweak scale; the shallowness of the Higgs potential. The Higgs quartic coupling even seems to vanish at around the Planck scale within the uncertainties of the top quark mass and the strong gauge coupling. We show that the shallowness of the Higgs potential might be an outcome of supersymmetry breaking at around the Planck scale. There, the electroweak fine-tuning in the Higgs quadratic terms leads to an almost vanishing quartic coupling at around the Planck scale.

• *Peccei-Quinn Symmetric Pure Gravity Mediation*

In collaboration with the members of ICRR, IPMU and Minnesota U.

Successful models of Pure Gravity Mediation (PGM) with radiative electroweak symmetry breaking can be expressed with as few as two free parameters which can be taken as the gravitino mass and $\tan\beta$. These models easily support a $125-126$ GeV Higgs mass at the expense of a scalar spectrum in the multi-TeV range and a much lighter wino as the lightest supersymmetric particle. In these models, it is also quite generic that the Higgs mixing mass parameter, $\mu$, which is determined by the minimization of the Higgs potential is also in the multi-TeV range. For $\mu > 0$, the thermal relic density of winos is too small to account for the dark matter. The same is true for $\mu < 0$ unless the gravitino mass is of order 500 TeV. Here, we consider the origin of a multi-TeV $\mu$ parameter arising from the breakdown of a Peccei-Quinn (PQ) symmetry. A coupling of the PQ-symmetry breaking field, $P$, to the MSSM Higgs doublets, naturally leads to a value of $\mu \sim \langle P\rangle^2/M_P \sim O(100)$ TeV and of order that is required in PGM models. In this case, axions make up the dark matter or some fraction of the dark matter with the remainder made up from thermal or non-thermal winos. We also provide solutions to the problem of isocurvature fluctuations with axion dark matter in this context.

• *Testing the Minimal Direct Gauge Mediation at the LHC*

In collaboration with the members of ICRR, IPMU and University of Tokyo

We reexamine the models with gauge mediation in view of the minimality. As a result, we arrive at a very simple model of direct gauge mediation which does not suffer from the flavor problems nor the CP problems. We show that the parameter space which is consistent with the Higgs boson mass at around 126 GeV can be tested through the stable stau searches at the 14TeV run of the LHC. The gravitino is a viable candidate for a dark matter. We also give a short discussion on a possible connection of our model to the recently discovered X-ray line signal at 3.5 keV in the XMM Newton X-ray observatory data.

## Bibliography


[1] J. L. Evans, K. A. Olive, M. Ibe and T. T. Yanagida, Eur. Phys. J. C **73**, 2611 (2013) [arXiv:1305.7461 [hep-ph]].

[2] K. Harigaya, M. Ibe, K. Schmitz and T. T. Yanagida, Phys. Rev. D **88**, no. 7, 075022 (2013) [arXiv:1308.1227 [hep-ph]].

[3] K. Harigaya, M. Ibe and T. T. Yanagida, JHEP **1312**, 016 (2013) [arXiv:1310.0643 [hep-ph]].

[4] J. L. Evans, M. Ibe, K. A. Olive and T. T. Yanagida, Eur. Phys. J. C **74**, 2775 (2014) [arXiv:1312.1984 [hep-ph]].

[5] M. Ibe, S. Matsumoto and T. T. Yanagida, Phys. Lett. B **732**, 214 (2014) [arXiv:1312.7108 [hep-ph]].

[6] J. L. Evans, M. Ibe, K. A. Olive and T. T. Yanagida, arXiv:1402.5989 [hep-ph].

[7] K. Hamaguchi, M. Ibe, T. T. Yanagida and N. Yokozaki, arXiv:1403.1398 [hep-ph].


## *Particle Cosmology*


[Spokesperson : M. Kawasaki]
ICRR, The Univ. of Tokyo, Kashiwa, Chiba 277-8582


### Inflation and Thermal History in the early Universe

• *Heavy gravitino in hybrid inflation*

In collaboration with the members of ICRR, IPMU and University of Tokyo

It is known that supersymmetric hybrid inflation model may require severe tunings on the initial condition for large gravitino mass of order $100-1000$ TeV due to the constant term in the superpotential. We propose a modified hybrid inflation model, where the constant term is suppressed during inflation and generated after inflation by replacing a constant term with dynamical field. In this modified model, successful inflation consistent with large gravitino mass takes place without severe tunings on the initial condition. Constraint from cosmic strings is also relaxed [1].

• *Domain wall and isocurvature perturbation problems in axion models*

In collaboration with the members of ICRR and IPMU

Axion models have two serious cosmological problems, domain wall and isocurvature perturbation problems. In order to solve these problems we investigate the Linde's model in which the field value of the Peccei-Quinn (PQ) scalar is large during inflation. In this model the fluctuations of the PQ field grow after inflation through the parametric resonance and stable axionic strings may be produced, which results in the domain wall problem. We study formation of axionic strings using lattice simulations. It is found that in chaotic inflation the axion model is free from both the domain wall and the isocurvature perturbation problems if the initial misalignment angle $\theta_a$ is smaller than $O(10^{-2})$. Furthermore, axions can also account for the dark matter for the breaking scale $v \simeq 10^{12-16}\,\mathrm{GeV}$ and the Hubble parameter during inflation $H_{\rm inf} \lesssim 10^{11-12}\,\mathrm{GeV}$ in general inflation models [2].

• *Decay rates of Gaussian-type I-balls and Bose-enhancement effects in 3+1 dimensions*

In collaboration with the members of ICRR and IPMU.

I-balls/oscillons are long-lived spatially localized lumps of a scalar field which may be formed after inflation. In the scalar field theory with monomial potential nearly and shallower than quadratic, which is motivated by chaotic inflationary models and supersymmetric theories, the scalar field configuration of I-balls is approximately Gaussian. If the I-ball interacts with another scalar field, the I-ball eventually decays into radiation. Recently, it was pointed out that the decay rate of I-balls increases exponentially by the effects of Bose enhancement under some conditions and a non-perturbative method to compute the exponential growth rate has been derived. In this paper, we apply the method to the Gaussian-type I-ball in $3+1$ dimensions assuming spherical symmetry, and calculate the partial decay rates into partial waves, labelled by the angular momentum of daughter particles. We reveal the conditions that the I-ball decays exponentially, which are found to depend on the mass and angular momentum of daughter particles and also be affected by the quantum uncertainty in the momentum of daughter particles.

• *A new algorithm for calculating the curvature perturbations in stochastic inflation*

In collaboration with the members of ICRR and IPMU

We propose a new approach for calculating the curvature perturbations produced during inflation in the stochastic formalism. In our formalism, the fluctuations of the e-foldings are directly calculated without perturbatively expanding the inflaton field and they are connected to the curvature perturbations by the $\delta N$ formalism. The result automatically includes the contributions of the higher order perturbations because we solve the equation of motion non-perturbatively. In this paper, we analytically prove that our result (the power spectrum and the nonlinearity parameter) is consistent with the standard result in single field slow-roll inflation. We also describe the algorithm for numerical calculations of the curvature perturbations in more general inflation models [4].

## Bibliography


[1] M. Kawasaki, N. Kitajima, K. Nakayama and T. T. Yanagida, JCAP **1306**, 037 (2013) [arXiv:1301.6281, arXiv:1301.6281 [hep-ph]].

[2] M. Kawasaki, T. T. Yanagida and K. Yoshino, JCAP **1311**, 030 (2013) [arXiv:1305.5338 [hep-ph]].

[3] M. Kawasaki and M. Yamada, arXiv:1311.0985 [hep-ph].

[4] T. Fujita, M. Kawasaki, Y. Tada and T. Takesako, JCAP **1312**, 036 (2013) [arXiv:1308.4754 [astro-ph.CO]].


**Dark Matter, Baryogenesis, Big-Bang nucleosynthesis**

• *Baryogenesis from the Gauge-mediation type Q ball and the dark matter New type Q ball*

In collaboration with the members of ICRR and Kanagawa University

We investigate that the two types of the Q balls explain the baryon asymmetry and the dark matter of the universe in the gauge-mediated supersymmetry breaking. The gauge-mediation type Q balls of one flat direction produce baryon asymmetry, while the new type Q balls of another flat direction become the dark matter. We show that the dark matter new type Q balls are free from the neutron star constraint. $n = 5$ gauge mediation type and $n = 6$ new type Q balls are displayed as an example, where the potential is lifted by the superpotential $\Phi^n$. These dark matter Q balls may be detected by future observations, such as in advanced IceCube-like observations [1].

• *Axions as Hot and Cold Dark Matter*

In collaboration with the members of ICRR, DESY and Tohoku University

The presence of a hot dark matter component has been hinted at $3\sigma$ by a combination of the results from different cosmological observations. We examine a possibility that pseudo Nambu-Goldstone bosons account for both hot and cold dark matter components. We show that the QCD axions can do the job for the axion decay constant $f_a < O(10^{10})$ GeV, if they are produced by the saxion decay and the domain wall annihilation. We also investigate the cases of thermal QCD axions, pseudo Nambu-Goldstone bosons coupled to the standard model sector through the Higgs portal, and axions produced by modulus decay [2].

• *Baryon Asymmetry, Dark Matter, and Density Perturbation from PBH*

In collaboration with the members of ICRR and IPMU

We investigate the consistency of a scenario in which the baryon asymmetry, dark matters, as well as the cosmic density perturbation are generated simultaneously through the evaporation of primordial black holes (PBHs). This scenario can explain the coincidence of the dark matter and the baryon density of the universe, and is free from the isocurvature perturbation problem. We show that this scenario predicts the masses of PBHs, right-handed neutrinos and dark matters, the Hubble scale during inflation, the non-gaussianity and the running of the spectral index. We also discuss the testability of the scenario by detecting high frequency gravitational waves from PBHs [3, 4].

• *Dark Matter Production in Late Time Reheating*

In collaboration with the members of ICRR, IPMU, and Tokyo Univ.

We estimate dark matter density for the Universe with a reheating temperature smaller than the mass of dark matter, assuming dark matter to be a weakly interacting massive particle. During the reheating process, an inflaton decays and releases high-energy particles, which are scattered inelastically by the thermal plasma and emit many particles. Dark matters are produced through these inelastic scattering processes and pair creation processes by high-energy particles. We properly take account of the Landau-Pomeranchuk-Migdal effect on inelastic processes and show that the resultant energy density of dark matter is much larger than that estimated in the literature and can be consistent with that observed when the mass of dark matter is larger than $O(100)$ GeV (see Fig. 20).

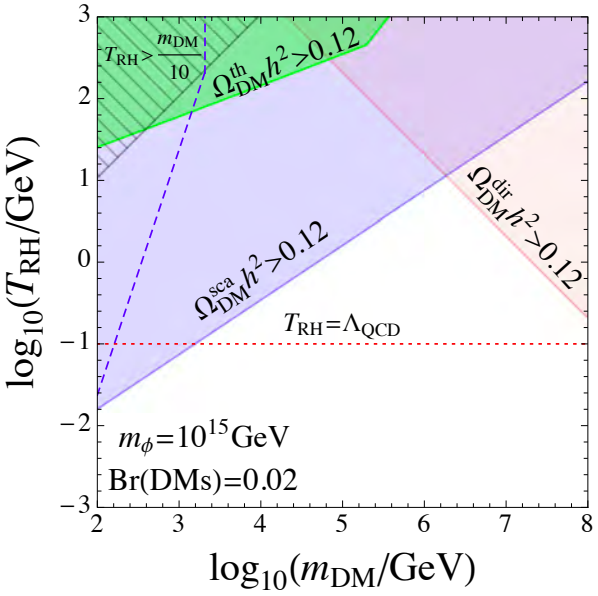


Fig. 20. Exclusion plot in a scenario with low reheating temperature. The abundance of DM produced from thermal production ($\Omega^{\rm th}_{\rm DM}h^2$), direct decay of inflaton ($\Omega^{\rm dir}_{\rm DM}h^2$), and inelastic scatterings ($\Omega^{\rm sca}_{\rm DM}h^2$) is larger than that observed in the green, red, and blue shaded regions, respectively. The striped regions are $T_{\rm RH} > m_{\rm DM}/10$, in which DM is produced only thermally. The abundance of DM is less than that observed above the blue dashed line due to its annihilation. The red dotted lines represent the reheating temperature below which $\Omega^{\rm sca}_{\rm DM}h^2$ is over-estimated.

## Bibliography


[1] S. Kasuya and M. Kawasaki, arXiv:1402.4546 [hep-ph].

[2] K. S. Jeong, M. Kawasaki and F. Takahashi, JCAP **1402**, 046 (2014) [arXiv:1310.1774 [hep-ph], arXiv:1310.1774].

[3] T. Fujita, K. Harigaya and M. Kawasaki, Phys. Rev. D **88**, 123519 (2013) [arXiv:1306.6437 [astro-ph.CO]].

[4] T. Fujita, M. Kawasaki, K. Harigaya and R. Matsuda, Phys. Rev. D **89**, 103501 (2014) [arXiv:1401.1909 [astro-ph.CO]].

[5] K. Harigaya, M. Kawasaki, K. Mukaida and M. Yamada, Phys. Rev. D **89**, 083532 (2014) [arXiv:1402.2846 [hep-ph]].


### Gravitational waves

• *On the estimation of gravitational wave spectrum from cosmic domain walls*

In collaboration with the members of ICRR, Kyoto University and Tokyo Institute of Technology

We revisit the production of gravitational waves from unstable domain walls analyzing their spectrum by the use of field theoretic lattice simulations with grid size 10243, which is larger than the previous study. We have recognized that the reexists an error in the code used in the previous study, and the correction of the error leads to the suppression of the spectrum of gravitational waves at high frequencies. The peak of the spectrum is located at the scale corresponding to the Hubble radius at the time of the decay of domain walls, and its amplitude is consistent with the naive estimation based on the quadrupole formula. Using the numerical results, the magnitude and the peak frequency of gravitational waves at the present time are estimated. It is shown that for some choices of parameters the signal of gravitational waves is strong enough to be probed in the future gravitational wave experiments [1].

• *Gravitational waves from a curvaton model with blue spectrum*

In collaboration with the members of ICRR.

We investigate the gravitational wave background induced by the first order scalar perturbations in the curvaton models.

We consider the quadratic and axion-like curvaton potential which can generate the blue-tilted power spectrum of curvature perturbations on small scales and derive the maximal amount of gravitational wave background today. We find the power spectrum of the induced gravitational wave background has a characteristic peak at the frequency corresponding to the scale reentering the horizon at the curvaton decay, in the case where the curvaton does not dominate the energy density of the Universe. We also find the enhancement of the amount of the gravitational waves in the case where the curvaton dominates the energy density of the Universe. Such induced gravitational waves would be detectable by the future space-based gravitational wave detectors or pulsar timing observations, as shown in Fig. 21.

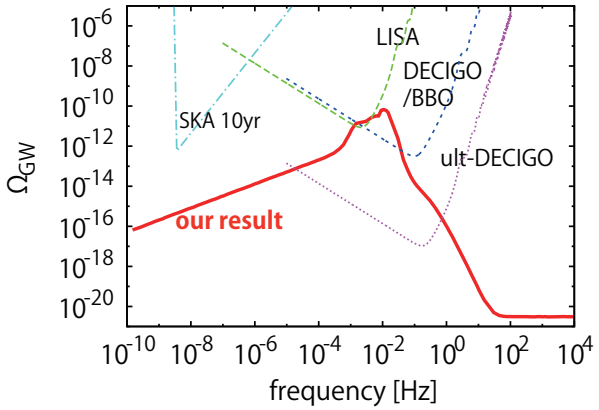


Fig. 21. One example of the spectrum of the gravitational background shown in Ref. [2]. The red thick line is the resultant spectrum in Ref. [2]. We also show the sensitivity curves of LISA (dashed green), DECIGO/BBO (dotted blue), ultimate-DECIGO (small dotted magenta) and the pulsar timing observation by SKA (dash dotted cyan).

## Bibliography

[1] T. Hiramatsu, M. Kawasaki and K. 'i. Saikawa, JCAP **1402**, 031 (2014) [arXiv:1309.5001 [astro-ph.CO]].

[2] M. Kawasaki, N. Kitajima and S. Yokoyama, JCAP **1308**, 042 (2013) [arXiv:1305.4464 [astro-ph.CO]].

### Primordial non-Gaussianity, Structure formation in the Universe

• *Higher order statistics of curvature perturbations in IFF model and its Planck constraints*

In collaboration with the members of ICRR and Kavli IPMU.

We compute the power spectrum $P_\zeta$, and non-linear parameters $f_{nl}$ and $\tau_{nl}$ of the curvature perturbation induced during inflation by the electromagnetic fields in the kinetic coupling model (IFF model). By using the observational result of $P_\zeta$, $f_{nl}$ and $\tau_{nl}$ reported by the Planck collaboration, we study the constraint on the model comprehensively. Interestingly, if the single slow-rolling inflation is responsible for the observed $P_\zeta$, the constraint from $\tau_{nl}$ is most stringent. We also find a general relationship between $f_{nl}$and $\tau_{nl}$ generated in this model. Even if $f_{nl} \sim O(1)$, a detectable $\tau_{nl}$ can be produced.

• *CMB distortion anisotropies due to the decay of primordial magnetic fields*

In collaboration with the members of ICRR, Nagoya Univ. and Arizona State Univ..

We investigate the power spectrum of the distortion of Cosmic Microwave Background (CMB) due to the decay of the primordial magnetic fields. It is known that there are two-types of the CMB distortions, so-called $\mu$- and $y$-types and we find that the signal of the y-type distortion becomes larger than that of the $\mu$-type one. We also discuss cross power spectra between the CMB distortions and the CMB temperature anisotropy, which are naturally generated due to the existence of the primordial magnetic fields. We find that such cross power spectra have small amplitudes compared with the auto-power spectra of the CMB distortions because of the Silk damping effect of the temperature anisotropy. We also investigate the possibility of detecting such signal in the future CMB experiments, including not only absolutely calibrated experiments such as PIXIE but also relatively calibrated experiments such as LiteBIRD and CMBpol.

• *Halo/Galaxy Bispectrum with Primordial non-Gaussianity from integrated Perturbation Theory (iPT)*

In collaboration with the members of ICRR, Nagoya Univ. and YITP.

We derive a formula for the halo/galaxy bispectrum on the basis of the integrated Perturbation Theory (iPT). In addition to the gravity-induced non- Gaussianity, we consider the non-Gaussianity of the primordial curvature perturbations, and investigate in detail the effect of such primordial non-Gaussianity on the large-scale halo/galaxy bispectrum. In iPT, the effects of primordial non-Gaussianity are wholly encapsulated in the linear (primordial) polyspectra, and we systematically calculate the contributions to the large-scale behaviors arising from the three types of primordial bispectrum (local-, equilateral-, and orthogonal-types), and primordial trispectrum of the local-type non-Gaussianity. We find that the equilateral- and orthogonal-type non-Gaussianities show distinct scale-dependent behaviors which can dominate the gravity-induced non-Gaussianity at very large scales. For the local-type non-Gaussianity, higher-order loop corrections are found to give a significantly large contribution to the halo/galaxy bispectrum of the squeezed shape, and eventually dominate over the other contributions on large scales. A diagrammatic approach based on the iPT helps us to systematically investigate an impact of such higher-order contributions to the large-scale halo/galaxy bispectrum.

• *Critical constraint on inflationary magnetogenesis*

In collaboration with the members of ICRR and Kavli IPMU.

Recently, there are several reports that the cosmic magnetic fields on Mpc scale in void region is larger than $10^{-15}$G with an uncertainty of a few orders from the current blazar observations. On the other hand, in inflationary magnetogenesis models, additional primordial curvature perturbations are inevitably produced from iso-curvature perturbations due to generated electromagnetic fields. We explore such induced curvature perturbations in a model independent way and obtained a severe upper bound for the energy scale of inflation from the observed cosmic magnetic fields and the observed amplitude of the curvature perturbation, as $\rho_{inf}^{1/4} < 30\text{GeV} \times (B_{\rm obs}/10^{-15}\text{G})^{-1}$ where $B_{\rm obs}$ is the strength of the magnetic field at present. Therefore, without a dedicated low energy inflation model or an additional amplification of magnetic fields after inflation, inflationary magnetogenesis on Mpc scale is generally incompatible with CMB observations.

• *Probing small-scale cosmological fluctuations with the 21 cm forest: effects of neutrino mass, running spectral index and warm dark matter*

In collaboration with the members of ICRR, Nagoya Univ. and MPI.

Although the cosmological paradigm based on cold dark matter and adiabatic, nearly scale-invariant primordial fluctuations is consistent with a wide variety of existing observations, it has yet to be sufficiently tested on scales smaller than those of massive galaxies, and various alternatives have been proposed that differ significantly in the consequent small-scale power spectrum (SSPS) of large-scale structure. Here we show that a powerful probe of the SSPS at $k \gtrsim 10$ Mpc$^{-1}$ can be provided by the 21 cm forest, that is, systems of narrow absorption lines due to intervening, cold neutral hydrogen in the spectra of high-redshift background radio sources in the cosmic reionization epoch. Such features are expected to be caused predominantly by collapsed gas in starless minihalos, whose mass function can be very sensitive to the SSPS. As specific examples, we consider the effects of neutrino mass, running spectral index (RSI) and warm dark matter (WDM) on the SSPS, and evaluate the expected distribution in optical depth of 21 cm absorbers out to different redshifts. Within the current constraints on quantities such as the sum of neutrino masses $\sum m_\nu$, running of the primordial spectral index $dn_s/d\ln k$ and WDM particle mass $m_{\rm WDM}$, the statistics of the 21 cm forest manifest observationally significant differences that become larger at higher redshifts. In particular, it may be possible to probe the range of $m_{\rm WDM} \gtrsim 10$ keV that may otherwise be inaccessible. Future observations of the 21 cm forest by the Square Kilometer Array may offer a unique and valuable probe of the SSPS, as long as radio sources such as quasars or Population III gamma-ray bursts with sufficient brightness and number exist at redshifts of $z \gtrsim 10$ - 20, and the astrophysical effects of reionization and heating can be discriminated.

## Bibliography


[1] T. Fujita and S. Yokoyama, JCAP **1309**, 009 (2013) [arXiv:1306.2992 [astro-ph.CO]].

[2] K. Miyamoto, T. Sekiguchi, H. Tashiro and S. Yokoyama, Physical Review D **89**, 063508 (2014) *American Physical Society*, [arXiv:1310.3886 [astro-ph.CO]].

[3] S. Yokoyama, T. Matsubara and A. Taruya, Phys. Rev. D **89**, 043524 (2014) [arXiv:1310.4925 [astro-ph.CO]].

[4] T. Fujita and S. Yokoyama, JCAP **1403**, 013 (2014) [Erratum-ibid. **1405**, E02 (2014)] [arXiv:1402.0596 [astro-ph.CO]].

[5] H. Shimabukuro, K. Ichiki, S. Inoue and S. Yokoyama, arXiv:1403.1605 [astro-ph.CO].

# OBSERVATORIES and A RESEARCH CENTER

**Location of the Institute and the Observatories in Japan**

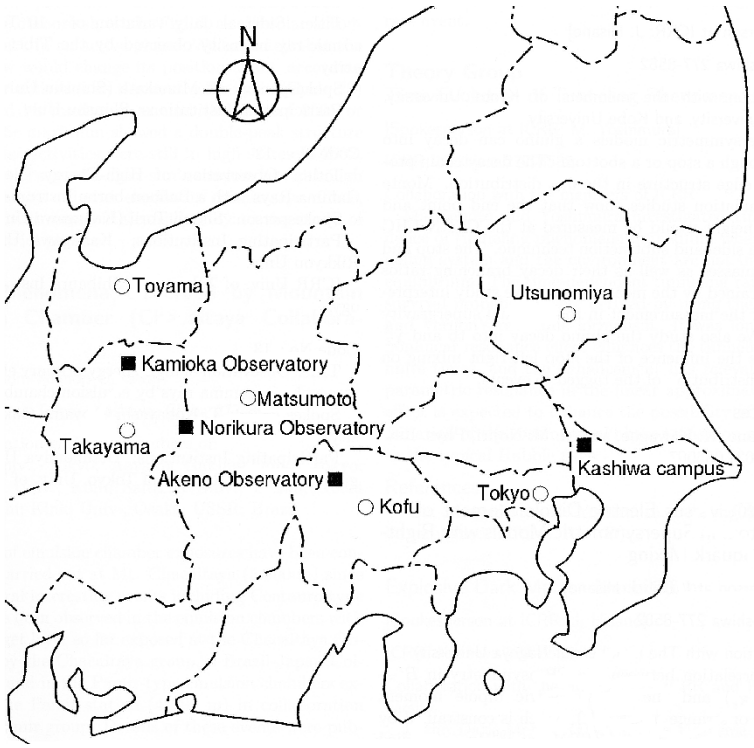


## Norikura Observatory

| | |
|---|---|
| Location: | Norikuradake, Nyukawa-cho, Takayama-shi, Gifu Prefecture 506-2100<br>N 36°06′, E 137°33′, 2770 m a.s.l. |
| Telephone (Fax): | +263-33-7456 |
| Telephone (satellite): | 090-7721-5674 |
| Telephone (car): | 090-7408-6224 |

## Akeno Observatory

| | |
|---|---|
| Location: | 5259 Asao, Akeno-machi, Hokuto-shi, Yamanashi Prefecture 408-0201<br>N 35°47′, E 138°30′, 900 m a.s.l. |
| Telephone / Fax: | +551-25-2301 / +551-25-2303 |

## Kamioka Observatory

| | |
|---|---|
| Location: | 456 Higashi-mozumi, Kamioka-cho, Hida-shi, Gifu Prefecture 506-1205<br>N 36°25′26″, E 137°19′11″, 357.5 m a.s.l. |
| Telephone / Fax: | +578-85-2116 / +578-85-2121 |

## Research Center for Cosmic Neutrinos

| | |
|---|---|
| Location: | 5-1-5 Kashiwanoha, Kashiwa, Chiba Prefecture 277-8582 |
| Telephone / Fax: | +4-7136-3138 / +4-7136-3115 |

# NORIKURA OBSERVATORY

## Introduction

Norikura Observatory (36.10°N and 137.55°E) was founded in 1953 and attached to ICRR in 1976. It is located at 2770 m above sea level, and is the highest altitude manned laboratory in Japan. Experimental facilities of the laboratory are made available to all the qualified scientists in the field of cosmic ray research and associated subjects. The AC electric power is generated by the dynamo and supplied throughout the observatory. In 1996, two dynamos of 70 KVA each were replaced with the new ones. The observatory can be accessed easily by car and public bus in summer (July-September). The 50th anniversary of Norikura Observatory was celebrated in 2003.

Fig. 1. Norikura Observatory.

The feasibility of the automatic operation of Norikura Observatory during winter period has been tested since winter 2004 in order to study the possibilities to reduce maintenance and labor costs without seriously damaging to the use of researches. A long-distance (∼40km) wireless LAN system (11M bps) was set up in 2003. Two new easy-to-handle and easy-to-maintain dynamos of 115 KVA each were installed in 2004 as well. The unmanned operation of Norikura Observatory has been mostly successful in winter, during which the battery backed-up solar panels and/or wind power generators kept supplying the electricity to the wireless LAN and on-going cosmic-ray experiments. The 60th anniversary of Norikura Observatory was celebrated in 2013.

Present major scientific interests of the laboratory is focused on the modulation of high energy cosmic rays in the interplanetary space associated with the solar activity and the generation of energetic particles by the solar flares, both of which require long-term monitoring. This research has been carried out by the group of universities, where ICRR provides them with laboratory facility. A part of the facility has been open for the environmental study at high altitude such as


Fig. 2. A dynamo of 115KV.

aerosol-related mechanism in the atmosphere, observation of total ozone and UV solar radiation, for botanical study in the high-altitude environment, etc.

## Cosmic Ray Physics

A neutron monitor has been continuously operated to study the correlation of solar activities and cosmic ray flux for a long time. It is the only active one in Japan now. The neutron monitor data are open to researchers worldwide as a world observation network point (WDC). In addition, space weather observation is actively made by a 25 $m^2$ muon hodoscope at Norikura Observatory[1], [2], [3], [4], [5], [6], [7], [8], [9].

The anisotropy observed with the global muon detector network (GMDN) provides us with a unique information of the spatial gradient of the GCR density which reflects the large-scale magnetic structure in the heliosphere. The solar cycle variation of the gradient gives an important information on the GCR transport in the heliosphere, while the short-term variation of the gradient enables us to deduce the large-scale geometry of the magnetic flux rope and the interplanetary coronal mass ejection (ICME). Real-time monitoring of the precursory anisotropy which has often been observed at the Earth preceding the arrival of the ICME accompanied by a strong shock may provide us with useful tools for forecasting the space weather with a long lead time. By using a self-supporting power system utilizing the solar panels and batteries, we keep a 25 $m^2$ muon hodoscope running at the Mt. Norikura Cosmic Ray Observatory as an important component detector of the GMDN. The total power consumption of this detector has been suppressed as low as 36 Watt by replacing all amplifier boards with those using CMOS ICs and by introducing a new recording system using the FPGA. This new system, in which the observation has been automatically carried out by a PC connected with the internet, also enabled us

to monitor the data on the real-time basis for the space weather study.

The Sun is the nearest site to the Earth capable of accelerating particles up to high energies. When the Sun becomes active, flares are frequently observed on its surface. The flare accelerates the proton and ion to high energy and they are detected on the Earth soon after the flare. Among the particles generated by the flare, high energy neutrons provide the most direct information about the acceleration mechanism as they come straight from the flare position to the Earth without deflected by the magnetic field.

Observation of solar neutron has been conducted at the Norikura Observatory since 1990. Neutron is used to clarify the acceleration mechanism of high energy particles in association with solar flares, because the neutron is not reflected by the interplanetary magnetic field. The 64m$^2$ solar neutron telescope was constructed in 1996, which is one of 7 solar neutron telescopes deployed at different longitudes to make up a network of 24 hour observation of solar neutrons. The Norikura 64m$^2$ solar neutron telescope has been operated by solar batteries and windmills since 2004.

This collaborative work has started since fiscal 2007 succeeding to the previous project titled 'Observation of solar neutrons by using a new method.' Although solar cycle 24 has started since 2008, the solar activity has continued to be inactive, and no new solar neutron event has been detected by the network since 2006. The last solar neutron event was on September 7, 2005. This event is unique because it indicates ions were accelerated or trapped at the acceleration region longer than electrons. The summary of 11 solar neutron events detected until 2005 shows that it may not be probable that a very efficient acceleration such as the shock acceleration works for ions at solar flares. This is given by deriving the energy spectrum of neutrons at the solar surface for each solar neutron event with a power law. Power law indices obtained span from 3 to 7. The energy spectrum of the original ions is softer than that of neutron. Therefore an efficient acceleration has not been detected by the observation of solar neutrons so far.This work continues in solar cycle 24 to accumulate more events to obtain definite results related with particle acceleration at the solar surface.

Another effort aiming at observation of highest-energy solar cosmic rays started at the Norikura Observatory. The Sun is an accelerator of protons and electrons in the universe. In association with large solar flares, protons and electrons are accelerated into high energies. It is known that protons are accelerated over 50 GeV in the largest solar flares[24]. These high energy particles produce the Ground Level Enhancement (GLE).

In order to understand the acceleration mechanism of protons, we have prepared several solar neutron telescopes at the high altitude laboratories in the world. They are located at Gornergrat (3,135m), Mt. Aragats in Armenia (3,200m), Tibet (4,200m), Mauna-Kea in Hawaii (4,200m), Mt. Chacaltaya in Bolivia (5,250m), and at Mt. Sierra Negra in Mexico (4,900m). We have constructed a solar neutron telescopes at Mt. Norikura Cosmic Ray Observatory (2,770m) in 1990 and operated it until 2004[21]. However due to the lack of power supply during the winter time since 2005, the first solar neutron telescope (36 m$^2$) has not been operated.

From 2008 to 2009, we have decided to make a new solar neutron telescope to utilize the large amount of the plastic scintillator (0.5m$^3$), as shown in Fig. 3, left at the observatory.

Fig. 3. 0.5-m$^2$ plastic scintillation counter for a new neutron telescope.

The new solar neutron telescope with use of the recycled plastic scintillator consists of main target where neutrons are converted into protons and of the anti-counters surrounding the target. The signals of neutrons converted into protons are observed by using one photomultiplier from bottom side to reduce the electric power. Furthermore a lead plate with the thickness of 1cm is located over the target and the lead plate is sandwiched by two layers of the plastic scintillator to identify gamma-rays from neutrons.

The new solar neutron telescope has a function to reject charged particles with an efficiency of 90%. Therefore the new solar neutron telescope has capability of 1/3 of the 64m$^2$ large solar neutron telescope located at the same place. We are waiting large solar flares over our detectors.

In addition to the long-term cosmic-ray observations mentioned above, various kinds of short-dated experiments are carried out every year taking an advantage of the high altitude of the observatory.

High-energy radiations from thunderstorms have been observed by flight measurement, high-mountain observations and

ground-based measurement. There are two types of those radiations associated with thunderstorms. One is short-duration radiations with duration of 1 ms or less. The other is long-duration emissions lasting for a few seconds to a few minutes, or a few tens of minutes on rare occasions. It is believed that both emissions originate from electrons accelerated in strong electric fields formed in lightning and thunderclouds. However, compared with the former, the latter has remained less understood due to lack of a large sample of observations.

To investigate production mechanism of long-duration emissions and the relevant electron acceleration, we installed at Norikura Cosmic-ray Observatory a radiation detection system and environmental sensors to measure light and electric fields during 2008−2010. The radiation system consists of a spherical NaI scintillator and a thin plastic scintillator that is placed just above the NaI counter. During the period, the system detected one long-duration bursts as well as five short-duration events.

Fig. 4 (top) shows the long-duration event observed during thunderstorms on 2008 September 20th [25]. The event lasted for 90 sec. Fig. 4 (bottom) represents an observed photon spectrum extending from 10 keV to 10 MeV. This indicates that electrons can be accelerated to at least 10 MeV in a quasi-stable thundercloud electric field. In addition, we compared the observed spectrum with model ones, and concluded that a gamma-ray source is located 60 m−130 m (at 90% confidence level) apart from our detector. Given these results, the observed emission was found to consist of not only gamma rays but also electrons. This was the first simultaneous observation of gamma rays and electrons in long-duration bursts

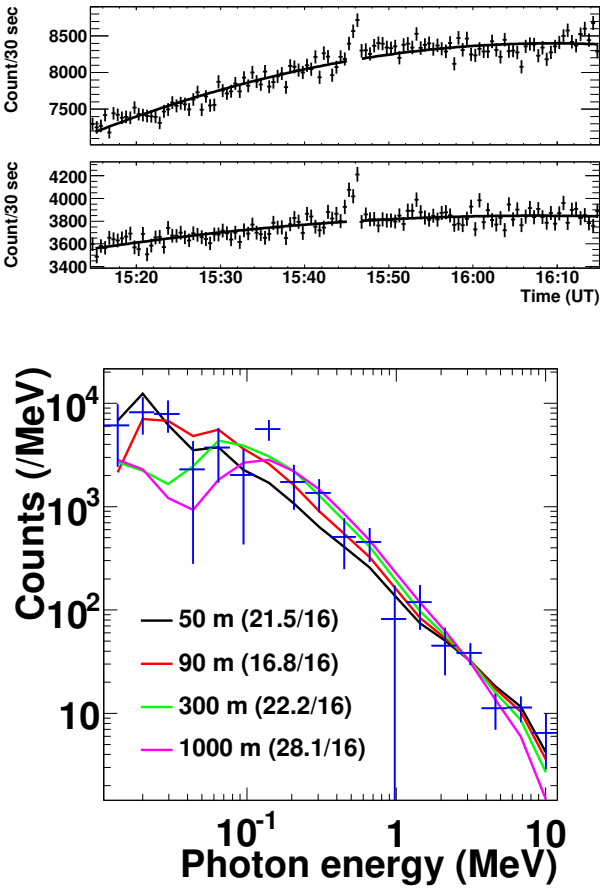


Fig. 4. (Top) Count rates per 30 sec observed by the >10 keV NaI scintillator (upper) and > 100 keV plastic one (lower). (Bottom) The photon spectrum observed by the NaI scintillator.

Observation of night sky background is carried out at Mt. Norikura for basic study of ultra high energy cosmic-ray physics.

The JEM-EUSO mission is going on in order to study ultra high energy cosmic rays (UHECRs), especially above $10^{20}$eV. A 2.5m telescope with 60° FoV will be attached to the International Space Station in 2017 and detect fluorescence in near UV band from extensive air showers induced by UHECRs. Observation of UHECRs from a satellite orbit has not been done yet, so that the knowledge of background light intensity is important to realize the observation. We have measured it from a balloon altitude, but the opportunity is limited. We started the background measurement at Mt. Norikura.

Two 1 inch multi-anode photomultipliers (MAPMTs) developed for EUSO was used with UV filters. The center wavelengths of the filters were 337, 350, 358, 370, 380, 391, 400nm with 10nm band width. In addition BG3 filter was used to detect light in wider range from 330nm to 430nm. The MAPMTs were collimated to 7° FoV. The data was taken with the photon counting method.

We have observed several nights for three years. The intensity at zenith was almost constant at 600-800 photons/ns∼sr $m^2$ for BG3 filter. The spectral intensity was about 1.5-2 times larger than those measured at La Palma and Namibia. The estimated portion of star light and zodiacal light was ∼30% and artificial light and nightglow at upper atmosphere may be the main components at Mt.Norikura.

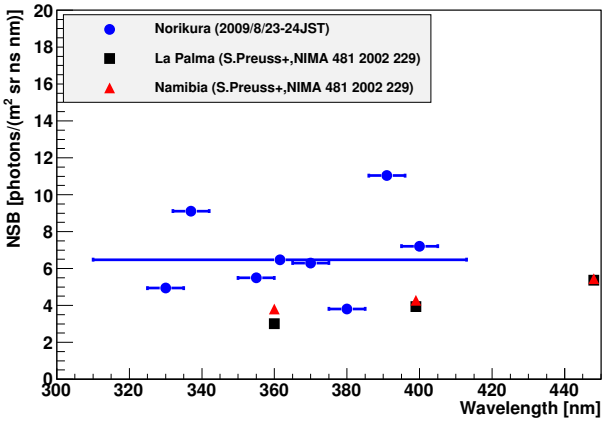


Fig. 5. Spectrum of night sky background measured at Mt.Norikura compared with those at La Palma and Namibia.

## Environmental Study

One of the interesting topics is atmospheric environment especially relating with atmospheric aerosol particles and water soluble gases. The cosmic ray observatory at Mt. Norikura provides us very unique opportunity for the observations of atmosphere at free-tropospheric conditions with its high altitude, AC power supply at the site, accommodation facility,

and easy accessibility. From year 2000 to 2007, we conducted continuous monitoring (mostly mid-May to mid-October) of meteorological parameters, number-size distribution of aerosols, aerosol chemical composition, ozone and radon concentrations, and column amount of aerosols from sky radiometer and ceilometers. We also collected rain, fog, water-condensed aerosol samples. These samples combined with other observed parameters were used in publications in the following subjects [26, 27, 28]:

(1) Polluted air pumping effects over central Japanese Alps in summer
(2) Seasonal variation of aerosol chemistry in free troposphere
(3) Vertical profiles of aerosols and clouds near the top of the atmospheric boundary layer.

Ceilometer (lidar with small output energy) was installed in summer 2002, and was operated in 6 summer seasons. The aerosol and cloud profiles near the top of the atmospheric boundary layer have been observed. Some events of Asian dust were detected.

Observations of total ozone and UV solar radiation with Brewer spectrophotometer on the Norikura mountains are also made[29, 30, 31].

Aerological Observatory started " Observations of total ozone and UV solar radiation with Brewer spectrophotometer at Norikura mountains " as a joint project with Institute for Cosmic Ray Research (ICRR), University of Tokyo at the Norikura Observatory of ICRR (Brewer site: 36.11 N, 137.56 E, 2,772 m a.s.l.), locating at the Northern Japanese Alps in every summer seasons from 2009 (Ito *et al.*: 2011). Purpose of this study is based on the concept of developing Regional Brewer Calibration Centre in Asia and study of total ozone, total sulfur oxide and global/diffuse UV included solar radiation on the high mountains. Observation results by using Brewer spectrophotometers and other instruments for the observation period of three summer seasons of recent three years between 2009 to 2011 are summarized as follows;

(1) Daily means of ds $O_3$ (total ozone) at Norikura for the observation periods were approx. 280 to 290 m atm-cm and were running on the lower values of approx. -3 to -6% compared to the value at Tsukuba (36.06 N, 140.13 E, 39 m a.s.l.) at almost same latitude. Day-to-day variations at Norikura were also small against Tsukuba. On the other hand, daily mean of ds $SO_2$ (total sulfur oxide) values were not recognized at Norikura.

(2) Absolute calibration of Brewers for ds $O_3$ and ds $SO_2$ observations could be carried out within the range of air mass from 7.928 (maximum) to 1.028 (minimum) at Norikura in the clear day. $O_3$ and $SO_2$ Extra-Terrestrial Coefficients (=ETC) of Brewers could be produced as about 10 samples satisfying the condition of "$R^2 > 0.9997$" by the calibrations. As an example of the calibration in 2011, the average of $O_3$ ETC of Brewers was identical within 1% to the currently used coefficient.

(3) In comparison to the data acquired at Tsukuba, the average of daily total $GL_{UV}$ (global UV, e.g. CIE) for the observation periods indicated the intensities of approx. +23 % in 2009 to -6 % in 2011. The low intensity in 2011 was due to the bad weather on the Norikura Mountain. In the case of clear days, the $GL_{UV}$ at Norikura indicated high intensities of approx. +35 to +52 % against the values at Tsukuba. On the other hand, the $GL_{UV}$ increased in the short wavelength range at Norikura against the average at Tsukuba. The altitudinal increasing rate of $GL_{UV}$ in the clear day indicated the calculated amounts of approx. +13 to +18 % per 1,000 m.

This joint project had been clarifying the low total $O_3$, high UV in clear day, low turbidity and etc. at Norikura against the value at Tsukuba. Those environmental conditions are useful for the intercomparison and the absolute calibrations with Brewers. The continuous observations with Brewers and other instrument are very important for the clarification of the seasonal variation and the coefficient trends.

## Botanical Study

Effects of snow cover on pine shrub Pinus pumila in the alpine region of Mt. Norikura

High mountainous habit is one of the most severe habits for plant life and sometimes dwarf shrubs cannot survive. In the alpine regions of Japan, the dwarf shrub Pinus pumila (Japanese name : Haimatsu) forms communities together with small alpine plants, whereas dwarf shrubs occur only in the transition zone between the alpine region and the subalpine forest in Europe and North America. This characteristic of alpine vegetation is considered to be owing to winter heavy snow in the alpine regions of Japan. The purpose of this study is to elucidate how snow cover protects Haimatsu from winter environmental stresses in the alpine region of Mt. Norikura.

Study site

Tree height of Haimatsu and snow depth differ greatly as a result of slight difference in topography. Two site of the study area were selected. (i) site P (wind-protected) and (ii) site E (wind-exposed). At site P, mean tree height was 1.1 m. There was a lot of snow accumulation and Haimatsu was almost entirely covered with snow during the winter. Needle browning and death occurred rarely. At site E, mean tree height was 0.4 m. Snow accumulation was minimal, and Haimatsu was not entirely covered with snow. Needle browning and death was observed frequently.

Winter needle death in Haimatsu[32]

At site E, the browning and death of needles of Haimatsu occurred mainly in early spring at the point where the shoot protrudes from the snowpack. They are thought to be caused by excessive water loss due to mechanical damage to the cuticle and/or to a thinner cuticle. However, needle browning and death in Haimatsu were not related to mechanical damage of the cuticle but might be due to changes in the quality and structure of the cuticle wax and resultant increase in water loss from needle cells.

Photosynthetic capacity in Haimatsu[33]

At site E, needles of Haimatsu had lower biomass, nitrogen, Rubisco (enzyme) and cell wall per unit area, and had higher photosynthetic capacity and shorter needle life-span than Haimatsu at site P. These results suggest that Haimatsu at wind-exposed site produces needles at low cost with high productivity to compensate for a short leaf life-span which may be imposed by wind stress when needles appear above the snow surface in winter.

## Bibliography


[1] K. Munakata, S. Yasue, C. Kato, J. Kota, M. Tokumaru, M. Kojima, A. A. Darwish, T. Kuwabara and J. W. Bieber, "On the cross-field diffusion of galactic cosmic rays into the magnetic flux rope of a CME", *Advances in Geosciences*, 2, 115-124, eds. W. H. Ip and M. Duldig (World Scientific Publishing Co., USA), (2006).

[2] T. Kuwabara, J. W. Bieber, J. Clem, P. Evenson, R. Pyle, K. Munakata, S. Yasue, C. Kato, S. Akahane, M. Koyama, Z. Fujii, M. L. Duldig, J. E. Humble, M. R. Silva, N. B. Trivedi, W. D. Gonzalez and N. J. Schuch, "Real-time cosmic ray monitoring system for space weather", *Space Weather*, 4, S08001-1 10, (2006).

[3] M. R. Da Silva, A. Dal Lago, E. Echer, A. de Lucas, W. D. Gonzalez, N. J. Schuch, K. Munakata, L. E. A. Vieira, and F. L. Guarnieri, "Muon and neutron observations in connection with the corotating interaction regions", *Adv. Space Res.*, 40, pp348-352, (2007).

[4] Y. Okazaki, A. Fushishita, T. Narumi, C. Kato, S. Yasue, T. Kuwabara, J. W. Bieber, P. Evenson, M. R. Da Silva, A. Dal Lago, N. J. Schuch, Z. Fujii, M. L. Duldig, J. E. Humble, I. Sabbah, J. Kóta and K. Munakata, "Drift effects and the cosmic ray density gradient in a solar rotation period: First observation with the Global Muon Detector Network (GMDN)", *Astrophys. J.*, 681, 693-707, (2008).

[5] T. Kuwabara, J. W. Bieber, P. Evenson, K. Munakata, S. Yasue, C. Kato, A. Fushishita, M. Tokumaru, M. L. Duldig, J. E. Humble, M. R. Silva, A. Dal Lago, and N. J. Schuch, "Determination of ICME Geometry and Orientation from Ground Based Observations of Galactic Cosmic Rays", *J. Geophys. Res., 114*, A05109-1 10, doi:10.1029/2008JA013717, (2009).

[6] A. Fushishita, T. Kuwabara, C. Kato, S. Yasue, J. W. Bieber, P. Evenson, M. R. Da Silva, A. Dal Lago, N. J. Schuch, M. Tokumaru, M. L. Duldig, J. E. Humble, I. Sabbah, H. K. Al Jassar, M. M. Sharma, and K. Munakata, "Precursors of the Forbush Decrease on 2006 December 14 observed with the Global Muon Detector Network (GMDN)", *Astrophys. J.*, 715, 1239-1247, (2010).

[7] A. Fushishita, Y. Okazaki, T. Narumi, C. Kato, S. Yasue, T. Kuwabara, J. W. Bieber, P. Evenson, M. R. Da Silva, A. Dal Lago, N. J. Schuch, M. Tokumaru, M. L. Duldig, J. E. Humble, I. Sabbah, J. Kóta, and K. Munakata, "Drift effects and the average features of cosmic ray density gradient in CIRs during successive two solar minimum periods", *Advances in Geosciences*, eds. W. H. Ip and M. Duldig (World Scientific Publishing Co., USA), 21, 199-210, (2010).

[8] M. Tokumaru, M. Kojima, K. Fujiki, K. Munakata, T. Kuwabara and K. Marubashi, "Relation between loop-shaped interplanetary disturbances and the magnetic flux rope", *Advances in Geosciences*, eds. W. H. Ip and M. Duldig (World Scientific Publishing Co., USA), 21, 21-32, (2010).

[9] M. Rockenbach, A. Dal Lago, W. D. Gonzalez, K. Munakata, C. Kato, T. Kuwabara, J. W. Bieber, N. J. Schuch, M. L. Duldig, J. E. Humble, H. K. Al Jassar, M. M. Sharma, and I. Sabbah, "Geomagnetic Storms Precursors Observed from 2001 to 2007 with the Global Muon Detector Network GMDN", *Geophys. Res. Lett.*, 38, L16108-1 4, doi:10.1029/2011GL048556, (2011).

[10] "Solar neutron events of October—November 2003", Watanabe, K. *et al.*, Astrophys. J., **636**, 1135–1144, 2006.

[11] "Solar neutron events in association with large solar flares in November 2003", Watanabe, K. *et al.*, Adv. Space Res., **38**, 425–430, 2006.

[12] "Long-lived solar neutron emission in comparison with electron-produced radiation in the 2005 September 7 solar flare", Sako, T. *et al.*, Astrophys. J., **651**, L69–L72, 2006.

[13] "Highly significant detection of solar neutrons on 2005 September 7", Watanabe, K. *et al.*, Adv. Space Res., **39**, 1462–1466, 2007.

[14] "A solar neutron telescope in Tibet and its capability examined by the 1998 November 28th event", Muraki, Y. *et al.*, Astroparticle Phys., **28**, 119–131, 2007.

[15] "Simultaneous detection of high-energy solar neutrons and protons at Chacaltaya observatory on April 15, 2001", Muraki, Y. *et al.*, in Proc. 30th Int. Cosmic Ray Conf, Merida, **1**, 25–28, 2007.

[16] "Search for solar neutrons associated with series of X-class flares during the declining period of solar cycle 23", Matsubara, Y. *et al.*, in Proc. 30th Int. Cosmic Ray Conf, Merida, **1**, 29–32, 2007.

[17] "Ion acceleration and neutral emission mechanisms for 2005 September 7 flare", Watanabe, K. *et al.*, in Proc. 30th Int. Cosmic Ray Conf, Merida, **1**, 45–48, 2007.

[18] "Emission profile of solar neutrons obtained from the ground-based observations for the 7 September 2005 event", Sako, T. *et al.*, in Proc. 30th Int. Cosmic Ray Conf, Merida, **1**, 53–56, 2007.

[19] "Energy spectrum for the solar neutron event of September 7 2005, derived from the SNT at Sierra Negra", Gonzalez, L. X. *et al.*, in Proc. 30th Int. Cosmic Ray Conf, Merida, **1**, 57–60, 2007.

[20] “Status of the world-wide network of solar neutron telescopes in solar cycle 24”, Matsubara, Y. *et al.*, in Proc. 31st Int. Cosmic Ray Conf, Lodz, **1**, On Conference homepage, 2009.

[21] “Detection of high-energy solar neutrons and protons by ground level detectors on April 15, 2001”, Muraki, Y. *et al.*, Astropart. Phys., **29**, 229–242, 2008.

[22] “Solar neutron events as a tool to study particle acceleration at the Sun”, Valdes-Galicia, J. F. *et al.*, Adv. Space Res., **43**, 565–572, 2009.

[23] “Physics of ion acceleration in the solar flare on 2005 September 7 determines $\gamma$-ray and neutron production”, Watanabe, K. *et al.*, Adv. Space Res., **44**, 789–793, 2009.

[24] “Observation of solar neutrons associated with the large flare on 1991 June 4”, Muraki, Y. *et al.*, ApJ, **400**, L75-L78 , 1992.

[25] “Observation of an energetic radiation burst from mountain-top thunderclouds”, H. Tsuchiya *et al.*, Phys. Rev. Lett. **102**, 255003 (2009), Citation Index:13.

[26] Nishita, C., K. Osada, K. Matsunaga, Y. Iwasaka, e, J. Geophys. Res., **113**, D06202, doi:10.1029/2007JD009302, 2008.

“Nucleation mode particles in up-slope valley winds at Mt. Norikura, Japan: implications for the vertical extent of new particle formation events in the lower tropospher”, Nishita, C., K. Osada, K. Matsunaga, Y. Iwasaka, J. Geophys. Res., **113**, D06202, doi:10.1029/2007JD009302, 2008.

[27] “Temporal variation of water-soluble ions of free tropospheric aerosol particles over central Japan”, Osada, K., Kido, M., Nishita, C., Matsunaga, K., Iwasaka, Y., Nagatani, M., Nakada, H., Tellus, **59B**, 742-754, 2007.

[28] “Number-size distributions of free tropospheric aerosol particles at Mt. Norikura, Japan: effects of precipitation and air-mass transportation pathways”, Nishita, C., K. Osada, K. Matsunaga, Y. Iwasaka, J. Geophys. Res., 112, doi:10.1029/2006JD007969, 2007.

[29] “Observations of total ozone and UV solar radiation with Brewer spectrophotometers on the Norikura mountains in 2009.”, Ito, M., M. Takano, H. Oguri, M. Takita, H. Shimodaira and H. Ishitsuka, Jour. of the Aerological Observatory, **69**, 41-54 2011.

[30] “Observations of total ozone and UV solar radiation with Brewer spectrophotometers on the Norikura mountains, Northern Japanese Alps, from 2009.”, Ito, M., S. Shimizu, Y. Noto, T. Shimamura, M. Takano, M. Takita, H. Shimodaira and H. Ishitsuka, The 13th WMO Biennial Brewer Workshop, Beijing, China in 2011, 2011.

[31] “Total ozone and UV solar radiation with Brewer spectrophotometers at Norikura of Northern Japanese Alps, in recent three years.”, Ito, M., S. Shimizu, Y. Noto, T. Shimamura, M. Takita, H. Shimodaira and H. Ishitsuka, Jour. of the Aerological Observatory, **70**, in contribution.

[32] “Needle browning and death in Pinus pumila in the alpine region of central Japan were not related to mechanical damage of cuticle and cuticle thickness.”, Nakamoto A., Ikeda T., Maruta E., Can. J. For. Res. 42, 167-178 (2012).

[33] “Needle traits of an evergreen, coniferous shrub growing at wind-exposed and protected sites in a mountain region: does Pinus pumila produce needles with greater mass per area under wind-stress conditions?”, Nagano S., Nakano T., Hikosaka K and Maruta E., Plant Biology 11(Suppl.1), 94-100, (2009).

# AKENO OBSERVATORY

## Introduction

The Akeno Observatory is situated in Akeno of Hokuto-city, 20 km northwest of Kofu and 130 km west of metropolitan Tokyo. The location is at the longitude of 138.5°E and the latitude of 35.8°N. The altitude is ∼900 m above sea level. It was established in 1977 as a research center for air shower studies in the very high energy region, and it has been administered by the ICRR as a facility of joint-university-use.

## Akeno Air Shower Experiments

The Akeno Air Shower Experiment started in 1979 with an array covering 1 km$^2$ area (the 1 km$^2$ array, see Fig.1). The array was enlarged to 20 km$^2$ in 1984 and was gradually expanded to Akeno Giant Air Shower Array (AGASA) of approximately 100 km$^2$ area by 1990. The AGASA was built

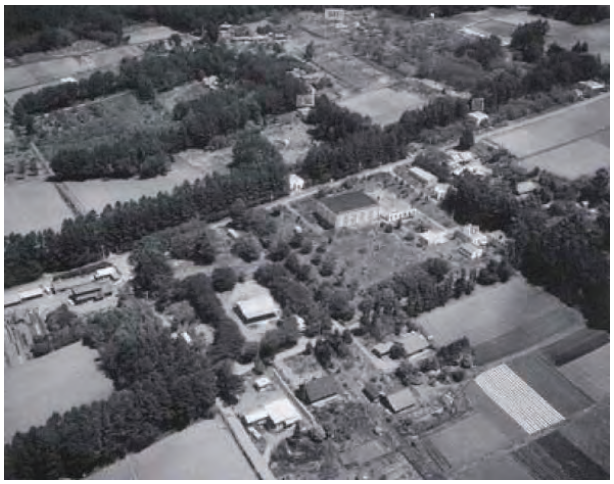

Fig. 1. Aerial View of Akeno Observatory and 1 km$^2$ Array Area

to detect Ultra-High Energy Cosmic Rays (UHECRs) in the energy range of $10^{20}$ eV.

One of the distinctive features of Akeno experiments is that the measurements were made over five decades of energies well covering $10^{15}$ eV - $10^{20}$ eV by using both the surface detector for electromagnetic component, and the shielded detector for muon component (Fig.2). The wide energy coverage was accomplished by the arrays of scintillation detectors of various inter-detector spacings from 3 m to 1 km and with different triggering conditions. This feature of Akeno air shower measurement is well demonstrated in Fig.3, in which the spectra from Akeno 1 km$^2$ array for $10^{14.5}$ eV - $10^{18.8}$ eV [7] and AGASA for $10^{18.5}$ eV - $10^{20.3}$ eV [8] are plotted.

Fig. 2. One of the muon detector housings with concrete shielding.

## AGASA

The AGASA was composed of 111 surface detectors, each with plastic scintillator of 2.2 m$^2$ area and 5 cm thickness. The counters were deployed with ∼1 km spacing covering the ground area of about 100 km$^2$ in the suburban area of Akeno, outside of the observatory campus. All counters were connected with optical fibers for the timing measurement and digital data transfer to the observatory. The AGASA served as the largest air shower array in the world since its commissioning in 1990 until it stopped data taking in January 2004, when the construction of the succeeding experiment, Telescope Array (TA), started in Utah. It was dismantled in 2007 together with other Akeno air shower arrays.

An exposure of 5.8 $\times$ $10^{16}$ m$^2$ s sr above $10^{19}$ eV was accumulated by AGASA in 13 years of operation. Extensive air showers with zenith angles smaller than 45° and with core locations inside the array area were used for the analysis. The AGASA reported an extension of the energy spectrum beyond the predicted Greisen-Zatsepin-Kuzmin (GZK) cutoff in 1998 [9] and a total of eleven UHECR events were observed above $10^{20}$ eV by 2003.

## Measurement of UHECRs

Since the AGASA measurement in 1998, High Resolution Fly's Eye (HiRes) [10], Pierre Auger Observatory (PAO) [11], and Telescope Array (TA) [12] measured the energy spectra of UHECRs with higher statistics.

The HiRes observed the UHECR using the fluorescence telescope. The PAO and TA measure the spectrum using the surface array consisting of either water tanks (PAO) or plastic

*7 M. Nagano et al., J. Phys. **G10**, 1295 (1984); M. Nagano et al., J. Phys. **G18**, 423 (1992).
*8 M. Takeda et al., Astropart. Phys. **19**, 447 (2003).
*9 M. Takeda et al., Phys. Rev. Lett. **81**, 1163 (1998).
*10 R.U. Abbasi et al., Phys. Rev. Lett. **100**, 101101 (2008).
*11 J. Abraham et al., Phys. Lett. **B685**, 239 (2010).
*12 T. Abu-Zayyad et al., arXiv:1205.5067v1 (2012).

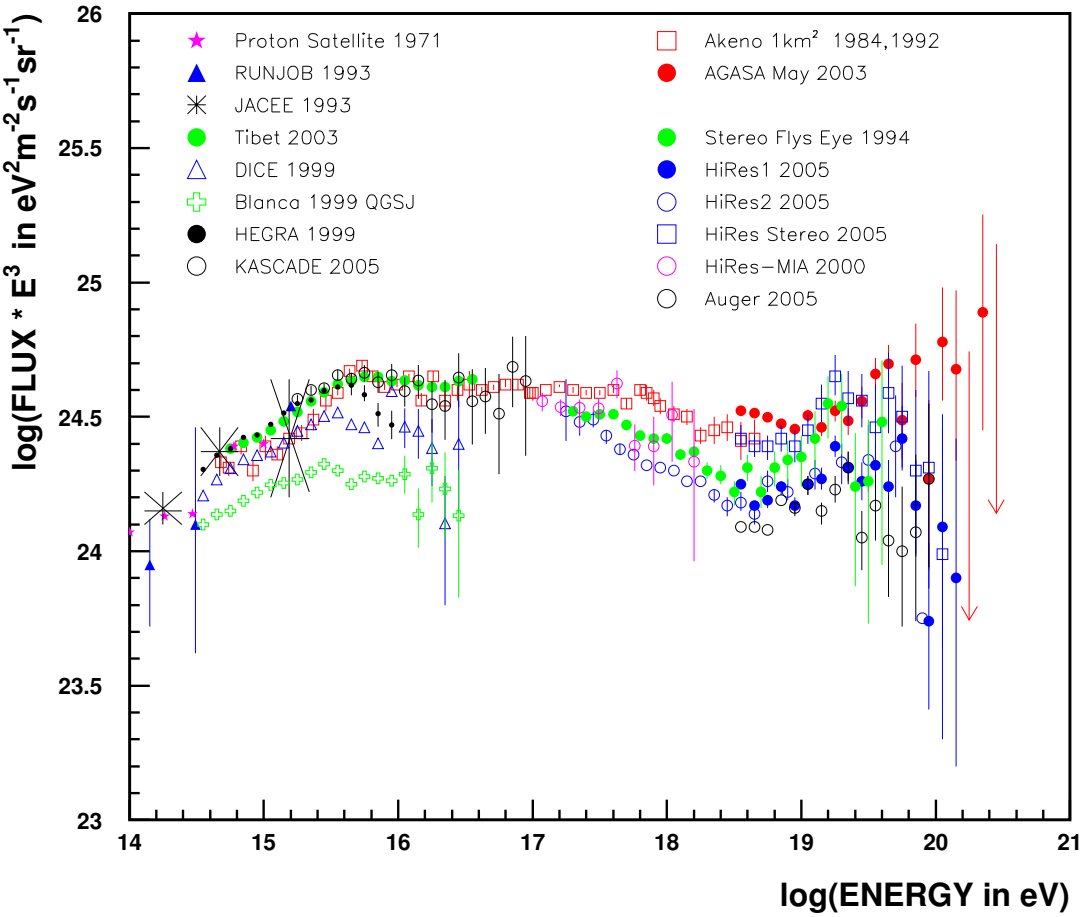


Fig. 3. Akeno energy spectrum measurements for $10^{15}$ eV - $10^{20}$ eV.

scintillators (TA), but the energy scale of the array is determined by the fluorescence telescope using a subset of events observed by the fluorescence telescope and surface array at the same time. The adoption of the energy scale by the fluorescence telescopes is based on its small dependence on the air shower simulation.

The energy spectra above $10^{18}$ eV by AGASA and other experiments are compiled and compared by the working group represented by UHECR experiments in the UHECR-2012 symposium held at CERN for Feb. 13th - 16th, 2012 [13]. The result is plotted in Fig.4 with the energy scale of each experiment adjusted to a reference energy, which is set halfway between the PAO and TA/HiRes.

Following factors were applied for the energy scale; $\times 1.10$ for PAO, $\times 0.91$ for TA and HiRes, $\times 0.65$ for AGASA and $\times 0.56$ for Yakutsk.

As seen in Fig.4, the overall agreement between experiments is good, and a "dip" structure was seen around $10^{18.7}$ eV by all experiments. The HiRes, PAO and TA confirmed a strong flux suppression above approximately $10^{19.7}$ eV. Although the AGASA spectrum does not demonstrate the cutoff structure, the number of events above $10^{20}$ eV became only two after the energy rescaling, making the claim of the extended spectrum statistically insignificant. The estimate of systematic uncertainty of the energy measurement is approximately 20% for all the experiments, and rescalings for the TA/HiRes and PAO are within this limit. Rescaling of the surface array energy, $\times 0.65$ for AGASA and $\times 0.56$ for Yaktsuk, indicates that there exist larger systematic uncertainties than originally estimated by running the air shower simulation. This difference of energy scale obtained by the surface array and by the fluorescence telescope remains as a basic question in the understanding of the air shower phenomena.

## Recent Research Activities

The study of UHECRs by AGASA in Akeno was succeeded by the Telescope Array (TA) experiment in Utah, USA since 2008. After the cessation of AGASA, the Akeno observatory has been used for small scale cosmic ray experiments, astrophysical observations and as a test and maintenance facility of TA by the ICRR and university researchers. Research activities in JFY 2013 (April 2013 - March 2014) are described in the following.

*[13] http://indico.cern.ch/conferenceDisplay.py?confId=152124

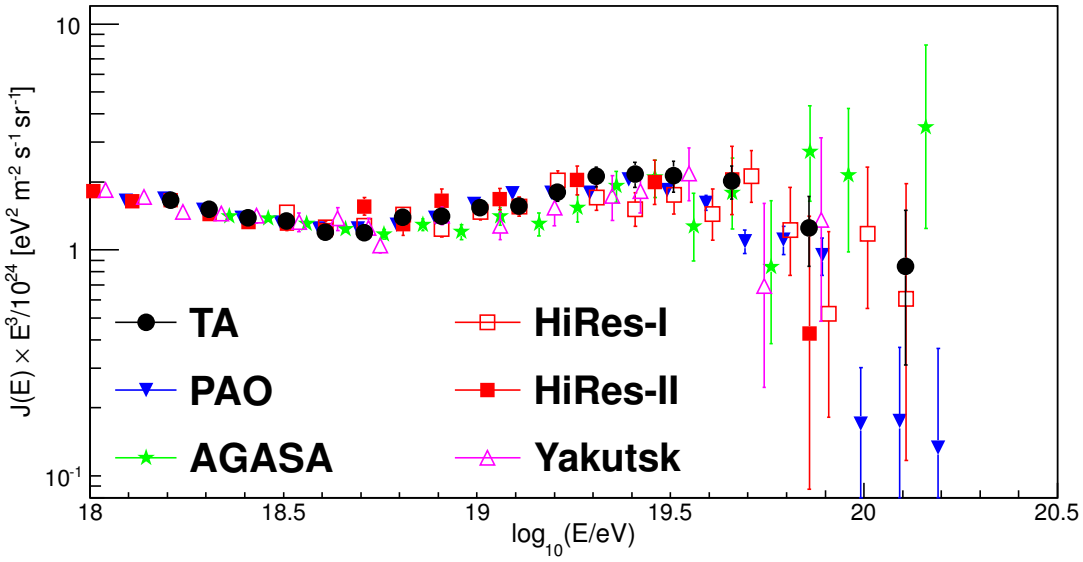


Fig. 4. Recent compilation of UHECR energy spectra. The energy scale of each experiment is adjusted as described in the text.

***Research and development for the Telescope Array observation in Utah by the TA collaboration***

All the fluorescence imaging cameras and a part of the surface detectors of TA were assembled in the Akeno observatory by the TA collaboration team. The detectors were tested in Akeno and shipped to the Utah observation site for the installation. All the unit mirrors of the TA fluorescence telescope were tested in Akeno and the atmospheric monitoring lidar of TA using YAG laser was developed in Akeno. In JFY 2013, a certain number of scintillator counters were assembled for TA muon detectors and were sent to Utah. A part of the experimental hall was prepared for the test of the vibration control equipment and temporary storage of the KAGRA gravitational antenna equipment.

***Observation by the multi-color imager for transients, survey and monstrous explosions (MITSuME) by N. Kawai (Tokyo Institute of Technology) et al.***

One of the three MITSuME robotic telescopes was installed in the Akeno observatory in 2003 on the roof of the unused concrete muon house. The telescope has an aperture of 50 cm, an FOV of 28' $\times$ 28' and is equipped with a tricolor CCD camera capable of $g'R_CI_C$-bands photometry. It is operated remotely from the Tokyo Tech using dedicated ADSL connections. Upon receiving a GRB alert from Swift or Fermi satellite, it quickly directs the telescope (9°/s maneuverability) toward the GRB direction, and makes a prompt observation of the GRB and its afterglow. In JFY 2013, 46 GRBs were observed, and 5 were identified as visible objects. Other burst objects were also observed. The whole sky monitor was installed 10 m away from the telescope dome, and this information is opened to the public via Internet. Since the air conditioning was controlled remotely, the focusing function was improved during summer season.

***Observation of galactic cosmic rays by large area muon telescope by S. Shibata (Chubu University) et al.***

Four layers of proportional counter telescopes, each with 25 m$^2$ area, were installed in three muon houses in Akeno (Fig.2) and have been continuously measuring the cosmic ray muons since 2003. The mode energy of the primary cosmic rays is approximately 2.5 GeV corresponding to 2m thick concrete ceiling of the muon house and the latitude of Akeno observatory. The measurement in Akeno is combined with a simultaneous measurement in Ooty, India, and the modulation effects of galactic cosmic rays by the solar activity such as the Forbush decrease and its precursor have been continuously monitored [14]. In JFY 2013, the network router was replaced to improve the access from the outside, and the UPS was installed to operate the data server stably. And the observation was continued.

***Research and development for a small atmospheric Cherenkov telescope in Akeno observatory by T. Yoshikoshi, M. Ohishi (ICRR) et al.***

A small alt-azimuth telescope is being setup in Akeno for prototype tests with atmospheric Cherenkov observations of gamma rays [15]. The optical axis of segmented mirrors was adjusted. The system of reflectivity measurement and the system of telescope position calibration were developed. The data acquisition system was installed to this telescope.

*[14] T. Nonaka.et al, Proc. of the 29th ICRC, **1**, 363-366 (2005).
*[15] M. Ohishi et al., 33rd ICRC, (Rio deJaneiro), **9**, in press (2013).

# KAMIOKA OBSERVATORY

Kamioka observatory is located at 1000 m underground (2700 m water equivalent) in the Kamioka Mine, Gifu prefecture, about 200 km west of Tokyo. The observatory was established in 1995 in order to operate Super-Kamiokande experiment (SK). The underground laboratories are located under Mt.Ikeno-yama and accessible to the experimental site through a 1.7 km horizontal tunnel. The observatory also has surface research buildings and a dormitory located at the distance of 15 minutes drive from the entrance of the underground laboratories.

The Super-Kamiokande experiment had discovered neutrino oscillations through the observations of atmospheric and solar neutrinos (see the section for Neutrino and Astroparticle Division). The atmospheric neutrino oscillation was confirmed by the long baseline neutrino oscillation experiment, K2K, using accelerator neutrino beam, which was conducted between 1999 and 2004. A new long baseline neutrino oscillation experiment (the T2K experiment) using a high intensity beam, 50 times of the K2K neutrino beam, by the J-PARC proton accelerator has started in 2009. In 2011, the experiment has observed 6 $\nu_e$ appearance events indicating non-zero $\theta_{13}$ which was as yet determined the last neutrino oscillation parameter. In 2012 and 2013, the collaboration accumulated more electron neutrino appearance events and strengthen the discovery of non-zero $\theta_{13}$.

The low cosmic ray flux and low seismic noise environment in the underground site enables us to conduct various researches. There is a 100 m long laser interferometer, which is a proto-type of the 3 km gravitational wave antenna (see section of Astrophysics Gravity Division) under construction. Using the low radioactive background environment in the Kamioka Mine, a dark matter experiment, called XMASS is operated in Lab-C. The XMASS group constructed a 800kg liquid xenon detector and started commissioning run in late 2010. In 2013, the detector was improved to remove backgrounds on the inner surface of the PMT plane. The R&D study of a tracking type detector for dark matter detection lead by the Kobe University group (the NEWAGE experiment) has also been performed in Lab-B. The commissioning run of the CANDLE experiment in Lab-D (Osaka Univ.), a double beta decay experiment is now conducted. The study to improve the neutrino detection sensitivity by adding gadolinium to Super-Kamiokande is on going. A 200 ton test tank dedicated for the R&D study of the gadolinium project was constructed in Lab-E and a feasibility study has been performed. In order to support those experiments and also related R&D works, the Observatory is equipped with low background Germanium detector in Lab-1 and Lab-A, ICP-MS and so on to measure extremely low radioactive backgrounds.

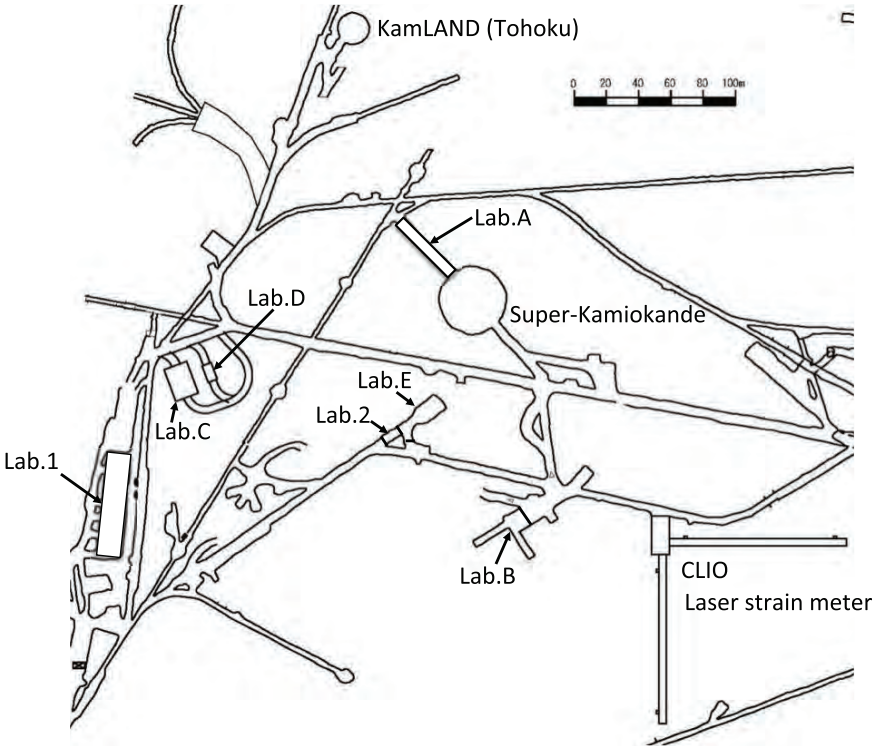


Fig. 1. Kamioka Underground Observatory.

# RESEARCH CENTER FOR COSMIC NEUTRINOS

The Research Center for Cosmic Neutrinos (RCCN) was established in April, 1999. The main objective of this center is to study neutrinos based on data from various observations and experiments. In order to promote studies of neutrino physics, it is important to provide the occasion to discuss theoretical ideas and experimental results on neutrino physics. Therefore, one of the most important tasks of this center is the organization of neutrino-related meetings. On January 20, 2014, we hosted this year's domestic neutrino workshop, whose topic was on the measurement of absolute neutrino masses by terrestrial experiments and cosological measurements. About 40 physicists participated in this meeting.

Members of this center have been involved in the Super-Kamiokande and T2K experiments, carrying out researches in neutrino physics. (Please see the Super-Kamiokande and T2K pages for the scientific results.) Atmospheric neutrino data from Super-Kamiokande give one of the most precise pieces of information on neutrino oscillations. With increased data, it is more important to have better predictions of the neutrino flux. Therefore, in addition to data analysis of the above experiments, we work on the calculation of the atmospheric neutrino flux.

It is important to share our scientific achievements with the general public. For this reason, we hold public lectures every year. Since FY2009, ICRR and the Kavli Institute for the Physics and Mathematics of the Universe (Kavli-IPMU) have co-sponsored two public lectures each year. The public lecture held in Spring is co-organized by RCCN and the Public Relation Office of ICRR. The Spring public lecture in FY2013 was held on April 13, 2013. Two scientists lectured on the observations of the Universe and the physics of the Higgs particle.

RCCN, together with the computer committee of ICRR, is in charge of operating the central computer system in ICRR. In FY 2013, the computer system was upgraded to a much high performance one. Since then, the system has been operated without any serious problems. RCCN also supports the users of the computer system, including physicists in the cosmic ray community in Japan.

Since 2004, RCCN has been acting as a body for accepting the ICRR inter-university programs related to the low-background underground facility in the Kashiwa campus. The facility is currently equipped with 4 Ge detectors mainly for the measurements of cosmic radioactive isotopes. The scientific activities related to this facility is described elsewhere.

# APPENDICES

# A. ICRR Workshops and Ceremonies

## 4th Korea-Japan workshop on KAGRA

Date: June 10-11, 2013
Place: Osaka University, Japan

**Outline:** This workshop was the 4th Korea-Japan workshop on KAGRA, and was held at Osaka University. The workshop was organized by the scientific advisory committee, the scientific organizing committee chaired by Seiji Kawamura (ICRR), and the local organizing committee chaired by Hideyuki Tagoshi (Osaka University).

The workshop consisted of several sessions: the opening, plenary, instrument, data analysis, theory, detector characterization, data management, and discussion about the future collaboration sessions. After the opening talk given by Takaaki Kajita (ICRR), in the plenary session Hyung Mok Lee (Seoul National University) explained the activities of the Korean gravitational wave group and Kazuaki Kuroda (ICRR) gave a talk about the overview on the current KAGRA. In each session of subsystems, the past activities and the future plans were presented and discussed, including a talk on the activities of the KAGRA data analysis subsystem by Hideyuki Tagoshi (Osaka University) and a talk on the status of KAGRA detector characterization by Kazuhiro Hayama (Osaka City University). In the instrument session Kyuman Cho (Sogang University) gave a talk about the precision tilt and radius curvature sensor using a double-pass AOM, and indicated the possibility of using it for KAGRA.

In the discussion session, first, some progress in the framework of the collaboration was reported, including the JSPS core-to-core program KAGRA had obtained, the appointment of Tai Hyun Yoon (Korea University) as an ICRR visiting professor, and the gravitational wave summer school that would be held in August, 2013 at Pohang, Korea. Then we discussed the future collaboration on each subsystem. For the instrument, we agreed that we would investigate the possibility of using the tilt sensor for KAGRA, we would continue inviting Korean researchers and students using the JSPS core-to-core program, and we would keep the efforts of finding other Korean experimentalists interested in joining KAGRA. For the detector characterization, we defined several projects for developing tools equipped to identify noise artifacts and to localize their sources, and decided to have a bi-weekly telecon in the group. For the data analysis, we agreed that the bayesian parameter estimation was a good starting research to establish closer collaboration. Finally we decided that the next workshop would be held on November 29 - 30, 2013 at Seoul National University, Seoul, Korea.

**Participants:** 34 participants.
**Website:** http://vega.ess.sci.osaka-u.ac.jp/korea-japan/

Fig. 1. 4th Korea-Japan workshop on KAGRA.

## 5th Japan-Korea workshop on KAGRA

Date: November 29-30, 2013
Place: Seoul National University, Seoul, Korea

**Outline:** This workshop was the 5th Japan-Korea workshop on KAGRA, and was held at Seoul National University, Seoul, Korea. The workshop was organized by the scientific advisory committee, the scientific organizing committee chaired by Hyung Mok Lee (Seoul National University) and Seiji Kawamura (ICRR), and the local organizing committee chaired by Hyung Mok Lee (Seoul National University).

The workshop consisted of several sessions: the opening, plenary, detector characterization and data management, instrument, optical follow-up, theory and data analysis, and discussion on the next steps sessions. After the opening talk given by Hyung Mok Lee (Seoul National University), Ho Jung Paik (University of Maryland) gave a talk about a low frequency gravitational wave detector with superconducting instrumentation, and Shinji Miyoki (ICRR) explained the present status of KAGRA. In each session of subsystems, the past activities and the future plans were presented and discussed, including a talk on the status of KAGRA detector characterization by Kazuhiro Hayama (Osaka City University), a talk on the current status of the KAGRA cryogenics by Chihiro Tokoku (ICRR), and a talk on the status of the KAGRA data analysis subsystem by Hideyuki Tagoshi (Osaka University). In the instrument session Tai Hyun Yoon (Korea University) gave a talk about the high-finesse fiber ring cavity for compact laser frequency stabilization system of KAGRA and reported the progress he made during his visit to ICRR

an a visiting professor. In this workshop we decided to have the optical follow-up session for the first time because of the importance of the multi-messenger science, and Michitoshi Yoshida (Hiroshima University) gave a talk about the optical-infrared telescope network for follow-up observation of gravitational wave transients in Japan.

In the discussion session, for the instrument, we agreed that we would investigate the possibility of using the fiber ring cavity which Tai Hyun Yoon (Korea University) developed for KAGRA, and we would investigate the possibility of inviting Tai Hyun Yoon (Korea University) and Kyuman Cho (Sogang University) to ICRR as a visiting professor. For the detector characterization, we were discussing the KAGRA mock data challenge and an EMD-based event-trigger-generation development using CLIO data. For the data analysis, several collaboration research projects were explained, and the group planned to have a monthly telecon. For the data management, we had some discussion about the data transfer test, etc. Finally we decided that the next workshop would be held on June 20 - 21, 2014 at National Astronomical Observatory of Japan, and the workshop after next would be held in December, 2014 at Toyama University.

**Participants:** 36 participants.
**Website:** https://kgwg.nims.re.kr/kagra5th/kagra5th/Home.html

Fig. 2. 5th Japan-Korea workshop on KAGRA.

# EliTES 2nd General Meeting

Date: Dec 4-5, 2013
Place:Deligation of the Eureopean Union to Japan & Sanjo Conference Hall, the University of Tokyo, Japan

**Outline:** The ELiTES program is initiated by partners; European Gravitational Observatory sponsored by Italy and France, ICRR (Japan), Universit di Roma "La Sapienza" (Italy), Friedrich-Schiller Universitaet, Jena (Germany), University of Glasgow (UK), FOM (Nitherland), MPG (Germany), Universit degli Studi del Sannio (Italy), University of West Scotland (UK). The acronym ELiTES stands for ET LCGT(KAGRA, at present) interferometric Telescopes: Exchanges of Scientists. It is an initiative supported (2012-2016) by the European Commission under FP7-people. In particular, ELiTES is supported as IRSES: International Research Staff Exchange Scheme (RISE in H2020). ELiTES supports the exchange of GW scientists between EU and Japan (and the Japanese counterpart set-up a mirror initiative, consequent to ELiTES). ELiTES idea born during the second ET general meeting, focusing on the ET-KAGRA common aspects:

- Cryogenics and Underground facilities
- Very active and productive links are sustained through

ELiTES consists of four working packages, WP1: Suspensions design and test, WP2: Suspensions materials and fibers, WP3: Infrastructures & Vacuum apparatuses and WP4: organization. Under this ELiTES program, we have one technical workshop in Europe and one general meeting in Japan. In this financial year, ICRR hosted the second general meeting in Tokyo as in the previous year. Since the program is sponsored by EU, the first day was held in EU representative house in Tokyo. First half of the beginning session of the first day consisted of invited talks. First one was given by Dr. Barbara Rhode who is the Head of Science and Technology Section of the delegation of EU to Japan (EU house in Tokyo). The second one was given by Mr. Shintaro Seto who is the director for Scientific Research Coordination, Scientific Research Institutes Devision, Research Promotion Bureau, Ministry of Eduation, Culture, Sports, Science and Technology. After this invited talks, KAGRA project by Raffaele Flaminio, Advanced Virgo status by Fulvio Ricci, Advanced LIGO status by James Hough, and The Einstein Telescope Project by Harald Lueck were presented in the morning. The afternoon was devoted to WP3-Infrasgtructures. Three talks focused on KAGRA underground facility and one talk was for site study of ET project.We had discussed about underground environmental sensors. Also correlated magnetic noise in Kamioka was reported.

The second day, the meeting venue was moved to Sanjo Hall in Hongo campus of UTokyo. WP1-WP2 joint activities were presented and discussed. Modeling and testing of cryogenic sapphire suspensions is introduced and study of radiation shield vibration was reported by a KAGRA member. Also the issues of vertical filters in crytogenic environment need to be sorted out for both KAGRA and ET. Thermal noise relating to bulk material and optical coating was handled by plural presentations. Practically study of bonding sapphire fibers on the main mirror was the most interested subject by KAGRA suspension group. All presentations this year were satisfactory from the point of view of research development and let listeners recognize steady advancement of the collaborative work between Europe and Japan.

**Participants:** 46 people 6 countires on 4th, December 80 people 7 countries on 5th, December

## CTA LST General Meeting

Date: January 14 2014 - Jaunuary 17 2014
Place: Kashiwa Library, the University of Tokyo, Japan

**Outline:** The CTA LST General meeting was held to discuss the science with the CTA large-sized telescopes and to finalize the design of the CTA large-sized telescope, time schedule and to define the responsibilities, validation and verification procedures for individual telescope elements.

**Participants:** 83 participants.

# B. ICRR Seminars

1. April 4, 2013: Sadakazu Haino (National Central University), "Status of AMS-02"
2. June 25, 2013: Shigeki Aoki (Kobe University), "GRAINE project: Cosmic Gamma-ray Observation with Balloon-Borne Emulsion Telescope"
3. July 5, 2013: Anne Verhamme (The Observatory of Geneva, Switzerland), "Lyman-alpha radiation transfer effects in galaxies"
4. July 19, 2013: Shoei Nakayama (ICRR, the University of Tokyo), "The latest results from T2K"
5. July 24, 2013: Martin A. Lee (University of New Hampshire), "What is new in the outer heliosphere: Voyager and IBEX?"
6. September 25, 2013: Rutger Van Haasteren (Jet Propulsion Laboratory), "Detecting gravitational-waves by observing pulsars, nature's most accurate natural clocks"
7. October 23, 2013: Eduardo de la Fuente Acosta (Departamento de Fisica, CUCEI, Universidad de Guadalajara), "The "High Altitude Water Cerenkov (HAWC)" Gamma Ray Observatory"
8. November 28, 2013: Kenneth Long (Imperial College London), "Neutrinos from stored muon beams"
9. February 18, 2014: Razmik Mirzoyan (Max-Planck-Institute for Physics, Munich, Germany), "Strong Boost of PMT and SiPM Parameters for Astro-Particle Physics Experiments"
10. March 11, 2014: Yoshinari Hayato (ICRR, the University of Tokyo), "The latest results from the T2K experiment"

# C. List of Publications

## (a) Papers Published in Journals


1. "Calibration of the Super-Kamiokande Detector", The Super-Kamiokande Collaboration, Nucl. Instr. & Meth, A **737**C (2014) [arXiv:1307.0162].
2. "First Indication of Terrestrial Matter Effects on Solar Neutrino Oscillation", The Super-Kamiokande Collaboration, Phys. Rev. Lett. **112**, 091805(2014)[arXiv:1312.5176].
3. "Evidence for the Appearance of Atmospheric Tau Neutrinos in Super-Kamiokande", The Super-Kamiokande Collaboration, Phys. Rev. Lett. **110**, 181802 (2013).
4. "Future long-baseline neutrino facilities and detectors", M. Diwan, R. Edgecock, T. Hasegawa, T. Patzak, M. Shiozawa, and J. Strait, Advances in High Energy Physics Volume 2013 (2013), Article ID 460123.
5. "Search for inelastic WIMP nucleus scattering on 129Xe in data from the XMASS-I experiment, status and results", U. Uchida et al. (XMASS collaboration), Prog. Theor. Exp. Phys. 2014, **063**C01.

6. “Baryon Number Violation”, Baryon Number Violation Group. Report of the Community Summer Study (Snowmass 2013), Intensity Frontier.

7. “Progress and open questions in the physics of neutrino cross sections”, L. Alvarez-Ruso, Y. Hayato, Invited review article for New Journal of Physics.

8. “Monte-Carlo neutrino event generators”, H. Gallagher, Y. Hayato, Invited review article for Review of Particle Physics ( 2014 ).

9. “The Development of a Hybrid Photo-Detector (HPD) for the Hyper-Kamiokande Project”, Seiko Hirota et al., Nucl. Instrum. Meth. A **732** (2013) 303.

10. “XMASS detector”, The xmass Collaboration, Nucl. Instr. and Meth. in Phys.Res.A**716** (2013) 78-85.

11. “Search for solar axions in XMASS, a large liquid-xenon detector”, The xmass Collaboration, Phys.Lett. B**724** (2013) 46-50.

12. “Observation of Electron Neutrino Appearance in a Muon Neutrino Beam”, The T2K Collaboration, Phys. Rev. Lett. **112**, 061802 (2014).

13. “Measurement of Neutrino Oscillation Parameters from Muon Neutrino Disappearance with an Off-axis Beam”, The T2K Collaboration, Phys. Rev. Lett. **111**, 211803 (2013).

14. “Measurement of the Inclusive NuMu Charged Current Cross Section on Carbon in the Near Detector of the T2K Experiment”, The T2K Collaboration, Phys. Rev. D **87**, 092003 (2013).

15. “Evidence of Electron Neutrino Appearance in a Muon Neutrino Beam”, The T2K Collaboration, Phys. Rev. D **88**, 032002 (2013).

16. “Search for Very-High-Energy Gamma Rays from the z = 0.896 Quasar 4C +55.17 with the MAGIC telescopes”, MAGIC collaboration, Aleksić et al. MNRAS **440** (2014) 530.

17. “Optimized dark matter searches in deep observations of Segue 1 with MAGIC MAGIC collaboration”, Aleksić et al. JCAP **02** (2014) .

18. “Discovery of very high energy gamma-ray emission from the blazar 1ES 1727+502 with the MAGIC Telescopes MAGIC collaboration”, Aleksić et al. A&A **563** (2014).

19. “MAGIC upper limits on the GRB 090102 afterglow MAGIC collaboration”, Aleksić et al. MNRAS **437** (2014) 3103-3111.

20. “Multifrequency Studies of the Peculiar Quasar 4C+21.35 during the 2010 Flaring Activity MAGIC collaboration”, Ackermann et al. ApJ **786** (2014) 157.

21. “Discovery of GeV Emission from the Circinus Galaxy with the Fermi Large Area Telescope”, M.Hayashida et al., ApJ **779** (2013) id131 (7pp).

22. “Introducing the CTA concept”, CTA Consortium, Astropart. Phys. **43** (2013) 3.

23. “Gamma-ray burst science in the era of the Cherenkov Telescope Array”, CTA Consortium, Astropart. Phys. **43** (2013) 252.

24. “Observations of the magnetars 4U 0142+61 and 1E 2259+586 with the MAGIC telescopes MAGIC collaboration”, Aleksić et al. A&A **549** (2013) A23.

25. “The simultaneous low state spectral energy distribution of 1ES 2344+514 from radio to very high energies MAGIC collaboration”, Aleksić et al. A&A **556** (2013) A67.

26. “Very high energy gamma-ray observation of the peculiar transient event Swift J1644+57 with the MAGIC telescopes and AGILE MAGIC collaboration”, Aleksić et al. A&A **552** (2013) A11.

27. “Upper limit on the flux of photons with energies above $10^{19}$ eV using the Telescope Array surface detector”, T. Abu-Zayyada et al., Phys. Rev.D **88**,112005 (2013).

28. “CORRELATIONS OF THE ARRIVAL DIRECTIONS OF ULTRA-HIGH ENERGY COSMIC RAYS WITH EXTRA-GALACTIC OBJECTS AS OBSERVED BY THE TELESCOPE ARRAY EXPERIMENT”, T. Abu-Zayyada et al., Astrophys. J. 777, **88**(8pp), 2013.

29. “The energy spectrum of ultra-high-energy cosmic rays measured by the Telescope Array FADC fluorescence detectors in monocular mode”, T. Abu-Zayyada et al., Astropart. Phys. **48**(2013)16-24.

30. “THE COSMIC-RAY ENERGY SPECTRUM OBSERVED WITH THE SURFACE DETECTOR OF THE TELESCOPE ARRAY EXPERIMENT”, T. Abu-Zayyada et al., Astrophys. J. Lett., **768**:L1 (5pp), 2013.

31. “Probe of the Solar Magnetic Field Using the vCosmic-Ray Shadowy” of the Sun”, M.Amenomori et al., Physical Review Letters, **111**, 2013, 011101-1-5, [arXiv:1306.3009v2 [astro-ph.SR]].

32. “Wide-Band Spectra of Prompt Emission”, K. Asano, EAS Publications Series, Vol **61**, 115-122 (2013).

33. “Photon and Neutrino Spectra of Time-Dependent Photospheric Models of Gamma-Ray Bursts”, K. Asano & P. Meszaros, JCAP09(2013)008 [arXiv:1308.3563[astro-ph.HE]].

34. “Search for a correlation between giant radio pulses and hard X-ray emissions in the Crab pulsar”, Ryo Mikami, Toshio Terasawa, Shota Kisaka, Hideaki Miyamoto, Katsuaki Asano, Nobuyuki Kawai, Yosuke Yamakoshi, Kumiko Nagata, Ryuho Kataoka, Kazuhiro Takefuji, Mamoru Sekido, Hiroshi Takeuchi, Hirokazu Odaka, Tamotsu Sato, Yasuyuki T. Tanaka, JPS Conf. Proc. , 015106 (2014) [arXiv:1309.165[astro-ph.HE]].

35. “Constraint on Pulsar Wind Properties from Induced Compton Scattering off Radio Pulses”, Shuta J. Tanaka, Fumio Takahara, PTEP 2013 12, 123E01 [arXiv:1311.5337].

36. “Fermi-LAT Observations of the Gamma-Ray Burst GRB 130427A”, M. Ackermann, M. Ajello, K. Asano et al., Science Vol. 343 no. 6166 pp. 42-47 (2014).

37. “Neutrino and Cosmic-Ray Release from Gamma-Ray Bursts: Time-Dependent Simulations”, Katsuaki Asano, Peter Meszaros, ApJ **785** 54 (2014) [arXiv:1402.6057[astro-ph.HE]].

38. “The Evolution of High Temperature Plasma in Magnetar Magnetospheres and its Implications for Giant Flares”, Makoto Takamoto, Shota Kisaka, Takeru Suzuki, Toshio Terasawa, ApJ **787** 84 (2014) [arXiv:1404.2766[astro-ph.HE]].

39. “The First Fermi LAT Gamma-Ray Burst Catalog”, M. Ackermann, M. Ajello, K. Asano et al., ApJS **209**, 11(90pp) [arXiv:1303.2908[astro-ph.HE]].

40. “Spatially Resolved Spectroscopy of a Pulsar Wind Nebula in MSH 15-56”, Yoichi Yatsu, Katsuaki Asano, Nobuyuki Kawai, Yuki Yano, and Takeshi Nakamori, ApJ, **773**, 25(14 pp.), 2013.

41. “TARA:Forward-scattered radar detection of UHECR at the telescope array”, J. Belz, M. Abu Bakr Othman, C. Allen, E. Barcikowski,D. Besson B. Farhang-Boroujeny, D. Ikeda, W. Hanlon, S. Kunwar, J.P. Lundquist, I. Kravchenko, S. Larson, I.Myers, T. Nakamura, J.S. Rankin, H. Sagawa, P. Sokolsky, H. Takai, T. Terasawa and G.B. Thomson, the TARA Collaboratio, EPJ Web of Conferences **53** 08012 (2013).

42. “Sapphire mirror for the KAGRA gravitational wave detector”, Eiichi Hirose, Dan Bajuk, GariLynn Billingsley, Takaaki Kajita, Bob Kestner, Norikatsu Mio, Masatake Ohashi, Bill Reichman, Hiroaki Yamamoto, and Liyuan Zhang, Phys. Rev. D **89** (2014) 062003.

43. “Evaluation of heat extraction through sapphire fibers for the GW observatory KAGRA”, A Khalaidovski, G Hofmann, D Chen, J Komma, C Schwarz, C Tokoku, N Kimura, T Suzuki, A O Scheie, E Majorana, R Nawrodt and K Yamamoto, Class. Quantum Grav. **31** 105004, 2014.

44. “Precise measurement of laser power using an optomechanical system”, Kazuhiro Agatsuma, Daniel Friedrich, Stefan Ballmer, Giulia DeSalvo, Shihori Sakata, Erina Nishida, and Seiji Kawamura, Optics Express, **22** (2014) 2013-2030.

45. “Interferometer design of the KAGRA gravitational wave detector”, Yoichi Aso, Yuta Michimura, Kentaro Somiya, Masaki Ando, Osamu Miyakawa, Takanori Sekiguchi, Daisuke Tatsumi, and Hiroaki Yamamoto (The KAGRA Collaboration), Phys. Rev.D, **88**, 43007(2013).

46. “Cryogenics System for the Interferometric Cryogenics Gravitationak Wave Telescope, KAGRA -Design, Fabrication, and Performance Test -,” C. Tokoku, N. Kimura, S. Koike, T. Kume, Y. Sakakibara, T. Suzuki, K. Yamamoto, S. Miyoki, D. Chen, S. Goto, M. Tanaka, S. Ioka, K. Nakamoto, H. Nezuka, T. Uchiyama, M. Ohashi, and K. Kuroda, Adv. Cryog. Eng. **59**B (2014), pp.1254-1261.

47. “A Study of Cooling Time Reduction of Interferometric Cryogenic Gravitational Wave Detectors Using a High-Emissivity Coating”, Y. Sakakibara, N. Kimura, T. Suzuki, K. Yamamoto, D. Chen, S. Koike, C. Tokoku, T. Uchiyama, M. Ohashi and K. Kuroda, Adv. Cryog. Eng., AIP Publishing, AIP Conf. Proc. **1573** pp.1176-1183 (2014).

48. "Calibrating [O II] star formation rates at $z < 1$ from dual H$\alpha$-[O II] imaging from HiZELS", Hayashi, M., et al., Monthly Notices Roy. Astron. Soc., **430**, 1042-1050, 2013, [arXiv:1212.4905 [astro-ph.CO]].

49. "New Constraints on Cosmic Reionization from the 2012 Hubble Ultra Deep Field Campaign", Robertson, B., et al., Astrophys. J., **768**, 71, 2013, [arXiv:1301.1228 [astro-ph.CO]].

50. "The UV Luminosity Function of Star-forming Galaxies via Dropout Selection at Redshifts $z \sim 7$ and 8 from the 2012 Ultra Deep Field Campaign", Schenker, M. A., et al., Astrophys. J., **768**, 196, 2013, [arXiv:1212.4819 [astro-ph.CO]].

51. "First Spectroscopic Evidence for High Ionization State and Low Oxygen Abundance in Ly$\alpha$ Emitters", Nakajima, K., Ouchi, M., et al., Astrophys. J., **769**, 3, 2013, [arXiv:1208.3260 [astro-ph.CO]].

52. "SEDS: The Spitzer Extended Deep Survey. Survey Design, Photometry, and Deep IRAC Source Counts", Ashby, M. L. N., et al., Astrophys. J., **769**, 80, 2013.

53. "A new multifield determination of the galaxy luminosity function at $z = 7-9$ incorporating the 2012 Hubble Ultra-Deep Field imaging", McLure, R. J., et al., Monthly Notices Roy. Astron. Soc., **432**, 2696-2716, 2013, [arXiv:1212.5222 [astro-ph.CO]].

54. "The UV continua and inferred stellar populations of galaxies at $z \simeq 7-9$ revealed by the Hubble Ultra-Deep Field 2012 campaign", Dunlop, J. S., et al., Monthly Notices Roy. Astron. Soc., **432**, 3520-3533, 2013, [arXiv:1212.0860 [astro-ph.CO]].

55. "Evolution of star formation in the UKIDSS Ultra Deep Survey field - I. Luminosity functions and cosmic star formation rate out to $z = 1.6$", Drake, A. B., et al., Monthly Notices Roy. Astron. Soc., **433**, 796-811, 2013, [arXiv:1305.1305 [astro-ph.CO]].

56. "Star Formation on Subkiloparsec Scale Triggered by Non-linear Processes in Nearby Spiral Galaxies", Momose, R., et al., Astrophys. J. (Letters), **772**, L13, 2013, [arXiv:1306.5531 [astro-ph.CO]].

57. "Physical Properties of Spectroscopically Confirmed Galaxies at $z \geq 6$. I. Basic Characteristics of the Rest-frame UV Continuum and Ly$\alpha$ Emission", Jiang, L., et al., Astrophys. J., **772**, 99, 2013, [arXiv:1303.0024 [astro-ph.CO]].

58. "Resolved Giant Molecular Clouds in Nearby Spiral Galaxies: Insights from the CANON CO (1–0) Survey", Donovan Meyer, J., et al., Astrophys. J., **772**, 107, 2013, [arXiv:1305.5275 [astro-ph.GA]].

59. "Physical Properties of Spectroscopically Confirmed Galaxies at $z \geq 6$. II. Morphology of the Rest-frame UV Continuum and Ly$\alpha$ Emission", Jiang, L., et al., Astrophys. J., **773**, 153, 2013, [arXiv:1303.0027 [astro-ph.CO]].

60. "The Galaxy Environment of a QSO at $z \sim 5.7$", Bañados, E., et al., Astrophys. J., **773**, 178, 2013, [arXiv:1306.6642 [astro-ph.CO]].

61. "On the evolution and environmental dependence of the star formation rate versus stellar mass relation since $z \sim 2$", Koyama, Y., et al., Monthly Notices Roy. Astron. Soc., **434**, 423-436, 2013, [arXiv:1302.5315 [astro-ph.CO]].

62. "Evolution of the Sizes of Galaxies over $7 < z < 12$ Revealed by the 2012 Hubble Ultra Deep Field Campaign", Ono, Y., Ouchi, M., et al., Astrophys. J., **777**, 155, 2013, [arXiv:1212.3869 [astro-ph.CO]].

63. "The 2012 Hubble Ultra Deep Field (UDF12): Observational Overview", Koekemoer, A. M., et al., Astrophys. J. Suppl., **209**, 3, 2013, [arXiv:1212.1448 [astro-ph.CO]].

64. "An Intensely Star-forming Galaxy at $z \sim 7$ with Low Dust and Metal Content Revealed by Deep ALMA and HST Observations", Ouchi, M., et al., Astrophys. J., **778**, 102, 2013, [arXiv:1306.3572 [astro-ph.CO]].

65. "The Nature of H$\alpha$-selected Galaxies at $z > 2$. I. Main-sequence and Dusty Star-forming Galaxies", Tadaki, K., et al., Astrophys. J., **778**, 114, 2013, [arXiv:1311.4259 [astro-ph.CO]].

66. "First Systematic Search for Oxygen-line Blobs at High Redshift: Uncovering AGN Feedback and Star Formation Quenching", Yuma, S., Ouchi, M., et al., Astrophys. J., **779**, 53, 2013, [arXiv:1306.5246 [astro-ph.CO]].

67. "A fundamental metallicity relation for galaxies at $z = 0.84-1.47$ from HiZELS", Stott, J. P., et al., Monthly Notices Roy. Astron. Soc., **436**, 1130-1141, 2013, [arXiv:1309.0506 [astro-ph.CO]].

68. "The Nature of H$\alpha$-selected Galaxies at $z > 2$. II. Clumpy Galaxies and Compact Star-forming Galaxies", Tadaki, K., et al., Astrophys. J., **780**, 77, 2014, [arXiv:1311.4260 [astro-ph.CO]].

69. ""Direct" Gas-phase Metallicities, Stellar Properties, and Local Environments of Emission-line Galaxies at Redshifts below 0.90", Ly, C., et al., Astrophys. J., **780**, 122, 2014, [arXiv:1307.7712 [astro-ph.CO]].

70. "Extragalactic science, cosmology, and Galactic archaeology with the Subaru Prime Focus Spectrograph", Takada, M., et al., Publ. Astron. Soc. Japan, **66**, 1, 2014, [arXiv:1206.0737 [astro-ph.CO]].

71. "The mass-metallicity relation at $z \sim 1.4$ revealed with Subaru/FMOS", Yabe, K., et al., Monthly Notices Roy. Astron. Soc., **437**, 3647-3663, 2014, [arXiv:1311.2624 [astro-ph.CO]].

72. "Mapping the large-scale structure around a $z = 1.46$ galaxy cluster in 3D using two adjacent narrow-band filters", Hayashi, M., et al., to be published in Monthly Notices Roy. Astron. Soc., 2014, [arXiv:1401.3919 [astro-ph.CO]].

73. "What is the Physical Origin of Strong Ly$\alpha$ Emission? I. Demographics of Ly$\alpha$ Emitter Structures", Shibuya, T., Ouchi, M., et al., to be published in Astrophys. J., 2014, [arXiv:1401.1209 [astro-ph.CO]].

74. "Dark Matter Production in Late Time Reheating", K. Harigaya, M. Kawasaki, K. Mukaida and M. Yamada, Phys. Rev. D **89**, 083532 (2014) [arXiv:1402.2846 [hep-ph]].

75. "Critical constraint on inflationary magnetogenesis", T. Fujita and S. Yokoyama, JCAP **1403**, 013 (2014) [Erratum-ibid. **1405**, E02 (2014)] [arXiv:1402.0596 [astro-ph.CO]].

76. "Baryon Asymmetry, Dark Matter, and Density Perturbation from PBH", T. Fujita, M. Kawasaki, K. Harigaya and R. Matsuda, Phys. Rev. D **89**, 103501 (2014) [arXiv:1401.1909 [astro-ph.CO]].

77. "Flat Higgs Potential from Planck Scale Supersymmetry Breaking", M. Ibe, S. Matsumoto and T. T. Yanagida, Phys. Lett. B **732**, 214 (2014) [arXiv:1312.7108 [hep-ph]].

78. "One-loop anomaly mediated scalar masses and $(g-2)_m u$ in pure gravity mediation", J. L. Evans, M. Ibe, K. A. Olive and T. T. Yanagida, Eur. Phys. J. C **74**, 2775 (2014) [arXiv:1312.1984 [hep-ph]].

79. "Lower Bound on the Garvitino Mass $m_{3/2} > O(100)$ TeV in $R$-Symmetry Breaking New Inflation", K. Harigaya, M. Ibe and T. T. Yanagida, Phys. Rev. D **89**, 055014 (2014) [arXiv:1311.1898 [hep-ph]].

80. "Decay rates of Gaussian-type I-balls and Bose-enhancement effects in 3+1 dimensions", M. Kawasaki and M. Yamada, JCAP **1402**, 001 (2014) [arXiv:1311.0985 [hep-ph]].

81. "Hypercharged Dark Matter and Direct Detection as a Probe of Reheatingff, B. Feldstein, M. Ibe and T. T. Yanagida, Phys.ReV.Lett. **112**, 101301 (2013) [ arXiv:1310.7495 [hep-ph]] .

82. "Halo/Galaxy Bispectrum with Primordial non-Gaussianity from integrated Perturbation Theory (iPT)", S. Yokoyama, T. Matsubara and A. Taruya, Phys. Rev. D **89**, 043524 (2014) [arXiv:1310.4925 [astro-ph.CO]].

83. "Axions as Hot and Cold Dark Matter", K. S. Jeong, M. Kawasaki and F. Takahashi, JCAP **1402**, 046 (2014) [arXiv:1310.1774 [hep-ph]].

84. "A Closer Look at Gaugino Masses in Pure Gravity Mediation Model/Minimal Split SUSY Model", K. Harigaya, M. Ibe and T. T. Yanagida, JHEP **1312**, 016 (2013) [arXiv:1310.0643 [hep-ph]].

85. "On the estimation of gravitational wave spectrum from cosmic domain walls", T. Hiramatsu, M. Kawasaki and K. 'i. Saikawa, JCAP **1402**, 031 (2014) [arXiv:1309.5001 [astro-ph.CO]].

86. "A new algorithm for calculating the curvature perturbations in stochastic inflation", T. Fujita, M. Kawasaki, Y. Tada and T. Takesako, JCAP **1312**, 036 (2013) [arXiv:1308.4754 [astro-ph.CO]].

87. "Peccei-Quinn symmetry from a gauged discrete R symmetry", K. Harigaya, M. Ibe, K. Schmitz and T. T. Yanagida, Phys. Rev. D **88**, 075022 (2013) [arXiv:1308.1227 [hep-ph]].

88. "Large Scale Cosmic Perturbation from Evaporation of Primordial Black Holes", T. Fujita, K. Harigaya and M. Kawasaki, Phys. Rev. D **88**, 123519 (2013) [arXiv:1306.6437 [astro-ph.CO]].

89. "Higher order statistics of curvature perturbations in IFF model and its Planck constraints", T. Fujita and S. Yokoyama, JCAP **1309**, 009 (2013) [arXiv:1306.2992 [astro-ph.CO]].

90. "Non-Universalities in Pure Gravity Mediation", J. L. Evans, K. A. Olive, M. Ibe and T. T. Yanagida, Eur. Phys. J. C **73**, 2611 (2013) [arXiv:1305.7461 [hep-ph]].

91. “Domain wall and isocurvature perturbation problems in axion models”, M. Kawasaki, T. T. Yanagida and K. Yoshino, JCAP **1311**, 030 (2013) [arXiv:1305.5338 [hep-ph]].

92. “Gravitational waves from a curvaton model with blue spectrum”, M. Kawasaki, N. Kitajima and S. Yokoyama, JCAP **1308**, 042 (2013) [arXiv:1305.4464 [astro-ph.CO]].

93. “AMS-02 Positrons from Decaying Wino in the Pure Gravity Mediation Model”, M. Ibe, S. Matsumoto, S. Shirai and T. T. Yanagida, JHEP **1307**, 063 (2013) [arXiv:1305.0084 [hep-ph]].

94. “Recent Result of the AMS-02 Experiment and Decaying Gravitino Dark Matter in Gauge Mediation”, M. Ibe, S. Iwamoto, S. Matsumoto, T. Moroi and N. Yokozaki, JHEP **1308**, 029 (2013) [arXiv:1304.1483 [hep-ph]].

95. “Muon g-2 and 125 GeV Higgs in Split-Family Supersymmetry”, M. Ibe, T. T. Yanagida and N. Yokozaki, JHEP **1308**, 067 (2013) [arXiv:1303.6995 [hep-ph]].

96. “Implications of Planck results for models with local type non-Gaussianity”, T. Suyama, T. Takahashi, M. Yamaguchi and S. Yokoyama, JCAP **1306**, 012 (2013) [arXiv:1303.5374 [astro-ph.CO]].

97. “Focus point gauge mediation in product group unification”, F. Brümmer, M. Ibe and T. T. Yanagida, Phys. Lett. B **726**, 364 (2013) [arXiv:1303.1622 [hep-ph]].

98. “Statistics of general functions of a Gaussian field-application to non-Gaussianity from preheating”, T. Suyama and S. Yokoyama, JCAP **1306**, 018 (2013) [arXiv:1303.1254 [astro-ph.CO]].

99. “Universality in Pure Gravity Mediation”, J. L. Evans, M. Ibe, K. A. Olive and T. T. Yanagida, Eur. Phys. J. C **73**, 2468 (2013) [arXiv:1302.5346 [hep-ph]].

100. “Heavy gravitino in hybrid inflation”, M. Kawasaki, N. Kitajima, K. Nakayama and T. T. Yanagida, JCAP **1306**, 037 (2013) [arXiv:1301.6281, arXiv:1301.6281 [hep-ph]].

101. “A Simple Solution to the Polonyi Problem in Gravity Mediation”, K. Harigaya, M. Ibe, K. Schmitz and T. T. Yanagida, Phys. Lett. B **721**, 86 (2013) [arXiv:1301.3685 [hep-ph]].

102. “Natural supersymmetryfs last hope: R-parity violation via UDD operators”, B. Bhattacherjee, J. L. Evans, M. Ibe, S. Matsumoto and T. T. Yanagida, Phys. Rev. D **87**, 115002 (2013) [arXiv:1301.2336 [hep-ph]].

103. “Axions: Theory and Cosmological Role”, M. Kawasaki and K. Nakayama, Ann. Rev. Nucl. Part. Sci. **63**, 69 (2013) [arXiv:1301.1123 [hep-ph]].

104. “Revisiting the Cosmological Coherent Oscillation”, M. Kawasaki, N. Kitajima and K. Nakayama, Phys. Rev. D **87**, 023513 (2013) [arXiv:1112.2818 [hep-ph]].

## (b) Conference Papers

1. “Future of Super-Kamiokande and Hyper-Kamiokande”, M. Nakahata, Proceedings of the 13th International Conference on Topics in Astroparticle and Underground Physics(TAUP2013), Asilomar, California USA, September 8-13, 2013.

2. “XMASS experiment”, K. Abe, Proceedings of Dark Matter 2014, February, 2014.

3. “Status of the XMASS experiment”, S. Moriyama, Proceedings of TAUP2013, September, 2013.

4. “Design of low-energy calibration sources for liquid xenon dark matter detectors”, K. Hosokawa, Proceedings of TAUP2013, September, 2013.

5. “Low background techniques from XMASS”, H. Ogawa, Proceedings of LRT2013, April, 2013.

6. “Neutrino Physics (rapporteur talk)”, M. Nakahata, Proceedings of the 33rd International Cosmic Ray Conference (ICRC2013), to be published, Rio de Janeiro, Brazil, July 2-9, 2013.

7. “Solar neutrino analysis of Super-Kamiokande”, H. Sekiya, Proceeding of 33rd International Cosmic Ray Conference (ICRC 2013), Jul, 2013.

8. “Recent results from XMASS”, K. Hiraide, Proceedings of 48th Rencontres de Moriond on Very High Energy Phenomena in the Universe.

9. “The Hyper-Kamiokande project”, M. Shiozawa, Proceeding of Neutrino Oscillation Workshop (NOW 2012), September, 2012, published in Nuclear Physics B Proceedings Supplement.

10. “Super-Kamiokande Atmospheric Neutrino Oscillation Analysis”, R. Wendell, Proceeding of Neutrino Oscillation Workshop (NOW 2012), September, 2012, published in Nuclear Physics B Proceedings Supplement.

11. “Super-Kamiokande Low Energy Results”, H. Sekiya, Proceeding of Neutrino Oscillation Workshop (NOW 2012), September, 2012, published in Nuclear Physics B Proceedings Supplement.

12. “Atmospheric neutrino oscillation and mass hierarchy determination in Super-Kamiokande”, K. Okumura, Proceedings of TAUP2013, September, 2013.

13. “Detection of the Atmospheric Showers with Telescope Array (TA) Experiment”, H. Sagawa for the TA collaboration, Proceedings of the Conference on Calorimetry for the High Energy Frontier (CHEF2013), April 22-25, 2013, Paris.

14. “Highlights from the Telescope Array Experiment”, H. Sagawa for the TA collaboration, Proceedings of the 33rd International Cosmic Ray Conference (ICRC2013), July 2-9, 2013, Rio de Janeiro.

15. “The Plan of the Telescope Array Experiment for the Next Five Years”, H. Sagawa for the TA collaboration, Proceedings of ICRC2013, Rio de Janeiro.

16. “SD energy spectrum of TA and its fitting with the energy loss model of UHECR protons”, E. Kido for the TA collaboration, Proceedings of the ICRC2013, Rio de Janeiro.

17. “Search for Ultra-High Energy Photons and Neutrinos using the Telescope Array Scintillator Array Data”, G. I. Rubtsov for the TA collaboration, Proceedings of the ICRC2013, Rio de Janeiro.

18. “Telescope Array Measurements of the UHECR Energy Spectrum”, D. Bergman for the TA collaboration, Proceedings of the ICRC2013, Rio de Janeiro.

19. “Study on Mass Composition of Ultra-High Energy Cosmic Rays by Telescope Array”, Y. Tsunesada for the TA collaboration, Proceedings of the ICRC2013, Rio de Janeiro.

20. “TA anisotropy summary”, P. Tinyakov for the TA collaboration, Proceedings of the ICRC2013, Rio de Janeiro.

21. “Composition Analysis of a Multispecies UHECR Spectrum Compatible with Auger Data via Telescope Array Hybrid Reconstruction”, W. F. Hanlon for the TA collaboration, Proceedings of the ICRC2013, Rio de Janeiro.

22. “Measuring Large-Scale Anisotropy in the Arrival Directions of Cosmic Rays Detected at the Telescope Array and the Pierre Auger Observatory above $10^{19}$ eV”, O. Deligny for the Telescope Array and Pierre Auger Collaborations, Proceedings of the ICRC2013, Rio de Janeiro.

23. “Absolute energy calibration of the Telescope Array Fluorescence detector with an Electron Linear Accelerator”, T. Shibata for the TA collaboration, Proceedings of the ICRC2013, Rio de Janeiro.

24. “The Telescope Array Low Energy Extension”, S. Ogio for the TA collaboration, Proceedings of the ICRC2013, Rio de Janeiro.

25. “The mass composition of ultra-high energy cosmic rays measured by new fluorescence detectors in the Telescope Array experiment”, T. Fujii for the TA collaboration, the 13th International Conference on Topics in Astroparticle and Underground Physics (TAUP2013), Sept. 8-13, 2013, Asilomar.

26. “Recent results from Telescope Array”, T. Okuda for the TA collaboration, Symposium on Cosmology and Particle Astrophysics (CosPA2013), Nov. 12-15, 2013, Honolulu.

27. ““Cosmic-ray shadow” of the Sun at 3 TeV observed by the Tibet Air Shower Array”, M. Amenomori et al., Proceedings of The 33rd International Cosmic Ray Conference, Rio de Janeiro, Brazil, July 2 - July 9, 2013, ID=0340.

28. “A Northern Sky Survey for TeV gamma-ray steady point sources using the Tibet-III air shower array”, M. Amenomori et al., Proceedings of The 33rd International Cosmic Ray Conference, Rio de Janeiro, Brazil, July 2 - July 9, 2013, ID=0498.

29. “Average mass of primary cosmic rays in the knee energy region inferred from Tibet experiment”, M. Amenomori et al., Proceedings of The 33rd International Cosmic Ray Conference, Rio de Janeiro, Brazil, July 2 - July 9, 2013, ID=0525.

30. “Observation of Multi-TeV Gamma Rays from MGRO J2019+37 and MGRO J2031+41 with the Tibet Air Shower Array”, M. Amenomori et al., Proceedings of The 33rd International Cosmic Ray Conference, Rio de Janeiro, Brazil, July 2 - July 9, 2013, ID=0513.

31. “Observation of thundercloud-related charged particles in Tibet”, M. Amenomori et al., Proceedings of The 33rd International Cosmic Ray Conference, Rio de Janeiro, Brazil, July 2 - July 9, 2013, ID=0505.

32. “The TIBET AS+MD Project; progress report 2013”, M. Amenomori et al., Proceedings of The 33rd International Cosmic Ray Conference, Rio de Janeiro, Brazil, July 2 - July 9, 2013, ID=0508.

33. “A Monte Carlo study to measure heavy-component spectra of the primary cosmic-rays at the knee by a new hybrid experiment (YAC-II+Tibet-III+MD)”, L.M. Zhai et al., Proceedings of The 33rd International Cosmic Ray Conference, Rio de Janeiro, Brazil, July 2 - July 9, 2013, ID=1049.

34. “Hadronic interaction and EAS muon investigated with the (YAC + Tibet-III + MD) hybrid experiment”, M. Amenomori et al., Proceedings of The 33rd International Cosmic Ray Conference, Rio de Janeiro, Brazil, July 2 - July 9, 2013, ID=1051.

35. “Observation of the large-scale sidereal anisotropy of the galactic cosmic ray at 300 TeV with the Tibet Air shower Array”, M. Amenomori et al., Proceedings of The 33rd International Cosmic Ray Conference, Rio de Janeiro, Brazil, July 2 - July 9, 2013, ID=0256.

36. “Primary proton and helium spectra at energy range from 50 TeV to $10^{15}$ eV observed with (YAC+Tibet-III ) hybrid experiment”, M. Amenomori et al., Proceedings of The 33rd International Cosmic Ray Conference, Rio de Janeiro, Brazil, July 2 - July 9, 2013, ID=1047.

37. “Progress Report on the MD-A under TIBET III array”, M. Amenomori et al., Proceedings of The 33rd International Cosmic Ray Conference, Rio de Janeiro, Brazil, July 2 - July 9, 2013, ID=1018.

38. “Study on the primary mass sensitivity of muon multiplicity measured with (YAC-II +Tibet-III + MD) experiment”, J.S. Liu et al., Proceedings of The 33rd International Cosmic Ray Conference, Rio de Janeiro, Brazil, July 2 - July 9, 2013, ID=1057.

39. “Test of the hadronic interaction model EPOS-LHC and QGSJETII-04 with Tibet EAS core data”, M. Amenomori et al., Proceedings of The 33rd International Cosmic Ray Conference, Rio de Janeiro, Brazil, July 2 - July 9, 2013, ID=1056.

40. “Progress report on the TIBET AS+MD Project”, M. Amenomori et al., Proceedings of the 12th Asia Pacific Physics Conference, Makuhari Messe, Chiba, Japan, July 14 - July 19, 2013, JPS Conf. Proc. 1, 2014, 013124-1-4.

41. “Wide-Band Spectra of Prompt Emission”, K. Asano, Proceedings of Gamma-ray Bursts: 15 Years of GRB Afterglows.

42. “Broadband Emission Structure of Pulsar Wind Nebulae”, S. J. Tanaka, Proceedings of the 33rd International Cosmic Ray Conference 2013.

43. “High Energy Emission from Spherically Symmetric Pulsar Wind Nebulae”, S. J. Tanaka, Proceedings of SUZAKU-MAXI 2014.

44. “Synchrotron Emission from Old Pulsars”, S. J. Tanaka and S. Kisaka, Proceedings of SUZAKU-MAXI 2014.

45. “Electric field screening at the pulsar polar cap”, S. Kisaka and T. Terasawa Proceedings of SKA Science Workshop in East Asia.

46. “Axisymmetric and stationary magnetic field structures in neutron star crusts under various boundary conditions”, K. Fujisawa and S. Kisaka Proceedings of IAU Symposium 302, Magnetic fields throughout stellar evolution, 2013.

47. “Hard X-ray observations with Suzaku HXD at the time of giant radio pulses from the Crab pulsar”, R. Mikami, T. Terasawa, S. Kisaka, K. Asano, S. J. Tanaka, M. Sekido, K. Takefuji, H. Takeuchi, H. Odaka, T. Sato, Y. T. Tanaka and N. Kawai, Proceedings of SUZAKU-MAXI 2014.

48. “CALET observational performance expected by CERN beam test”, Y. Akaike for the CALET collaboration, Proceedings of the 33rd International Cosmic Ray Conference 2013.

49. “The CALET Structure and Thermal Model used for beam test at CERN”, Y. Ueyama, S. Torii, K. Kasahara, S. Ozawa, T. Niita, M. Nakamura, S. Kaneko, R. Katahira, A. Murata, T. Tamura, Y. Katayose, Y. Akaike, Y. Shimizu, Proceedings of the 33rd International Cosmic Ray Conference 2013.

50. “CALET Calibration on ISS Orbit Using Cosmic Rays”, T. Niita and the CALET collaboration, Proceedings of the 33rd International Cosmic Ray Conference 2013.

51. “The Calorimetric Electron Telescope (CALET) for High Energy Astroparticle Phsycis on the International Space Station”, S. Torii for the CALET collaboration, Proceedings of the 33rd International Cosmic Ray Conference 2013.

52. “Expected Performance of CALET as a High Energy Gamma Ray Observatory”, M. Mori for the CALET collaboration, Proceedings of the 33rd International Cosmic Ray Conference 2013.

53. “Dark Matter Search with CALET”, K. Yoshida for the CALET collaboration, Proceedings of the 33rd International Cosmic Ray Conference 2013.

54. “CALET perspectives in high-energy gamma-ray observations”, A. Moiseev for the CALET collaboration, Proceedings of the 33rd International Cosmic Ray Conference 2013.

55. “Particle Beam Tests of the Calorimetric Electron Telescope”, T. Tamura for the CALET collaboration, Proceedings of the 33rd International Cosmic Ray Conference 2013.

56. “CALET measurements with cosmic nuclei and performance of the charge detectors”, P. S. Marrocchesi for the CALET collaboration, Proceedings of the 33rd International Cosmic Ray Conference 2013.

57. “CALET Positron/Electron Measurements Using the Geomagnetic Field”, B. Rauch for the CALET collaboration, Proceedings of the 33rd International Cosmic Ray Conference 2013.

58. “CALET Measurement of Ultra-Heavy Cosmic Rays”, B. Rauch for the CALET collaborationP. S. Marrocchesi for the CALET collaboration, Proceedings of the 33rd International Cosmic Ray Conference 2013.

59. “The CALorimetric Electron Telescope (CALET) ground data handling and processing system”, T. Guzik for the CALET collaboration, Proceedings of the 33rd International Cosmic Ray Conference 2013.

60. “CALET Gamma-ray Burst Monitor (CGBM)”, K. Yamaoka for the CALET collaboration, Proceedings of the 33rd International Cosmic Ray Conference 2013.

61. “Search for PeV-EeV Tau Neutrinos and Optical Transients from Violent Objects with Ashra-1”, M.Sasaki, Proceedings of 14th ICATPP Conference on Astroparticle, Particle, Space Physics and Detectors for Physics Applications, 2013.

62. “Ashra NTA: Towards Survey of Astronomical Tau Neutrino Sources”, Y. Aita, T. Aoki,Y.Asaoka, H.M Motz, M. Sasaki, C. Abiko, C.Kanokohata, S.Ogawa ,H. Shibuya, T. Takada, T. Kimura, J. G. learned, S.Matsuno, S. Kuze, P. Chang, *G.W-S. Hou, Y.B. Hsiung, J-G. Shu, K. Ueno, M. Wang, P. M. Binder, J. Goldman, N. Sugiyama, Y. Watanabe, C-C. Hsu (Ashra NTA Collaboration), Proceedings of the 12th Asia Pacific Physics Conference of AAPPS ASEPS3 The third Asia-Europe Physics Summit, 2013.

63. “Trigger and readout system for the Ashra-1 detector”, Aita, T. Aoki,Y.Asaoka, Y.Moromoto, H.M Motz, M. Sasaki, C. Abiko, C. Kanokohata, *S.Ogawa, H. Shibuya, T. Takada, T. Kimura, J. G. learned, S.Matsuno, S. Kuze, P. M. Binder, J. Goldman, N. Sugiyama, Y. Watanabe (Ashra-1 Collaboration), Proceedings of the 12th Asia Pacific Physics Conference of AAPPS ASEPS3 The third Asia-Europe Physics Summit, 2013.

64. “Search for PeV-EeV Tau Neutrinos and Optical Transients from Violent Objects with Ashra-1”, Y. Aita, T. Aoki, Y.Asaoka, H.M Motz,*M. Sasaki, C. Abiko, C.Kanokohata, S.Ogawa, H. Shibuya, T. Takada, T. Kimura, J. G. learned, S.Matsuno, S. Kuze, P. M. Binder,J. Goldman, N. Sugiyama, Y. Watanabe (Ashra-1 Collaboration), Proceedings of 33th Intl. Cosmic Ray Conf. (Rio), 2013.

65. “Ashra NTA: Towards Survey of Astronomical Tau Neutrino Sources”, Y. Aita, T. Aoki, Y.Asaoka, H.M Motz, M. Sasaki, C. Abiko, C.Kanokohata,S.Ogawa, H. Shibuya, T. Takada, T. Kimura, J. G. learned, S.Matsuno, S. Kuze, P. Chang, *G.W-S. Hou, Y.B. Hsiung, J-G. Shu, K. Ueno, M. Wang, P. M. Binder, J. Goldman, N. Sugiyama, Y. Watanabe, C-C. Hsu (Ashra NTA Collaboration), Proceedings of 33th Intl. Cosmic Ray Conf. (Rio), 2013.

66. “Neutrino Telescope Array (NTA)”, G. W.-S. Hou on behalf of the NTA Collaboration, The 7th International Workshop on Very High Energy Particle Astronomy - Next Generation Explorer for Cosmic Ray Origin - (Kashiwa), 2014.

67. “Real Time Control for KAGRA 3km Cryogenic Gravitational Wave Detector”, Osamu Miyakawa and KAGRA collaboration, ICALEPCS 2013, 2013/10/5-10/11, San Francisco U.S.A, Proceedings of the 14th International Conference on Accelerator & Large Experimental Physics Control Systems, 23-26, 2013.

68. “Mahalo-Subaru: Mapping Star Formation at the Peak Epoch of Massive Galaxy Formation”, Kodama, T., Hayashi, M., et al., Proceedings of the International Astronomical Union, 295, 74-77, 2013.

69. “From Mahalo-Subaru to Gracias-ALMA: Resolving Galaxy Formation at Its Peak Epoch”, Kodama, T., Tanaka, I., Hayashi, M., et al., ASP Conference Series, 476, 37, 2013.

70. “Axino dark matter and baryon number from $Q$-ball decay”, S. Kasuya, E. Kawakami and M. Kawasaki, J. Phys. Conf. Ser. **485**, 012025 (2014).

## (c) ICRR Reports

1. ICRR-Report-652-2013-1
“AMS-02 Positrons from Decaying Wino in the Pure Gravity Mediation Model”
Masahiro Ibe, Shigeki Matsumoto, Satoshi Shirai, Tsutomu T. Yanagida.

2. ICRR-Report-653-2013-2
“Domain wall and isocurvature perturbation problems in axion models”
Masahiro Kawasaki, Tsutomu T. Yanagida, Kazuyoshi Yoshino.

3. ICRR-Report-654-2013-3
“Implications of Planck results for models with local type non-Gaussianity”
Teruaki Suyama, Tomo Takahashi, Masahide Yamaguchi, Shuichiro Yokoyama.

4. ICRR-Report-655-2013-4
“Higher order statistics of curvature perturbations in IFF model and its Planck constraints”
Tomohiro Fujita, Shuichiro Yokoyama.

5. ICRR-Report-656-2013-5
“Large Scale Cosmic Perturbation from Evaporation of Primordial Black Holes”
Tomohiro Fujita, Keisuke Harigaya, and Masahiro Kawasaki.

6. ICRR-Report-657-2013-6
“The Peccei-Quinn Symmetry from a Gauged Discrete R Symmetry”
Keisuke Harigaya, Masahiro Ibe, Kai Schmitz, Tsutomu T. Yanagida.

7. ICRR-Report-658-2013-7
“A new algorithm for calculating the curvature perturbations in stochastic inflation”
Tomohiro Fujita, Masahiro Kawasaki, Yuichiro Tada, Tomohiro Takesako.

8. ICRR-Report-659-2013-8
“On the estimation of gravitational wave spectrum from cosmic domain walls”
Takashi Hiramatsu, Masahiro Kawasaki, Ken’ichi Saikawa.

9. ICRR-Report-660-2013-9
“A Closer Look at Gaugino Masses in Pure Gravity Mediation Model/Minimal Split SUSY Model”
Keisuke Harigaya, Masahiro Ibe, Tsutomu T. Yanagida.

10. ICRR-Report-661-2013-10
“Axions as Hot and Cold Dark Matter”
Kwang Sik Jeong, Masahiro Kawasaki, Fuminobu Takahashi.

11. ICRR-Report-662-2013-11
“I-ball formation with logarithmic potential”
Masahiro Kawasaki, Naoyuki Takeda.

12. ICRR-Report-663-2013-12
“Halo/Galaxy Bispectrum with Primordial non-Gaussianity from integrated Perturbation Theory (iPT)”
Shuichiro Yokoyama, Takahiko Matsubara, Atsushi Taruya.

13. ICRR-Report-664-2013-13
“Hypercharged Dark Matter and Direct Detection as a Probe of Reheating”
Brian Feldstein, Masahiro Ibe, Tsutomu T. Yanagida.

14. ICRR-Report-665-2013-14
“Lower Bound on the Garvitino Mass $m_{3/2} > O(100)$ TeV in R-Symmetry Breaking New Inflation”
Keisuke Harigaya, Masahiro Ibe, Tsutomu T. Yanagida.

15. ICRR-Report-666-2013-15
"Mixed (Cold+Warm) Dark Matter in the Bino-Wino co-annihilation scenario"
Masahiro Ibe, Ayuki Kamada, Shigeki Matsumoto.

16. ICRR-Report-667-2013-16
"Decay rates of Gaussian-type I-balls and Bose-enhancement effects in 3+1 dimensions"
Masahiro Kawasaki, Masaki Yamada.

17. ICRR-Report-668-2013-17
"Baryon Asymmetry, Dark Matter, and Density Perturbation from PBH"
Tomohiro Fujita, Keisuke Harigaya, Masahiro Kawasaki, Ryo Matsuda.

18. ICRR-Report-669-2013-18
"Critical constraint on inflationary magnetogenesis"
Tomohiro Fujita, Shuichiro Yokoyama.

19. ICRR-Report-670-2013-19
"Probing small-scale cosmological fluctuations with the 21 cm forest: effects of neutrino mass, running spectral index and warm dark matter"
Hayato Shimabukuro, Kiyotomo Ichiki, Susumu Inoue, and Shuichiro Yokoyama.

20. ICRR-Report-671-2013-20
"Dark Matter Production in Late Time Reheating"
Keisuke Harigaya, Masahiro Kawasaki, Kyohei Mukaida, Masaki Yamada.

21. ICRR-Report-672-2013-21
"Baryogenesis from the Gauge-mediation type Q ball and the dark matter New type Q ball"
Shinta Kasuya, Masahiro Kawasaki.

22. ICRR-Report-673-2013-22
"Neutrino masses, leptogenesis, and sterile neutrino dark matter"
Takanao Tsuyuki.

23. ICRR-Report-674-2013-23
"Compensation for large tensor modes with iso-curvature perturbations in CMB anisotropies"
Masahiro Kawasaki, Shuichiro Yokoyama.

# D. Doctoral Theses

1. "Cosmological implications from supersymmetric axion models– origin of matter and its fluctuations",
E. Kawakami,
Ph.D Thesis, Mar. 2013.

2. "Primordial blackhole formation and gravitational wave production in a curvaton model",
N. Kitajima,
Ph.D Thesis, Mar. 2013.

3. "The Effective Masses of Scalar Fields in the Radiation Dominated Universe",
T. Takesako,
Ph.D Thesis, Mar. 2013.

# E. Public Relations

## (a) ICRR News

ICRR News is a quarterly publication written in Japanese about scientific and educational activities at ICRR. It includes :

1. reports on scientific activities of ICRR staff members and those conducted at one or more of its facilities,

2. reports of international conferences on topics relevant to ICRR's research activities,
3. reports on topics discussed at ICRR's Committees,
4. list of publications published by ICRR [ICRR-Report],
5. list of seminars held at ICRR,
6. announcements, and
7. other items of relevance.

Below lists the main topics in the issues published in FY 2013:

**No.85** (June 30, 2013)

- Report of ICRR Spring School 2013, Masahiro Teshima.
- TA Low energy Extention (TALE) Experiment, Shoichi Ogio & Toshiyuki Nonaka.
- Staff reassignment.
- ICRR-Seminar.
- ICRR-Report.

**No.86** (September 30, 2013)

- AMS-02 positron flux anomaly and possibilities for dark matter in supersymmetric models, Masahiro Ibe.
- Probing the coronal magnetic field via the Sun's Shadow, Kazumasa Kawata & Masato Takita.
- The current status of the T2K Experiment -search for the electron neutrino appearance-, Yoshinari Hayato.
- Staff reassignment.
- ICRR-Seminar.
- ICRR-Report.

**No.87** (December 27, 2013)

- Report of the speech and the ceremony commemorating the 60th anniversary of Norikura Observatory, Masato Takita.
- KAGRA's Y-arm tunnel is now complete, Misato Hayashida.
- Report of 2013 Kashiwa Open Campus, Misato Hayashida.
- Staff reassignment.
- ICRR-Seminar.
- ICRR-Report.

**No.88** (March 31, 2014)

- Precision measurement of neutrino oscillation parameters in T2K experiment, Yasuhiro Nishimura.
- Report of the 3rd ICRR Graduate Students Workshop, Misato Hayashida.
- Staff reassignment.
- ICRR-Seminar.
- ICRR-Report.

## (b) Public Lectures

- ”Gallery talk”, Apr. 7, 2013, Toyama Science Museum, Toyama-city, Toyama, Masaki Yamashita & Jun kameda (ICRR, the University of Tokyo).
- ”SSH The Shizuoka-kita High School”, Apr. 25, 2013, Kamioka-cho, Hida-city, Gifu, Atsushi Takeda (ICRR, the University of Tokyo).
- ”Hirameki Tokimeki Science”, Apr. 7, 2013, Kamioka-cho, Hida-city, Gifu, Atsushi Takeda & Jun kameda (ICRR, the University of Tokyo).
- ”GSA Science seminar”, July. 29, 2013, Kamioka-cho, Hida-city, Gifu, Yoichiro Suzuki (ICRR, the University of Tokyo).
- “SSH The Kyoto Prefectural Momoyama Senior High School”, July. 29, 2013, Kamioka-cho, Hida-city, Gifu, Makoto Shiozawa (ICRR, the University of Tokyo).
- “SSH The Tochigi Ashikaga High School”, July. 30, 2013, Kamioka-cho, Hida-city, Gifu, Jun Kameda (ICRR, the University of Tokyo).
- “SSH The Fujishima Senior High School”, Aug. 7, 2013, Kamioka-cho, Hida-city, Gifu, Yoichiro Suzuki (ICRR, the University of Tokyo).
- “Yumenotamago-Jyuku”, Aug. 9, 2013, Kamioka-cho, Hida-city, Gifu, Hiroyuki Sekiya (ICRR, the University of Tokyo).
- “SSH The Yamanashi Eiwa Junior & Senior High School”, Aug. 19, 2013, Kamioka-cho, Hida-city, Gifu, Jun Kameda (ICRR, the University of Tokyo).
- “Yume Challenge”, Aug. 20, 2013, Kashiwa, Chiba, Shigetaka Moriyama (ICRR, the University of Tokyo).
- “SSH The Senior High School Attached to Kyoto University of Education”, Aug. 21, 2013, Kamioka-cho, Hida-city, Gifu, Makoto Miura (ICRR, the University of Tokyo).
- “School of Engineering The University of Tokyo”, Aug. 27, 2013, Kamioka-cho, Hida-city, Gifu, Shigetaka Moriyama (ICRR, the University of Tokyo).
- “School of Engineering The University of Tokyo”, Aug. 27, 2013, Kamioka-cho, Hida-city, Gifu, Yoshinari Hayato (ICRR, the University of Tokyo).
- “SSH The kaisei Academy (The kaisei Junior and Senior High Schools)”, Aug. 28, 2013, Kamioka-cho, Hida-city, Gifu, Shigetaka Moriyama (ICRR, the University of Tokyo).
- “Science cafe”, Sep. 23, 2013, Nigata-city, Nigata, katsuki Hiraide (ICRR, the University of Tokyo).
- “SSH The Nanao High School”, Oct. 2, 2013, Kamioka-cho, Hida-city, Gifu, Ko Abe (ICRR, the University of Tokyo).
- “SSH The Senri Senior High School”, Oct. 10, 2013, Kamioka-cho, Hida-city, Gifu, Roger Wendell (ICRR, the University of Tokyo).
- “Science cafe at Astronomical Observatory of Toyama”, Oct. 19, 2013, Toyama-city, Toyama, Yoichiro Suzuki (ICRR, the University of Tokyo).
- “Lecture”, Oct. 26, 2013, Toyama Science Museum, Toyama-city, Toyama, Yoichiro Suzuki (ICRR, the University of Tokyo).
- “Science cafe”, Dec. 21, 2013, Gifu-sinbunsya, Gifu-city, Gifu, Yoichiro Suzuki (ICRR, the University of Tokyo).
- “The University of Twente, Oranda”, Feb. 25, 2014, Gifu-sinbunsya, Gifu-city, Gifu, Yasuhiro Kishimoto (ICRR, the University of Tokyo).
- “Detecting Cosmic Rays in Desert”, May 11, 2013, The University of Tokyo, Tokyo, T. Nonaka (ICRR, the University of Tokyo).
- “Mt. Katakake-Mozumi Ginzan to Kamioka mine–Towards KAGRA Project”, Forth Saturdays of Apr. through Sep., 2013, Inotani-Sekisho-Kan, Toyama, S. Miyoki, O. Miyakawa, T. Ohashi, and S. Kawamura (ICRR, the University of Tokyo).

- “KAGRA’s detection method: Michelson Interferometer”, September 8, 2013, Inotani-Sekisho-Kan, Toyama, S. Miyoki, O. Miyakawa (ICRR, the University of Tokyo).
- “Introduction to Gravitational Wave Detector KAGRA - Hands-on Michelson Interferometer -”, September 28-29, 2013, Toyama University, Toyama, O. Miyakawa (ICRR, the University of Tokyo).
- “Gravitational Waves: The melody of the universe predicted by Einstein”, November 23, 2013, Osawano Center for Lifelong Lerning, Toyama, O. Miyakawa (ICRR, the University of Tokyo).
- “Detection Physics and Technology of Gravitational Waves”, July 30-August10, 2013, Numerical Relativity & Gravitational waves School in Pohang 2013, Korea, K. Kuroda (ICRR, the University of Tokyo).
- “The new ear of the 21st century to hear the universe - Gravitational Waves”, October 26, 2013, Sawayaka Plaza, Chiba, S. Miyoki (ICRR, the University of Tokyo).
- “Physics and Gravitational Waves, Study and Research in Germany and Japan”, October 18, 2013, Inotani-Sekisho-Kan, Toyama, S. Miyoki & Alexander Khalaidovski (ICRR, the University of Tokyo).
- “Cryogenic system for the interferometric cryogenic gravitational wave telescope, KAGRA”, July 12, 2013, Wroc*l*aw University of Technology, Poland, N. Kimura (KEK).
- “Cosmic History Probed by the Deepest Observations”, April 13, 2013, Amuser Kashiwa, Chiba, M. Ouchi (ICRR, the University of Tokyo).
- “From Bangkok to the Early Universe”, July 27, 2013, Kofu Higashi High School, Yamanashi, S. Yuma (ICRR, the University of Tokyo).
- “Cosmic History Studied with the Large Telescopes”, October 25, 2013, ICRR, Chiba, M. Ouchi (ICRR, the University of Tokyo).
- “Galaxy formation and evolution revealed by resent observations”, October 25, 2013, ICRR, Chiba, M. Hayashi (ICRR, the University of Tokyo).
- “Cosmic History Studied with the Large Telescopes”, November 20, 2013, Tokyo Metropolitan Musashi High School, Tokyo, M. Ouchi (ICRR, the University of Tokyo).
- “Galaxies in the Universe”, March 15, 2013, Kavli IPMU, Chiba, R. Momose (ICRR, the University of Tokyo).
- “The Standard Model and Higgs particle”, December 1, 2013, the University of Tokyo. Tokyo, M. Ibe (ICRR, the University of Tokyo).

## (c) Visitors

KASHIWA Campus
(Total: 11 groups, 328 peoples)

- Higashi-Katsushika High School
- RKU Kashiwa High School
- Miyazaki Nishi High School
- Others: 8 groups

KAMIOKA Observatory
(Total: 159 groups, 3,024 peoples)

- Yumeno Tamago Jyuku (Hida Academy for High School Students)
- MEXT Super Science High School (SSH) project: total 14 schools
- Schools and Universities: total 13 groups
- Researchers: total 13 groups
- Others: 118 groups

# F. Inter-University Research Activities

## Numbers of Researchers

| | Number of Applications | Number of Adoptions | Number of Researchers |
|---|---|---|---|
| Facility Usage | | | |
| Kamioka Observatory | 34 | 33 | 1,030 |
| Akeno Observatory | 4 | 4 | 47 |
| Norikura Observatory | 9 | 9 | 86 |
| Low-Level Radioisotope Measurement Facility | 5 | 5 | 33 |
| Cryogenic Laser Interferometer in Kashiwa | 21 | 21 | 423 |
| Laboratorial Facility in Kashiwa | 9 | 9 | 246 |
| Computer Facility in Kashiwa | 17 | 17 | 287 |
| Conference Facility in Kashiwa | 7 | 7 | 292 |
| Over Sea Facilities | 12 | 12 | 146 |
| Annual Sums | 118 | 117 | 2,590 |

| | | | |
|---|---|---|---|
| Joint Research | | | |
| Neutrino and Astroparticle Research | 35 | 34 | 1,035 |
| High Energy Cosmic Ray Research | 49 | 49 | 952 |
| Astrophysics and Gravity Research | 23 | 23 | 470 |
| Research Center for Cosmic neutrinos | 11 | 11 | 133 |
| Annual Sums | 118 | 117 | 2,590 |

## Research Project Titles

1. Precise measurement of Day/Night effect for B8 solar neutrinos
2. Energy spectrum measurement of solar neutrinos in Super-Kamiokande
3. Study of Solar Neutrino Flux
4. Study of simulation for atmospheric neutrino
5. Study of atmospheric neutrino flux and neutrino oscillations
6. Study of three flavor oscillation in atmospheric neutrinos
7. Study of flavor identification of atmospheric and beam neutrinos
8. Study for Supernova monitor
9. Study of Supernova Relic Neutrinos
10. Study of proton decay $p \to \nu K^+$
11. Search for proton decay via $e^+\pi^0$ mode
12. Study in upward-going muons and high energy neutrinos
13. Sidereal daily variation of $\sim$10TeV galactic cosmic ray intensity observed by the Super-Kamiokande
14. Tokai to Kamioka Long Baseline Experiment T2K
15. Neutrino interaction study using accelerator data
16. Study for the electron neutrino appearance search in the T2K experiment
17. Energy calibration for Super-Kamiokande

18. Development of low concentration radon detection system
19. R&D of a Mton water Cherenkov Hyper-Kamiokande
20. Development of the Hybrid Photo Detector
21. Neutrino workshop
22. Direction-sensitive dark matter search experiment
23. Strain, tilt, seismic measurement in Kamioka-mine
24. Study for double beta decay of $^{48}Ca$
25. Studies on steady removal of noble gas impurities using laser resonance ionization
26. Integration of crustal activity observation around the Atotsugawa fault
27. Microdetermination of impurity gas in Xe
28. Development of radon detector for purified gases
29. Calibration study of liquid xenon detector
30. A study on infrared emission of liquid xenon scintillator
31. Study for upgrade of XMASS detector
32. A Search for Dark Matter using Liquid Xenon Detector
33. Study of annual modulation for dark matter search
34. Study for lowering backgrounds of radioisotopes in large volume detectors
35. R&D for a Small Atmospheric Cherenkov Telescope in Akeno Observatory
36. Reconstruction of the optical system of a small Cherenkov telescope at the Akeno Observatory
37. Multi-Color Imager for Transients, Survey and Monstrous Explosions
38. Observation of Galactic Cosmic Ray Intensities using Large Area Muon Telescopes
39. Observation of solar neutrons in solar cycle 24
40. Space weather observation using muon hodoscope at Mt. Norikura
41. Evaluation of altitude dependent doses of secondary cosmic neutrons
42. Observation of cosmogenic nuclides concentrations with temporal variability at Mt. Norikura
43. Alpine vegetation study on Mt. Norikura
44. Observations of total ozone and UV solar radiation with Brewer spectrophotometer on the Norikura mountains
45. In-Situ Conservation - Establishment of handling method of chicks for one month after hatching by cage captivity
46. Dynamics of Abies mariesii forests of forest line of Mt. Norikura
47. Evaluation of Response to the Gamma-ray of the Emulsion Telescope
48. Experimental Study of High-energy Cosmic Rays in the Tibet AS $\gamma$ Experiment
49. Sidereal daily variation of $\sim$10TeV galactic cosmic ray intensity observed by the Tibet air shower array
50. Cosmic ray interactions in the knee and the highest energy regions
51. Study of High Energetic Radiation from Thundercloud in Tibet
52. Study of the composition of cosmic-rays at the Knee
53. A study on variation of interplanetary magnetic field with the cosmic-ray shadow by the sun

54. BASJE (Bolivian Air Shower Joint Experiment)
55. Towards the imaging of the massive black hole in SgrA*
56. Observation with the All-sky Survey High Resolution Air-shower detector (Ahsra)
57. Test and installation of image pipeline for Ashra observation
58. Automatization of Ashra observation
59. Test of the sensor to detect cosmic rays for Ashra observation
60. Integration of the optical fiber trigger system for Ashra
61. Study of Extremely-high Energy Cosmic Rays by Telescope Array
62. Development of new surface detector for observation of ultra high energy cosmic ray at Telescope Array site
63. Study of radio detection of highest energy cosmic rays
64. Development of the steering system on CLF at the Telescope Array Experiment
65. Calibration for TA FD with RC helicopter
66. Study of absolute energy calibration of air shower by a compact electron linac
67. Improvementof low-energy sensitivity of the TA surface detector (TALE project) and study of the cosmic-ray anisotropy
68. Calibration of TA-EUSO 64ch multi-anode PMT and comparison with CRAYS
69. Observation of airshower fluorescence light at the TA FD site by using an Imaging UV telescope
70. Research and development of detectors for MBR microwave radiations
71. CTA Project R&D
72. Development of the readout system for the CTA large-size telescopes
73. Development of Foal Plane Instruments for the CTA Large Scale Telescope
74. Development of camera for CTA small-sized telescopes
75. Development of advanced photon counter for the future IACT
76. CTA-Japan Physics Research
77. CTA Monte Carlo Simulation
78. The extreme Universe viewed in very high energy gamma-rays 2013
79. Study of High Energy Gamma-ray Objects with the MAGIC telescopes
80. Development of a high-sensitivity cosmic gamma-ray detector exploring 0.5-30 MeV
81. Study on High Energy Cosmic Ray Sources by Observations in Space
82. Observational study of particle acceleration in the Crab nebula/pulsar
83. Comparative study of astrophysical particle acceleration phenomena
84. Research and Development for the ultra high sensitivity quantum interferometer in KAGRA
85. Data analysis using CLIO data (IV)
86. Real time control for interferometer using computers (II)
87. Gravitational Wave Detector in Kamioka (XII)
88. Development of optical cavities for ultranarrow stable lasers
89. Development of the output mode-cleaner for KAGRA

90. Numerical simulation of Electric-Magnetic Wave Propagation in Gravitational wave Detector
91. Application of geophysical observations in the Kamioka mine to the dynamics of snow and water
92. Research on ultra-low frequency anti-vibration system for KAGRA
93. Development of beam position minitoring and controling systems for KAGRA
94. Development of Sapphire Mirror Suspension for KAGRA(LCGT) (X)
95. Study for KAGRA data analysis and Research for its System (III)
96. Development of precision profiler for mirrors of LCGT interferometer 3
97. Development of Very Low Vibration Cryo-Cooler System
98. Research on cryogenic payload for KAGRA
99. Research of Large-scale Gravitational wave Telescope (III)
100. The development of a super sensitive shadow sensor for a gravitational antenna
101. Gravitational Wave Detection using Non-Harmonic Analysis
102. Characterization of Sapphire mirror for KAGRA using electron spin resonance
103. Development of a stabilization system for the KAGRA laser source
104. R&D for the intensity stabilization of the laser system in KAGRA
105. Cosmic Reionization Probed with Large Optical Near-Infrared Telescopes
106. Evolution of the universe and particle physics
107. Frontier of the planetary material science
108. Nondestructive characterization of planetary materials using Imaging Plates
109. Detection of time variations for cosmogenic Be-7
110. Observation of global air-mass motion measuring radionuclides of Cs in the air
111. Study on solar and cosmic-ray effects on climate variations
112. Continuous Environment Measurement of the Kashiwa Underground Laboratory
113. Evaluation of the erupted radioactivities into the environment.
114. Precise calculation of the atmospheric neutrino flux
115. Simulation study for the IceCube Neutrino Observatory
116. CRC workshop for future plans in cosmic ray research
117. The 7th International Workshop on Very High Energy Particle Astronomy (VHEPA2014) - Next Generation Explorer for Cosmic Ray Origin -

# G. List of Committee Members

**(a) Board of Councillors**

| | |
|---|---|
| KAJITA, Takaaki | ICRR, the University of Tokyo |
| FUKUSHIMA, Masaki | ICRR, the University of Tokyo |
| KAWASAKI, Masahiro | ICRR, the University of Tokyo |
| NAKAHATA, Masayuki | ICRR, the University of Tokyo |
| AIHARA, Hiroaki | The University of Tokyo |
| MATSUMOTO, Yoichiro | The University of Tokyo |
| YAMAUCHI, Masanori | KEK |
| SASAKI, Misao | YITP, Kyoto University |
| HAYASHI, Masahiko | National Astronomical Observatory of Japan |
| YUDA, Toshinori | The University of Tokyo |
| MURAKI, Yasushi | Nagoya University |
| MASAIKE, Akira | Kyoto University |
| MAKINO, Fumiyoshi | Institute of Space and Astronautical Science |
| SUGIYAMA, Naoshi | Nagoya University |
| KOMAMIYA, Yukio | ICEPP, the University of Tokyo |

**(b) Advisory Committee**

| | |
|---|---|
| KAJITA, Takaaki | ICRR, the University of Tokyo |
| HISANO, Junji | Nagoya University |
| SUGIYAMA, Naoshi | Nagoya University |
| HAZUMI, Masashi | KEK |
| KISHIMOTO, Tadafumi | Osaka University |
| YOKOYAMA, Masashi | The University of Tokyo |
| KANDA, Nobuyuki | Osaka City University |
| ITOW, Yoshitaka | Nagoya University |
| NISHIJIMA, Kyoshi | Tokai University |
| OGIO, Shoichi | Osaka City University |
| SUZUKI, Yoichiro | ICRR, the University of Tokyo |
| KURODA, Kazuaki | ICRR, the University of Tokyo |
| NAKAHATA, Masayuki | ICRR, the University of Tokyo |
| KAWASAKI, Masahiro | ICRR, the University of Tokyo |
| TERASAWA, Toshio | ICRR, the University of Tokyo |
| TESHIMA, Masahiro | ICRR, University of Tokyo |

**(c) Inter-University Research Advisory Committee**

| | |
|---|---|
| NISHIJIMA, Kyoshi | Tokai University |
| MUNAKATA, Kazuoki | Shinshu University |
| TAJIMA, Hiroyasu | Nagoya University |
| MASUDA, Kimiaki | Nagoya University |
| YAMAMOTO, Tokonatsu | Konan University |
| ANDO, Masaki | The University of Tokyo |
| TSUNESADA, Yoshiki | Tokyo Institute of Technology |
| KUBO, Hidetoshi | Kyoto University |
| TERASAWA, Toshio | ICRR, the University of Tokyo |
| TAKITA, Masato | ICRR, the University of Tokyo |
| SAGAWA, Hiroyuki | ICRR, the University of Tokyo |
| OHASHI, Masatake | ICRR, the University of Tokyo |
| KISHIMOTO, Yasuhiro | ICRR, the University of Tokyo |

# H. List of Personnel

**Director** KAJITA, Takaaki,

**Vice-Director** TERASAWA, Toshio,

**Kamioka Observatory (Neutrino and Astroparticle Division)**

| | | | |
|---|---|---|---|
| Scientific Staff | ABE, Ko, | HAYATO, Yoshinari, | HIRAIDE, Katsuki, |
| | ICHIMURA, Koichi, | IKEDA, Motoyasu, | KAMEDA, Jun, |
| | KISHIMOTO, Yasuhiro, | KOBAYASHI, Kazuyoshi, | MIURA, Makoto, |
| | MORIYAMA, Shigetaka, | NAKAHATA, Msayuki, | NAKAYAMA, Shoei, |
| | OGAWA, Hiroshi, | SEKIYA, Hiroyuki, | SHIOZAWA, Masato, |
| | SUZUKI, Yoichiro, | TAKEDA, Atsushi, | TANAKA, Hidekazu, |
| | TOMURA, Tomonobu, | YAMASHITA, Masaki, | YANG, Byeongsu, |
| | WENDELL, Roger Alexandre, | | |
| Administrative Staff | OIDA, Yoshihito, | TANAKA, Masahiro, | |
| Technical Staff | NOZAWA, Noriyuki, | ONOUE, Tatsuya, | TAMORI, Yukio, |
| Research Fellow | BAI, Lili, | WILKING, Michael Joseph, | |
| Secretary | OKURA, Yoko, | TANIMURA, Naoko, | YONEZAWA, Keiko, |

**Research Center for Cosmic Neutrinos (Neutrino and Astroparticle Division)**

| | | | |
|---|---|---|---|
| Scientific Staff | KAJITA, Takaaki, | MASUDA, Kimiaki, | NISHIMURA, Yasuhiro, |
| | OKUMURA, Kimihiro, | | |
| Technical Staff | SHINOHARA, Masanobu, | | |
| Secretary | KITSUGI, Atsuko, | WATANABE, Keiko, | |

**High Energy Cosmic Ray Division**

| | | | |
|---|---|---|---|
| Scientific Staff | ASANO, Katsuaki, | ENOMOTO, Ryoji, | FUKUSHIMA, Masaki, |
| | HAYASHIDA, Masaaki, | IKEDA, Daisuke, | KAWATA, Kazumasa, |
| | MIRZOYAN, Razmik, | NONAKA, Toshiyuki, | NAKAJIMA, Daisuke, |
| | TAKEDA, Masahiro, | TAKITA, Masato, | TERASAWA, Toshio, |
| | TESHIMA, Masahiro, | OHNISHI, Munehiro, | OHISHI, Michiko, |
| | SASAKI, Makoto, | SHIBATA, Tatsunobu, | YOSHIKOSHI, Takanori, |
| Technical Staff | AOKI, Toshifumi, | KOBAYASHI, Takahide, | NIWA, Hiroki, |
| | OOKI, Kaoru, | SUZUKI, Masao, | |
| Research Fellow | AITA, Yuichi, | AKAIKE, Yosui, | |
| | FUJII, Toshihiro, | HANABATA, Yoshitaka, | INOUE, Susumu, |
| | KIDO, Eiji, | KISAKA, Shota, | KUMAR, Rahul, |
| | MIYAMOTO, Hideaki, | SAITO, Koji, | SAKO, Takashi, |
| | TANAKA, Syuta, | | |
| Secretary | KOKUBUN, Yayoi, | OKAMURA, Takako, | SUGAHARA, Midori, |

**Akeno Observatory (High Energy Cosmic Ray Division)**

| | | | |
|---|---|---|---|
| Scientific Staff | SAGAWA, Hiroyuki, | | |
| Tecnical Staff | OHOKA, Hideyuki, | SHIMIZU, Kanetoshi, | |

**Norikura Observatory (High Energy Cosmic Ray Division)**

| | | | |
|---|---|---|---|
| Technical Staff | AGEMATSU, Yoshiaki, | ISHITSUKA, Hideki, | OKAZAKI, Nao, |
| | SHIMODAIRA, Hideaki, | TOKOKU, Chihiro, | USHIMARU, Tsukasa, |

**Astrophysics and Gravity Division**

| | | | |
|---|---|---|---|
| Scientific Staff | HIROSE, Eiichi, | IBE, Masahiro, | KAWAMURA, Seiji, |
| | KAWASAKI, Masahiro, | KIMURA, Nobuhiro, | KURODA, Kazuaki, |
| | MIYAKAWA, Osamu, | MIYOKI, Shinji, | OHASHI, Masatake, |
| | OHISHI, Naoko, | ONO, Yoshiaki, | OUCHI, Masami, |
| | SAITO, Yoshio, | SUZUKI, Toshikazu, | TAKAHASHI, Ryutaro, |
| | UCHIYAMA, Takashi, | YAMAMOTO, Kazuhiro, | YOON Tai Hyun, |
| Administrative Staff | TAKAYAMA, Kyouichi, | | |
| Technical Staff | FURUTA, Kiyoshi, | IWASAKI, Utako, | KAMIIZUMI, Masahiro, |
| | SAKATA, Shihori, | | |
| Research Fellow | FRIEDRICH, Daniel Dieter, | HARIKANE, Yuichi, | HAYASHI, Masao, |
| | KHALAIDOVSKI, Alexander , | MOMOSE, Rieko, | NISHIDA, Erina, |
| | SHIBUYA, Takatoshi, | SHIOMI, Sachie, | YAMANAKA, Yuji, |
| | YOKOYAMA, Shuichiro, | YUMA, Suraphong, | |
| Secretary | KAWAKAMI, Akiko, | KIKUCHI, Rie, | MASHIMA, Chieko, |
| | OKINAKA, Mihoko, | | |

**Graduate Students**

| | | | |
|---|---|---|---|
| Doctor | CHEN, Dan, | IRVINE, Tristan James, | IYOGI, Kazuki, |
| | KAWAKAMI, Etsuko, | KITAJIMA, Naoya, | MIKAMI, Ryo, |
| | NAKANO, Yuuki, | OBI, Yoshio, | RICHARD, Euan Neil, |
| | SAKAKIBARA, Yusuke, | SEKIGUCHI, Takanori, | TAKACHIO, Osamu, |
| | TAKEDA, Naoyuki, | TAKEISHI, Ryuji, | TAKESAKO, Tomohiro, |
| | YAMADA, Masaki, | YOSHINO, Kazuyoshi, | |
| Master | AIZAWA, Tasuku, | HAGA, Yuto, | HAYAKAWA, Taku, |
| | HIGUCHI, Chika, | HONG, Jeong Pyong, | ISHIGAKI, Masaufumi, |
| | ISHIO, Kazuma, | KAMETANI, Isao, | KOBAYASHI, Masatoshi, |
| | KOJIMA, Takumi, | KONISHO, Shiori, | KONNO, Akira, |
| | NAITO, Yoshiaki, | NAKAGAWA, Katsuma, | NAKAJIMA, Tateo, |
| | NAKANO, Masayuki, | NISHIMURA, Tsubasa, | OGINO, Momoko, |
| | OKA, Naoya, | ONO, Kenji, | ORII, Asato, |
| | SASAKI, Kento, | SHIN, Heungsu, | TAKAHASHI, Mitsunari, |
| | TAMAZAWA, Hiroko, | TEJIMA, Koudai, | TO, Sho, |
| | TSUYUKI, Takanao, | WATANABE, Atsushi, | |

**Administrative Division**

| | | | |
|---|---|---|---|
| Administrative Staff | AKIYAMA, Makiko, | ASAKA, Sadako, | FUJIE, Tamiko, |
| | IRIMAJIRI, Aki, | ISHII, Yoshikazu, | MARUMORI, Yasuko, |
| | MORITSUBO, Shigeru, | NAKAMURA, Saori, | OCHI, Masashi, |
| | SAITO, Akiko, | WATANABE, Wataru, | YAMAGUCHI, Akiko, |
| Research Administrator | SATO, Ritsuko, | | |
| Outreach Staff | HAYASHIDA, Misato | | |